TÜBİTAK

TÜRKİYE BİLİMSEL VE
TEKNİK ARAŞTIRMA KURUMU

THE SCIENTIFIC AND TECHNICAL
RESEARCH COUNCIL OF TURKEY

Yer Deniz Atmosfer Bilimleri ve
Çevre Araştırma Grubu

Earth Marine Atmospherical Sciences and
Environmental Researches Grant Group

Orta Doğu Teknik Üniversitesi
Deniz Bilimleri Enstitüsü

Özsoy, Emin

TÜRKİYE BİLİMSEL VE TEKNİK ARAŞTIRMA KURUMU
(TÜBİTAK)

2001-92

(YDABÇAG - 137)

KIYI GEOMETRİSİ İLE TABAN TOPOGRAFYASININ KIYI VE KITA SAHANLIĞI AKIMLARININ YAPISI VE GİRDAP OLUŞUMLARINA ETKİSİ

PROJE KESİN RAPORU

Erdemli, Nisan 2000

KIYI GEOMETRİSİ İLE TABAN TOPOGRAFYASININ KIYI VE KITA SAHANLIĞI AKIMLARININ YAPISI VE GİRDAP OLUŞUMLARINA ETKİSİ

İÇİNDEKİLER

Öz. Tr. En

KIYI GEOMETRİSİ İLE TABAN TOPOGRAFYASININ KIYI VE KITA SAHANLIĞI AKIMLARININ YAPISI VE GİRDAP OLUŞUMLARINA ETKİSİ

Özet ve Raporun Organizasyonu

Bu proje'nin amacı, kıyısal akimlar dinamiğinin incelenmesi ve bu akımların topoğrafya, kiyisal geometri, rüzgar gerilimi gibi çevre koşullarından nasıl etkilendiğinin belirlenmesidir. Anılan türden etkileşimler, küresel okyanus'u çevreleyen kıyısal bölgelerin pek çoğunda geçerlidir. Bu bölgelerdeki kıyısal akımların dinamiği çoğu kez menderesler, girdaplar ve puüsküller gibi, açık denizle ısı, tuzluluk, besin tuzları *vbg* özelliklerin alışverişini etkileyen yapılarca belirlenir.

Bu araştırma projesinde çeşitli yöntemler kullanılmıştır: Uydu ve yer ölçümlerine dayanan önceki gözlemler, bizleri bazı düşsel veya uygulamalı problemler için analitik veya sayısal çözümler geliştirmek yolunda teşvik etmiştir. Türkiye kıyılarında gözlenen özel durumlar bu yönde önemli bir rol oynamışlardır. Temel bir kavrayış için, kontrollü durumlardaki geometrik veya topoğrafik özelliklerin etkileri incelenmiştir. Ancak, incelenebilecek düşsel durumların kapsadığı alanın çok geniş olabileceği gözönüne alınarak, basitleştirilmiş durumlardan oluşan bir set problem ele alınmıştır. Bu özel problemlere ek olarak, taban akımlırının basit bir modeli, gözlemlerden de yararlanılarak, İstanbul ve Çanakkale Boğazları'nın komşu denizlere ulaşan dip akımlarına uygulanmıştır.

Bu raporda öncelikle barotropik bir kıyısal akımın geometrik ve topoğrafik olarak kontrolü problemini formüle etmekteyiz. Daha sonra, dönen yerküre üzerinde, taban sürtünmesi ve topoğrafya değişimleri tarafından dengelenen bir kıyısal akımı incelemekteyiz. Asimptotik bir profil ile yaklaşan bir akımın basitleştirilmiş durağan d'namiği öncelikle ele alınmaktadır. Daha sonra, analitik çözümlerle yapilan karşılaştırma yoluyla modelin durağan olmayan koşullara uygulanması denenmektedir.

Kıta sahanlığı akımlarının ikinci bir uygulaması olarak, Türkiye denizleri'nden iyi bilinen iki örnek seçilmektedir: İncelenen kıta sahanlığı akımları, İstanbul ve Çanakkale Boğazları'nın komşu denizlere olan yoğun su akımları'dır. Komşu kıta sahanlığı bölgelerindeki akımlar Boğazlar'daki momentum veya yoğunluk farkı kaynaklarınca sürülür, ve ortaya çıkan yerçekimi akıntılarının yapısı büyük ölçüde taban topoğrafyası, taban sürtünmesi ve türbülanslı girişim tarafından belirlenir.

Yaklaşımımız, herhangi bir yapıyı modeller yardımı ile benzeştirmeden önce, gözlemlerin dikkatlice gözden geçirilmesine dayanmaktadır. Deneyimimiz, bu yaklaşımın gerekliliğini göstermiştir. Sonuçlar, kıta sahanlığı topoğrafyasınının küçük ayrıntılarına fazlaca duyarlıdır. Boğazlar'dan dışarı akan suların kaderi, ve dolaylı olarak belirledikleri komşu Deniz'lerin yenilenme süreçleri, kıta sahanlığı üzerindeki akım yoluna ve gerçekleşen karışıma duyarlı bir şekilde bağlıdır.

Rapor'un ilk bölümü kıyısal akımların gözden geçirilmesine ve Türkiye Denizleri'nden örneklere ayrılmıştır. Uydu ve yer gözlemleri ile ilgili yayınlar gerçekleşen durumları örnelemek amacı ile Rapor'a eklenmiştir.

İkinci bölümde barotropik kıyısal akımları belirleyen denklemlerin geliştirilmesi ve özel durumları, kullanılan modellerin ayrıntıları ile birlikte anlatılmaktadır. Seçilmiş düşsel durumlardaki analitik ve sayısal çözümler arasında karşılaştırmalar yapılmaktadır.

İstanbul ve Çanakkale Boğazları'ndan komşu denizlere yoğun su akışı ile ilgili gözlem ve modellere dayanan sonuçların bir özeti, yayımlanmak üzere gönderilen biri İngilizce diğeri Türkçe iki makale aracılığıyla Ek 1 de verilmiştir. Ek 2 de ise konuyla ilgili daha önceki yayınlarımız bütünleyici olmaları için sunulmaktadir.

THE EFFECTS OF COASTAL GEOMETRY AND BOTTOM TOPOGRAPHY ON THE STRUCTURE OF COASTAL / CONTINENTAL SHELF CURRENTS AND ON THE FORMATION OF EDDIES AND MEANDERS

TABLE OF CONTENTS

THE EFFECTS OF COASTAL GEOMETRY AND BOTTOM TOPOGRAPHY ON THE STRUCTURE OF COASTAL / CONTINENTAL SHELF CURRENTS AND ON THE FORMATION OF EDDIES AND MEANDERS

Summary and Organization of the Report

The present project aims for preliminary investigations of the dynamics of coastal currents as influenced by interactions with topography, coastal geometry, wind-stress, and ambient conditions. Such interactions seem to be active in many coastal environments of the global ocean, where the coastal current dynamics is often associated with meanders, rings, eddies, filaments, which are able to exchange heat, salinity, nutrients *etc.* with the open ocean waters.

In this research project, a combination of tools are used: Previous observations based on satellite or *in-situ* measurements have motivated us to seek analytical / numerical solutions for idealized, as well as application oriented problems. Special cases observed along the Turkish coastal seas have a special role in this respect. To develop a basic understanding, simple effects of geometrical and topographical features under specific controls have been considered. Because this area of research covers a very wide range of possible idealised cases to be investigated, a cursory examination of a set of simplified cases is investigated. In addition to simplified problems, a simple model of bottom flows is applied to specific conditions of the Bosphorus and Dardanelles outflows, guided by observations.

We first formulate the problem of geometrical and topographical controls of a barotropic coastal flow. We then investigate coastal flows on a rotating earth, balanced by bottom friction and topographical variations. Simplified steady dynamics is first investigated for approaching flows with assymptotic characteristics. Comparison to analytical solutions are then used to test the model for unsteady development.

As a second application to shelf flows, we consider the two well known examples from Turkish Seas: The shelf flows investigated are the dense water outflows from the Dardanelles and Bosphorus Straits. The flows on the adjacent shelf regions are driven by the sources of momentum and negative buoyancy at the Strait exits, and the structure of the resulting gravity currents is greatly determined by the shelf topography, bottom friction and the entrainment into these turbulent flows. We base our approach on careful consideration of the observed features, before using a model to simulate these features. Our experience has verified the need for these considerations. The results are very sensitive to small details of the shelf topography. Therefore the fate of the outflowing water, which in turn determines the internal renewal processes of the adjacent Seas, sensitively depends on the flow route and the mixing achieved on the shelf.

The first chapter of the report is devoted to a review of coastal flows, followed by examples from Turkish Seas. Papers on the satellite and in-situ observations are appended to exemplify these features.

The second chapter gives the development of the equations governing barotropic coastal flows and the theory for limiting cases, together with the detailed descriptions of the models used. It then displays the solutions and idealised comparisons for selected cases.

The third chapter provides a summary of results obtained from combined observational and modelling experiments for the dense water outflows from the Bosphorus and the Dardanelles Straits. A draft manuscript of a submitted paper on the Bosphorus outflow, and a summary of results from a student thesis on the Dardanelles outflow are included in this section. In Appendix 1, copies of previously published papers are given for completeness.

Chapter 1
A REVIEW OF COASTAL FLOWS WITH EXAMPLES FROM THE TURKISH SEAS

Scope and Importance of the Subject

Intensive industrial and other activities along the coasts, including fishing and transportation, and the need for protection and rational utilization of natural resources, demonstrate the importance of coastal seas in the world ocean. It is often due to these activities that there is an immediate need for a better understanding of the coastal ocean.

In addition, the coastal ocean has emerged as a sensitive area within the context of 'global change', i.e. with respect to its role as a land-ocean-atmosphere interface, as signified by the LOICZ (Land Ocean Interactions in the Coastal Zone) core project of IGBP (International Geosphere - Bisphere Program) (IGBP, 1995). The roles of the coastal ocean in the global system, in terms of supporting high rates of primary production and receiving river inputs and pollution from land, and the impacts of global change on sea-level and ecosystem changes adjacent to the coast, motivate high priorities to be assigned to the coastal ocean. In the present world, where the global contests of superpowers of former decades have been overwhelmed with the present regional conflicts, increasing military importance is assigned to coastal regions.

On the other hand, the interdisciplinary problems of the coastal zone, in the context of interactions between the coastal ocean, the land, the atmosphere and the open ocean regions have not been fully resolved. An important workshop (IOC, 1994, Brink and Robinson, 1998; Robinson and Brink, 1998) recently called for an international emphasis on studies of the coastal ocean. It is recognised that the coastal zones of the world display considerable heterogeneity, when compared to the open ocean (IGBP, 1995), which pose methodological problems in addressing the role of coasts in a global perspective. Therefore it seems necessary that individual cases be understood with confidence, before generalizations can be made.

It is in this spirit that the coastal ocean processes bordering the Anatolian peninsula are investigated. As also evident in other parts of the world, the coastal processes defining the physical and ecological system behaviour of Turkish coastal seas are extremely complex. Among these, the effects of coastal geometry and bottom topography constitute the most easily identified, yet not necessarily easily understood component of system behaviour. The scope of the problems that could be generated is very wide in terms of possible geometric

configurations, and parametric space. The basic dynamical problems are by nature non-linear and defined by competitive first order contributions of the various physical factors in a wide range of possible settings. Hence the approach adopted here: the analytical / numerical investigations of possible flow configurations will be motivated by observed cases along the Turkish coastal seas, it will then be possible to address simplified versions of these problems, *e.g.* barotropic or baroclinic currents as influenced by the particular geometry and topography, stratification, and wind or buoyancy forcing in the correct parametric ranges for each individual problem.

A Review of Coastal Currents

In the Turkish coastal seas, it is possible to find many examples of coastal currents interacting with local topography, geometry, buoyancy sources, or wind stress distributions.

The 'rim current' of the Black Sea is a good example of an unstable boundary current in an environment of a prograde coastal front driven by buoyancy sources (the major rivers such as Danube) further upstream. Typically, the unstable motions are triggered when the current core attached to the continental slope region approaches the Sakarya Canyon, a wide, deep depth discontinuity along the Anatolian coast (Sur *et al.*, 1994, 1995), whereupon meanders and eddies develop along the coast, and evolve into a fully turbulent structure separated from the coast at Cape Kerempe, a sharp corner where slope changes occur. In winter, the cold water mass formed along the western shelf moves in the region as a shallow front attached to the coast, and becomes separated at Cape Baba, a sharp rectangular headland.

An interesting consequence of the boundary current instability, of interest in the Black Sea, is the rather unexpected patterns of upwelling generated in summer, when a transient, modulated upwelling structure develops near Cape Kerempe, even in the absence of favorable winds (Sur *et al.*, 1994, 1995).

In the eastern Black Sea, the Batumi eddy is a large anticyclonic circulation trapped in the angular corner of the Black Sea where the Caucasian and Anatolian coastlines merge. On occasions, this eddy escapes the geometric confines and develops into a large meander motion along the Caucasian coast (Sur *et al.*, 1994, 1995).

Whatever may be the cause leading to the meandering and filamented structures of boundary currents, they are of primary importance in determining the exchange between the shelf

regions and the deep ocean, with many bio-geo-chemical implications. In a basin of relatively small size such as the Black Sea, cross-shelf exchanges are of central importance because (*i*) occasionally the horizontal scales in the bursts of exchanges are almost of the same scale as the basin itself, (*ii*) a significant amount of the fresh water, nutrients and other materials are input from major rivers (*e.g.* the Danube), and advected along the coast by the boundary current, finally being injected into the basin interior via turbulent exchanges (Sur *et al.*, 1994, 1995). Episodes such as the unstable, seprated currents in the southeastern Black Sea, or the large meander instabilities alomg the Caucasian coast, are expected to be extremely important for transport of fish eggs and larvae, as well as other materials.

Along the Eastern Mediterranean (northeastern Levantine Sea) coast of Anatolia, the meandering Asia Minor current (Özsoy *et al.*, 1993) is a well defined feature, which interacts and reorganises itself with incident eddies arriving through the Cilician Channel, or leads to the semi-permanent Antalya anticyclonic eddy, possibly as a result of current instabilities (Özsoy *et al.*, 1993; Feliks and Ghil, 1993). The Rhodes Gyre is a permanent feature, and the Cretan eddy is a semi-permanent coherent eddy, formed along this current (Özsoy *et al.*, 1993).

It is possible to find many examples of the interactive, and often unstable dynamics of coastal currents in many coastal areas of the world oceans. In general strong coastal currents in frontal regions tend to follow the topographic slopes, and become strongly influenced by relatively small changes in the influential factors, such as topography, coast geometry, wind-stress forcing, existing stratification, *etc.*. These factors have been demonstrated to play leading roles in the separation from the coast of large current systems; and even in the case of majestic currents such as the Gulf Stream (Haidvogel *et al.*, 1991).

Instabilities often lead to meso-scale variability along the boundary currents. Unstable waves, meanders, dipoles, or paired eddies with opposite signed vorticity have frequently been reported along density-driven boundary currents in many parts of the world ocean: near Vancouver Island (Thomson 1984; Ikeda *et al.*, 1984), in the California Current (Ikeda and Emery, 1985), off the southern coast of Alaska (Ahlnäs *et al.*, 1987), in the Norwegian Coastal Current (Carstens *et al.*, 1984; Johannessen *et al.*, 1989; Ikeda *et al.*, 1989), in the Sea of Okhotsk and the Subarctic Polar Frontal Zone (Fedorov and Ginsburg, (1989), in the Fram Strait Marginal Ice Zone (Johanessen *et al.*, 1987, Ginsburg and Fedorov, 1989), off the Labrador Coast (Ikeda, 1987), in the East China Sea (Qiu *et al.*, 1988), in the Leeuwin Current along western Australia (Cresswell and Golding, 1980; Legeckis and

Cresswell, 1981; Thompson, 1984; Griffiths and Pearce, 1985), along the Ligurian Coastal Current (Crepon *et al.*, 1982), and along the Algerian Current (Millot, 1985, 1991).

Baroclinic instability could be one of the most relevant mechanisms generating time-dependent motions along frontal regions. Realistic boundary flows with horizontal density gradients are often found to be unstable to small perturbations (*e.g.* Mysak and Schott, 1977; Griffiths and Linden, 1981; Ikeda *et al.*, 1984, 1989; Qiu *et al.*, 1988; Chao, 1988; Beckers and Nihoul, 1992), and as a result, the unstable waves in many cases grow into large amplitude meanders or paired coherent vortices. Laboratory experiments of Condie (1989) show that the energy of the unstable motions, including coalescent eddies and dipoles, is extracted from the mean flow at the Rossby deformation radius scales, and later transferred to larger scales by nonlinear processes. During the nonlinear growth stage of the instability, Qiu *et al.*, (1988) showed that disturbances starting at the grid-scale were transformed into finite amplitude meanders with 'backward breaking' tendency, enhancing the cross-shelf exchanges. Laboratory experiments of Carstens *et al.*, 1984) indicated anomalous current loops separated from the coast. Chao (1990) differentiated between prograde (fronts rising to the surface in the same direction as the bottom topography, *e.g.* Gulf Stream or upwelling fronts) and retrograde (isobaths and isopycnals slanted in opposite senses, *e.g.* density driven boundary currents with buoyant water near the coast, such as in the Black Sea) fronts, arguing that prograde fronts are more amenable to slanted convection (baroclinic instability) than retrograde fronts. However, it was demonstrated that enhanced meander and eddy growth could occur due to relaxation processes, *e.g.* temporally varying buoyancy forcing, which seemed to be more important in the case of retrograde fronts and more effective than the other possible forms of external forcing (such as winds or small topographic variations).

Transient features of unexpected upwelling similar to those in the Black Sea have been found along boundary current systems by Qiu *et al.* (1988) and Chao (1990), and near anticyclonic members of coastal eddy pairs along the Algerian Current (Millot, 1991; Beckers and Nihoul, 1992).

In addition to the basic baroclinically unstable flow situations reviewed above, the interaction of a boundary current with the coastline geometry, or with the continental shelf / slope topography appears to be another possible mechanism that could lead to the unstable meanders, eddies or filaments along the Black Sea priphery.

The mechanism of generation of the oscillatory motions by the step topography is not clearly understood. We expect oscillatory motions to be generated by the interaction of a

topographic barrier with barotropic shelf / slope flows taking the coast (shallower depths) to the left in the northern hemisphere. Considering that the analogous effects of planetary vorticity gradient (β) and topography (*i.e.* contributions to variations in f/H, where f is the Coriolis parameter and H the depth of the flow), we can compare flows bounded on the left hand side with eastward flows in the case with planetary vorticity gradient. Oscillatory motions are created when an eastward flowing β-plane barotropic jet crosses a step topography, while a smooth readjustment occurs for westward flowing jets (Shetye and Rattray, 1982), confirming well known results of Batchelor (1970). The above results suggest that the western Anatolian jet flowing across the Sakarya Canyon would not be subjected to meandering or oscillatory motions if this jet were to be purely barotropic. On the other hand, Spitz and Nof (1991) indicate that a barotropic boundary current would be forced to separate from the coast when it encounters a large step with the depth increasing downstream, regardless of the direction of flow relative to the coast.

Sudden changes in topography are expected to lead to oscillatory motions even in the case of a right hand side coast, when baroclinic modes are included. In fact, barotropic flows impinging on a step topography can be expected to generate large amplitude baroclinic motions (*e.g.* Cushman-Roisin and O'Brien, 1987). Oscillatory motions created by interacting baroclinic and barotropic components of a boundary current near canyon or ridge topographies are illustrated by Häkkinen (1987).

Interactions with coastline perturbations were found to create standing waves, as well as baroclinic eddies and filaments in the case of upwelling fronts (Narimousa and Maxworthy, 1987), and to lead to meanders by pure geometrical adjustment to depth contours (without imposing baroclinic instability) in the case of ice-edge fronts (Ikeda, 1987). The role of bottom topographic features was found to augment the baroclinic instability in the case studied by Ikeda (1989). In the case of upwelling fronts, Narimousa and Maxworthy (1985) found large stationary meanders and filaments generated by a bottom ridge. Haidvogel *et al.* (1991) and Hoffmann *et al.* (1991) found offshore filaments generated by the interaction of a boundary current (upwelling front) with topographic variations. During later stages of development, the evolving filaments were shown to lead to self-advecting dipole eddies detached from the coastal region.

An important effect of topography we observe in the case of the west Anatolian boundary current is the separation of the jet from the coast at C. Kerempe, where the flow encounters a widening shelf topography. Leaman and Molinari (1987) studied the effects of a linearly

widening shelf and found that this situation can lead to vertically sheared flows perpendicular to the coast, resulting in flow separation. The change in the angle of the coastline near C. Kerempe can be a secondary factor leading to flow separation. Laboratory studies illustrate eddy shedding and separated flows downstream of headlands (*e.g.* Boyer and Chen, 1987).

Sharp corners in coastline geometry can lead to localized upwelling, even in the case of buoyant boundary currents with the coast on the right hand side, as shown by Cherniawsky and Leblond (1986). Most observations of topographically or geometrically induced upwelling elsewhere have been obtained either near permanent upwelling fronts (*e.g.* the California coast, Ikeda and Emery, 1984; Narimousa and Maxworthy, 1985, 1987; the southeastern coast of the U.S.A., Janowitz and Pietrafesa, 1982), or under conditions of favorable winds (*e.g.* the Gulf of Lions, Hua and Thomasset, 1983).

Eddies and filaments formed in regions of coastal currents elsewhere have been attributed to frontal dynamics of upwelling systems, or the effects of coastal headlands (Ramp *et al.*, 1991; Strub *et al.*, 1991; Haidvogel *et al.*, 1991). In the presence of deep canyons, tripole eddies are can be generated by the coastal current (Pingree and LeCann, 1992); conversely, the collision of an eddy with the coast can lead to a modified coastal current (Vidal *et al.*, 1992).

Dense Water Outflows from Straits

The communication between the Black Sea and the Aegean basin of the Mediterranean Sea is established through the Turkish Straits System (TSS), consisting of the Bosphorus and Dardanelles Straits and the Sea of Marmara. The flow through the System is in the form of a two-layer stratified exchange with the lighter surface waters flowing from the Black Sea to the Mediterranean, and the denser deep waters flowing in the other direction. The flow of dense water through the lower layer of both Straits is in the form of a bottom-arrested gravity current that feeds the deep waters of the adjacent basins and largely determines the internal deep structure of these seas.

Both dense water outflows at the entrances to the Marmara and Black Seas are strongly affected by local topography. In both cases the flow is initially confined to a canyon-like channel that exits from the strait into the sea, and later overflows the channel to flow along the local slopes of the continental shelf leading to the continental slope. Whether

the flow reaches the bottom of sea or not depends on the interior stratification, topography, entrainment and the initial conditions of the plume at the strait exit.

The properties of the Mediterranean water entering the Black Sea are transformed by turbulent entrainment as the water first follows the bottom conduit extending from the Strait onto the continental shelf, overflowing a sill, then spreading out on a very mild slope. At the shelf break the dense water cascades down the steep continental slope and loses its density contrast as a result of greatly increased entrainment, and reaches depths where it spreads horizontally into the interior and partially propagates east following the slope topography. The inflow largely determines the long-term properties of Black Sea deep water

The dense water inflow from the Dardanelles Strait into the Marmara Sea transports Mediterranean water into the basin and establishes the deep water stratification of the Marmara Sea. The lower-layer flow of the Dardanelles Strait is the only source that replenishes the deep waters of the Marmara Sea. A strong halocline, at a depth of $\sim 25m$, separates these waters from the low density surface waters of Black Sea origin, flowing in the opposite direction, *i.e.* entering the Marmara Sea from the Black Sea through the Bosphorus Strait, and leaving into the Aegean Sea through the Dardanelles Strait. Particular interest lies in the deep water renewals in the Marmara Sea owing to persistent oxygen deficiency of subhalocline waters.

A Review of the Numerical Modelling of Dense Water Outflows

The numerical modeling of gravity plumes in a rotating frame is initiated by the "streamtube" model of Smith (1975; cited in Baringer 1994). This model considers a laterally integrated streamtube with a variable cross-sectional area and, under the assumption of stationarity, it produces the path and the laterally averaged properties (density contrast, velocity) of the tube (plume) on a given, constant slope. The model includes bottom friction by means of a quadratic drag law and an entrainment rate proportional to the velocity, with both of these coefficients estimated diagnostically by finding the best fit to the observations.

This model has a number of convenient features such as being simple and effective in terms of computing power, however, the plume height is not predicted. The Smith model was applied to the Denmark Strait and the Mediterranean outflow with bottom friction and entrainment parameters tuned to fit the observations.

Modified and extended versions were later applied by Killworth (1977) to Antarctic slope convection and by Melling and Lewis (1982) to the shelf drainage flow in the Beaufort Sea. Pedersen (1980; cited in Baringer 1994) made the first attempt to include variable entrainment. Experimental data are examined to define a correlation function between entrainment and bottom slope. Using this new entrainment function reduces the unknown coefficients in the model to the bottom drag coefficient, but it also directly links entrainment to bottom drag. Baringer and Price (1990) used realistic topography and temperature and salinity data in their version they applied to the Mediterranean outflow. They reproduced the observed temperature and salinity structures, as well, but to avoid the drawback of getting only the cross-sectional area, they prescribed a plume width as if the plume were bounded by walls, which, in turn, is not realistic. Baringer (1994) applied a reduced gravity model with an active layer on the bottom to model the Mediterranean outflow. For the Dardanelles lower-layer inflow, Beşiktepe et al. (1993) applied a version of the streamtube model coupled with the interior heat and salt equations, namely the "filling box" model, to simulate the renewal mechanism, ignoring horizontal variations within the interior, and found it suitable for predicting and forecasting the interior vertical structure in response to variations in the inflow and outflow conditions of the Marmara Sea.

The model used by Jungclaus and Backhaus (1994) emerged from a need to investigate in more detail the plume dynamics over rugged topography of the continental slope, noting that laterally integrated model will not suffice, especially when splitting and joining is concerned.

Chapter 2
BAROTROPIC FLOW OVER TOPOGRAPHY

Governing Equations for Non-divergent, Frictional Coastal Flows

The *shallow water equations* for a homogeneous layer of fluid in a rotating frame of reference are

$$\frac{\partial \vec{u}}{\partial t} + \vec{u} \cdot \nabla \vec{u} + f\hat{k} \times \vec{u} = -\frac{1}{\rho}\nabla p + \frac{1}{\rho H}(\vec{\tau}^s - \vec{\tau}^b) + \frac{1}{H}\nabla \cdot H\underline{F} \qquad (1a)$$

$$\frac{\partial \eta}{\partial t} + \nabla \cdot H\vec{u} = 0 \qquad (1b)$$

The first of these is the horizontal momentum equation and the second one is the continuity equation. The variables $\vec{u}$, η and p are the fluid velocity, free surface elevation and pressure respectively. Of these variables, the velocity and pressure are three dimensional, depending on the cartesian coordinates $\vec{x} = (x, y, z)$ and time t, *i.e.* $\vec{u} = (u, v, w) = \vec{u}(\vec{x}, t) = \vec{u}(x, y, z, t)$, and $p = (\vec{x}, t)$, while the free surface depends on horizontal coordinates (x, y) and time t only, *i.e.* $\eta = \eta(x, y, t)$. The density of the fluid ρ is asumed to be a constant, *i.e.* the fluid is homogeneous. In essence, the equations are written on a *tangent plane* to the earth, where the vertical z coordinate points away from the center of the earth, and (x, y) lie in the plane tangent to the earth's surface at latitude ϕ_o at a point chosen to be the center of the coordinates at the area of interest. With these approximations to the original equations with the cartesian axes fixed on a spherical, rotating earth, the *Coriolis parameter* $f = 2\Omega\sin\phi$ represents the local effect of earth's rotation at latitude ϕ (with earth rotation speed of $\Omega = 2\pi/86400s^{-1}$). The total depth of the fluid at any point is $H = H(x, y, t) = h(x, y) + \eta(x, y, t)$ including the bottom depth h measured from the undisturbed sea surface, and the free surface elevation η (*i.e.* the deviation of the free surface from the undisturbed level). The second term on the *rhs* of (1a) is the surface forces acting horizontally on the a column of fluid, with $\vec{\tau}^s$ representing the wind stress at the free surface, and $\vec{\tau}^b$ representing the frictional stress at the bottom. The last term of (1a) represents the lateral friction where $\underline{F}$ is the shear stress acting between neighboring fluid columns.

We further simplify these equations based on approximations typical for problems to which they are applied. Firstly, since the vertical velocity of motion is assumed to be much smaller

than the horizontal velocities, the vertical momntum is approximated by hydrostatic pressure,

$$\frac{\partial p}{\partial z} = -\rho g, \quad \text{or} \quad p = \rho g(\eta - z)$$

by integration where g is the gravity, since (1b) implies $p = p(x, y)$ and (1b) implies $\vec{u} = \vec{u}(x, y)$ are two dimensional fields only. Secondly, we make the *rigid lid* assumption

$$\frac{\partial \eta}{\partial t} = 0$$

which amounts to the *nondivergent* approximation, since setting this term to zero equivalently sets the second term of (1b) to zero. Formally these approximations are justified through scale analysis. Finally, the lateral friction terms, i.e. the horizontal turbulent fluxes of momentum can be parameterized by

$$\frac{1}{H}\nabla \cdot H\underline{F} \simeq \nu \nabla^2 \vec{u}.$$

With the above approximations the equations of motion reduce to

$$\frac{D\vec{u}}{Dt} + f\hat{k} \times \vec{u} = -g\nabla\eta + \frac{(\vec{\tau}^s - \vec{\tau}^b)}{\rho H} + \nu\nabla^2\vec{u} \tag{2a}$$

$$\nabla \cdot H\vec{u} = 0 \tag{2b}$$

We define a *transport streamfunction* ψ according to

$$H\vec{u} = \hat{k} \times \nabla\psi$$

which satisfies continuity equation (2b) by virtue of simple vector identities. We then define *vorticity*

$$\zeta = \hat{k} \cdot \nabla \times \vec{u} = \hat{k} \cdot \nabla \times \frac{1}{H}\hat{k} \times \nabla\psi = \nabla \cdot \frac{1}{H}\nabla\psi.$$

Taking curl of equation (2a) yields

$$\frac{\partial}{\partial t}\nabla\times\vec{u}+\nabla\times(\vec{u}\cdot\nabla\vec{u})+f\nabla\times\hat{k}\times\vec{u}=\frac{1}{\rho}\nabla\times\frac{(\vec{\tau}^s-\vec{\tau}^b)}{H}+\nu\nabla^2\nabla\times\vec{u} \tag{3}$$

Now, after using the vector identities

$$\nabla\times(\vec{u}\cdot\nabla\vec{u})=\nabla\times\nabla(\frac{1}{2}\vec{u}\cdot\vec{u})-\nabla\times(\vec{u}\times\nabla\times\vec{u})=\nabla\times\hat{k}\zeta\times\vec{u}$$

equation (3) becomes

$$\frac{\partial}{\partial t}\hat{k}\zeta+\nabla\times[\hat{k}(\zeta+f)\times\vec{u}]=\frac{1}{\rho}\nabla\times\frac{(\vec{\tau}^s-\vec{\tau}^b)}{H}+\nu\hat{k}\nabla^2\zeta \tag{4}$$

Noting that the continuity equation can be written as

$$\nabla\cdot\vec{u}=-\frac{1}{H}\vec{u}\cdot\nabla H=-\frac{1}{H}\frac{DH}{Dt}$$

then yields the second term of (4) to be written as

$$\nabla\times[(\zeta+f)\hat{k}\times\vec{u}]=\vec{u}\cdot\nabla(\zeta+f)\hat{k}-\hat{k}\frac{\zeta+f}{H}\frac{DH}{Dt},$$

and combining terms, we obtain

$$\frac{D}{Dt}\left(\frac{\zeta+f}{H}\right)=\frac{1}{\rho H}\hat{k}\cdot\nabla\times\frac{(\vec{\tau}^s-\vec{\tau}^b)}{H}+\nu\frac{1}{H}\nabla^2\zeta \tag{5}$$

The bottom frictional stress τ^b can be parameterized in different ways (Csanady,). If we assume the well-stirred case, *i.e.* if the flow is turbulent, the bottom stress is related to the second power of velocity

$$\vec{\tau}^b=C_d|\vec{u}|\vec{u} \tag{6a}$$

which can be linearized, assuming $r = C_d|\vec{u}|$, approximating r to be a constant, to give

$$\frac{\vec{\tau}^b}{\rho H} = r\frac{\vec{u}}{H}. \tag{6b}$$

Instead if the flow is laminar, than the typical Ekman bottom boundary layer formulation would result in

$$\frac{\vec{\tau}^b}{\rho H} = s\vec{u}. \tag{7}$$

For shallow coastal flows the turbulent formulation is more appropriate. With the linearized turbulent version, (5) is

$$\frac{D}{Dt}\left(\frac{\zeta + f}{H}\right) = \frac{1}{\rho H}\hat{k}\cdot\nabla\times\frac{\vec{\tau}^s}{H} - r\frac{1}{H}\hat{k}\cdot\nabla\times\frac{\vec{u}}{H} + \nu\frac{1}{H}\nabla^2\zeta. \tag{8}$$

By multiplying (8) with H and expanding the first term we can write equation (8) as

$$\frac{\partial\zeta}{\partial t} + H\vec{u}\cdot\nabla\left(\frac{\zeta + f}{H}\right) = \frac{1}{\rho}\hat{k}\cdot\nabla\times\frac{\vec{\tau}^s}{H} - r\frac{1}{H}\hat{k}\cdot\nabla\times\frac{\vec{u}}{H} + \nu\nabla^2\zeta. \tag{9}$$

The bottom frictional term can alternatively be expressed as

$$\hat{k}\cdot\nabla\times\frac{\vec{u}}{H} = \hat{k}\cdot\nabla\times[\hat{k}\times\frac{1}{H^2}\nabla\psi] = \nabla\cdot\frac{1}{H^2}\nabla\psi, \tag{10}$$

or alternatively as

$$\nabla\cdot\frac{1}{H^2}\nabla\psi = \frac{1}{H}\nabla\cdot\frac{1}{H}\nabla\psi - \frac{1}{H^3}\nabla H\cdot\nabla\psi = \frac{1}{H^2}\nabla^2\psi - \frac{2}{H^3}\nabla H\cdot\nabla\psi. \tag{11}$$

By making use of (10) and using the definition of vorticity we can write

$$\frac{\partial\zeta}{\partial t} + \hat{k}\times\nabla\psi\cdot\nabla\left(\frac{\zeta + f}{H}\right) = \frac{1}{\rho}\hat{k}\cdot\nabla\times\frac{\vec{\tau}^s}{H} - r\nabla\cdot\frac{1}{H^2}\nabla\psi + \nu\nabla^2\zeta \tag{12a}$$

$$\nabla \cdot \frac{1}{H} \nabla \psi = \zeta \tag{12b}$$

to constitute closed form equations for streamfunction ψ and vorticity ζ. Equations (5), (8), (9) or (12) are different forms of the same equation, which is appropriately called the vorticity equation.

The Coriolis term

In general the Coriolis parameter f is a function of latitude, and if we expand about a central latitude angle ϕ_o,

$$\begin{aligned} f &= 2\Omega \sin\phi = 2\Omega \sin(\phi_o + \Delta\phi) \\ &= 2\Omega(\sin\phi_o \cos\Delta\phi + \sin\Delta\phi \cos\phi_o) \\ &= 2\Omega \sin\phi_o(\cos\Delta\phi + \sin\Delta\phi \cot\phi_o) \end{aligned}$$

where $\Delta\phi$ is the latitude deviation from the center latitude ϕ_o of the tangent plane. Orienting the y-axis along the logitude circles, and for a limited area of the tangent plane, $y \simeq R\Delta\phi$, f is approximated as

$$f \simeq 2\Omega \sin\phi_o(1 + \Delta\phi \cot\phi_o) = 2\Omega \sin\phi_o(1 + y \cot\phi_o/R) = f_o(1 + \beta y)$$

where R is the radius of the earth, $f_o = 2\Omega \sin\phi_o$ and $\beta = \cot\phi_o/R$.

The β effect can thus formally be included for ocean margins extending along latitudinal directions. However, for most coastal applications, the scales are usually much smaller, and therefore it will suffice to take $f = f_o$.

Non-dimensional Forms

Defining scales

$$x \sim L_o, t \sim f_o^{-1}, H \sim H_o, |\vec{u}| \sim u_o, |\vec{\tau}^s| \sim \Pi_o$$

implies $\psi \sim u_o H_o L_o$ and $\zeta \sim u_o/L_o$

substituting these scales results in the nondimensional equations

$$\frac{\partial \zeta}{\partial t} + \hat{k} \times \nabla\psi \cdot \nabla (\mathbf{R}\zeta + 1) = \lambda \hat{k} \cdot \nabla \times \frac{\vec{\tau}^s}{H} - \mu \nabla \cdot \frac{1}{H^2} \nabla\psi + \mathbf{E}\nabla^2 \zeta \qquad (11a)$$

$$\nabla \cdot \frac{1}{H} \nabla\psi = \zeta \qquad (11b)$$

where

$$\mathbf{R} = \frac{u_o}{f_o L_o}, \quad \mathbf{E} = \frac{\nu}{f_o L_o^2}$$

are respectively the *Rossby* and *Ekman* numbers, and

$$\mu = \frac{r}{f_o H_o}, \quad \lambda = \frac{\Pi}{\rho f_o u_o H_o}$$

are non-dimensional numbers measuring the relative importance of bottom friction and wind stress terms.

The values for parameters for typical shelf flows can be taken as $u_o = 0.1m/s$, $f_o = 10^{-4}s^{-1}$, $L_o = 100km$, $H_o = 100m$, $r = 10^{-3}$, $\nu = 100m^2/s$, the order of magnitude estimates for the nondimensional parameters are $\mathbf{R} \simeq 1$, $\mathbf{E} = 10^{-4}$, $\mu \simeq 0.1$ and $\lambda = 100$.

Solutions for Uniform Shelf

The solutions for a uniform shelf topography, *e.g.* $H = H(x)$ can be obtained for a steady ($\partial/\partial t = 0$), linearized flow ($\mathbf{R} \to 0$), with vanishing lateral viscosity ($\nu = 0$). With these approximations (12a,b) yield

$$-\frac{f_o}{H^2} \hat{k} \times \nabla\psi \cdot \nabla H = -r \nabla \cdot \frac{1}{H^2} \nabla\psi, \qquad (12)$$

and since $H = H(x)$, this is reduced to

$$-\frac{f_o}{H^2} \psi_y H_x = -r \left[\left(\frac{1}{H^2} \psi_x \right)_x + \left(\frac{1}{H^2} \psi_y \right)_y \right] \qquad (13).$$

After rearranging, this becomes

$$-\alpha(x)\psi_y + \gamma(x)\psi_x = \frac{1}{2}\nabla^2\psi \tag{14}$$

where

$$\alpha(x) = \frac{f_o}{2r}H_x \quad \text{and} \quad \gamma(x) = \frac{H_x}{H}. \tag{15a,b}$$

We can try separation of variables,

Let us consider a channel confined between $x = x_c$ and $x = x_l$, and assume that the flow (*e.g.* the streamfunction) is specified at $y = 0$, $\psi(x, 0) = \psi_o(x)$. We want to obtain solutions for all y subject to this initial condition. At the side boundaries, the boundary conditions are $\psi(x_c, y) = \psi_c$ and $\psi(x_l, y) = \psi_l$, where ψ_c and psi_l are constants.

We can try separation of variables,

$$\psi(x, y) = F(x)G(y)$$

so that equation () takes the form

$$-\alpha(x)FG_y + \gamma(x)F_xG = \frac{1}{2}\left(F_xx + G_{yy}\right), \tag{16}$$

or

$$-\frac{1}{2}\frac{F_xx}{F} + \gamma(x)\frac{F_x}{F} = \frac{1}{2}\frac{G_{yy}}{G} + \alpha(x)\frac{G_y}{G}. \tag{17}$$

Since we have a non-constant coefficient $\alpha(x)$ on the right hand side, separation of variables can not be achieved in general. However, for a specific form of the depth profile, *i.e.* $H(x) = H_c + a(x - x_c)$, $\alpha = af_o/2r$ becomes a constant and $\gamma(x) = a/H(x)$, so that we can write

$$-\frac{1}{2}\frac{F_x x}{F} + \gamma(x)\frac{F_x}{F} = \frac{1}{2}\frac{G_{yy}}{G} + \alpha\frac{G_y}{G} = \frac{1}{2}\lambda^2. \tag{18}$$

For this specific case, the separated equations are:

$$F_x x - 2\gamma(x)F_x + \lambda^2 F = 0, \tag{19a}$$

$$G_{yy} + 2\alpha G_y - \lambda^2 G = 0. \tag{19b}$$

The roots of the characteristic equation for the second equation are

$$m_+ = -\alpha + \sqrt{\alpha^2 + \lambda^2} \quad \text{and} \quad m_- = -\alpha - \sqrt{\alpha^2 + \lambda^2}.$$

It is seen that the character of the solution for $y > 0$ and $y < 0$ differ greatly. For an initial value $G(0) = \psi_o$ secified at cross-section $y = 0$ of the shelf, the decaying (evanescent) solutions m_+ for $y > 0$ and m_- for $y < 0$ must be chosen. It is clear that the solution for $y > 0$ decays at a much higher rate than the solution for $y < 0$.

For the more general case of an arbitrary $H = H(x)$, either analytical or numerical solutions must be sought, since separation of variables can not be applied.

Note that after some distance from the initial conditions at $y = 0$ either in the positive or negative y domain, the solution approaches an assymptotic state. In essence this assymptotic state represents the adjustment of the flow to the depth contours, and vanishing of the dependence on y. Under these conditions, the equation is much simplified to yield

$$\left(\frac{1}{H^2}\psi_x\right)_x = 0. \tag{20}$$

Integrating the above equation twice yields the general solution

$$\psi(x) = c\int_{x_c}^{x} H^2(x)\, dx + \psi_c. \tag{21}$$

The velocity along the shelf is calculated as

$$v = \frac{1}{H}\psi_x = \frac{1}{H}(cH^2)_x = cH(x) \tag{22}$$

and consequently the total flux of volume carried through the shelf is

$$Q = \int_{x_c}^{x_l} Hv \; dx = c\int_{x_c}^{x} H^2(x) \; dx = \psi_l - \psi_c, \tag{23}$$

which allows the calculation of the constant c to give

$$c = Q/\int_{x_c}^{x_l} H^2(x) \; dx. \tag{24}$$

The vorticity of the flow can also be calculated:

$$\zeta = \frac{\partial}{\partial x}\left(\frac{1}{H}\frac{\partial \psi}{\partial x}\right) = \frac{\partial}{\partial x} cH(x). \tag{25}$$

The solution for the linear depth profile

$$H(x) = H_c + S(x - x_c), \quad \text{where} \quad S = \frac{H_l - H_c}{x_l - x_c}, \quad H_l = H(x_l), \quad H_c = H(x_c) \tag{26}$$

is obtained as

$$\psi(x) - \psi_c = c\int_{x_c}^{x} [H_c + S(x - x_c)]^2 \; dx = \frac{c}{3S}\{[H_c + S(x - x_c)]^3 - H_c^3.\} \tag{27}$$

The constant c is evaluated as follows:

$$\psi(x_l) - \psi_c = \psi_l - \psi_c = Q = \frac{c}{3S}(H_l^3 - H_c^3). \tag{28}$$

Nonlinear inviscid solutions

Under steady, inviscid conditions, the nonlinear vorticity equation reduces to

$$-\frac{f_o}{H^2}\hat{k}\times\nabla\psi\cdot\nabla\left(\frac{\zeta+f}{H}\right) \tag{29}$$

which is simply the *Jacobian*

$$J(\psi,q)=0$$

where q is the potential vorticity defined as

$$q=\frac{\zeta+f}{H}=\frac{\nabla\frac{1}{H}\nabla\psi+f}{H}. \tag{30}$$

The above equation () has a special solution $q=K(\psi)$ which makes the Jacobian vanish, *i.e.*

$$q=\nabla\frac{1}{H}\nabla\psi+f=H\ K(\psi)$$

or

$$\nabla^2\psi-\frac{H_x}{H}\psi_x+\frac{H_y}{H}\psi_y+fH=H^2K(\psi). \tag{31}$$

The solution to the above equation is not unique and depends on the choice of $K(\psi)$ which has to satisfy the above equation as well as the initial and boundary conditions. The approaching flow would set an initial condition that could be used to determine $K(\psi)$. The uniform flow adjusted to the uniform depth variations $H=H(x)$ at a continental shelf has to satisfy

$$\psi_{xx}-\frac{H_x}{H}\psi_x+fH=H^2K(\psi). \tag{32}$$

Numerical Solution of the Vorticity Equation by PDE2D

The solutions for simple barotropic coastal flows are obtained by direct or iterative numerical solutions of the vorticity equations in a rectangular region enclosing the coast. The approach used in steady solutions of the linearized equations of motion for the coastal circulation is similar to that used in Ünlüata *et al.* (1983). For nonlinear cases, the vorticity equations are solved directly or iteratively for given boundary conditions, coastline configuration, and interior topography. In the numerical solutions, the PDE2D solver handling general, nonlinear partial differential equations is employed.

The numerical partial dfferential equation solver PDE2D, which is a follower of the PDE/PROTRAN developed by Sewell () solves n coupled PDE's of the form

$$C_i \frac{\partial u_i}{\partial t} = \frac{\partial A_i}{\partial x} + \frac{\partial B_i}{\partial y} - F_i \quad \text{in R} \tag{33}$$

for $i = 1, n$, where where each of the coefficients $A_i, B_i, B_2, C_i)$, $i = 1, n$ can be functions of the variables, or their first spatial derivatives. The system of PDE's should be accompanied by natural boundary conditions of either the 'fixed' or 'free' forms:

$$\begin{aligned} u_i &= FB_i(x, y, t) \quad \text{on } \partial R_1 \\ A_i n_x + B_i n_y &= GB_i(x, y, t, u_j) \quad \text{on } \partial R_2 \end{aligned} \tag{34a,b}$$

and initial conditions:

$$u_i = U0_i(x, y) \quad \text{at } t = t_o. \tag{35}$$

For equations (12a,b) we can have the form

$$\begin{aligned} C_1 \frac{\partial \zeta}{\partial t} &= \frac{\partial A_1}{\partial x} + \frac{\partial B_1}{\partial y} - F_1 \\ C_2 \frac{\partial \psi}{\partial t} &= \frac{\partial A_2}{\partial x} + \frac{\partial B_2}{\partial y} - F_2 \end{aligned} \quad \text{in R} \tag{36a,b}$$

where each of the coefficients $f_i = (A_1, A_2, B_1, B_2, C_1, C_2, F_1, F_2)$, $i = 1,8$ can be functions of the independent and dependent variables, or their first spatial derivatives, $f_i = (x, y, t, \zeta, \zeta_x, \zeta_y, \psi, \psi_x, \psi_y)$.

with 'fixed' boundary conditions:

$$\begin{aligned} \zeta &= FB_1(x,y,t) \\ \psi &= FB_2(x,y,t) \end{aligned} \quad \text{on } \partial R_1 \tag{37}$$

or 'free' boundary conditions:

$$\begin{aligned} A_1 n_x + B_1 n_y &= GB_1(x,y,t,\zeta,\psi) \\ A_2 n_x + B_2 n_y &= GB_2(x,y,t,\zeta,\psi) \end{aligned} \quad \text{on } \partial R_2 \tag{38a,b}$$

and initial conditions:

$$\zeta = Z0(x,y) \text{ and } \psi = P0(x,y) \text{ at } t = t_o. \tag{39}$$

if we let

$$C_1 = \frac{1}{r}, \quad C_2 = 0, \tag{40a,b}$$

$$A_1 = -\frac{\psi_x}{H^2} + \frac{\nu}{r}\zeta_x, \quad B_1 = -\frac{\psi_y}{H^2} + \frac{\nu}{r}\zeta_y \tag{40c,d}$$

$$A_2 = \frac{\psi_x}{H}, \quad B_2 = \frac{\psi_y}{H} \tag{40e,f}$$

$$F_1 = -\frac{1}{r\rho}\hat{k}\cdot\nabla\times\frac{\vec{\tau}^s}{H} + \frac{1}{r}H\vec{u}\cdot\nabla\left(\frac{\zeta+f}{H}\right), \quad F_2 = \zeta \tag{40g,h}$$

The equations solved by PDE2D by using the above definitons are the following:

$$\frac{1}{r}\frac{\partial\zeta}{\partial t} = \frac{\partial}{\partial x}\left(-\frac{\psi_x}{H^2} + \frac{\nu}{r}\zeta_x\right) + \frac{\partial}{\partial y}\left(-\frac{\psi_y}{H^2} + \frac{\nu}{r}\zeta_y\right) + \frac{1}{r\rho}\hat{k}\cdot\nabla\times\frac{\vec{\tau}^s}{H} - \frac{1}{r}H\vec{u}\cdot\nabla\left(\frac{\zeta+f}{H}\right)$$

$$0 = \frac{\partial}{\partial x}\left(\frac{\psi_x}{H}\right) + \frac{\partial}{\partial y}\left(\frac{\psi_y}{H}\right) - \zeta. \tag{41a,b}$$

Numerical Solutions for an Indented Coast with Linear Topography

The linear depth profile of a coastal region can be specified as

$$H(x) = H_c + S(x - x_c), \quad \text{where} \quad S = \frac{H_l - H_c}{x_l - x_c}, \quad H_l = H(x_l), \quad H_c = H(x_c)$$

defined in the domain (x_c, x_l), with the corresponding depths (H_c, H_l) and the slope S.

When normalized such that $h = H/H_o$ and $\hat{x} = x/L_o$ this becomes

$$\hat{H}(x) = H(x)/H_o = \hat{H}_c + s(\hat{x} - \hat{x}_c), \quad \text{where} \quad s = \frac{\hat{H}_l - \hat{H}_c}{\hat{x}_l - \hat{x}_c}, \quad \hat{H}_l = \hat{H}(\hat{x}_l), \quad \hat{H}_c = \hat{H}(\hat{x}_c)$$

such that the normalized slope is s.

In the first set of runs (y1a-f1f) the normalized along-shelf distance $\hat{y} = y/L_o$ spanned $(-2.5, 2.5)$, while the cross-shelf region extended between $\hat{x} = x/L_o$ values of $(\hat{x}_c, \hat{x}_l)$, which was $(0.25, 1.)$ for $y > 0$, and $(0., 1.)$ for $y < 0$, *i.e.*, a coast which is indented for $y > 0$, and the flow was in the negative y direction with normalized cross-shelf integrated flux $q = Q/(U_o L_o H_o) = -1$. The inflow boundary conditions with the vorticity and streamfunction boundary values at $\hat{y} = 2.5$ were calculated according to the uniform shelf assymptotic solutions described above. The boundary conditions at the coast and the offshore boundary were essentially those for a constant value of the transport streamfunction (the non-dimensional streamfunction $\hat{\psi} \equiv \psi/(U_o L_o H_o) = \hat{\psi}_c = 0$ on $\hat{x} = x_c/L_o$ and $\hat{\psi} = \hat{\psi}_l = -1$ on $\hat{x} = x_l/L_o = 1$, together with a vanishing flux of vorticity resulting from bottom and lateral friction, namely $\left(-\frac{\nabla\psi}{H^2} + \frac{\nu}{r}\nabla\zeta\right) \cdot \hat{n}$ at both horizontal boundaries $\hat{x} = \hat{x}_c$ and $\hat{x} = \hat{x}_l$. At the southern boundary, both the above vorticity flux and the u-velocity ψ_y/H were set equal to zero.

The dimensionless slope s was uniform for the entire domain, with a value of $s = 0.8$, although this value corresponded to different dimensional slope values $S = sH_o/L_o$ for given values of H_o and L_o. Similarly, the velocity U_o and the dimensional coefficients r and ν were changed to yield changes in the dimensionless parameter space of R, μ and E.

The unsteady runs were started from initial conditions in which both the vorticity and the streamfunction initial values were zero. Both the inflow and lateral boundary condition terms were increased with time to the final value, using a taper function $1 - e^{-\hat{t}}$ in terms of dimensionless time $\hat{t} = f_o t$. In nonlinear runs the nonlinear terms in the equations have also been multiplied with the same taper function to eliminate possible unstable solutions from developing.

run	U_o (m/s)	H_o (m)	L_o (km)	ν (m/s^2)	r (m/s)	**R**	**E**	μ	**E**/μ
y1a	0.2	100.	50.	10^2	3×10^{-2}	0.04	4×10^{-2}	3	1.33×10^{-2}
y1b	0.2	10.	50.	10^2	3×10^{-2}	0.04	4×10^{-4}	30	1.33×10^{-5}
y1c	0.2	10.	5.	10^{-2}	3×10^{-2}	0.4	4×10^{-6}	30	1.33×10^{-7}
y1d	0	100.	50.	10^{-2}	3×10^{-4}	0	4×10^{-8}	0.03	1.33×10^{-5}
y1d0	1	100.	50.	10^{-2}	3×10^{-4}	2	4×10^{-8}	0.03	1.33×10^{-5}
y1e	0.5	100.	5.	10^{-2}	3×10^{-2}	1	4×10^{-6}	3	1.33×10^{-6}
y1f	1	100.	50.	10^{-2}	3×10^{-5}	2	4×10^{-8}	0.003	1.33×10^{-5}

			—— $\hat{y} > 0$ ——			—— $\hat{y} < 0$ ——				
run	H_o (m)	L_o (km)	$\hat{x}_c$ $\frac{x_c}{L_o}$	$\hat{h}_c$ $\frac{h_c}{H_o}$	s $\frac{H_l - H_c/H_o}{x_l - x_c/L_o}$	$\hat{x}_c$ $\frac{x_c}{L_o}$	$\hat{h}_c$ $\frac{h_c}{H_o}$	s $\frac{H_l - H_c/H_o}{x_l - x_c/L_o}$	$\hat{y}_{in}$ $\frac{y_{in}}{L_o}$	q $\frac{Q}{(U_o L_o H_o)}$
y1e	100.	5.	0.25	0.4	0.8	0.	0.2	0.8	+2.5	-1
y2e	100.	5.	0.25	0.4	0.8	0.	0.1	0.9	+2.5	-1
y3e	100.	5.	0.25	0.4	0.8	0.	0.4	0.6	+2.5	-1
y4e	100.	5.	0.25	0.4	0.8	0.	1.0	0.0	+2.5	-1
p2e	100.	5.	0.25	0.4	0.8	0.	0.2	0.8	-2.5	+1
p4e	100.	5.	0.25	1.0	0.0	0.	0.2	0.8	-2.5	+1
z2e	100.	5.	0.0	0.2	0.8	0.25	0.4	0.8	-2.5	+1
z4e	100.	5.	0.0	1.0	0.0	0.25	0.4	0.8	-2.5	+1

In the second set of runs (y1e-y4e, p2e, p4e, z2e, z4e) both the slope of the channel and the position of the indented coastal boundary were changed for the domains $y > 0$ and

$y < 0$, as well as reversing the flow direction with inflow bounday conditions specified at $\hat{y} = -2.5$ rather than specified at $\hat{y} = +2.5$.

The runs with different values of parameters are tabulated in the table. and the results of the runs are given in the Figures.

The results show that the frictional coastal flows along sloping continental shelves respond to rather smoothly to the changes in coastal geometry and bottom topography. The solution develops at different distance scales for positive and negative y directions. The lateral friction along the coastal and offshore boundaries induces oscillations in the solutions resulting from vorticity generation at the side boundaries, which differs from the assymptotic analytical solutions described above. The flow adjusts to the assymptotic solution in ashort distance downstream of the inflow boundary. In non-linear flows a further oscillation near the inflow boundary is induced before the flow adjusts to the frictinal flows long sloping topography.

The effects of changing the bottom slope at the location of the indentation results in an adjustment process which also takes place in rather short distances (on the same order as the shelf width). In the cases of reversal in flow direction, the solutions are assymmetric, but essentially display similar features.

Overall, no erratic behaviour, such as meandering or oscillations and other unstable flows have not been developed in these barotropic flows.

CONCLUSIONS

Very few studies exist for coastal flows along the extended coastlines of Turkey. This tendency for a lack of specific studies for coastal flows is partly true for other parts of the world ocean, despite the recent interest. Because coastal flows can have a large variety of specific conditions (coastline geometry, rivers or bays, bottom topography, bottom roughness, wind stress distribution, stratification *etc.*) and regimes (frictional, barotropic, baroclinic, well-mixed, stratified *etc.*) their behaviour is difficult to predict. As a result, basic features of coastal flows applied to a specific region are often not well understood. Cycles of analysis and synthesis, guided by observations and modelling are required to better understand coastal systems.

Our attempt to study coastal flows from this viewpoint, both through idealized cases and through specific applications has only scratched the surface in terms of the many possible

varieties of coastal flows that are observed around the Turkish coasts. Yet, it has been demonstrated that detailed investigations are necessary in each specific case even to understand the simplest forms of idealized flows. The variety of cases worthy of investigations would increase with increasing numbers of parametric and geometric features, and one can make these cases as increasingly complex as one wishes. Applied problems and their models are similarly complex. It is often necessary to be guided by observations for identifying features that otherwise may pass unnoticed.

We cannot help but stress the need for further studies, both on theoretical grounds and from the point of view of applications. We have only looked at the physical features in this study, but the biogeochemical implications of the coastal flows are also very significant. It is also a matter of scales when one talks about coasts. The engineer and earth scientist often have different scales. This may also be true for biologists, chemists and geologists, with different ranges of interests. Of course, the need is for a unified multidisciplinary approach that requires great concentration of resources.

FIGURES

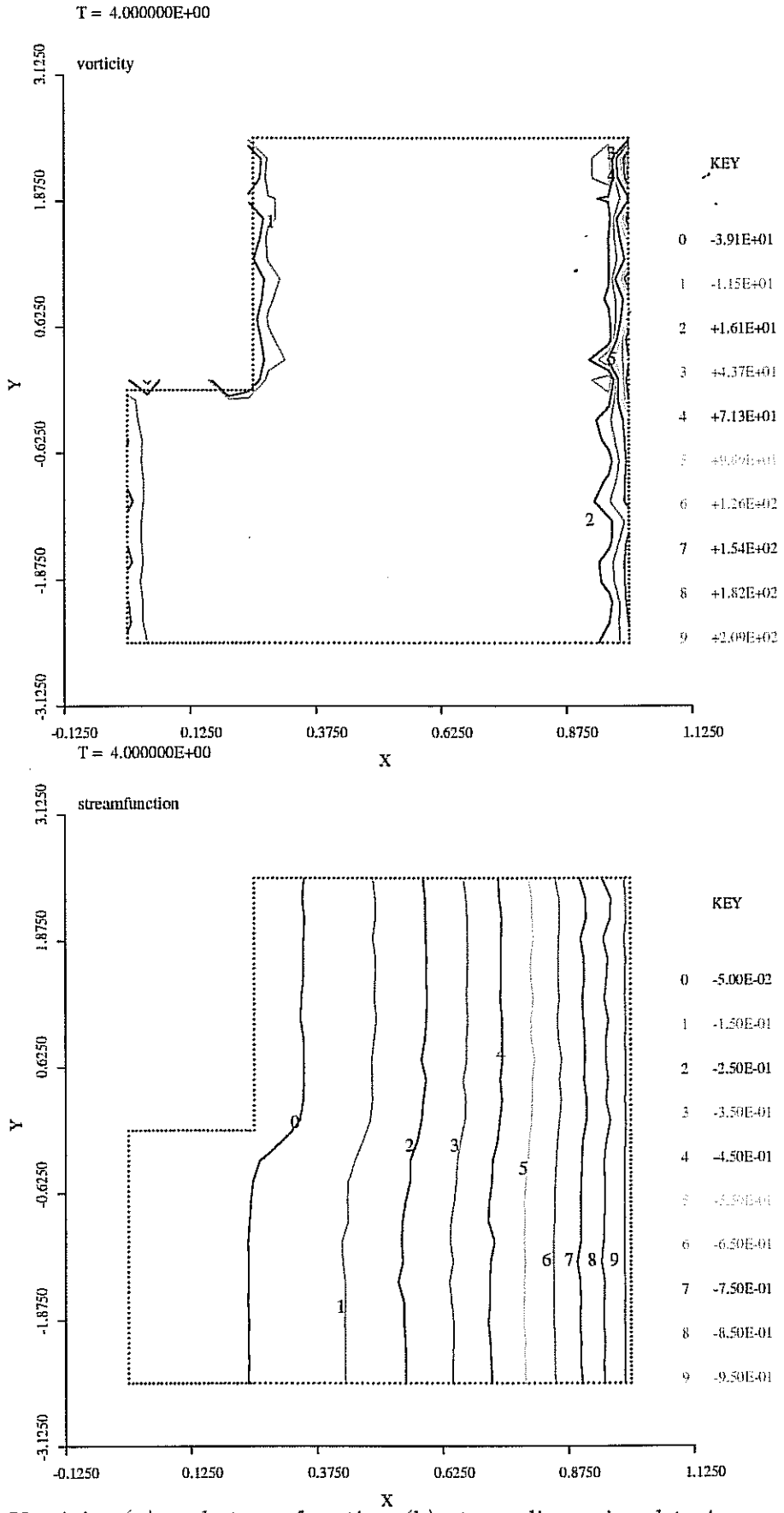

Figure 1. Vorticity (a) and streamfunction (b) at nondimensional t=4, run y1a

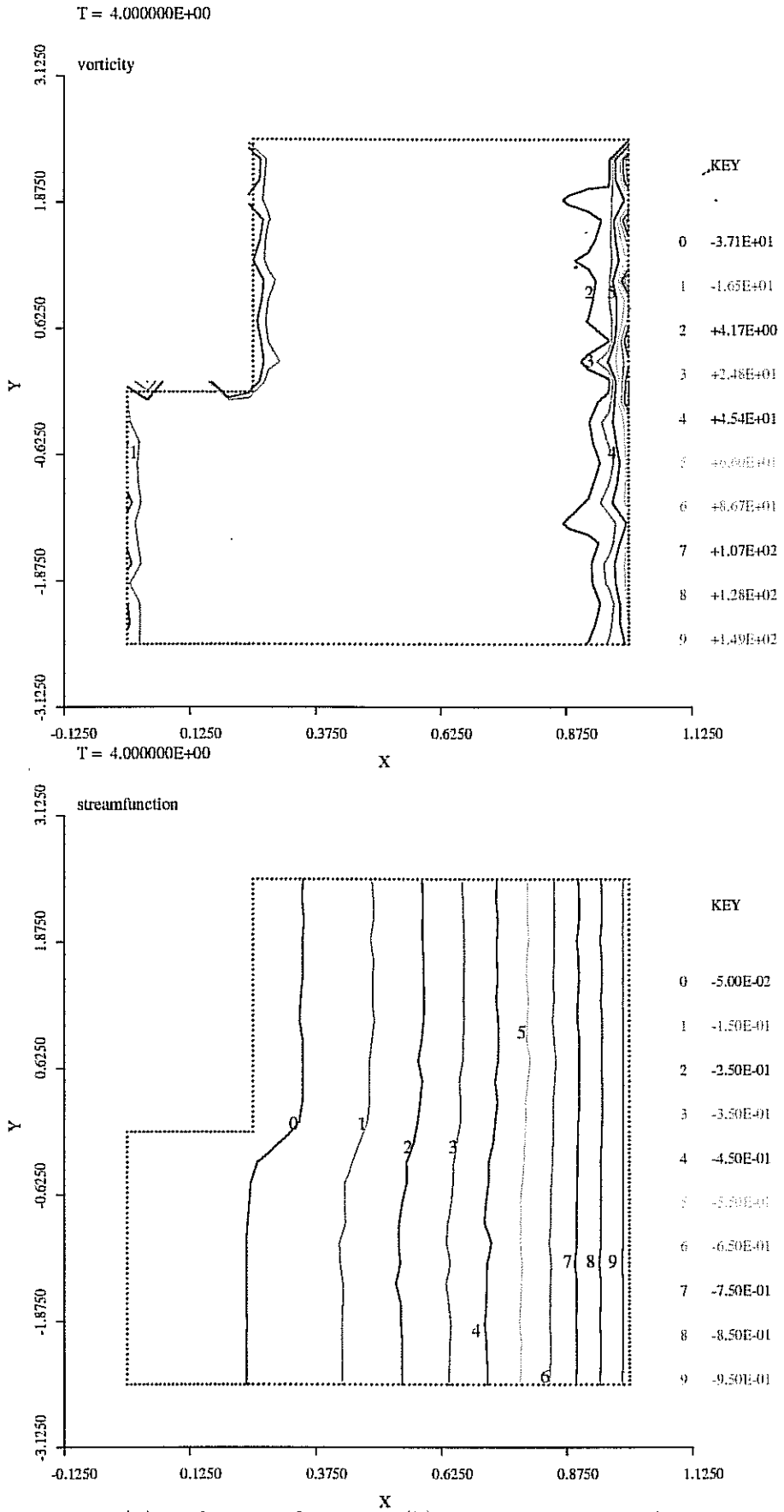

Figure 2. Vorticity (a) and streamfunction (b) at nondimensional t=4, run y1b

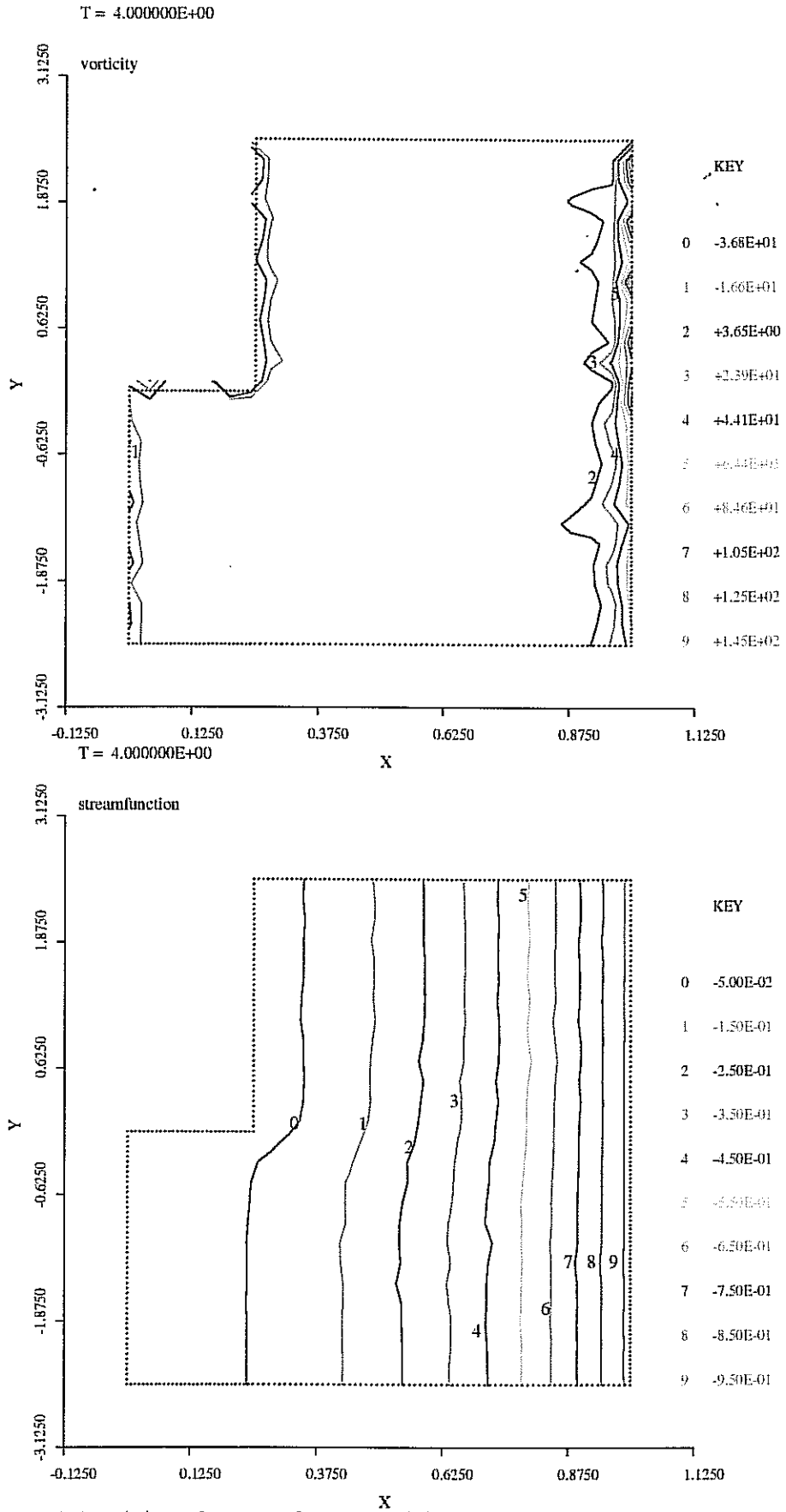

Figure 3. Vorticity (a) and streamfunction (b) at nondimensional t=4, run y1c

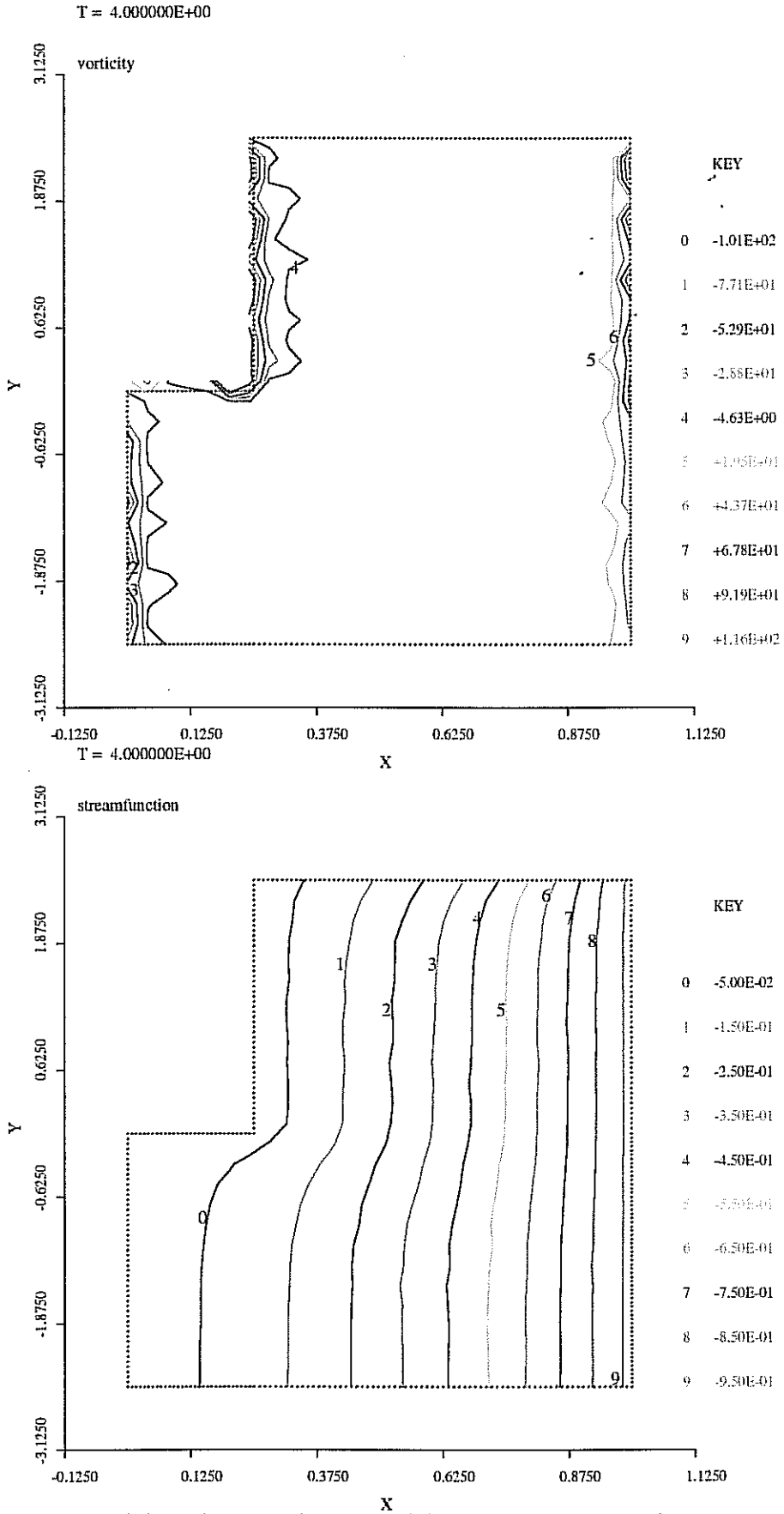

Figure 4. Vorticity (a) and streamfunction (b) at nondimensional t=4, run y1d

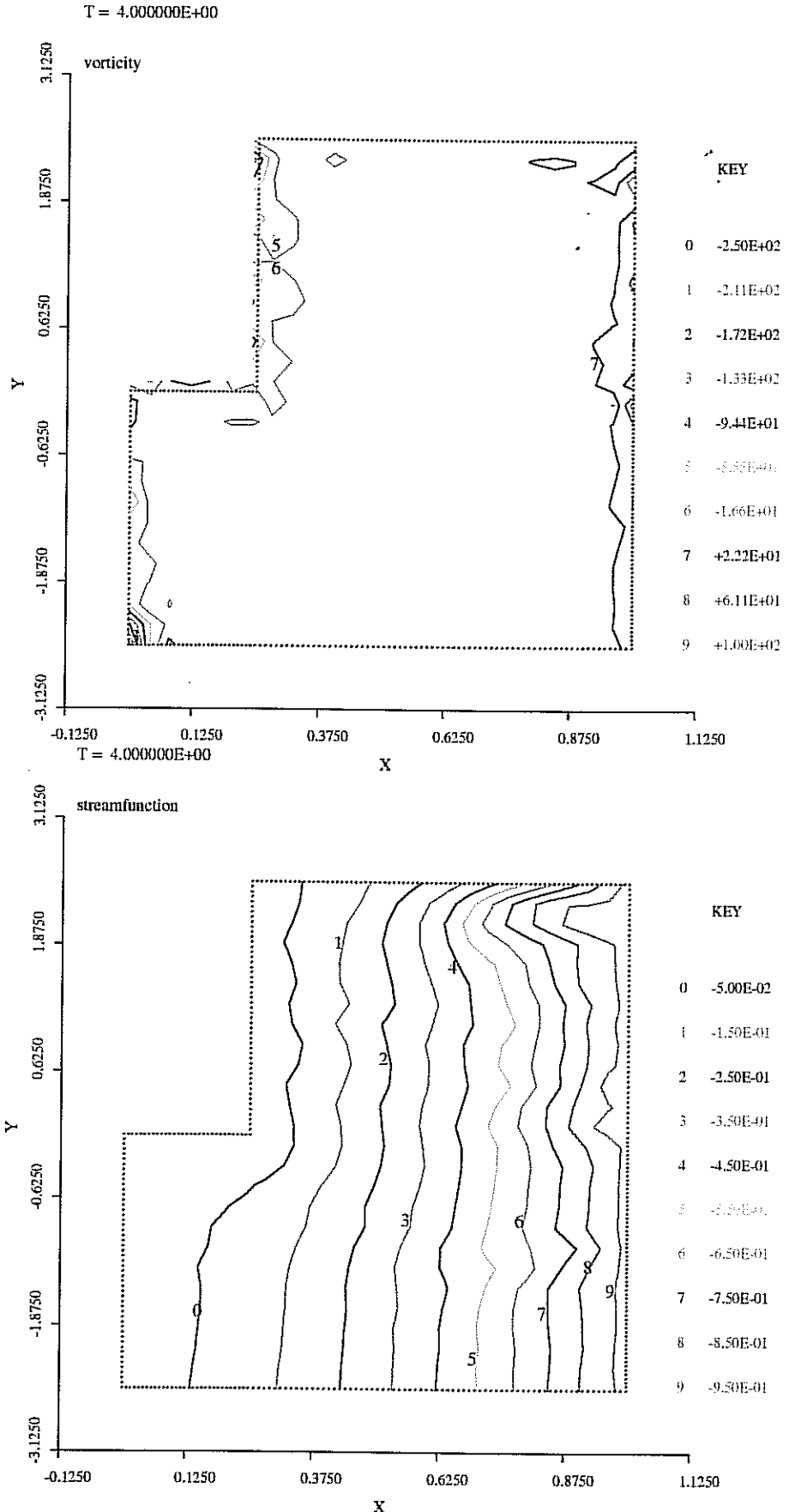

Figure 5. Vorticity (a) and streamfunction (b) at nondimensional t=4, run y1d0

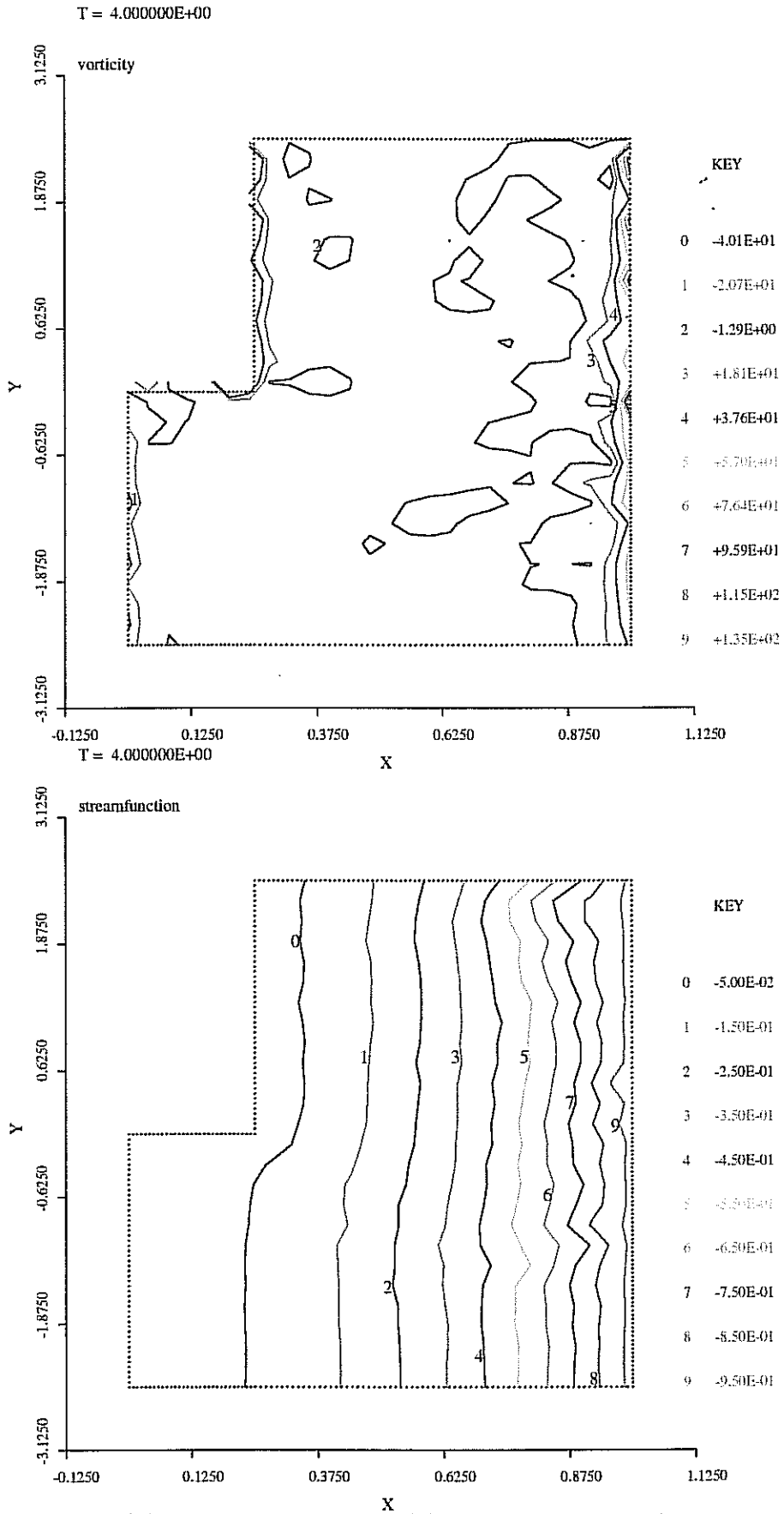

Figure 6. Vorticity (a) and streamfunction (b) at nondimensional t=4, run y1e

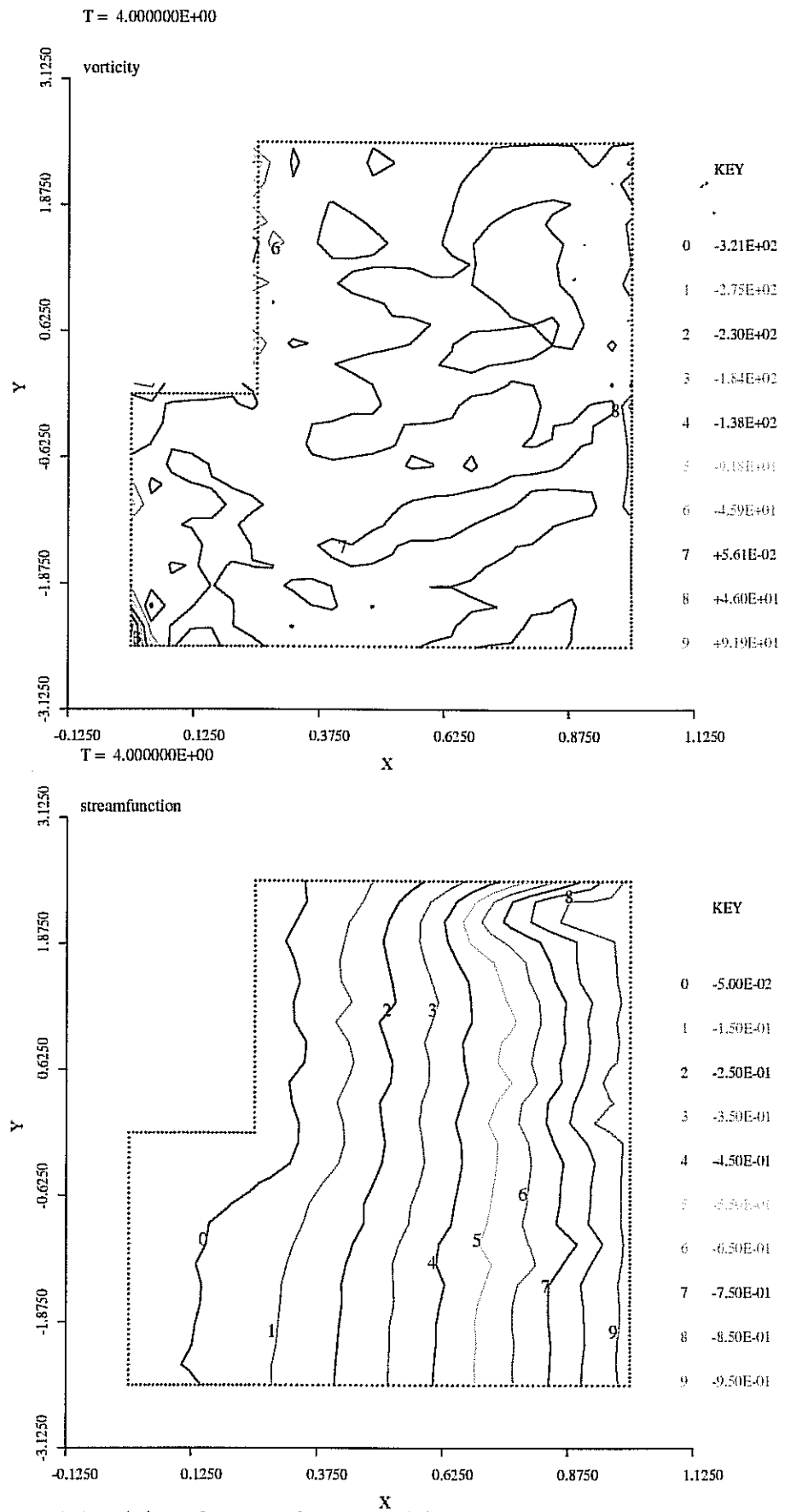

Figure 7. Vorticity (a) and streamfunction (b) at nondimensional t=4, run y1f

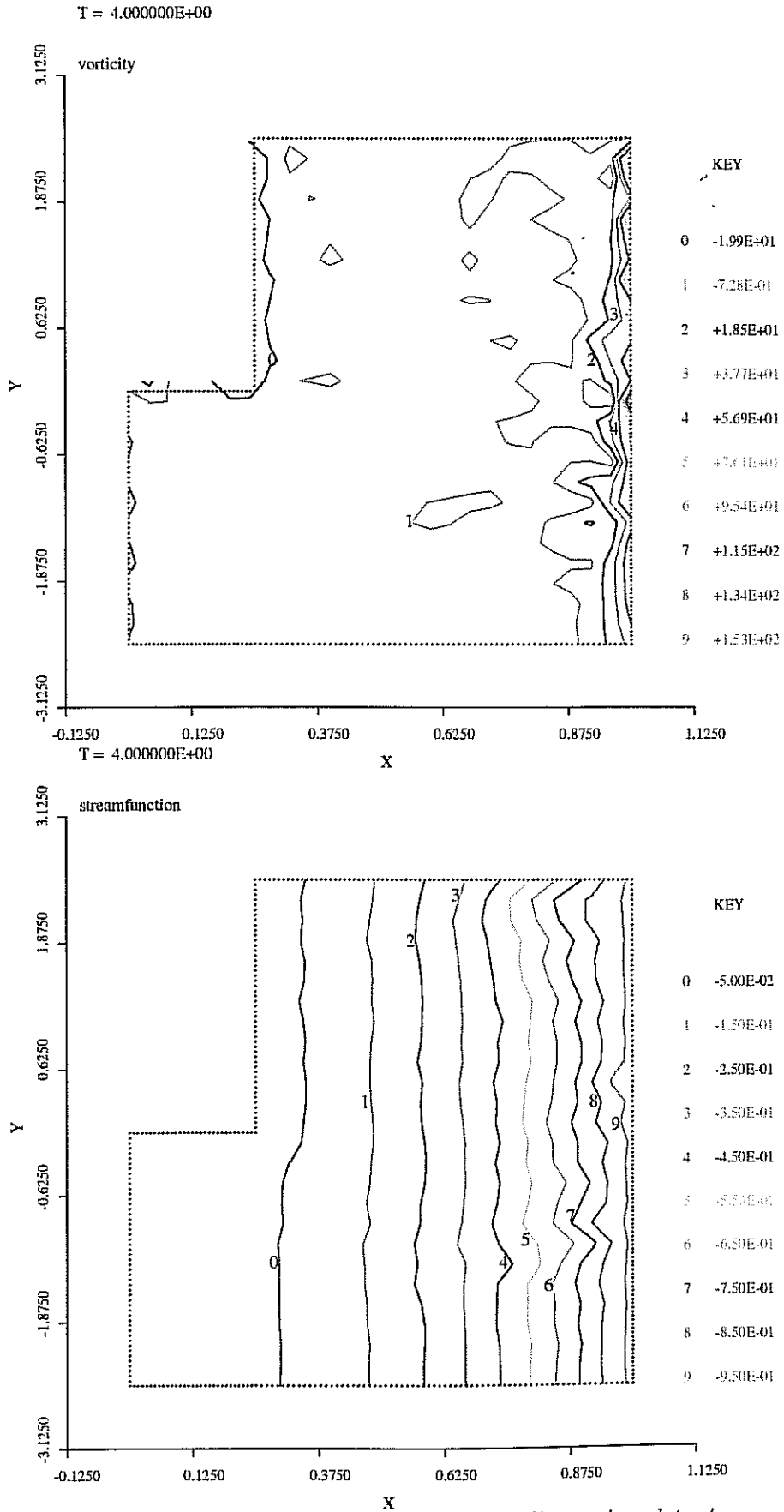

Figure 8. Vorticity (a) and streamfunction (b) at nondimensional t=4, run y2e

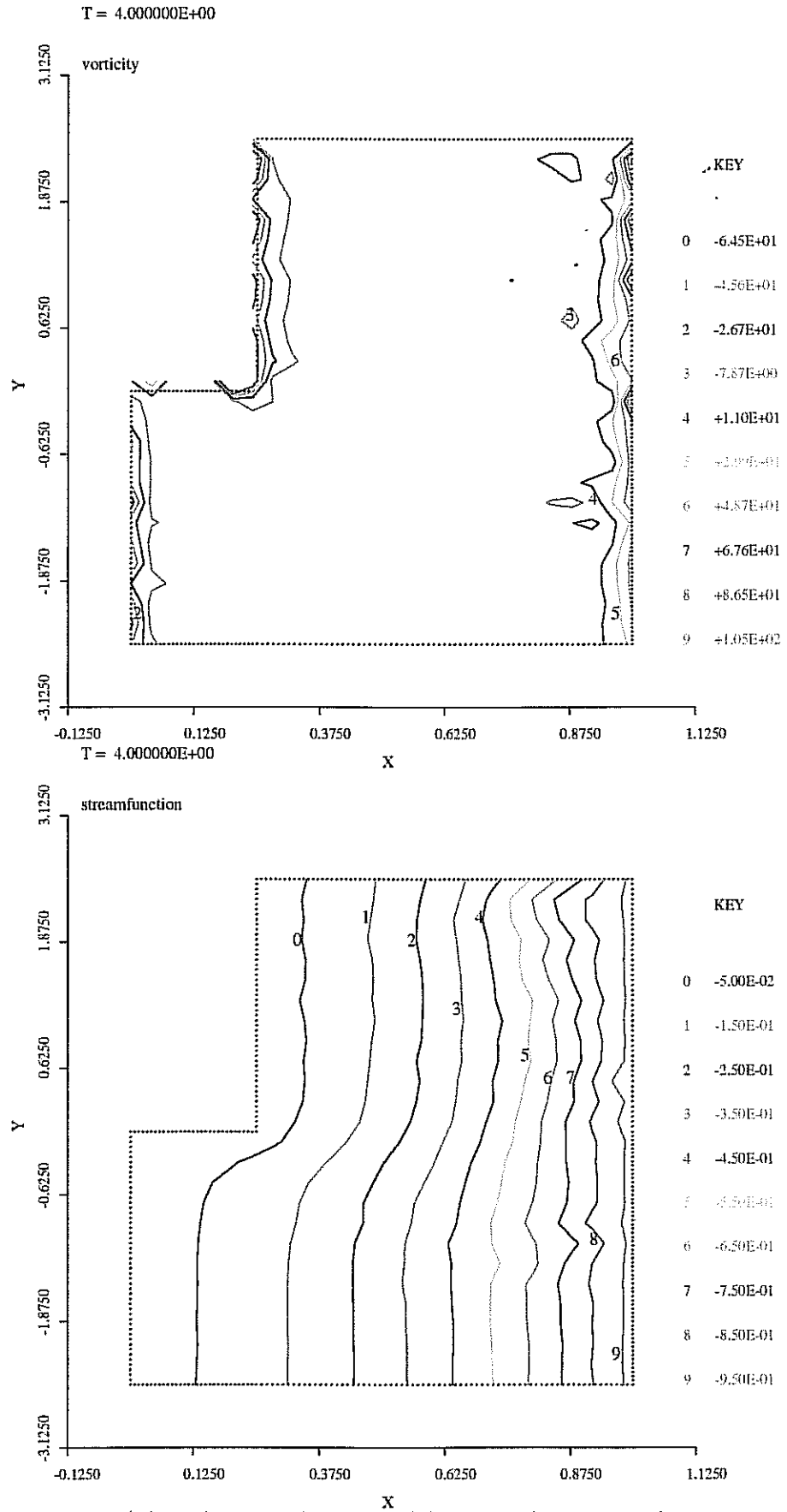

Figure 9. Vorticity (a) and streamfunction (b) at nondimensional t=4, run y3e

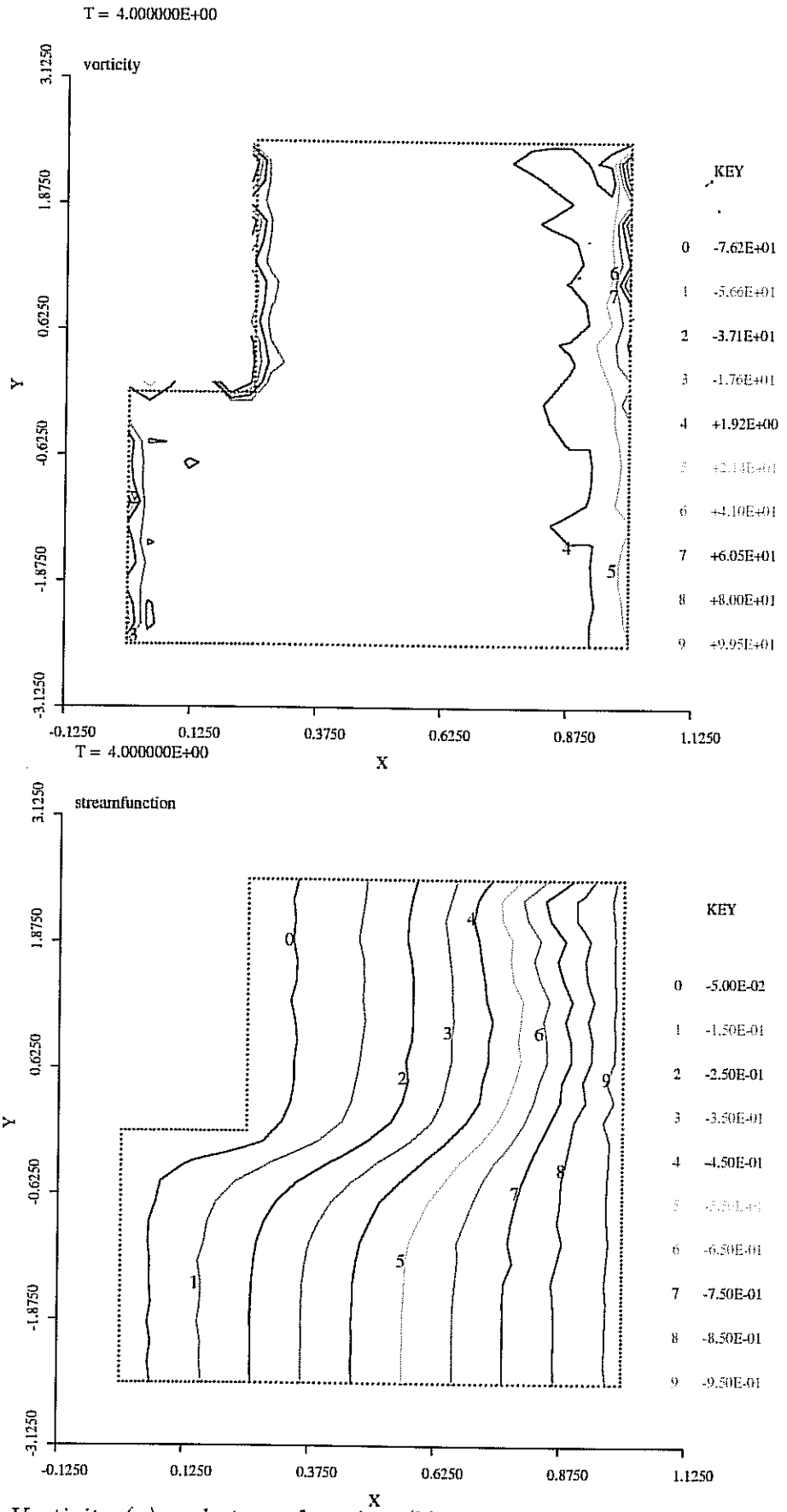

Figure 10. Vorticity (a) and streamfunction (b) at nondimensional t=4, run y4e

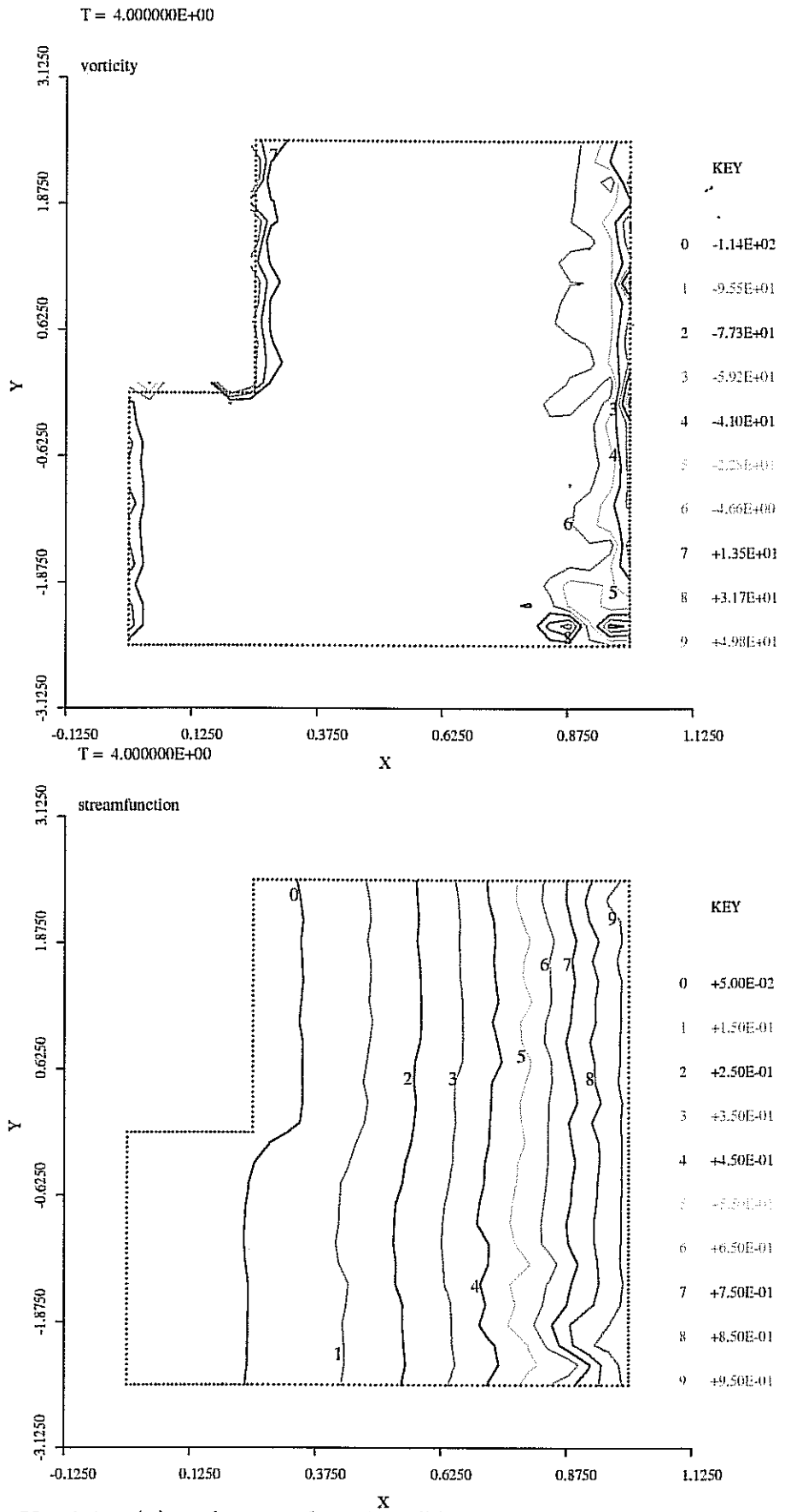

Figure 11. Vorticity (a) and streamfunction (b) at nondimensional t=4, run p2e

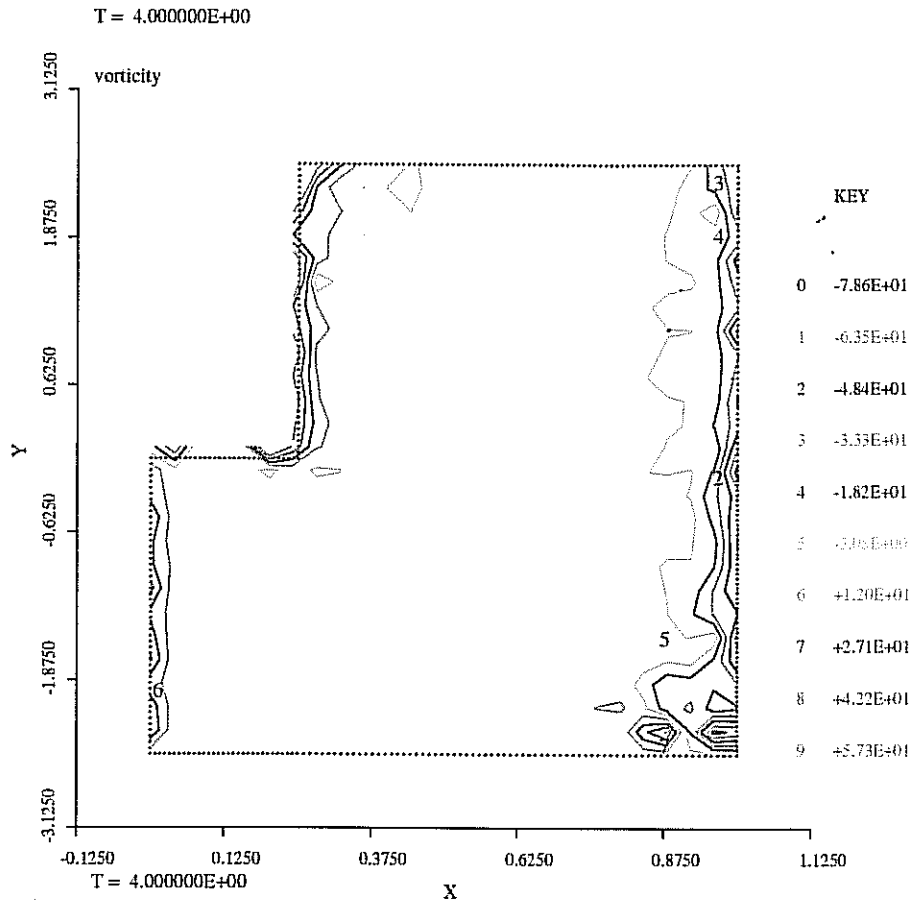

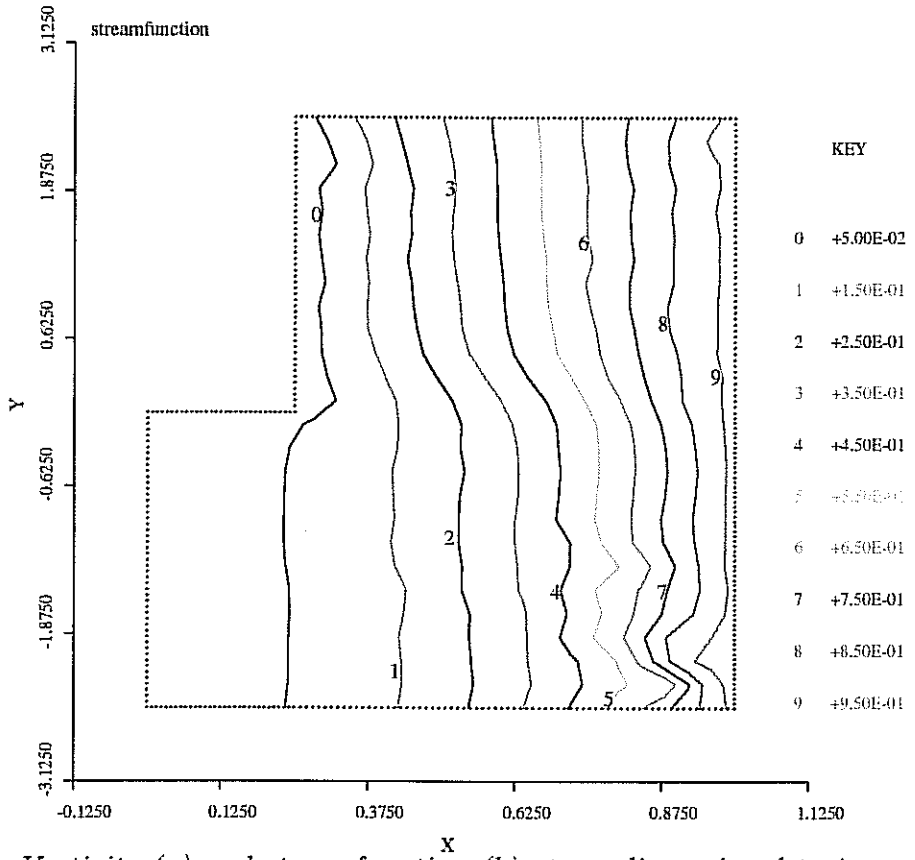

Figure 12. Vorticity (a) and streamfunction (b) at nondimensional t=4, run p4e

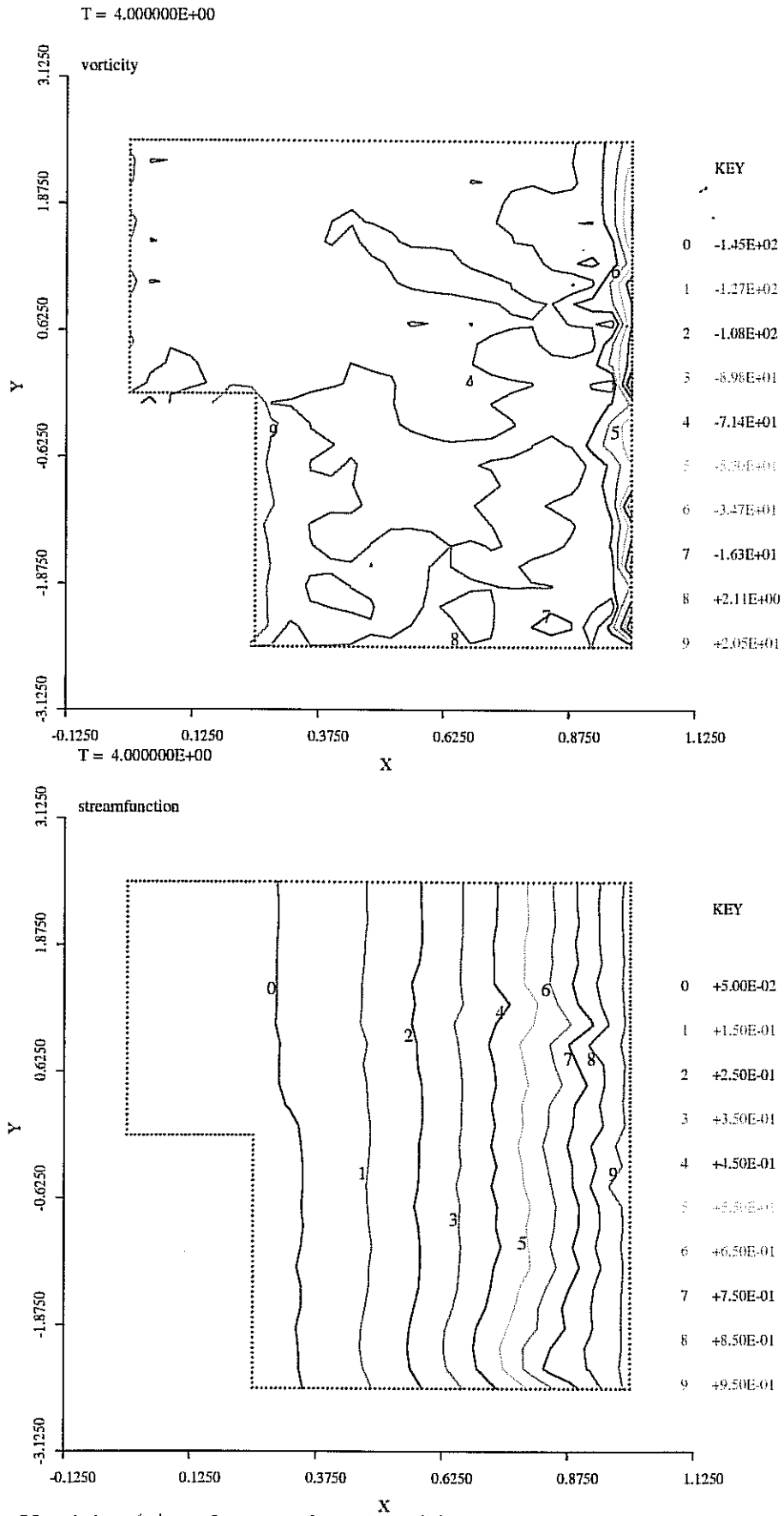

Figure 13. Vorticity (a) and streamfunction (b) at nondimensional t=4, run z2e

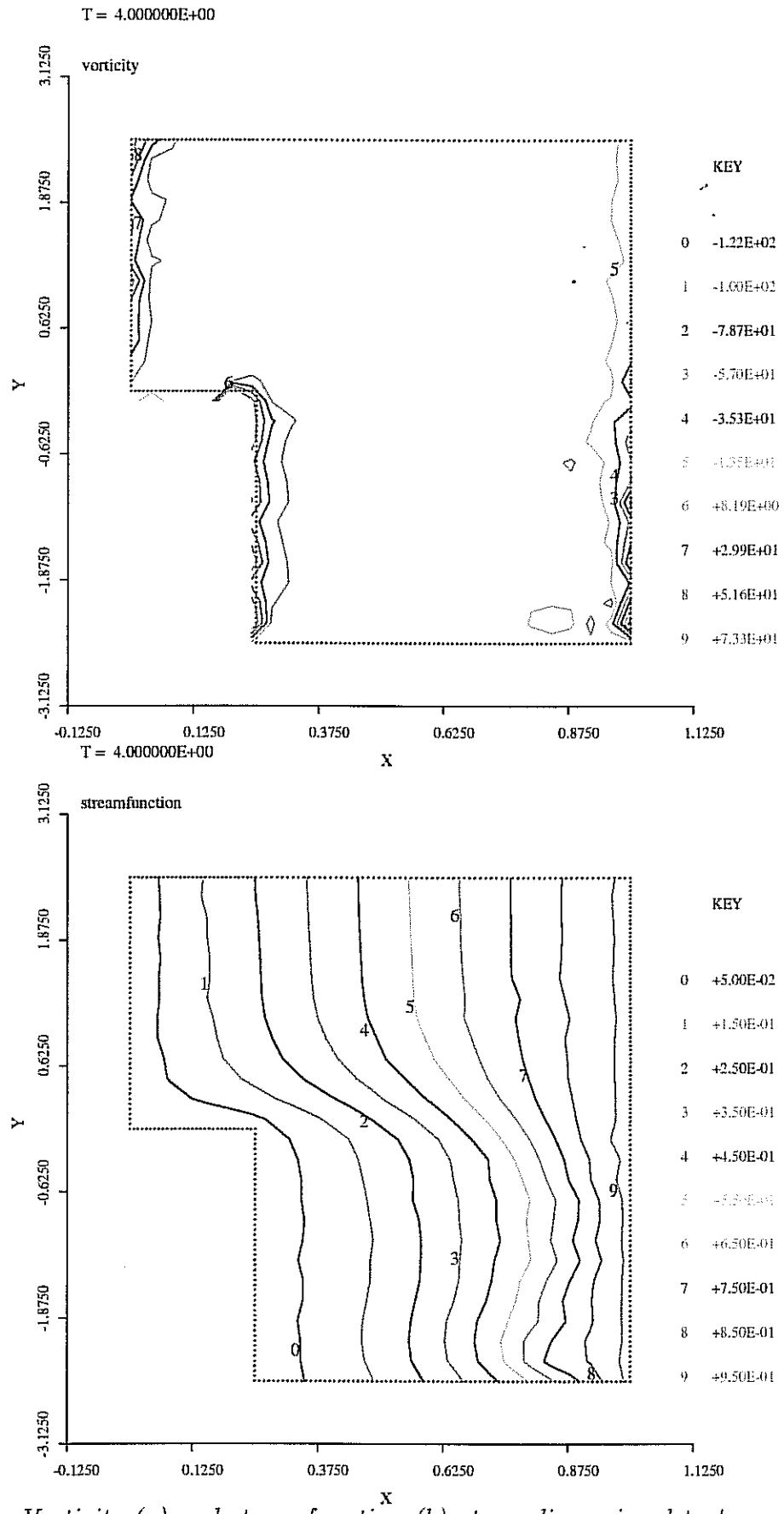

Figure 14. Vorticity (a) and streamfunction (b) at nondimensional t=4, run z4e

REFERENCES

Ahlnäs, K., T. C. Royer, and T. H. George, (1987). Multiple Dipole Eddies in the Alaska Coastal Current Detected with Landsat Thematic Mapper Data, *J. Geophys. Res.*, **92**, 13041-13047.

Armi, L. (1989). Hydraulic Control of Zonal Currents on a β-plane, *J. Fluid Mech.*, **201**, 357-377.

Arnone, R. A., and P. E. La Violette, (1986). Satellite Definition of the Bio-Optical and Thermal Variation of Coastal Eddies Associated With the African Current, *J. Geophys. Res.*, **91**, 2351-2364.

Batchelor, G. K. (1970) *An Introduction to Fluid Dynamics*, Cambridge University Press, 615 pp.

Boyer, D. L., and R. Chen (1987). On the Formation and Shedding of Vortices from Side-wall Mounted Obstacles in Rotating Systems, *Dyn. Atmos. Oceans*, **11**, 59-86.

Brink, K. H., and A. R. Robinson (1998). *The Global Coastal Ocean, Processes and Methods, The Sea*, bf 10, John Wiley and Sons Inc., New York.

Carstens, T., T. A. McClimans, and J. H. Nilsen, (1984). Satellite Imagery of Boundary Currents, in *Remote Sensing of Shelf Sea Hydrodynamics*, Nihoul, J. C. J., editor, Elsevier, 235-256.

Condie, S. A., (1989). Mesoscale Structures on Density Driven Boundary Currents, In: *Mesoscale / Synoptic Coherent Structures in Geophysical Turbulence*, J. C. J. Nihoul and B. M. Jamart, editors, Elsevier, Amsterdam, 197-210.

Chao, S-Y., (1990). Instabilities of Fronts over a Continental Margin, *J. Geophys. Res.*, **95**, 3199-3211.

Cherniawsky, J. and P. H. Leblond (1986). Rotating Flows along Indented Coastlines, *J. Fluid Mech.*, **169**, 379-407.

Cox, M. D. (1984). A Primitive Equation, Three Dimensional Model of the Ocean, GFDL Ocean Group Technical Report No. 1.

Crepon, M., L. Wald, and J. M. Monget, (1982). Low-Frequency Waves in the Ligurian Sea during December 1977, *J. Geophys. Res.*, **87**, 595-600.

Cresswell, G. R., and T. G. Golding, (1980). Observations of South-Flowing Current in the Southeastern Indian Ocean, *Deep Sea Res.*, **27**, 449-466.

Cushman-Roisin, B., and J. J. O'Brien, (1987). The Influence of Bottom Topography on Baroclinic Transports, *J. Phys. Oceanogr.*, **13**, 1600-1611.

Feliks, Y. and M. Ghil (1993). Downwelling Front Instability and Eddy Formation in the Eastern Mediterranean, *J. Phys. Oceanogr.*, **23**, 61-78.

Gill, A. E., and E. H. Schumann (1979). Topographically Induced Changes in the Structure of an Inertial Coastal Jet: Application to the Agulhas Current, *J. Phys. Oceanogr.*, **9**, 975-991.

Ginsburg, A. I. and K. N. Fedorov, (1989). On the Multitude of Forms of Coherent Motions in Marginal Ice Zones (MIZ), In: *Mesoscale / Synoptic Coherent Structures in Geophysical Turbulence*, J. C. J. Nihoul and B. M. Jamart, editors, Elsevier, Amsterdam, 25-40.

Griffiths, R. W., and P. F. Linden, (1981). The Stability of Buoyancy-driven Coastal Currents, *Dyn. Atmos. Oceans*, **5**, 281-306.

Griffiths, R. W., and A. F. Pearce, (1985). Instability and Eddy Pairs on the Leeuwin Current South of Australia, *Deep-Sea Res.*, **32**, 1511-1534.

Haidvogel, D., A. Beckmann, and K. Hedström, (1991). Dynamical Simulations of Filament Formation and Evolution in the Coastal transition Zone, *J. Geophys. Res.*, **96**, 15017-15040.

Haidvogel, D. B., McWilliams, J. C. and P. R. Gent (1992). Boundary current separation in a quasi-geostrophic eddy-resolving ocean circulation model, *J. Phys. Oceanogr.*, **22**, 892-902, 1902.

Häkkinen, S., (1987). Feedback Between Ice Flow, Barotropic Flow and Baroclinic Flow in the Presence of Bottom Topography, *J. Geophys. Res.*, **92**, 3807- 3820.

Heburn, G. W. and P. E. La Violette (1990). Variations in the Structure of the Anticyclonic Gyres Found in the Alboran Sea, *J. Geophys. Res.*, **95**, 1599-1613.

Hoffmann, E. E., K. Hedström, J. Moisan, D. Haidvogel, and D. L. Mackas, (1991). Use of Simulated Drifter Tracks to Investigate General Transport Patterns and Residence Times in the Coastal Transition Zone, *J. Geophys. Res.*, **96**, 15041-15052.

Hua, B-L., and F. Thomasset (1983). A Numerical Study of Coastline Geometry on Wind-Induced Upwelling in the Gulf of Lions, *J. Phys. Oceanogr.*, **13**, 678-694.

Hughes, R. L. (1985). On Inertial Currents over a Sloping Continental Shelf, *Dyn. Atmos. Oceans*, **9**, 49-73.

Hughes, R. L. (1986) On the Role of Criticality in Coastal Flows Over Irregular Bottom Topography, *Dynamics of Atmospheres and Oceans*, **10**, 129-147.

Huthnance, J. M. (1992). Extensive Slope Currents and the Ocean-Shelf Boundary, *Prog. Oceanogr.*, **29**, 161-196.

IGBP (1995). Pernetta, J. C. and J. D. Milliman, *editors*, *Land - Ocean Interactions in the Coastal Zone, Implementation Plan*, Global Change report No. 33, The International Geosphere-Biosphere Programme: A Study of Glabal Change (IGBP) of the International Council of Scientific Unions (ICSU), 215 p., Stockholm.

Ikeda, M. (1984). Coastal Flows Driven by a Local Density Flux, *J. Geophys. Res.*, **89**, 8008-8016.

Hurlburt, H. E. and J. D. Thompson (1980). A Numerical Study of Loop Current Intrusions and Eddy Shedding, *J. Phys. Oceanogr.*, **8**, 1611-1651.

Ikeda, M., L. A. Mysak, and W. J. Emery, (1984). Observation and Modelling of Satellite-Sensed Meanders and Eddies off Vancouver Island, *J. Phys. Oceanogr.*, **14**, 3-21.

Ikeda, M., and M. J. Emery (1985). Observation and Modelling of Meanders in the California Current System off Oregon and Northern California, *J. Phys. Oceanogr.*, **14**, 1434-1450.

Ikeda, M., (1987). Modelling Interpretation of the Ice Edge off the Labrador Coast Observed in NOAA Satellite Imagery, Northern California, *J. Phys. Oceanogr.*, **17**, 1468-1483.

Ikeda, M., J. A. Johanessen, K. Lygre, and S. Sandven, (1989). A Process Study of Mesoscale Meanders and Eddies in the Norwegian Coastal Current, *J. Phys. Oceanogr.*, **19**, 20-35.

IOC (Intergovernmental Oceanographic Commission) (1994). First IOC-CEC-SCOR Workshop on Coastal Ocean Advanced Science and Technology Study (COASTS), Liege, Belgium, 5-9 May 1994, IOC Workshop Report No. 102, Unesco, Paris.

Janowitz, G. S. and L. J. Pietrafesa (1982). The Effects of Alongshore Variation in Bottom Topography on a Boundary Current, *Cont. Shelf Res.*, **1**, 123-141.

Johanessen, O. M., J. A. Johanessen, E. Svendsen, R. A. Schuchman, W. J. Campbell, and E. Josberger, (1987). Ice- Edge Eddies in the Fram Strait Marginal Ice Zone, *Science*, **236**, 427-429.

Johannessen, J. A., E. Svendsen, O. M. Johannessen, and K. Lygre, (1989). Three-Dimensional Structure of Mesoscale Eddies in the Norwegian Coastal Coastal Current, *J. Phys. Oceanogr.*, **19**, 3-19.

Leaman, K. D. and R. L. Molinari, (1987). Topographic Modification of the Florida Current by Little Bahama and Great Bahama Banks, *J. Phys. Oceanogr.*, **17**, 1724-1736.

Legeckis, R., and G. Cresswell, (1981). Satellite Observations of Sea Surface Temperature Fronts off the Coast of Western and Southern Australia, *Deep Sea Res.*, **28**, 279-306.

Mied, R. P., J. C. McWilliams, and G. J. Lindemann, (1991). The Generation and Evolution of Mushroom-like Vortices, *J. Phys. Oceanogr.*, **21**, 489-510.

Millot, C., (1985). Some Features of the Algerian Current, *J. Geophys. Res.*, **90**, 7169-7176.

Millot, C., (1991). Mesoscale and Seasonal Variabilities of the Circulation in the Western Mediterranean, *Dyn. Atmos. Oceans*, **15**, 179-214.

Mysak, L. A. and F. Schott, (1977). Evidence for Baroclinic Instability of Norwegian Current, *J. Geophys. Res.*, **82**, 2087-2095.

Narimousa, S., and T. Maxworthy, (1985). Two-Layer Model of Shear-Driven Coastal Upwelling in the Presence of Bottom Topography, *J. Fluid Mech.*, **159**, 503-531.

Narimousa, S., and T. Maxworthy, (1987). A note on the Effects of Coastline Perturbations on Coastal Currents and Fronts, *J. Phys. Oceanogr.*], **17**, 1296-1303.

Nof, D., (1984). Shock Waves in Currents and Outflows, *J. Phys. Oceanogr.*, **14**, 1683-1702.

Özsoy, E., Ünlüata, Ü., and M. Aral (1982). Coastal Amplification of Tsunami Waves in the Eastern Mediterranean, *J. Phys. Oceanogr.*, **12**, 117-126.

Özsoy, E., Lozano, C. and A. R. Robinson, (1992). A Baroclinic Quasigeostrophic Model for Closed Basins or Semi-Enclosed Seas with Islands, *Mathematics and Computers in Simulations*, **34**, 51-79.

Özsoy, E., Hecht, A., Ünlüata, Ü., Brenner, S., Sur, H. İ., Bishop, J., Latif M. A., Rozentraub, Z. and, T. Oğuz, (1993). A Synthesis of the Levantine Basin Circulation and Hydrography, 1985-1990, *Deep-Sea Research*, **40** 1075-1119.

Pingree, R. D. and B. LeCann (1992). Anticyclonic eddy in the southern Bay of Biscay, May 1991 to February 1992, *J. Geophys. Res.*, **97**, 14353-67.

Qiu, B., N. Imasato, and T. Awaji, (1988). Baroclinic Instability of Buoyancy-Driven Coastal Density Currents, *J. Geophys. Res.*, **93**, 5037-5050.

Ramp, S. T., Jessen, P.F., Brink, K. H., Niiler, P. P., Daggett, F. L. and J. S. Best (1991). The physical structure of cold filements near Point Arena, California, during June 1987, *J. Geoph. Res.*, **96**, 14859-83.

Robinson, A. R., Arango, H. G., Lozano, C. J., Halay, P. J., Sloan, N. Q., and A. Gangopadhyay (1994). Development of a Generic Forecasting and Simulation System for Coupled Coastal and Deep Seas, 26^{th} International Liège Colloquium on Ocean Hydrodynamics, 2-6 May 1994.

Robinson, A. R., and K. H. Brink (1998). *The Global Coastal Ocean, Regional Studies and Syntheses, The Sea*, bf 10, John Wiley and Sons Inc., New York.

Shetye, S. R. and M. Rattray (1982). The Effect of Varying Bathymetry on Steady, Zonal Equivalent-Barotropic Jets, *Deep-Sea Res.*, **29**, 17-44.

Spitz, Y. H., and D. Nof (1991). Separation of Boundary Currents due to Bottom Topography, *Deep-Sea Res.*, **38**, 1-20.

Stern, M. E. (1980). Geostrophic Fronts, Bores Breaking and Blocking Waves, *J. Fluid Mech.*, **99**, 687-703.

Strub, P. T., Kosro, P. M. and A. Huyer (1991). The nature of cold filaments in the California current, *J. Geoph. Res.*, **96**(C8), 14743-69.

Sur, H. İ., Özsoy, E. and Ü. Ünlüata, (1994). Boundary Current Instabilities, Upwelling, Shelf Mixing and Eutrophication Processes In The Black Sea, *Prog. Oceanog.*, **33**, 249-302.

Sur, H. İ., Y. P. Ilyin, E. Özsoy and Ü. Ünlüata (1994). The Impacts of Continental Shelf / Deep Water Interactions in the Black Sea, submitted for publication, (*J. Marine Tech.*).

Thompson, R. O. R. Y., (1984). Observations of the Leeuwin Current off Western Australia, *J. Phys. Oceanogr.*, **14**, 623-628.

Thomson, R. E. (1984). A Cyclonic Eddy over the Continental Margin of Vancouver Island: Evidence for Baroclinic Instability, *J. Phys. Oceanogr.*, **14**, 1326-1348.

Ünlüata, Ü., Oğuz, T., and E. Özsoy (1983). Blocking of Steady Circulation by Coastal Geometry, *J. Phys. Oceanogr.*, **13**, 1055-1062.

Vidal, V. M. V., Vidal, F. F. and J. M. Perez-Molero (1992). Collision of a loop Current anticyclonic ring against the continental shelf - slope of the western Gulf of Mexico - *J. Geophys. Res.*, **97**, 2155-72.

van Heijst G. J. F., and J. B. Flor, (1989). Laboratory Experiments on Dipole Structures in a Stratified Fluid, In: *Mesoscale / Synoptic Coherent Structures in Geophysical Turbulence*, J. C. J. Nihoul and B. M. Jamart, editors, Elsevier, Amsterdam, 591-608.

Voropayev, S. I., (1989). Flat Vortex Structures in a Stratified Fluid, In: *Mesoscale / Synoptic Coherent Structures in Geophysical Turbulence*, J. C. J. Nihoul and B. M. Jamart, editors, Elsevier, Amsterdam, 671-690.

APPENDIX 1

DENSE WATER OUTFLOWS FROM STRAITS INTO ADJACENT SEAS

Paper 1

Emin Özsoy, Daniela Di Iorio, Michael C. Gregg and Jan O. Backhaus
Mixing in the Bosphorus Strait and the Black Sea Shelf:
Observations and a Model of Dense Water Outflow
Submitted, Journal of Marine Systems

Paper 2

Emin Özsoy, Şükrü Beşiktepe and Muhammed A. Latif
Türk Boğazlar Sistemi'nin Fiziksel Oşinografisi,
Marmara Denizi 2000 Sempozyumu, 11-12 Kasım 2000, İstanbul

Paper 1

Emin Özsoy, Daniela Di Iorio, Michael C. Gregg and Jan O. Backhaus
Mixing in the Bosphorus Strait and the Black Sea Shelf:
Observations and a Model of Dense Water Outflow
Submitted, Journal of Marine Systems

MIXING IN THE BOSPHORUS STRAIT AND THE BLACK SEA CONTINENTAL SHELF: OBSERVATIONS AND A MODEL OF THE DENSE WATER OUTFLOW

Emin Özsoy[1], Daniela Di Iorio[2],
Michael C. Gregg[3] and Jan O. Backhaus[4]

[1] *Institute of Marine Sciences, Middle East Technical University,*
P. O. Box 28, Erdemli, Icel 33731 Turkey. e-mail: ozsoy@ims.metu.edu.tr
[2] *Dept of Marine Sciences, University of Georgia,*
Marine Sciences Building, Athens GA 30602 USA. e-mail: daniela@arches.uga.edu
[3] *Applied Physics Laboratory, College of Ocean and Fishery Sciences, University of Washington,*
1013 NE 40th St., Seattle, Washington 98105-6698 USA. e-mail: gregg@apl.washington.edu
[4] *Institut für Meereskunde an der Universität Hamburg,*
Troplowitzstrasse 7, D-22529 Hamburg, Germany. e-mail: backhaus@dkrz.de

Abstract

The exchange and mixing across the Bosphorus Strait and on the Black Sea shelf of waters originating from the adjacent seas are described, based on recent measurements. The properties of the two counterflowing layers derived from the adjacent Black Sea and the Mediterranean Sea, evolve rapidly within the Strait through interfacial mixing. The upper layer entrains water from below mainly in the southern Bosphorus, while the lower layer continuously entrains water from the upper layer as it flows towards the Black Sea. The Black Sea exit of the Strait joins a wide continental shelf with a mild slope but complex bottom topography. The features of the bottom are much like those found in a river delta, and are only adequately described by combining the results of high resolution surveys using ADCP and SWATH instruments. The properties of the Mediterranean water entering the Black Sea are further transformed by turbulent entrainment as the water first follows the bottom conduit extending from the Strait onto the continental shelf, overflowing a sill, then spreading out on a very mild slope. At the shelf break the dense water cascades down the steep continental slope and loses its density contrast as a result of greatly increased entrainment, and reaches depths where it spreads horizontally into the interior and partially propagates east following the slope topography. Experimental observations reveal the structure of this flow and the way it is introduced to the Black Sea. Modelling of the density current using a reduced gravity model confirms the crucial importance of the fine scale topographical features. Sensitivity of the flow to environmental parameters is investigated. When the topography is adequately represented in the model, the flow features are found to be less sensitive to changes in the parameters.

Introduction

The communication between the Black Sea and the Aegean basin of the Mediterranean Sea is established through the Turkish Straits System (TSS), consisting of the Bosphorus and Dardanelles Straits and the Sea of Marmara. Among the two Straits, the Bosphorus plays a more important role in regard to restricting and controlling the exchange between the adjacent seas (*e.g.* [36]). The Bosphorus Strait is located in a region that is sensitive to climatic changes and contrasts [28], and is able to create large environmental changes in the adjacent basins. The effects of sea-level change on the exchanges at the Strait and the recently recovered evidence on the abrupt flooding of the Black Sea about 7,500 years BP [30] attests to the level of impact of the possible climatic changes.

An overview of the flows through the Bosphorus Strait and its effects on the adjacent regions are shown in the SAR image of Figure 1. Surface currents are visualised in SAR images through their influence on sea surface roughness. Shallow bottom topographic features can also be recovered from SAR data if methodologies are used to quantify the interaction with existing currents [38]. In particular, the southward flowing surface jet issuing into the Marmara Sea from the Bosphorus is clearly visible in Figure 1. The narrow jet carrying Black Sea Water extends impinges on the Bozburun peninsula at the southern coast of Marmara, where it excites an internal wave pattern. A conspicuous feature observed in Figure 1 is the curved feature extending north from the Bosphorus into the Black Sea and joining a wider shadow covering the upper part of the image. This pattern appears to be the imprint of the submerged Mediterranean outflow into the Black Sea interacting with the Black Sea shelf, as it coincide well with the flow patterns investigated in the present paper.

The Bosphorus posesses remarkable geometric features [19, 36, 27] that are ideally located to create a 'maximal exchange' configuration [9] for hydraulically controlled two-layer strait flows. One of these is the contraction (the narrowest section) at about one third the length of the Strait from the southern end (Figure 2a), where both layers are expected to pass through a flow transition (i.e. the composite Froude number $G^2 = 1$ for the two-layers). The other control is the sill located about 5 km north of the northern end of the Strait (Figure 2a), located inside a bottom canyon through which the lower layer flows out into the Black Sea, where a transition ($G^2 = 1$) occurs once again. This feature serves as one of the main control sections of the Bosphorus, despite the fact that it is located outside the Strait.

The two-layer, hydraulically controlled flows across the Bosphorus Strait have direct influence on the local environment, as well as on the fate of the Black Sea, through its role in the ventilation of its anoxic waters [36, 19, 17, 37, 20, 22, 23, 24, 25, 26, 27, 12, 13, 14]. Extensive observations have shown that the Bosphorus, characterized with rapid along-strait variations in its geometry, a sharp stratification, nonlinear controls and temporary blocking of the flows in either direction, is driven by the combined effects of variable atmospheric pressure, wind set-up, sea level and water budgets in the adjacent basins [27, 8], resulting in time dependence on daily to interannual time scales.

The seawater properties in the two counter-flowing layers of the Turkish Straits System are continuously modified by two-way turbulent entrainment. Based on salinity measurements, the largest changes are known to occur in the Straits themselves, upon exit from the Strait into the adjacent seas, and especially past the hydraulic controls at the contraction in the southern part of the Bosphorus and the sill offshore of its northern exit *e.g.* [36].

In the 17th century, Count Marsigli had made the first scientific observations in the Bosphorus and performed insightful new experiments on stratified exchange flows [18]. Marsigli's observations confirmed a countercurrent flowing underneath the southerly surface current, a fact which was well known by local fishermen [4]. Although proven wrong by new observations a few decades later, incomplete observations in the mid 19th century cast a shadow on the existence of the countercurrent, resulting in a myth that surfaced a few times since the first half of the present century [4, 36]. Modern observations revealed features of a two-layer flow with intermittent blocking of either layer [17, 27], outflow into the Black Sea shelf [17, 12, 6, 7], and its intrusions into the Black Sea interior [20, 21].

In the following sections, we study the mixing of the waters transported by the counter-flowing currents along the Bosphorus Strait, and discuss mixing and flow features of the outflow along the continental shelf and slope regions of the Black Sea. A high resolution topography of the region is then generated by combining modern data from different sources, to be able to represent bottom features to the best level of detail required by realistic modelling of the Bosphorus outflow. We study the outflow using a

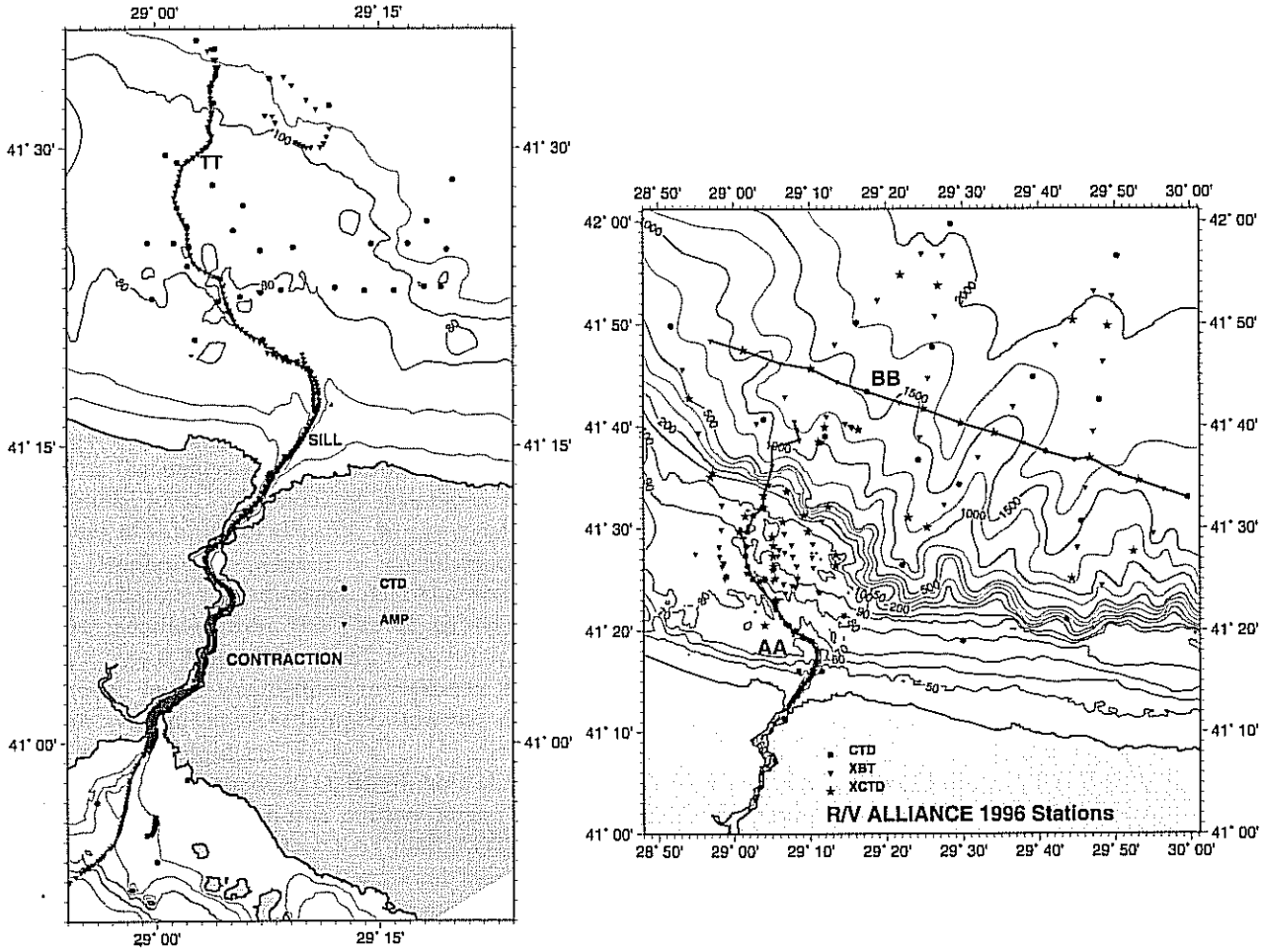

Figure 2: Location map showing the bathymetry and station positions during (a) R/V BİLİM surveys in September 1994, (b) R/V ALLIANCE surveys in June 1996.

reduced gravity model, investigating the effects of bottom friction, entrainment, earth's rotation and other environmental factors on the behaviour of the plume. The results are compared with recent observations and discussed in their light.

The Measurements

Hydrography and currents on the Black Sea continental shelf and slope regions adjacent to the Bosphorus exit have been investigated during numerous cruises of the R/V BİLİM of the IMS-METU from 1986 to the present [36, 19, 17, 37, 20, 22, 23, 24, 27, 21, 25, 26, 12, 13, 14].

The unique environment of Bosphorus Strait has also motivated collaborative studies of its hydrodynamics, turbulent dissipation and microstructure. In September 1994 scientists from the University of Washington (APL/UW) and IMS-METU carried out studies on board the R/V BİLİM, making intensive measurements using the ADCP, CTD, Advanced Microstructure Profiler (AMP), current meters, sea-level instruments and acoustic backscatter imaging of the physical features [14, 12]. The most detailed measurements of temperature and salinity as well as currents and microstructure turbulence in the Bosphorus till the present time were obtained during the 1994 survey of the R/V BİLİM, using the sensors of the AMP instrument as well as the CTD. Because the AMP drops were closely spaced and repeated for microstructure studies, they also provided the first opportunity to investigate the small scale changes along the Strait. The geographical locations of bursts of AMP stations mainly along the thalweg and the CTD stations in the region are shown in Figure 2a. The interfacial depths, and the upper and lower layer average properties along transect TT of Figure 2a, obtained from the 1994 measurements are presented in Figure 3, with corresponding temperature and salinity transects shown in Figure 4.

In the analyses of the along-strait variations of temperature and salinity, it was more appropriate to make local definitions of interfaces, rather than relying on artificial definitions based global fixed values of salinity or density. In the local definition we made use of the sharp two-layer stratification of the Bosphorus, seperated by an interfacial layer of $\sim 10\ m$ thickness. Since water properties in each layer change with distance, the characteristic upper and lower layer salinities S_s and S_b respectively were calculated from the 5 m depth averages of the water near the surface and bottom. Then, letting $S_1^* = S_s + 0.2(S_b - S_s)$ and $S_2^* = S_2 - 0.2(S_b - S_s)$ as the local limiting values for each layer, the transition between layers was defined in reference to these values. The interface depths and the upper and lower layer average values of temperature and salinity in Figures 3, 4 and 6 were computed between the limiting depths of each layer.

The visit of the NATO/SACLANT ship R/V ALLIANCE in 1996 facilitated the renewed collaborative studies of the Bosphorus outflow region in the Black Sea [7], with temperature and salinity obtained from CTD profilers and XBT and XCTD expendable sensors, fixed current meter and ADCP profile measurements of currents, sea-level measurements at fixed stations, acoustical backscatter imaging, as well as acoustical scintillography measurements of currents and turbulent dissipation, [7]. In addition, a high resolution depth survey was made with the SWATH instrument and the combined data from the 1995 and 1996 measurements of the R/V ALLIANCE were combined and processed to construct the detailed bottom topography shown in Figure 10c.

Mixing in the Bosphorus and the Black Sea Exit

The interfacial depths in the top panel of Figure 3 (also plotted in Figure 4) show the location of the interfaces separating the three layers identified: the upper and lower layers where the relatively uniform properties are averaged, and an interfacial layer between them assumed to contain the vertical gradients.

In Figure 3, the interfacial layer is relatively thin between the two control sections, *i.e.* the contraction and sill marked in Figure 2a, and also along the flat Black Sea shelf region, at a distance from the sill, where the lower layer also becomes very thin. There are two areas where the interface thickens: the southern Bosphorus and the Black Sea exit regions. The interfacial layer thickens and the upper layer salinity increases in the southernmost 10 km of the Strait, past the contraction (at 11 km in Figure 3) where one of the two main hydraulic controls takes place. A remarkable increase in salinity from 18

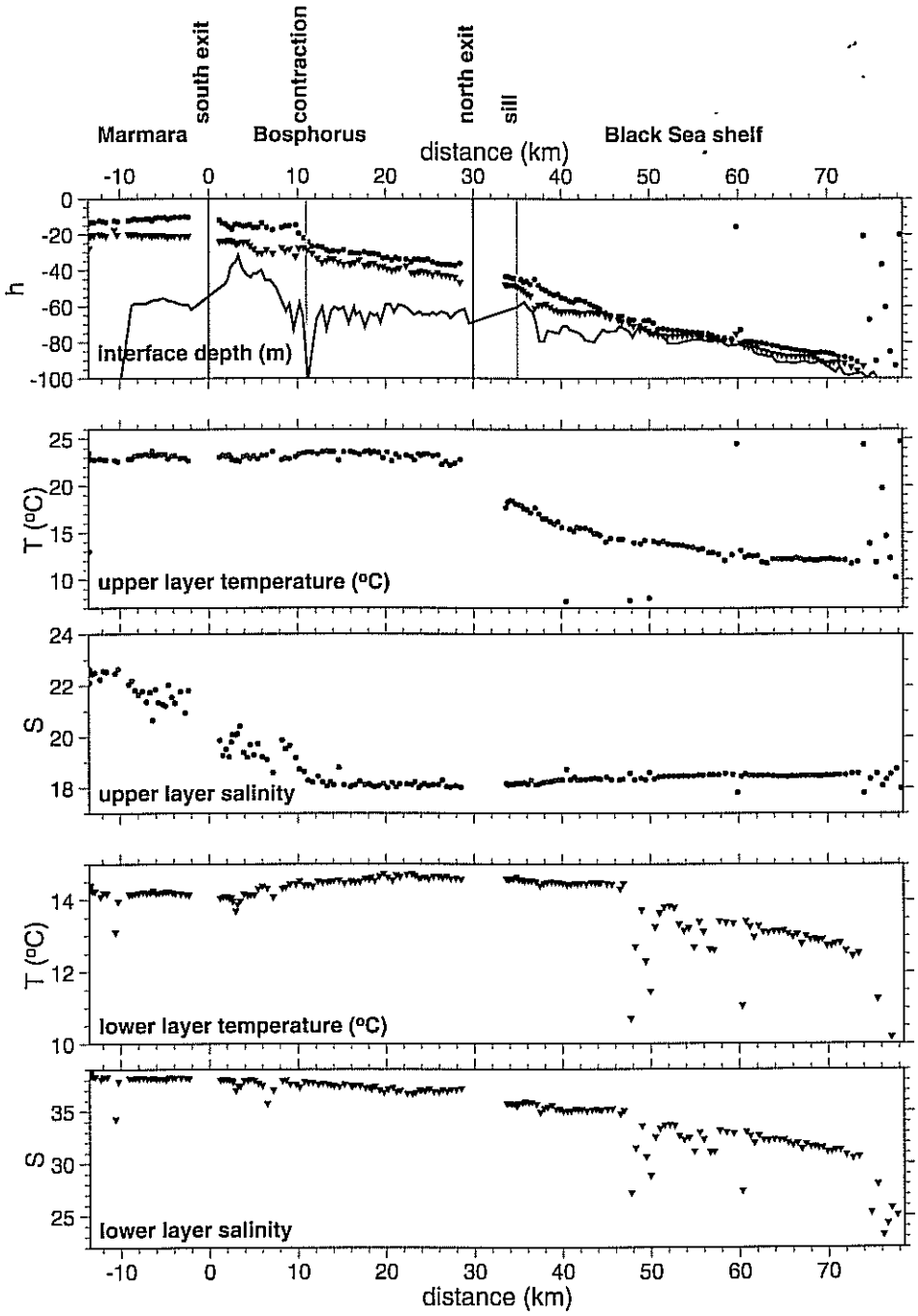

Figure 3: Variation of the upper and lower layer depths, average temperature and salinity, for the composite section of AMP drops along transect TT (Figure 2a) across the Bosphorus Strait (179 profiles) during 13-19 September 1994

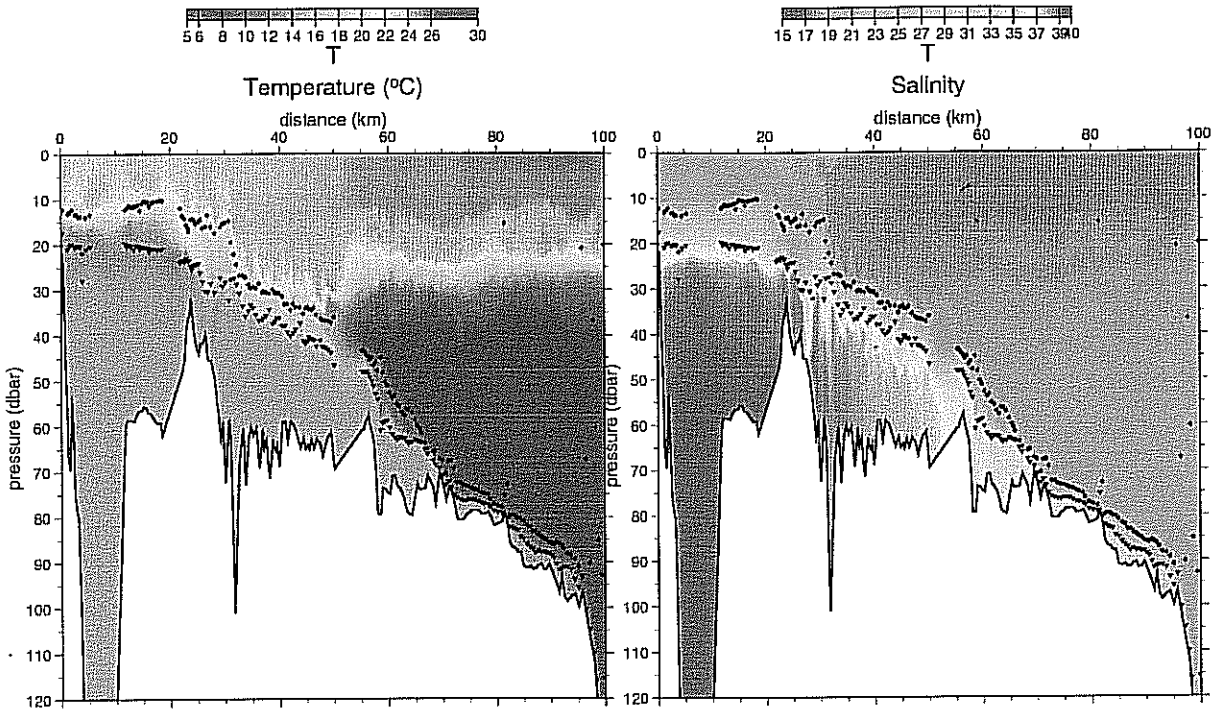

Figure 4: (a) salinity and (b) temperature section along transect TT constructed from the data of 179 AMP drops across the Bosphorus Strait during 13-19 September 1994, Figure 2a.

to 23 by almost 30 % accompanies the mixed layer thiickening in the southern Bosphorus, showing the importance of mixing in this region. The interfacial layer also thickens past the northern sill (5 km from the northern end) in the Black Sea, where the other hydraulic control takes place, and finally becomes much thinner when the flow emerges onto the flat shelf (20 km from the northern end) from the bottom channel extending out from the exit.

The temperature in the upper layer does not appear to change much in the Bosphorus because of the high contrast of the warm mixed layer at the surface originating from the Black Sea, but a slight decrease as a result of entrainment is evident south of the contraction. The rapid decrease in temperature towards the the Black Sea results from the inclusion in the upper layer average of two different layers with variable depths: the surface mixed layer and the underlying layer of Cold Intermediate Water (CIW) observed in Figure 4.

The lower layer temperature first rises as one proceeds north in the Bosphorus, by entrainment of warm water from the surface mixed layer in direct contact with it, and later decreases by entrainment of the overlying CIW in the northern Bosphorus and the Black Sea shelf. The salinity is perhaps a better indicator of entrainment for the lower layer, because it is a conservative property only affected by the relatively uniform upper layer source of entrainment. The lower layer salinity decreases continuously from Marmara to the Black Sea, with significant changes in its horizontal gradient in specific regions: In the northern Bosphorus where the interface stability is higher, the entrainment rate appears to be smaller than the southern part. In comparison to the Bosphorus, the flow past the northern sill ($5km$ from the northern end) on the Black Sea shelf has greater entrainment, and increases further when the flow exits the narrow northwestward bending channel topography and spreads on the flat shelf region ($20km$ from the northern end). Finally with the increased slope at the shelf edge ($55km$ from the northern end), the bottom layer can only be identified with difficulty, but few data points where it could be detected show entrainment increased by an order of magnitude in comparison to the flat region. Yet, the Mediterranean effluent survives with a temperature of 13°C and salinity of 31 before arriving at the shelf break, and completely loses its identity shortly thereafter.

In Figure 4, the temperature and salinity distribution across a transect extending through the Bosphorus into the Marmara and Black Sea open regions show the full details of the changes in properties, although discontinuities appear at certain regions, such as in the mixed layer at the northern end of the Bosphorus, because bursts of data taken over a period of few days are plotted together. In addition to the lengthwise variations in properties there are strong gradients at the interfacial layer, and as this layer

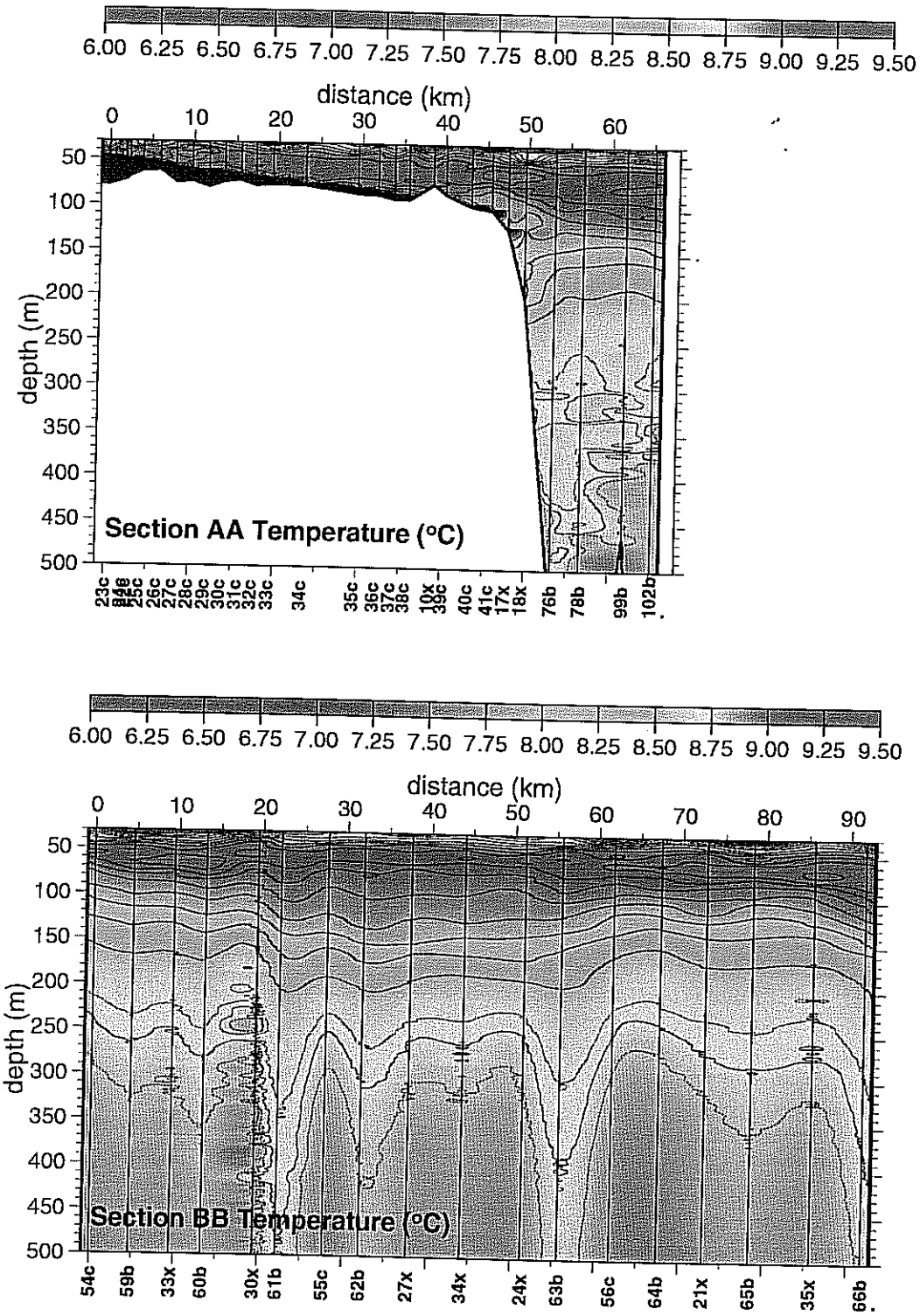

Figure 5: Contours of temperature along (a) cross-shore transect AA extending across the shelf from Bosphorus to the Black Sea, (b) off-shore transect BB extending parallel to the coast during June 1996. Transect locations are shown in Figure 2b. The dark area in (a) is the warm Mediterranean outflow waters, masked here in order to extend the range of contouring to the relatively smaller variations of temperature in deep waters.

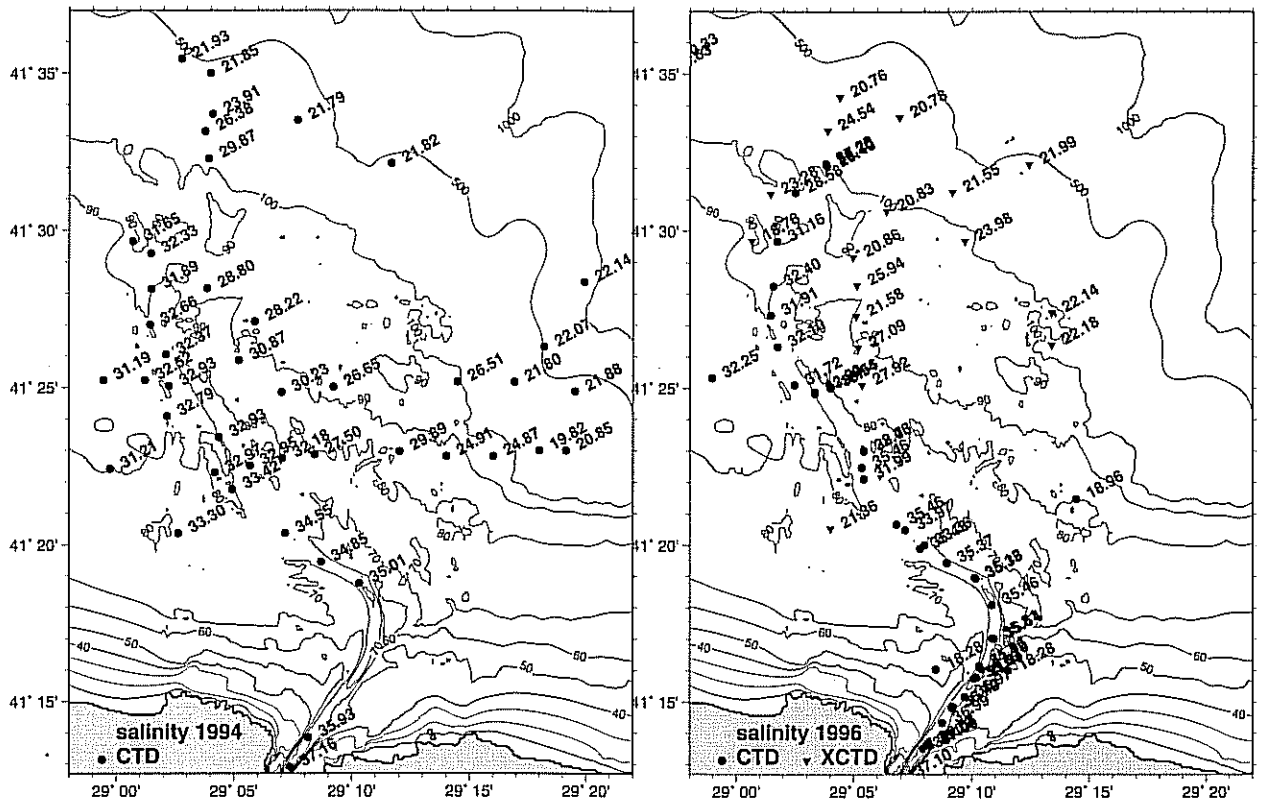

Figure 6: Salinity measurements averaged over the depth of the bottom layer in (a) September 1994, and (b) June 1996.

is approached from below and above. The Cold Intermediate Water (CIW) with a minimum temperature of 6°C stops at the Black Sea entrance of the Bosphorus because it wedges in between the mixed layer entering the strait from the Black Sea and the interface rising towards the south. Altough the CIW pinches off at the northern side of the Bosphorus, [12], traces of cold water trapped at the interface (< 14°C in Figure 4) reappear on the Marmara side, both as a result of a leakage of CIW from the Black Sea and the local production of cold water in the Marmara Sea during the colder time of the year [3].

In addition to the slow changes in properties with distance, there are marked oscillations on shorter horizontal distances in both layers, displayed in Figure 4. These oscillations have shorter scales, especially inside the Bosphorus, with wavelength on the order of 1 km, resulting from the turbulent structure of the flows. The oscillations are evident in the properties especially near the interfacial layer, whose limiting depths also fluctuate inside the Bosphorus. There are features with greater wavelengths in the adjacent basins, associated with meso-scale or smaller scale motions in those regions, and essentially of a different nature than the turbulent mixing between layers inside the Bosphorus.

The properties of the outflow determined during the 1994 and 1996 surveys were similar. The 1996 temperature distribution along transect AA (Figure 2b) in Figure 5a shows the outflow from the Bosphorus to change its thickness and properties almost the same way as that shown in Figures 3 and 4.

The bottom layer average salinity at stations where CTD and XCTD profiles were obtained during the 1994 and 1996 experiments are shown in Figure 6. In both surveys, as well as in those made earlier [17], the highest salinity was observed along the curved bottom groove extending from the Bosphorus to the shelf edge. The only area where water with large salinity values of up to 31-32 survive till the shelf edge (depth $\simeq$ 100 m) is within the bottom groove, until about a distance of 45 km from the Bosphorus exit (Figures 3 and 4). There is some indication in the 1994 measurements of moderately high salinity values decreasing to 28.6 at the shelf break east of the channel in the region gently sloping towards the head of the deep Bosphorus Canyon at around 29°15'E 41°25'N, which suggests leakage towards the east of saline waters inside the bottom groove. All measurements at the deeper locations on the slope are considerably smaller, with anomalous salinity values of about 28 detected at about 200m depth immediately offshore

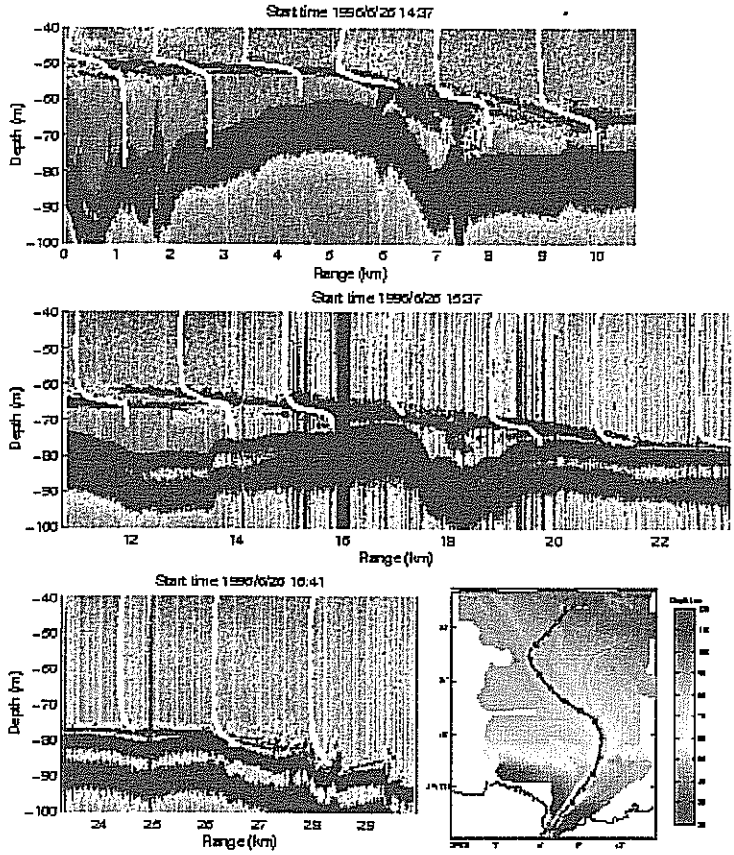

Figure 7: High resolution echo sounder image along a curved path (first following the canyon leading out from the Bosphorus until a range of 23 km, and sideways from it afterwards, shown in the lower right hand side), together with the overlaid temperature profiles from expendable sensors. Range is calculated along the path, starting from a point inside the Strait. Colour represents relative acoustic backscatter intensity, with darker colours corresponding to greater intensity.

of the bottom groove, and finally no sign of an anomalous distribution remains at depths of 500 m. These features either suggest that the waters cascading at the shelf edge are rapidly diluted or that they are not so easy to trace by measurements.

The water properties adjacent to the continental slope after the dense water cascades into deeper water at the shelf break are not well defined, both because of the difficulty of measurement very near the bottom, and because of the change in properties resulting from the intense mixing. The characteristic signature of the injected waters are discrete layers of double diffusive intrusions with anomalous cold temperature, as well as anomalous particle and nutrient concentrations, appearing intermittently over the entire southwestern Black Sea basin east of the Bosphorus outflow [20, 21].

Mixing along the slope is evident from the widening of the pycnocline (increased spacing between isotherms) in Figure 5a at about the depth of the shelf break. The deeper area between depths of 200-500 m adjacent to the continental slope in Figure 5a shows intrusions of cold water formed by mixing of the Mediterranean effluent on the shelf region with the the ambient waters, as decribed by [20] and [21]. Anomalous waters with intrusive structures in the deeper waters were only observed at stations offshore of the transect AA during the 1996 experiment, suggesting that the injection of the shelf waters to the offshore waters took place mainly through this route. The location of this transect on the shelf was deliberately chosen along the main channel based on earlier experiences. Although the intrusions would not necessarily be expected offshore of this transect and often extended east along the slope [20], in this particular survey they extended straight offshore from the channel. A temperature section along transect BB parallel to the coast and offshore of the continental slope in Figure 5b shows the intrusive fine scale structure in the lower part of the pycnocline at towards west, in the extension of transect AA. The isotherms suggest an anticyclonic feature in the middle part of the section and meso-scale eddies, belonging to the system of rim-current meanders found in the region during the experiment [7].

Turbulence measurements on the Black Sea shelf [13] has shown turbulent dissipation rates ϵ of 10^{-5} - 10^{-3} $W\ kg^{-1}$ (estimated over successive intervals of 0.5 m) within the outflow plume. Similar measurements using an acoustic scintillation system [6, 7] showed path integrated dissipation rates of up to 10^{-4} $W\ kg^{-1}$ within the Mediterranean water at the sill. The turbulent dissipation in the outflow plume was found to be slightly decreased until the shelf edge, but remained active at a distance of $5km$ from the the continental slope and up to a depth of 200 m (until where the measurements extended), with maximum values of up to 10^{-4} $W\ kg^{-4}$ [13], while the background turbulent dissipation of the Black Sea waters below the mixed layer and above the plume was found to correspond to some of the lowest diapycnal diffusivities observed in the world ocean, representing a background internal wave field that appeared to be the only source of turbulence in the absence of wind mixing and tides [11].

In Figures 7 and 8 the 120 Khz high resolution echosounder images along transects show a thin layer of water near the bottom, separated from the overlying waters by a sharp interface made visible by acoustic scatterers. Confirming the other measurements, these images help visualise the overflow of the dense Mediterranean waters over the sill and along the bottom channel. The details of the generally mildly sloping bottom show a terraced structure and submerged channels of the delta-like topography. The water trapped in the depressions of this topography are realtively thicker than the other regions but there is a leakage of dense waters away from these depressions to the surrounding areas, especially in the west to east sloping region east of the channel before the shelf break. In general the bottom flow in the flat shelf region is only a few meters in thickness, but covers a large area adjacent to the Bosphorus.

Topographical Features of the Continental Shelf

The bottom topography for the Black Sea shelf adjacent to the Bosphorus has been generated from a combination of data obtained from different sources: (*i*) digitized depth contours of UNESCO topographic maps for the Black Sea, (*ii*) digitized data from local hydrographic maps, (*iii*) ADCP depth measurements from R/V BİLİM cruise path in September 1994, with the combined data points shown in Figure 10a, (*iv*) the high resolution topography assembled from the measurements of the SWATH echosounder on board the R/V ALLIANCE in 1995 [6] and 1996 [7] shown in Figure 10c.

There were differences in the generated topography using different sources of data. The bottom topography generated when only ($i - iii$) depth data points of Figure 10a were used is shown in Figure

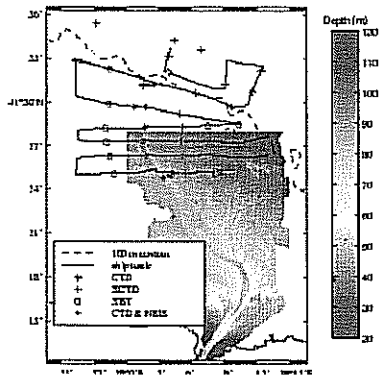

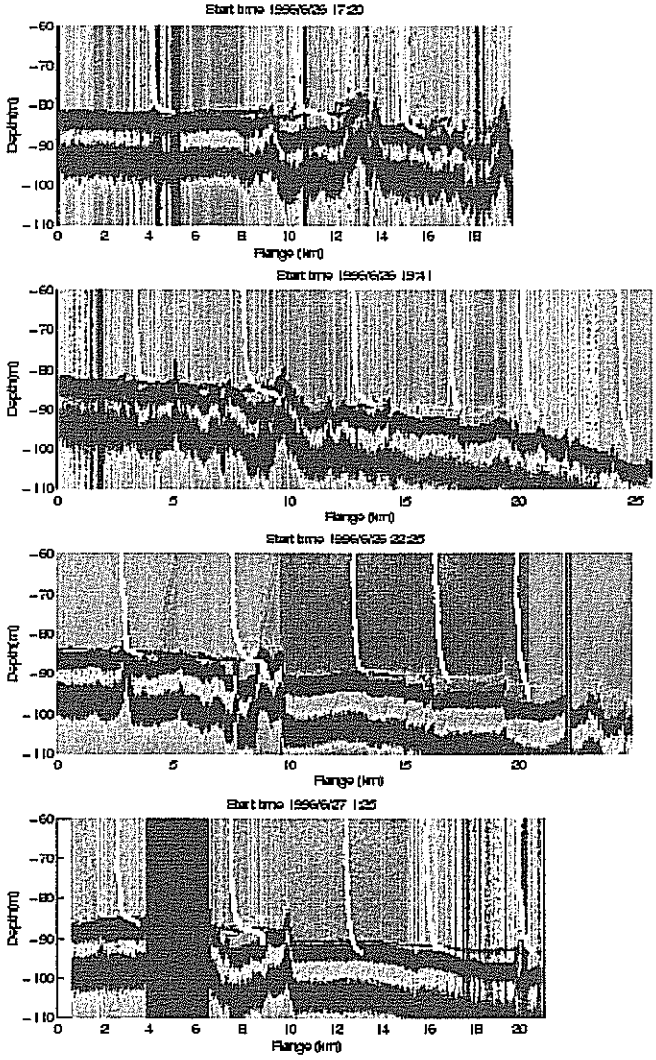

Figure 8: (a) High resolution echo sounding images along the west-east oriented transects, together with overlaid temperature profiles from expendable sensors. Range is calculated from the west end of each track. (b) Map showing the ship track.

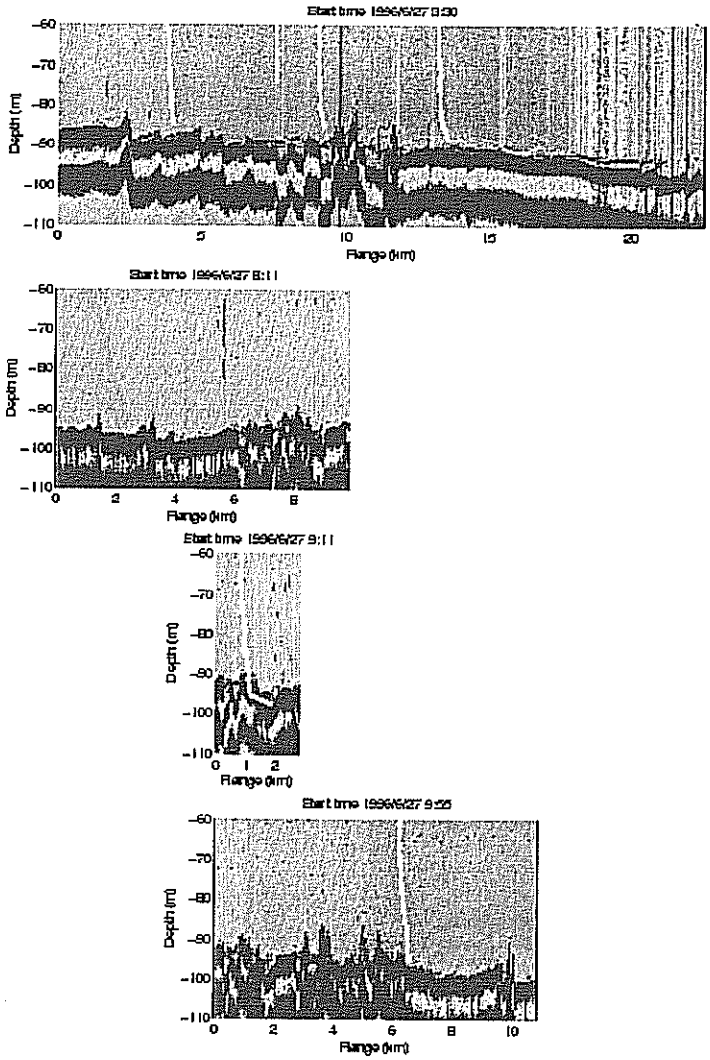

Figure 9: High resolution echo sounding images along the west-east oriented transects, together with overlaid temperature profiles from expendable sensors, continued From Figure 8

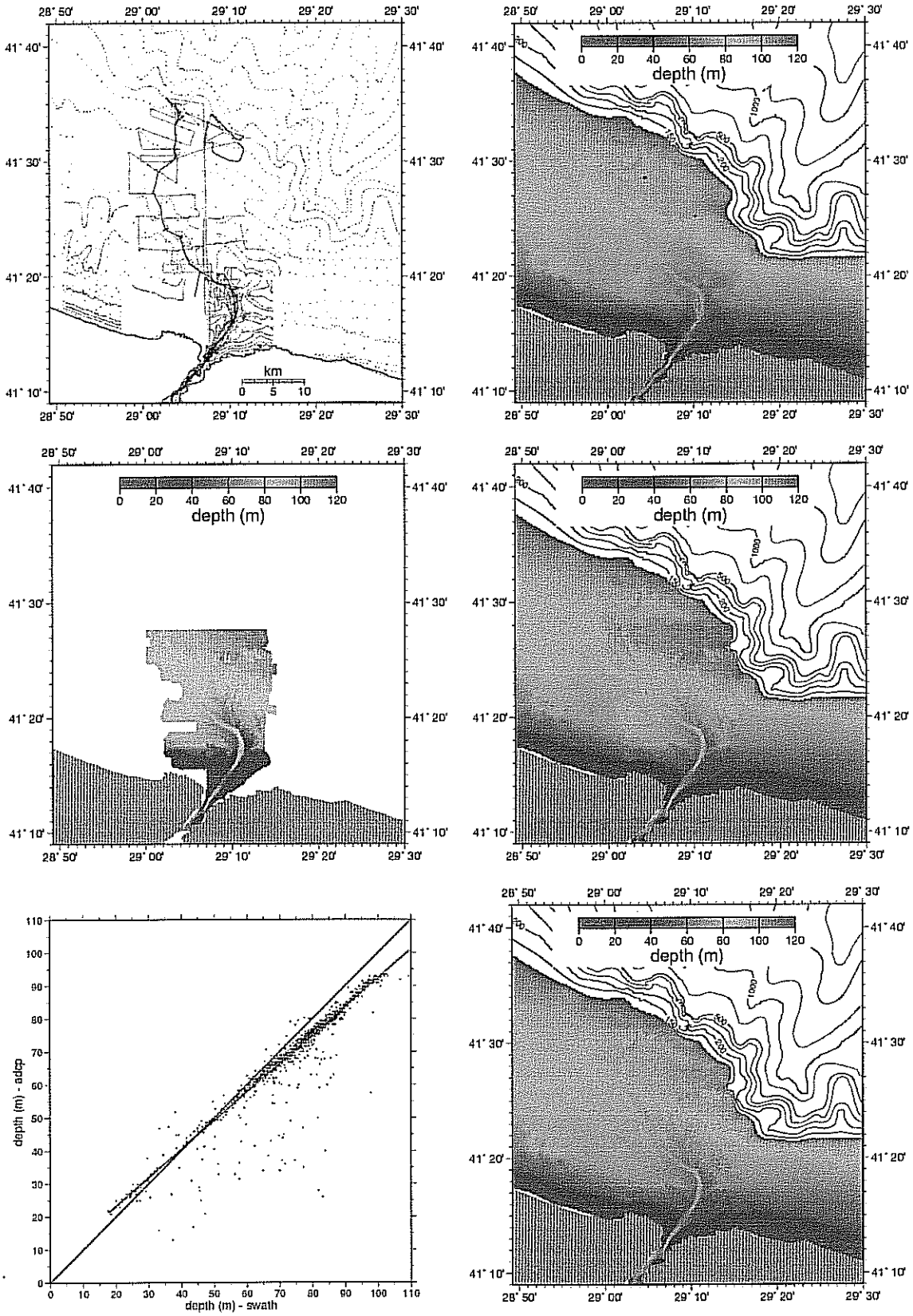

Figure 10: (a) The geographic locations of depth points obtained from hydrographic maps and the 1994 ADCP depth measurements interpolated onto a model grid, (b) the resulting bottom topography. (c) The high resolution bottom topography obtained from the combined data of the R/V ALLIANCE SWATH instrument in 1995 and 1996, and (d) the resulting topography when combined with the other data. (e) The correlation of ADCP versus SWATH depths at coinciding points, and the resulting topography when SWATH data are corrected according to the regression line.

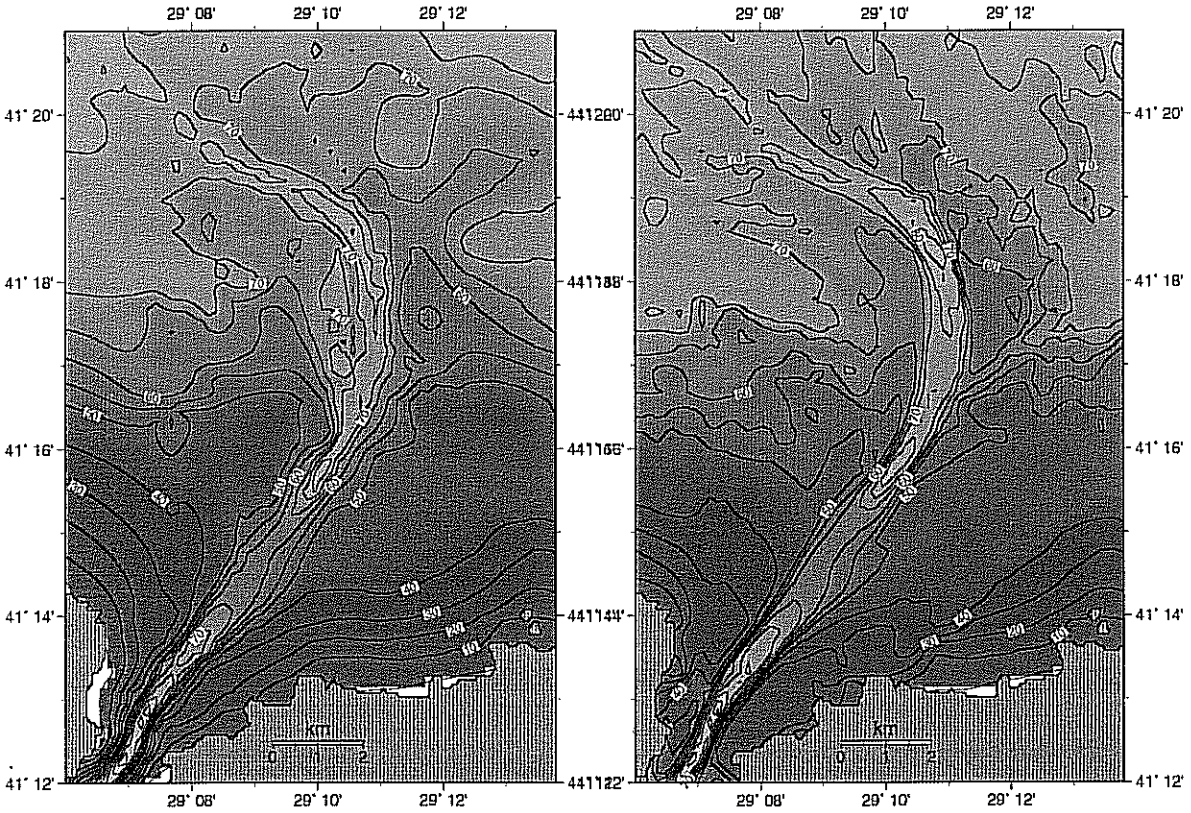

Figure 11: Bottom topography of the Bosphorus exit region, displaying features the northern sill and canyon when the topography is constructed from (a) hydrographic maps and adcp depth soundings, and (b) when these data are combined with SWATH data.

10b. The high resolution topography (*iv*) obtained in the region surveyed with the SWATH system [7] is shown in Figure 10c, and the topography reconstructed by combining all the data from $(i - iv)$ is shown in Figure 10d. It is immediately clear that the inclusion of the SWATH data (*iv*) has higher total weight and therefore makes a big difference in the topography, producing an abnormally deep area near the shelf edge in the same area as the SWATH coverage, not conforming to the general topography of the region obtained from the other sources. This is demonstrated by correlating the depth data obtained from ADCP and SWATH measurements where both types of measurements coincided, as shown in Figure 10e. The comparison in Figure 10e shows that the SWATH measurements had a positive bias yielding greater depths at the deeper areas, and did not agree with the other sources of data which had better internal consistency. This difference was important in the modelling because the artificially high slopes near the shelf edge imposed by the uncorrected topography had a tendency to channel dense water on the shelf towards the deep region in a way that contrasted eith the observations. By combining the the data from sources $(i - iv)$, with the SWATH data corrected according to the regression line in Figure 10e, a more consistent and highly resolved bottom topography was obtained as shown in Figure 10f.

The inclusion of the SWATH data makes a big difference especially near the exit canyon, making it much wider and deeper compared to the case when they are not included, as shown in Figures 11a,b. The other area with large differences is near the joining of the shelf region with the deeper Bosphorus canyon across the continental slope.

The long groove on the Black Sea shelf bottom leading from the Bosphorus exit to the shelf edge is a newly revealed feature, which comes out of the high resolution combined ADCP and SWATH data assembled together. The curved channel, its overflow ducts where the channel joins the wide shelf, and and a birdfoot delta structure separating into three channels upon approach to the shelf edge reminds us of the course of a river flowing into the Black Sea. A river of salty Mediterranean water exists now and may have existed in not so distant geological history. However it is not clear whether this river was ever a fresh water stream. Leaving the interpretation of its features and history to geologists who may be equally puzzled, we may speculate that the present 'river channel' was probably formed during the recent

past, when the flow cut through the holocene sediments it helped to accumulate on top of the bedrock.

In recent studies it has been speculated that 'the stream once running along the Bosphorus did not reach the shelf edge', based on the disappearence of the Bosphorus channel at mid-shelf and later coalescence into a wider channel further north [5]. These incomplete observations have incorrectly led to the speculations that 'no connection existed between the shelf edge channels (attributed to the erosive actions of debris flows and turbidity currents) and the Bosphorus channel'. Other studies have incorrectly attributed the alongshore undulations in sediment cover to transport along the coast by currents forming sand bars and waves perpendicular to the coast [1], and in their maps of bottom features connected the Bosphorus channel directly to the abyssal Bosphorus Canyon. In contrast to the above speculations, our detailed topography (Figure 10f) based on a synthesis of available data and repeated measurements of bottom salinity (Figure 6 and other published data, [17]), as well as model results shortly to be described, clearly indicate a continuous curved channel extending from the exit of the Strait to the shelf edge, while the Bosphorus outflow is found mainly to follow this groove.

The relationship of the 'river channel' to the abrupt flooding of the Black Sea by Mediterranean waters, linked to the rise of sea-level about 7,600 years BP [30, 31], is not so clear. A regional unconformity of strong acoustic reflection at a depth of $\sim$ 105 m, presumably the paleoshoreline before the 'flood' has been found at continental shelves both north and south of the Black Sea at about the present outline of the shelf break, but underlies the draped recent sediments that the Bosphorus 'river channel' cuts through [5, 1]. While [31] also link this erosion surface to abrupt flooding, the interpretation of [5] suggest that the breakthrough occurred tectonically. Indeed, the cross sections in Figures 7-9 as well as those given in [6] indicate previously undocumented terraces separated by sharp drops in depth, which could be part of the small scale compressional faulting found in the Bosphorus region [10]. Although the existence of a river prior to flooding is often suggested [30, 5], whether the Bosphorus outflow channel in its present form is in any way linked to this 'hidden river' seems doubtful, despite the fact that its delta at the shelf edge roughly coincides with the position and depth of the proposed ancient coastline.

Modelling of the Shelf Mixing and Spreading of Dense Water

We use the [16] model to study the Mediterranean plume in the Black Sea, incorporating the effects of the complex topography in the Bosphorus exit region. The model, described in Appendix A, is a reduced gravity single layer approximation to the primitive equations [15], including horizontal and bottom friction as well as entrainment from ambient waters. Either the Kochergin or the Pedersen entrainment parameterizations [16] can be specified, taking into account the ambient property distributions, represented by realistic vertical profiles of temperature and salinity in the Black Sea. In the present runs of the model, the ambient stratification was specified to be the observed profiles of temperature and salinity at station 7 of the 1988 R/V KNORR Leg 4 measurements [20]. The horizontal resolution of the model is $200m$. The combined and corrected bathymetry of Figures 10f or 11b was used in the model.

A central run of the model with indicated set of parameters and initial conditions is shown in Figure 12, for day 10 after start up, when the plume had covered the shelf and the flow had reached a steady state. The bottom drag coefficient r was found to be in the range of 0.003 to 0.015 from acoustical measurements of flow and dissipation over the sill carried out in both 1995 and 1996 [6, 7]. We have tested the model lower and upper bounds of this range in Figures 12 and 13d,e to investigate its effects on the flow. Most literature references quote a value close to r=0.003 for shallow seas [16, 32]. Increasing the bottom friction coefficient from r=0.003 in Figure 12 to r=0.015 results in smaller velocities in Figure 13d,e but does not greatly change the thickness or the salinity and temperature distribution (not shown). Decreasing the friction coefficient much further to r=0.001 while increasing the initial velocity to $u_o = 1.0$ m/s at the same time in Figure 14a,b results in increased velocities on the shelf as well as near the shelf edge, leading to the leakage of the dense water to the abyss at the continental slope. In the cases with higher friction values (Figures 12 and 13d,e), the flow on the continental slope region has been trapped to depths shallower than 500 m, in agreement with observations [20].

Entrainment is increased greatly at steep continental slope, and results in an order of magnitude increase in plume thickness, while the density contrast vanishes at the edges of the plume, making the reduced gravity approximation, and hence the model lose validity near the front. Furthermore, the model

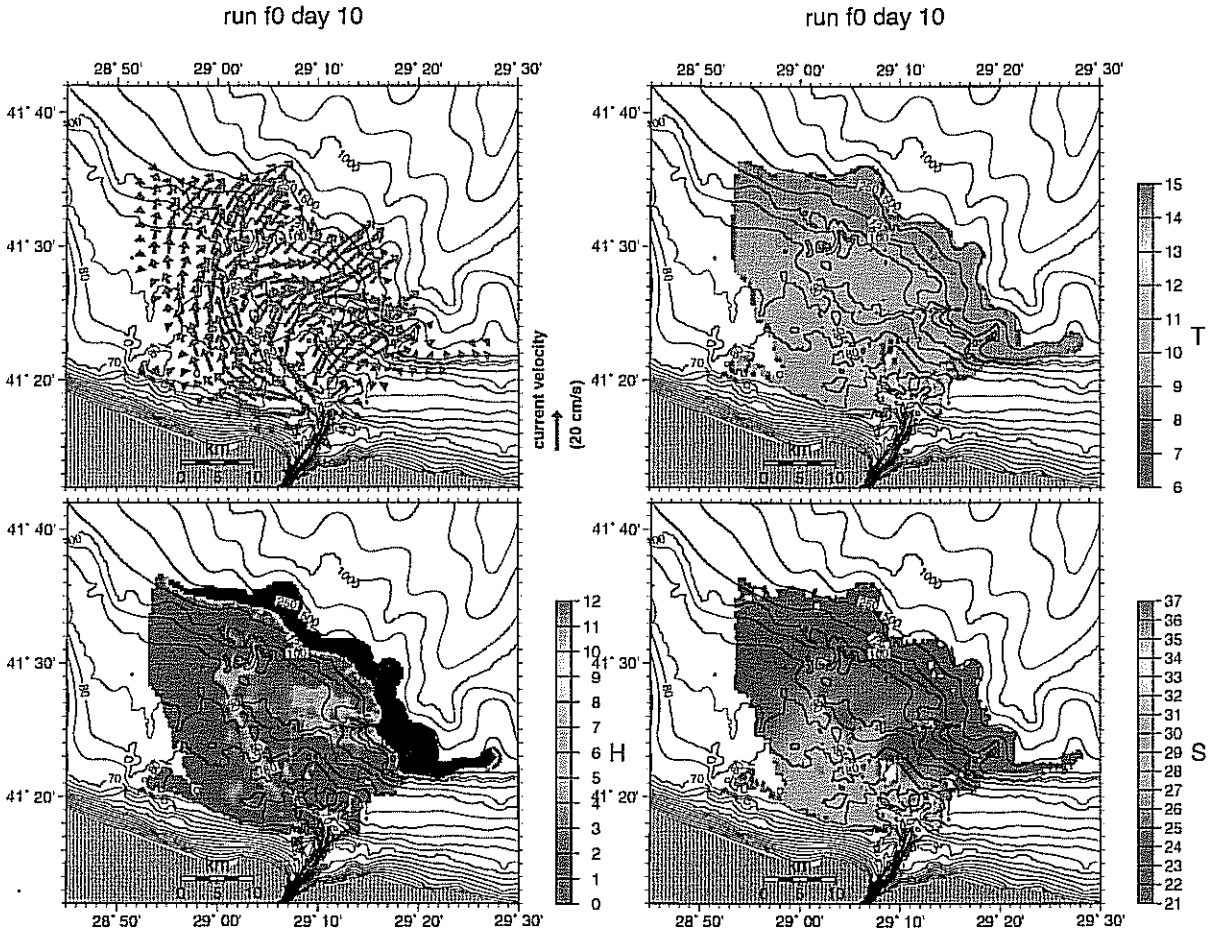

Figure 12: (a) flow velocity, (b) layer thickness, (c) temperature and (d) salinity 10 days after the initialization of the model with continuous outflow from the Bosphorus. Run parameters are: $A_h = 150m^2/s$, $r = 0.003$ for the horizontal eddy coefficient and bottom friction respectively, and $u_o = 0.7$ (direction 45^o) m/s, $S_o = 37$, $T_o = 14.5°C$, $H_o = 40m$ for the initial conditions specified at the Black Sea exit of the Bosphorus. The velocity vectors are plotted at every 10 points in the grid, to simplify the graphics. The thickness in the dark area along the continental slope is outside the scale range.

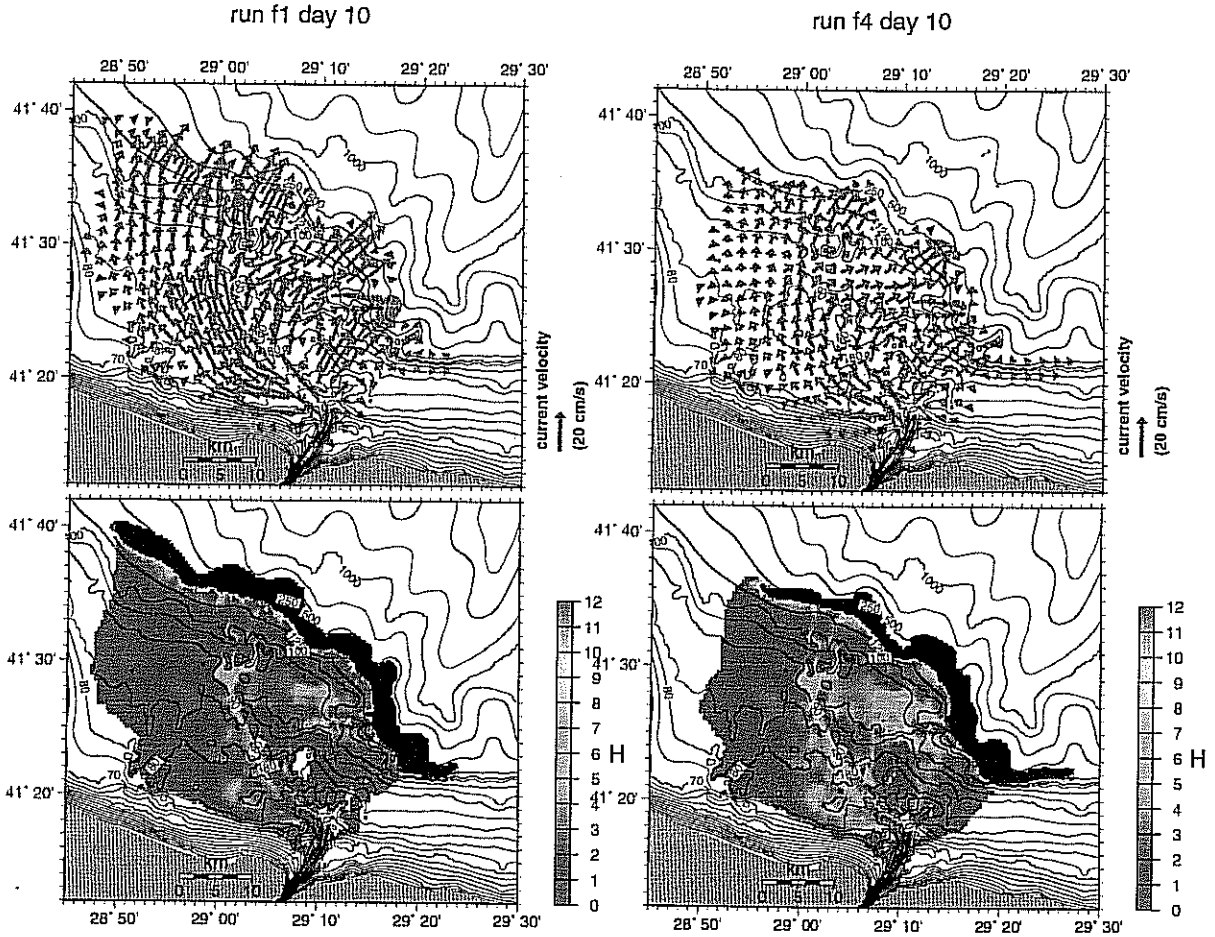

Figure 13: Model results for (a) flow velocity and (b) layer thickness 10 days after initialization, for the case when the effects of earth's rotation has been inactivated by setting the Coriolis parameter to f=0, while the other run parameters are the same as in Figure 12, (c) flow velocity and (d) layer thickness 10 days after start up, for run parameters the same as in Figure 12, except for the bottom friction $r = 0.015$.

also loses validity here because the water mass that loses its density contrast and momentum at the final level of the plume front would tend to either move along the bathymetric contours, in this case towards the east because of earth's rotation, or into the interior by isopycnal spreading, which however is not treated by the present model. In our results the waters at the plume front start to move east along bathymetric contours after reaching to a level of static equilibrium against the ambient stratification.

The other adjustable model parameter was the horizontal eddy coefficient, though changing it had little impact on the results. Similarly the use of linear versus nonlinear model equations were of very little consequence for the simulated flow on the shelf. We also made runs setting the Coriolis parameter $f = 0$ to test the effects of earth's rotation on the flow. The plume properties do not change much between the central run and the non-rotational case in Figure 13a,b, except that the plume in the non-rotating case was more spread out and thinner, while in the rotational case the flow was more confined and steered towards the east. The waters at the plume front moved in both directions along bathymetric contours in the non-rotational case, while the motion along the bathymetric contours of the slope region was always to the east in the case with rotation.

Different formulations of entrainment, *e.g.* Kochergin versus Pedersen formulations in Appendix A had little effect on the results except for slight differences along the continental slope (not shown), not affecting the penetration depth of the plume. In the extreme case when entrainment was totally eliminated in Figures 14d,e, a very thin layer of dense water conserving its initial properties flowed down the slope with great velocity, immediately reaching the abyssal depths.

The effects of ambient stratification were tested. However changing the ambient stratification within

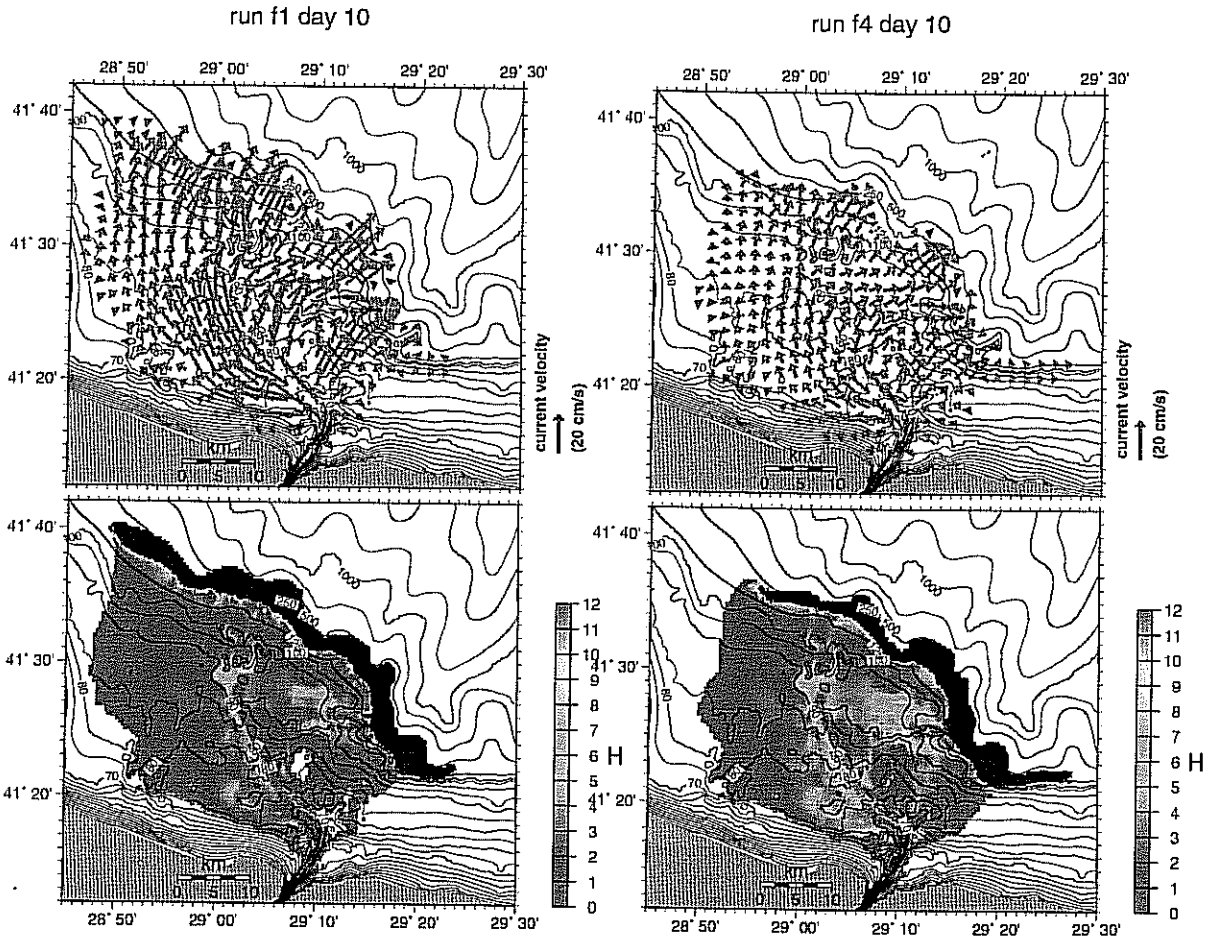

Figure 13: Model results for (a) flow velocity and (b) layer thickness 10 days after initialization, for the case when the effects of earth's rotation has been inactivated by setting the Coriolis parameter to f=0, while the other run parameters are the same as in Figure 12, (c) flow velocity and (d) layer thickness 10 days after start up, for run parameters the same as in Figure 12, except for the bottom friction $r = 0.015$.

also loses validity here because the water mass that loses its density contrast and momentum at the final level of the plume front would tend to either move along the bathymetric contours, in this case towards the east because of earth's rotation, or into the interior by isopycnal spreading, which however is not treated by the present model. In our results the waters at the plume front start to move east along bathymetric contours after reaching to a level of static equilibrium against the ambient stratification.

The other adjustable model parameter was the horizontal eddy coefficient, though changing it had little impact on the results. Similarly the use of linear versus nonlinear model equations were of very little consequence for the simulated flow on the shelf. We also made runs setting the Coriolis parameter $f = 0$ to test the effects of earth's rotation on the flow. The plume properties do not change much between the central run and the non-rotational case in Figure 13a,b, except that the plume in the non-rotating case was more spread out and thinner, while in the rotational case the flow was more confined and steered towards the east. The waters at the plume front moved in both directions along bathymetric contours in the non-rotational case, while the motion along the bathymetric contours of the slope region was always to the east in the case with rotation.

Different formulations of entrainment, *e.g.* Kochergin versus Pedersen formulations in Appendix A had little effect on the results except for slight differences along the continental slope (not shown), not affecting the penetration depth of the plume. In the extreme case when entrainment was totally eliminated in Figures 14d,e, a very thin layer of dense water conserving its initial properties flowed down the slope with great velocity, immediately reaching the abyssal depths.

The effects of ambient stratification were tested. However changing the ambient stratification within

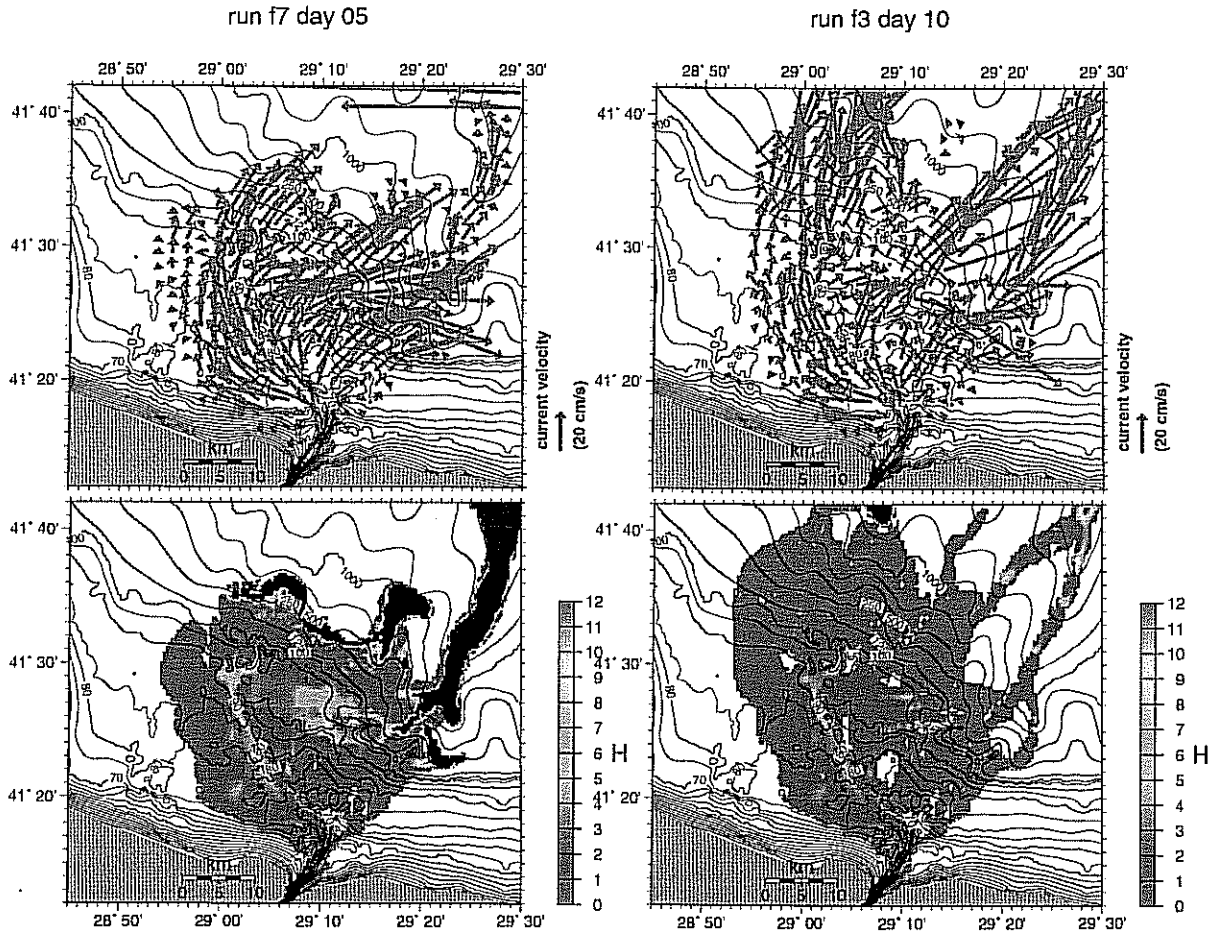

Figure 14: Model results for (a) flow velocity and (b) layer thickness 10 days after start up. with run parameters the same as Figure 12, except for reduced bottom friction $r = 0.001$ and increased initial velocity $u_o = 1.0m/s$ (direction 45°) specified at the Black Sea exit of the Bosphorus, (c) flow velocity and (d) layer thickness 10 days after start up, with run parameters the same as Figure 12, but without entrainment.

reasonable limits, *e.g.* lowering the ambient profile by $30m$ to simulate changes that would occur during a dynamically motivated change in the position of the pycnocline was found to have only very little effect on the dilution and velocity distribution of the plume.

The model results were highly sensitive to topographic details, bottom friction and entrainment, and less to variations of the other parameters. The plume reached a quasi-steady state on the shelf area after about 10 days from start-up. The flow along the continental slope is either in the form of a geostrophically adjusted motion along the bathymetric contours after it reaching a depth where it is arrested, or the precipitous flow down hill to abyssal depths, which continues to develop with time thereafter. The behaviour on the continental slope is rather erratic because the solutions reach limits of validity of the model itself: the rapid entrainment at the steep slope produces a very thick, diluted layer with vanishingly small density contrast at the edges of the plume. On the other hand, the assumptions with regard to entrainment are expected to break down in this steep region in relation to additional processes, such as due to double diffusive convection [20, 21], and interaction with the numerous small-scale canyon features probably not adequately resolved in the present topography.

Seemingly small differences in bathymetry had relatively large impact on the spreading, mixing and therefore penetration of the Mediterranean effluent into the Black Sea. To mention briefly, the model results based on the topography of Figure 10b or 11a lacking the resolution to define fine scale features resulted in flows which were not appropriately channeled. With the inclusion of the uncorrected SWATH data in Figure 10c, the falsified slopes in Figure 10d near the shelf edge transferred the thin layer of dense water on the adjacent shelf to the deeper Bosphorus Canyon region with less dilution, and hence greater

depth penetration. Consistent results were only obtained when the corrected high resolution topography of Figure 10f or 11b was utilized.

Discussion

Because the exchange and mixing at the Bosphorus have strong implications for the adjacent seas, and in particular for the Black Sea, it is important to obtain a sound understanding of these processes through observations and modelling. Continuing studies addressing the Bosphorus exchange and the ventilation of the Black Sea are important in their own right, for clarifying the local effects of hydrometeorological and climatic changes, but also have bearing on many applied problems, including the fate and conservation of the Black Sea and the Marmara Sea which are areas of intense human activity, including the regulation and safety of navigation through the Strait, subjected to increasing ship traffic threatening the well-being of the system.

We have offered a glimpse of these processes in this brief account. However, the time dependent regimes of exchange flows, mixing and entrainment in the Bosphorus and its Black Sea exit are possibly far more complex than described here. For example, the effects of ambient currents, *e.g.* the rim-current of the Black Sea, on forced drainage of the plume [32] and isopycnal or double diffusive spreading of the arrested plume front on the continental slope are more difficult to handle, and are not taken into account in the present model. On the other hand, analyses of the wealth of information obtained in the Bosphorus and the neigboring seas in recent years will certainly enhance the present understanding.

Some features of the topography of the shelf adjacent to the Bosphorus is much like a river delta, providing a conduit for the Mediterranean water to reach the shelf without extensive mixing, but at the same time the details of this topography are important in determining the plume momentum and other physical properties at the shelf edge, before the Mediterranean water cascading down the slope loses much of its identity by rapid dilution through entrainment. Although the model starts to lose its validity on approaching this frontal region, the behaviour of the plume is only stable when the details of the bottom topography are well resolved, and the model predicts maximum penetration of the plume to a depth of up to $500m$ under the present ambient stratification, inflow conditions and a reasonable range of parameters.

Appendix A: Model Description

The flow of the bottom layer of dense water is simulated by a hydrostatic, reduced gravity, two-dimensional primitive equation numerical model developed by [15]. The vertically integrated model predicts the spatial and temporal evolution of the flow field and the water mass changes within the gravity plume that descends on arbitrary topography. The turbulent lower layer flow has height H within a total fluid height of D overtopped by the ambient upper layer of thickness $\zeta = D - H$ assumed to be at rest. Hydrostatic, vertically integrated primitive equations (between $z = -\zeta$ and $z = -D$) for the bottom layer are used together with the kinematic and dynamical boundary conditions at the limiting surfaces. The integrated transport of the dense water is $\vec{\mathbf{U}} = (U, V) \equiv \int_{-D}^{-\zeta} \vec{\mathbf{u}}\, dz$ where $\vec{\mathbf{u}} = (u, v) \equiv \vec{\mathbf{U}}/H$ is the average velocity vector. The continuity and momentum equations for the dense water layer are

$$\frac{\partial \zeta}{\partial t} + \nabla \cdot \vec{\mathbf{U}} = w_e, \tag{1}$$

$$\frac{\partial \vec{\mathbf{U}}}{\partial t} + \nabla \circ (\vec{\mathbf{u}} \cdot \vec{\mathbf{U}}) + f\hat{\mathbf{k}} \times \vec{\mathbf{U}} = -g' H \nabla \zeta - \frac{gH^2}{2\rho_0} \nabla \rho + \nabla \cdot A_m H \nabla \vec{\mathbf{u}} - \frac{\vec{\tau}_b}{\rho_0}. \tag{2}$$

where the second term in 2 represents a dyadic operation, w_e is an 'entrainment velocity', f is the Coriolis parameter, and $g' \equiv (\rho - \rho_a)g/\rho_0$ is the reduced gravity (in which ρ_a denotes the ambient and ρ_0 the reference density), A_m is the horizontal mixing coefficient for momentum, and the bottom stress $\vec{\tau}_b$ has a quadratic drag representation $\vec{\tau}_b = \rho_0 r\, |\vec{\mathbf{u}}|\, \vec{\mathbf{u}}$.

The integrated conservation equations for heat and salt are in the following form

$$\frac{\partial T}{\partial t} + \vec{u} \cdot \nabla T + w_e \frac{T - T_a}{H} = \frac{A_t}{H} \nabla \cdot (H \nabla T) \tag{3}$$

for temperature, and an equivalent form for salinity, coupled through the equation of state for seawater density $\rho = \rho(T, S, z)$ based on UNESCO (1981).

Entrainment occurs from the upper into the lower layer, with vertical speed w_e pointed downwards, and creates variations of plume scalar properties. Since the upper layer is assumed to be at rest, entrainment terms do not appear in the flux form of the momentum equation, but entrainment terms representing interfacial friction would emerge if the equation of motion were to be written in terms of velocity rather than transport. Turner [34] parameterized the entrainment velocity as a function of the turbulent flow velocity, $w_e = E|\vec{u}|$, through a dimensionless entrainment coefficient E.

Substantial work exists on turbulent entrainment [34, 29], either in the case of a single turbulent layer entraining a non-turbulent fluid [2, 15] or the case when both entraining layers are turbulent [19], all of which suggest that the entrainment velocity, is a strong function of Richardson number

$$Ri = \frac{N^2}{\left|\frac{\partial \vec{u}}{\partial z}\right|^2} \quad \text{where} \quad N^2 = -\frac{g}{\rho_0} \frac{\partial \rho}{\partial z}. \tag{4}$$

The Richardson Number Ri measures the relative importance of the instability caused by shear with respect to the stabilizing influence of density stratification [34]. The Brunt-Väisälä (stratification) frequency N is a measure of static stability [34]. When the stratification consists of two layers, with one of the layers in motion, we redefine

$$Ri = \frac{g' H}{|\vec{u}|^2} \quad \text{and} \quad N^2 = -\frac{g \Delta \rho}{\rho_0 H} \tag{5}$$

where H is the plume height, and $\Delta\rho$ is the density difference between the layer and the ambience. Kullenberg (1977; cited in [15]) equated the turbulent buoyancy flux to the flux arising due to entrainment at the interface,

$$k_m \frac{\partial \rho}{\partial z} \equiv w_e \Delta \rho \tag{6}$$

where k_m represents the turbulent vertical exchange coefficient for density. Replacing the equivalent formulations for a single layer with uniform properties therefore yields

$$w_e = E|\vec{u}| = \frac{k_m}{H} = |\vec{u}| \frac{c_L^2}{S_m} \sqrt{1 + \frac{Ri}{S_m}}, \tag{7}$$

after using the formulation of Kochergin (1987, cited in [15]) which gives the entrainment coefficient E as a function of Ri on the *rhs* of the above equation. Here c_L is a constant of proportionality and S_m is the Schmidt number (the ratio of the momentum mixing coefficient k_i to the density mixing coefficient k_m)

$$S_m = \frac{k_i}{k_m} = \frac{Ri}{0.725 \left(Ri + 0.186 - \sqrt{Ri^2 - 0.316 Ri + 0.0346}\right)}. \tag{8}$$

Based on laboratory and field measurements, Pedersen [29] alternatively found the dimensionless entrainment parameter E to fit a theoretical function

$$E = 0.072 \left(\frac{r}{Ri}\right) \tag{9}$$

for values of $r/Ri < 10^{-2}$, where r is a dimensionless friction coefficient, typically having a value of $r = 0.003$.

The model utilizes both the Kochergin and Pedersen entrainment parameterizations as alternatives. Although Kochergin has derived $c_L = 0.05$, it is argued [16] convincingly that the E *versus* r/Ri curves for Kochergin and Pedersen entrainment parameterizations coincide for $r/Ri < 10^{-2}$ when the choices

for constants are made as $c_L = 0.0275$ and $r = 0.003$, but for higher Richardson numbers the curve for Kochergin parameterization flattens, which in fact prevents unrealistically high entrainment rates at the shallow edges of the flow to be numerically calculated. We use $c_L = 0.0275$ in our calculations but change r between 0.001 and 0.015.

The Numerical Scheme

The model discretization is made on the Arakawa staggered C grid, *i.e.* velocity is calculated at points displaced from the points where interface level (ζ), temperature and salinity are calculated. The points where the plume is absent are considered 'dry' (*i.e.*ζ equals total depth D). The horizontal extent of the plume movable boundary is determined by the application of a Boolean logic sequence to test 'dry' or 'wet' points: Defining the plume elevations H_E and H_W at two neighboring pressure points (*e.g.* respectively east and west of a velocity point), the point is set inactive if (*i*) both H_E and H_W points are dry, (*ii*) H_W point is dry and $\zeta_E > \zeta_W$, and (*iii*) H_E point is dry and $\zeta_W > \zeta_E$. In all other cases, the equation of motion is solved at the 'active' velocity point at each time step Δt. For integration in time, the model uses An explicit scheme with two-time levels is used for time integration, yielding plume height at $t + \Delta t$ and its extrapolation to $t + 2\,\Delta t$ so that negative plume heights are avoide at the edges of the flow, by introducing enhanced friction for the particular grid point to eliminate a consequence of numerical inaccuracies. Advection of momentum, as well as scalar properties (temperature and salinity) is done by using a conserving flux form of the equations, approximated by a selective (but numerically diffusive) vector upstream algorithm. The linear stability of the model is governed by

$$\frac{\Delta x}{\Delta t} > \sqrt{g\frac{\Delta\rho}{\rho}\zeta}. \tag{10}$$

Reflections at the open boundaries of the model grid are handled via a numerical "sponge" zone, where the horizontal diffusion terms and grid spacing perpendicular to the open boundary are gradually increased.

Acknowledgements

This study has been made possible by combined opportunities to collect and analyze the relevant data, and to make use of modelling for a synthesis. A number of different projects were instrumental in this respect: The data used in this study were obtained on board the R/V BİLİM of the IMS-METU, during research programs supported by the Municipality of İstanbul, Water and Wastewater Administration (İSKİ), the Turkish Council for Scientific and Technological Research (TÜBİTAK), as well as during a joint research activity of the IMS-METU and U. of Washington scientists with extra support from the Office of Naval Research (ONR) of the United States, and during a research cruise on board the R/V ALLIANCE supported by NATO/SACLANTCEN with the participation of scientists from IMS-METU and the Department of Navigation, Hydrography and Oceanography (SHOD) of the Turkish Navy. Research grants from the INCO-Copernicus Program of the European Union (ERBIC15CT960113) and TÜBİTAK (YDABÇAG 137) facilitated the analyses and modelling. The authors wish to express their gratitude to the cooperative efforts of the scientists, technicians and graduate students of the cooperating institutions who took part in the data collection and processing, and the captains and crew of the ships, who were involved in various stages of the work.

References

[1] Aksu, A. E., R. Hiscot, D. Yaşar and P. J. Mudie (1999). Deglacial and Postglacial Water Levels and Water Exchange across the Black Sea - Marmara Sea - Aegean Sea Shelves, Eastern Mediterranean Region. Land - Sea Link in Asia, International Workshop on Sediment Transport and Storage in Coastal Sea - Ocean System, Proceedings, 463-468, Tsukuba, Japan, 485 pp.

[2] Baringer, M. O. (1994). Mixing and Dynamics of the Mediterranean Outflow, Ph. D. Thesisi, Woods Hole Oceanographic Institution, / Massachusetts Institute of Technology Joint Program, Woods Hole, Massacusetts, USA.

[3] Beşiktepe, Ş., Sur, H. İ., Özsoy, E., Latif, M. A., Oğuz, T., and Ü. Ünlüata (1994). The Circulation and Hydrography of the Marmara Sea, *Prog. Oceanogr.*, **34**, 285-334.

[4] Deacon, M. B. (editor) (1971). *Scientists and the Sea 1650-1900 - A study of Marine Science*, Academic Press, 445p.

[5] Demirbağ, E., E. Gökaşan, F. Oktay, M. Şimşek and H. Yüce (1999). The last Sea Level Changes in the Black Sea: Evidence from the Seismic Data. *Mar. Geol.*, **157**, 249-265.

[6] Di Iorio, D. and H. Yüce (1998). Observations of Mediterranean Flow into the Black Sea, *J. Geopys. Res.*, **104**, 3091-3108.

[7] Di Iorio, D., T. Akal, P. Guerrini, H. Yüce, E. Gezgin and E. Özsoy (1999). Oceanographic Measurements of the West Black Sea: June 15 to July 1996, Saclant Undersea Research Centre report SR-305, 59 pp.

[8] Ducet, N., P.-Y. Le Traon, and P. Gauzelin (1999). Response of the Black sea mean level to atmospheric pressure and wind. *J. Mar. Sys.*, **22**, 311-327.

[9] Farmer, D. M. and L. Armi (1986). Maximal Two-Layer Exchange over a Sill and Through the Combination of a Sill and Contraction with Barotropic Flow, *J. Fluid Mech.*, **164**, 53-76.

[10] Gökaşan, E., E. Demirbağ, F. Y. Oktay, B. Ecevitoğlu, M. Şimşek and H. Yüce (1999). on the Origin of the Bosphorus, *Mar. Geol.*, **138**, 183-199.

[11] Gregg, M. C. (1998). Estimation and Geography of Diapycnal Mixing in the Stratified Ocean, In: J. Imberger, editor, *Physical Processes in Lakes and Oceans*, American Geophysical Uniion, Washington, D.C., pp. 305-338.

[12] Gregg M. C., E. Özsoy and M. A. Latif (1999). Quasi-Steady Exchange Flow in the Bosphorus *Geophysical Research Letters*, **26**, 83-86.

[13] Gregg M. C. and E. Özsoy (1999). Mixing on the Black Sea Shelf North of the Bosphorus *Geophysical Research Letters* **26**, 1869-1872.

[14] Gregg, M. C. and E. Özsoy (1999). Flow, Water Mass Changes and Hydraulics in the Bosphorus, (in preparation).

[15] Jungclaus, J. H. (1994), Ein numerisches Modell zur Simulation dichter Bodenströmungen im Ozean mit Anwendung auf den "Overflow" durch die Dänemarkstraße, Ph.D thesis, Zentrum für Meeres-und Klimaforschung der Universität Hamburg, Institut für Meereskunde, Hamburg, Germany

[16] Jungclaus, J. H. and J. O. Backhaus (1994). Application of a transient reduced gravity plume model to the Denmark Strait Overflow, *J. Geophys. Res*, **99**, 12,375–12,396.

[17] Latif, M. A., E. Özsoy, T. Oğuz and Ü. Ünlüata (1991). Observations of the Mediterranean inflow into the Black Sea, *Deep Sea Research*, **38**, Suppl. 2, S711-S723.

[18] Marsigli, L. F. (1681), *Osservazioni Intorno al Bosforo Tracio overo Canale di Constantinopoli Rappresentate in lettera all Sacra Real Maesta di Cristina Regina di Svezia*, Roma, 108+pp.

[19] Oğuz, T., Özsoy, E., Latif, M. A., and Ü. Ünlüata, (1990). Modelling of Hydraulically Controlled Exchange Flow in the Bosphorus Strait, *J. Phys. Oceanogr.*, **20**, 945-965.

[20] Özsoy, E., Ünlüata, Ü. and Z. Top, (1993). The Mediterranean Water Evolution, Material Transport by Double Diffusive Intrusions, and Interior Mixing in the Black Sea, *Progress in Oceanography*, **31**, 275-320.

[21] Özsoy, E. and Ş. Beşiktepe, (1995). Sources of Double Diffusive Convection and Impacts on Mixing in the Black Sea, pp. 261-274, in: Brandt, A. and H. J. S. Fernando (editors), *Double-Diffusive Convection*, Geophysical Monograph 94, American Geophysical Union, 334 pp.

[22] Özsoy, E., M. A. Latif, S. Tuğrul, and Ü. Ünlüata (1995a). Exchanges with the Mediterranean, Fluxes and Boundary Mixing Processes in the Black Sea, In: F. Briand, (editor), Mediterranean Tributary Seas, *Bulletin de l'Institut Oceéanographique, Monaco*, Special Number 15, CIESM Science Series No. 1, Monaco p. 1-25.

[23] Özsoy, E., Latif, M. A., Beşiktepe, Ş. and A. F. Gaines (1995b). Fluorescent Dye Measurements of the Mixing and Transport of Wastewater Discharge in the Bosphorus, *Wat. Sci. Tech.*, **32**(2), 61-68.

[24] Özsoy, E., M. A. Latif, H. İ. Sur and Y. Goryachkin (1996). A Review of the Exchange Flow Regimes and Mixing in the Bosphorus Strait, In: F. Briand, (editor), Mediterranean Tributary Seas, *Bulletin de l'Institut Oceéanographique, Monaco*, Special Number 17, CIESM Science Series No. 2, Monaco.

[25] Özsoy, E. and Ü. Ünlüata (1997). Oceanography of the Black Sea: A Review of Some Recent Results, *Earth Science Reviews*, **42**, 231-272.

[26] Özsoy, E. and Ü. Ünlüata (1998). The Black Sea, in: A. R. Robinson and K. Brink (editors), *The Sea: The Global Coastal Ocean: Regional Studies and Syntheses*, **11**, John Wiley and Sons, New York, pp. 889-914.

[27] Özsoy, E., Latif, M. A., Beşiktepe, Ş., Çetin, N., Gregg, N. Belokopytov, V., Goryachkin, Y. and V. Diaconu (1998). The Bosphorus Strait: Exchange Fluxes, Currents and Sea-Level Changes, in: L. I. Ivanov and T. Oğuz (editors), *Ecosystem Modeling as a Management Tool for the Black Sea*, NATO Science Series 2: Environmental Security **47**, Kluwer Academic Publishers, Dordrecht, vol. 1, 367pp + vol. 2, 385 pp.

[28] Özsoy, E. (1999). Sensitivity to Global Change in Temperate Euro-Asian Seas (the Mediterranean, Black Sea and Caspian Sea): A Review, in P. Malanotte-Rizzoli and V. N. Eremeev, (editors), *The Eastern Mediterranean as a Laboratory Basin for the Assessment of Contrasting Ecosystems*, NATO Science Series 2, Environmental Security, **51**, Kluwer Academic Publishers, Dordrecht, pp. 281-300.

[29] Pedersen, F. B. (1980). A Monograph on Turbulent Entrainment and Friction in Two-Layer Stratified Flow, Series Paper 25, Institute of Hydrodynamics and Hydraulic Engineering, Technical University of Denmark, Lyngby, Denmark.

[30] Ryan, W. and W. Pitman (1998). *Noah's Flood. The New Scientific Discoveries About the Event that Changed History*, Simon and Schuster, New York, 319 pp.

[31] Ryan, W. B. F., W. C. Pitman, C. O. Major, K. Shimkus, V. Moskalenko, G. A. Jones, P. Dimitrov, N. Görür, M. Sakınç, H. Yüce (1998). An Abrupt Drowning of the Black Sea Shelf, *Mar. Geol.*, **138**, 119-126.

[32] Shapiro, G. I. and A. Hill (1997). Dynamics of Dense Water Cascades at the Shelf Edge, *J. Phys. Oceanogr.*, **27**, 2381-2394.

[33] Stanev, E. V., J. Simeonov and E. Peneva (1999). Ventilation of the Black Sea Pycnocline by the Mediterranean Plume (submitted).

[34] Turner, J.S. (1973). *Buoyancy Effects in Fluids*, Cambridge University Press, London, 367 pp.

[35] UNESCO (1981). Tenth Report of the Joint Panel on Oceanographic Tables and Standards, UNESCO Technical Papers in Marine Science 36, UNESCO, Paris.

[36] Ünlüata, Ü., Oğuz, T., Latif, M. A., and E. Özsoy, (1990). On the Physical Oceanography of the Turkish Straits, in: *The Physical Oceanography of Sea Straits*, L. J. Pratt (editor), NATO/ASI Series, Kluwer, Dordrecht, 25-60.

[37] Yüce, H. (1990). Investigation of the Mediterranean Water in the Strait of İstanbul (Bosphorus) and the Black Sea, *Oc. Acta*, **13**, 177-186.

[38] Wensink, H. and G. Campbell (1997). Bathymetric Map Production Using the ERS SAR, *Backscatter*, **8**(1), 16-22.

Paper 2

Emin Özsoy, Şükrü Beşiktepe and Muhammed A. Latif
Türk Boğazlar Sistemi'nin Fiziksel Oşinografisi,
Marmara Denizi 2000 Sempozyumu, 11-12 Kasım 2000, İstanbul

Türk Boğazlar Sistemi'nin Fiziksel Oşinografisi

Emin Özsoy, Şükrü Beşiktepe ve Mohammed A. Latif
ODTÜ Deniz Bilimleri Enstitüsü, P.K.28 Erdemli İçel 33731

Özet

Marmara Denizi ve İstanbul ve Çanakkale Boğazlarından oluşan Türk Boğazlar Sistemi (TBS), birbirinden çok farklı özellikli büyük su ve kara kütleleri arasında yer alan küçük fakat dinamik bir sistemdir. Gerek eylemsizliğinin küçük olması gerekse Boğazlar aracılığıyla çevresinden kolay etkilenmesi, bu sistemin iklimsel duyarlılığını artırmaktadır. Öte yandan büyük yoğunluk farklılıklarının bulunduğu hızlı değişim ortamında gerçekleşen madde akıları nedeniyle, TBS komşu denizlerde de önemli etkiler yaratabilmekte ve o denizlerin iklimsel duyarlılığını da büyük oranda etkileyebilmektedir.

Giriş

Hızla çevresel bozulmaya uğrayan görece küçük boyutlardaki bir su kütlesi olan Marmara Denizi, dünyadaki yarı-kapalı özellikler taşıyan benzer denizler arasında özel bir öneme sahiptir ve sorunlarına acil çözüm beklemektedir. Hem Karadeniz'in bugünkü olumsuz koşullarından etkilenmesi, hem de çevresindeki yoğun sanayi ve yerleşim alanlarının etkileri sonucunda Marmara Denizi'nde kirlilik hizla artmakta ve bu denizimizi tehdit etmektedir. Bunun yanısıra, Boğazlardan geçen gemi trafiği de, gösterdiği artış eğilimi, yarattığı kirlilik ve kaza riskleri ile, önemli bir tehdit oluşturmaktadır.

Öte yandan, Türkiye'ye ait bir iç deniz olarak, buradaki kaynakların kullanımı, çevrenin korunması ve ekonomik, sosyal faktörler dikkate alınırsa, Marmara Denizi Türkiye için özel ve tartişilamaz bir öneme sahiptir. 1999 yılında gerçekleşen depremler ve bunların sonuçları da göstermiştir ki, Marmara Denizi, ülkemiz için sahip olduğu önemle orantılı kollektif bir sorumluluğu da gerektirmektedir.

Marmara Denizi, Akdeniz ve Karadeniz arasında yer alan oldukça küçük (yaklaşik 70 km x 250 km boyutlarında, 11,500 m^2 yüzey alanına ve 1390m maksimum derinliğe sahip) bir basendir. Avrupa ve Asya kıtaları arasında yer alması sonucunda sahip olduğu ekonomik ve sosyal önemine ek olarak, Akdeniz ve Karadeniz arasında sağladığı deniz iletişimi ve bağlantısı da bölgenin oşinografik yapisi ve değişkenliğinde önemli rol oynamaktadir, ve Çanakkale ve İstanbul Boğazları ile Marmara Denizi'nin birlikte oluşturdukları sistem, 'Türk Boğazlar Sistemi' (TBS) olarak adlandırılmaktadır. TBS'nin oşinografisi, geçmiş yıllarda yoğun biçimde araştırmalara konu olmuştur, ve özellikle fiziksel yapısı ve değişkenliği konusunda başta ODTÜ Deniz Bilimleri Enstitüsü'nde olmak üzere, elde oldukça geniş bir bulgu bazı bulunmaktadır (Özsoy et al., 1986, 1988; Ünlüata et al., 1990; Beşiktepe, et al., 1993, 1994).

Batimetri

Marmara Denizi'nin taban topoğrafyasında, güney kıyısı boyunca uzanan 100m derinliğindeki geniş kıta sahanlığı bölgesi ile, bunun kuzeyinde doğu - batı yönünde uzanan (batı'dan doğuya doğru sırasıyla 1100m, 1390m, ve 1240m) derin üç depresyon dikkat çekicidir (Şekil 1a). Bu derin depresyonları, yaklaşık 750m derinliği bulunan ve batıdaki 20 km, doğudaki ise 40 km uzunluğunda olan iki eşik yapısı birbirinden ayırmaktadır.

İstanbul Boğazı 30 km boyunda, Arnavutköy civarında en dar yeri 700 m genişliğinde, en derin yeri ise 100 m olan ve kıvrımlı bir kanaldır (Şekil 1b). İstanbul Boğazının güneyinde oldukça dar bir kıta sahanlığı bulunmakta ve doğu Marmara derin çukurundan keskin bir eğim ile ayrılmaktadır. Yine bu bölgeden Sarayburnu önlerine kadar ilerleyen 60-70 m derinliğindeki dar bir kanal Haliç'in güneyinde son bulmakta ve Beşiktaş yakınlarında her iki tarafından 40-50 m derinlikte kanallar geçen 35 m derinliğinde bir tümsek bulunmaktadır. Üsküdar önlerinde Anadolu tarafındaki derin kanal kuzeye doğru izlendiğinde Boğaz'ın kıvrımlarına uyar ve Arnavutköy civarındaki en dar kesitte 100m derinliğe ulaşır.

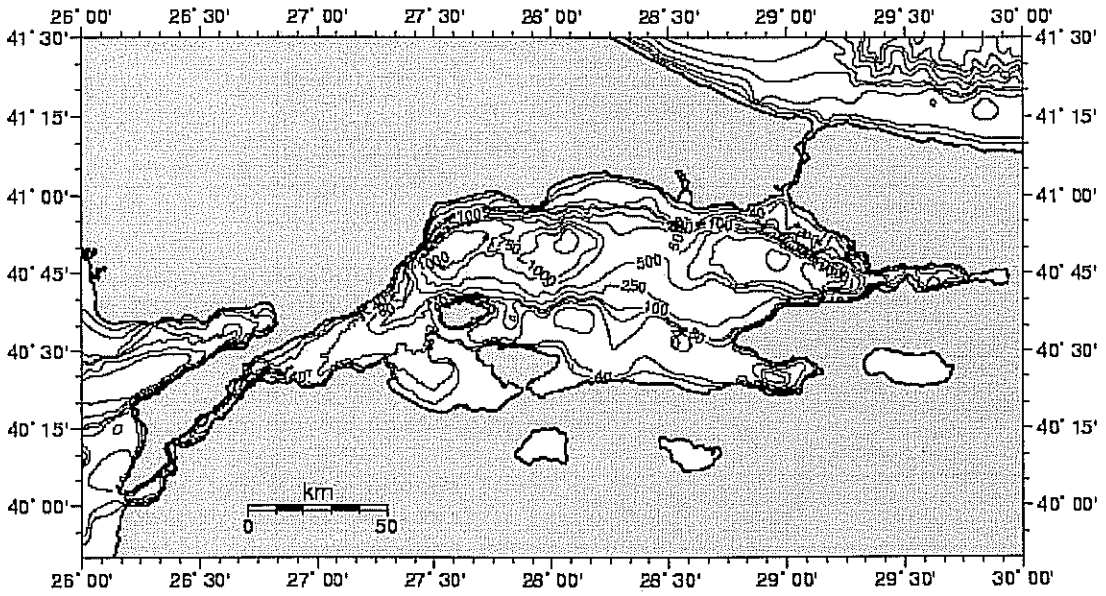

Şekil 1a. Türk Boğazlar Sistemi batimetri haritası

Çanakkale Boğazı, uzunluğu 60 km, genişliği ise en dar yeri olan Nara Burnu'nda 1300m olan bir kanal şeklindedir (Şekil 1c). Boğaz doğu yönünde genişleyerek Marmara Denizi'nin sığ güney kıta sahanlığı'na açılmaktadır, ancak Şekil 1b'de görülebileceği gibi Boğaz'ın güney kesimindeki 70 m derinliğinde belirgin yapıda bir kanal bulunmakta ve bu kanal doğu ucunda taban eğimi ile birleşerek Marmara Adası batısında batı Marmara derin çukuruna ulaşan bir kanyon şeklini almaktadır.

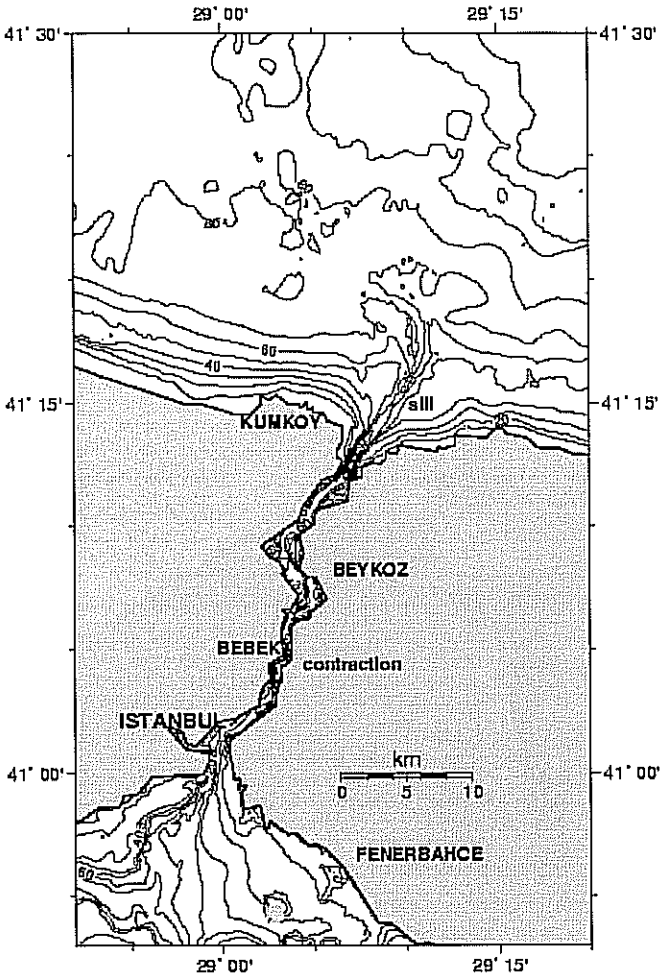

Şekil 1b İstanbul Boğazı batimetri haritası

İstanbul Boğazı'nın Karadeniz'e bağlandığı Karadeniz kıta sahanlığı bölgesinde batimetri oldukça ince ayrıntılara sahip ve karmaşıktır. Oysa buradaki ayrıntının iyi bilinmesi, ilerideki bölümlerde gösterileceği gibi Akdeniz suyunun Karadeniz'deki kaderinin belirlenmesi gibi önemli soruların ve buna bağlı diğer sorunların aydınlatılması için büyük öneme sahiptir.

İstanbul Boğazı'nın kuzey ucunda 70-80 m derinlikte bir kanal önce kuzeydoğu yönünde uzanır ve kanalın içinde yer alan 60 m derinlikteki bir eşiği geçtiğinde kuzeydoğuya dönerek 75 m derinliğe ulaşıncaya kadar ilerler. Bundan sonra eğimi azalan kıta sahanlığı bölgesinde derinlik farkı 2-3 m olan bir kanal şeklinde kuzeye ilerler ve üç kollu bir delta yapısı ile kıta eğimine ulaşır.

İstanbul Boğazı'na komşu Karadeniz kıta sahanlığı'nda, normal seyir haritaları'ndan elde edilebilen batimetri verileri oldukça yetersiz olduğundan aşağıdaki veriler kullanılarak bu bölgenin batimetrisi yeniden oluşturulmuştur (Özsoy *et al.*, 2000): (i) UNESCO Karadeniz batimetri haritalarının sayısallaştırılmış derinlik konturları, (ii) hidrografik seyir haritalarından sayısallaştırılmış veriler, (iii) Eylül 1994 tarihli R/V BİLİM seyirlerindeki ADCP cihazı ile elde edilen ve her istasyonda ses hızına göre düzeltilmiş derinlik verileri (Gregg ve Özsoy, 1999), (iv) 1995 ve 1996 tarihlerinde R/V ALLIANCE gemisi ile 'SWATH echosounder' kullanılarak elde edilen yüksek ayırımlı veriler (Di Iorio et al., 1998, 1999).

Bütün verilerin herhangi bir kontrol yapılmadan ve aynı anda kullanılması, veri setleri arasındaki uyumsuzluklar nedeniyle olanaklı olmamıştır. Örneğin Şekil 2a'da konumları gösterilen, sadece (i-iii) veri setleri kullanıldığında Şekil 2b'deki batimetri, sadece (iv) veri seti kullanıldığında ise Şekil 2c'deki batimetri, bütün veri setleri (i-iv) kullanıldığında ise Şekil 2d'deki batimetri elde edilmektedir.

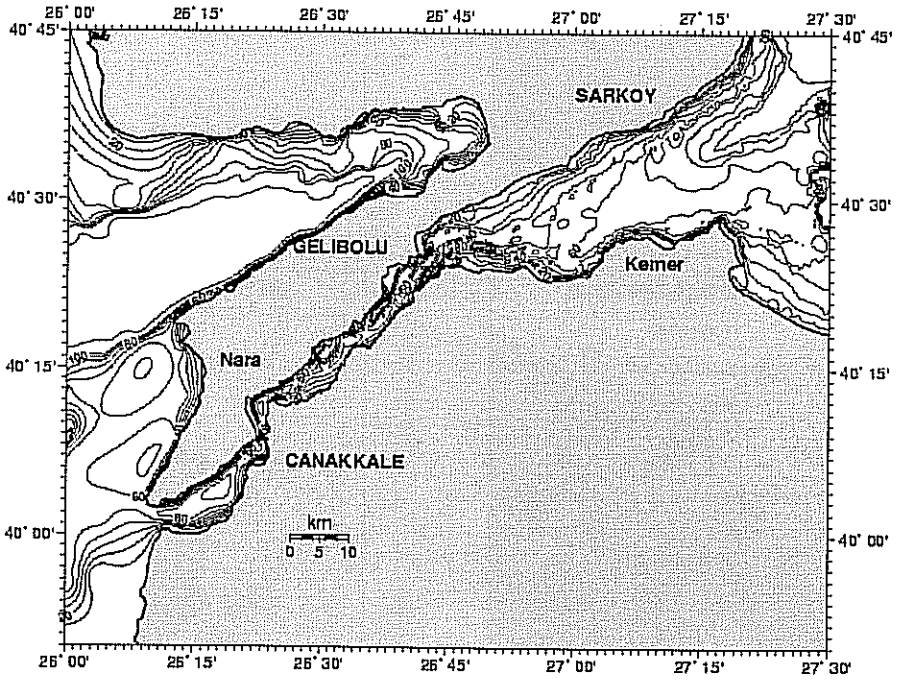

Şekil 1c Çanakkale Boğazı batimetri haritası

Bu şekillerin karşılaştırılmasından, yüksek ayırımlı (iv) SWATH verilerinin en büyük ağırlığa sahip olduğu ve başka veri bulunmayan bölgelerde sonucu en çok etkilediği görülmektedir. Örneğin kıta sahanlığı'nın derinleştiği ve SWATH'tan başka veri bulunmayan bölgelerde bu verilerin kullanılması, derinliği anormal olarak artan ve diğer veri kaynaklarının eğilimine uymayan bir alan yaratmaktadır (Şekil 2d). Veri kaynakları arasındaki bu farklılık, alındıkları yerler açısından çakışan ADCP ve SWATH derinlik ölçümleri arasında yapılan regresyon (Şekil 2e) ile ortaya çıkmaktadır. Bu hesaplamalara göre SWATH verileri yüksek yatay ayırıma sahip olmakla birlikte, derinlikle artan bir hata ile, herhangi bir noktanın derinliğini olduğundan fazla göstermektedir. Diğer veri setleri ise kendi içinde tutarlıdır. SWATH verilerinin yukarıdaki regresyon modelıne göre düzeltilmesinden sonra tüm verileın birleştirildiği durumda ise (Şekil 2f) yüksek ayırımlı ve mutlak derinliği daha doğru olan bir taban topoğrafyası elde edilmektedir. SWATH verilerinin kullanılması özellikle İstanbul Boğazı'nın kuzey ucundaki eşik (60m) geometrisini etkilemekte ve Boğaz'ı Karadeniz kıta sahanlığına bağlayan kanal batimetrisinin Duyarlı şekilde saptanabilmesini sağlamaktadır. Bu da ileride verilen model sonuçlarının doğruluğu yönünden büyük önem taşımaktadır.

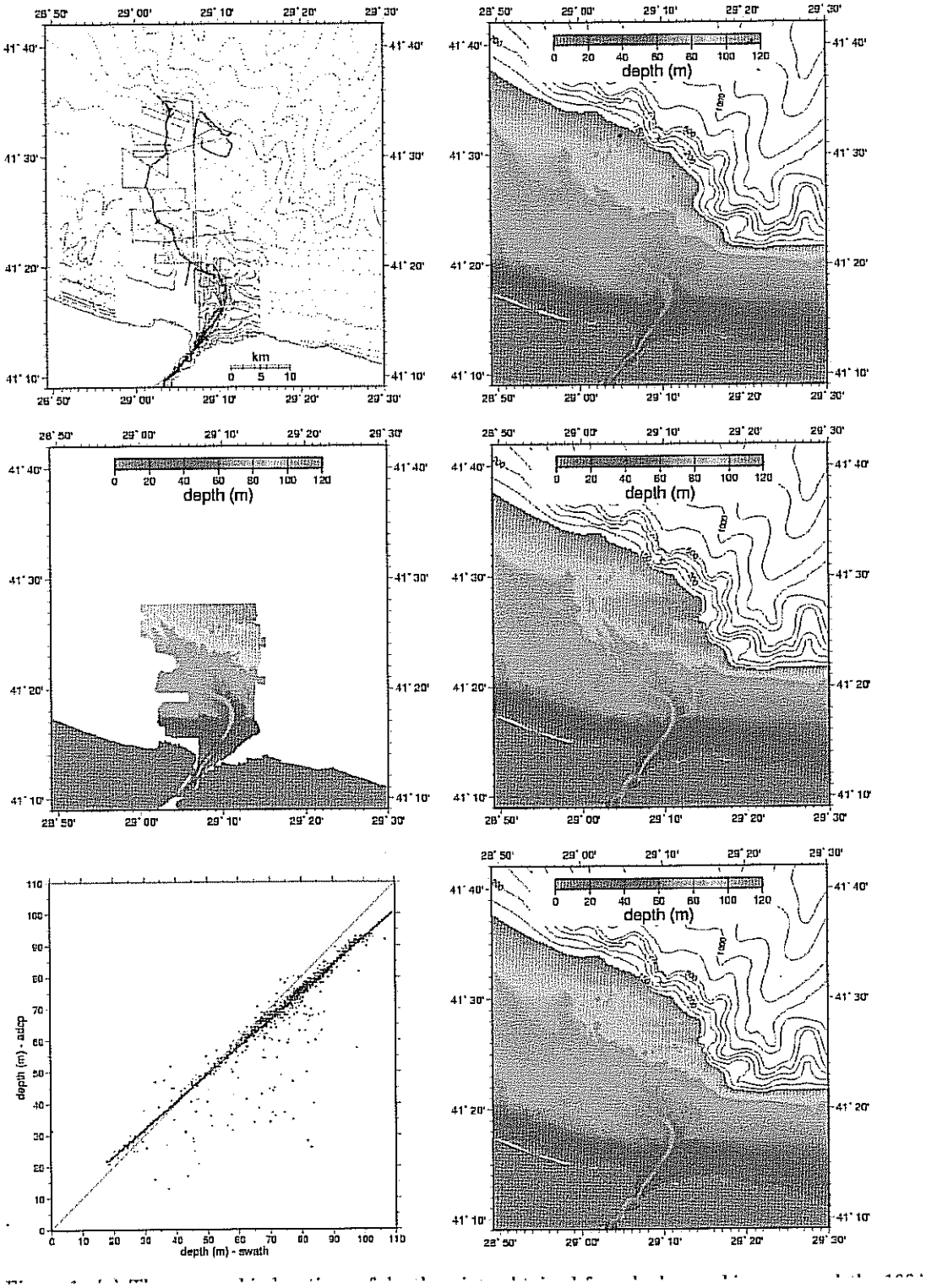

Şekil 2. (a) Hidrogrrafik haritalar ve 1994 ADCP ölçümlerinden elde edilen derinlik ölçüm noktaları, (b) bu ölçümlere dayanan taban topoğrafyası. (c) R/V ALLIANCE gemisinin 1995 ve 1996 seferlerinde SWATH cihazı ölçümleri ile ile elde edilen taban topoğrafyası, ve (d) bu ölçümler diğerleriyle birleştirildiğinde elde edilen taban topoğrafyası. (e) Yerleri çakışan ADCP ve SWATH derinlik ölçümleri arasındaki regresyon, ve (f) SWATH derinlik verileri regresyon modeline göre düzeltildikten sonra elde edilen birleşik taban topoğrafyası.

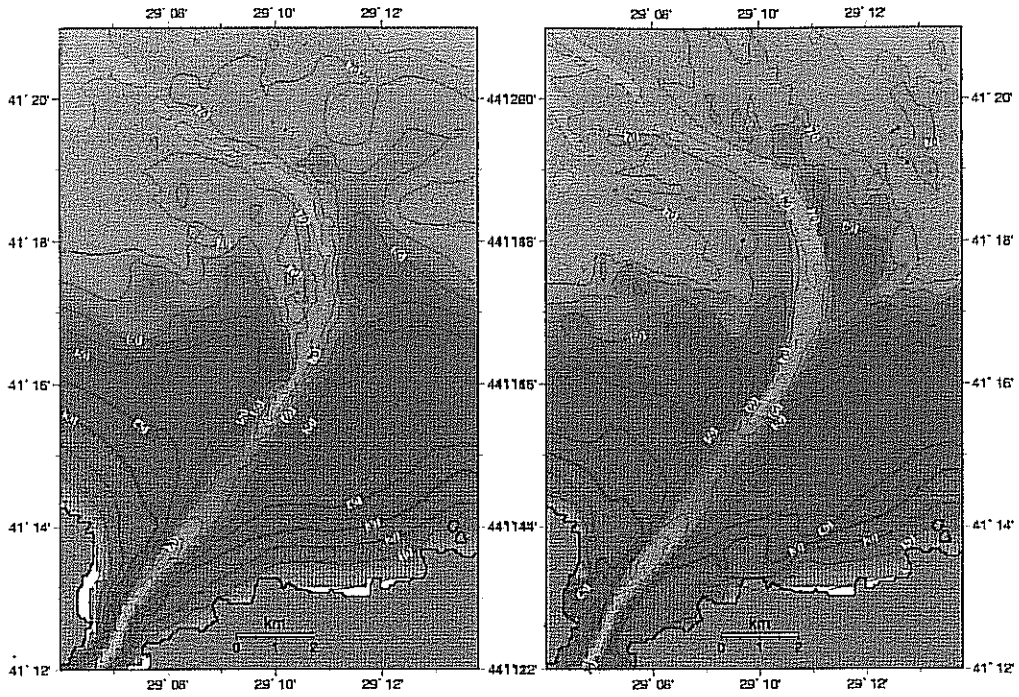

Şekil 3. İstanbul Boğazı Karadeniz çıkışında (a) hidrografik haritalar ve ADCP verilerine dayanan, veya (b) bu verilerle birlikte SWATH verilerine dayanılarak hazırlanan yüksek ayırımlı taban topğrafyası.

Şekil 2 ve 3 te ortaya çıkan şaşırtıcı ayrıntılar, verilerin birleştirilmesiyle ilk defa ortaya çıkmaktadır. Boğaz çıkışında kanal içerisinde ilerleyen Akdeniz suyunun zaman zaman yanlara doğru taşabileceği alçak kanallar bulunmaktadır (Şekil 3). Öte yandan, kıta sahanlığı üzerinde kıvrılarak ilerleyen kanalın varlığı öteden beri bilinmesine karşın ilk kez bu kadar ayrıntılı bir şekilde ortaya konulmaktadır. Şekil 2f'de görüldüğü gibi kanal Boğaz çıkışından 100m derinlikteki kıta sahanlığı sınırına kadar sürekli bir yapıya sahiptir ve kıta sahanlığı sınırına yakın bir nehir deltasını andıran üç ayaklı bir delta yapısı oluşturmaktadır. Gerçekten de şu anda tuzlu bir 'nehir' olan Akdeniz suyu bu kanaldan akmakta ve kıta yamacına ulaşmaktadır (Latif et al. 1991). Ancak, bu nehrin, bundan yaklaşık 7500 yıl önce Karadeniz'de su seviyesi şimdikinden 105m daha aşağıdayken (Ryan et al., 1998) deltası o zamanki kıyı çizgisinde olan bir nehir yatağı olup olmadığı açık değildir. Bazı yayınlarda Boğaz'da eskiden bulunduğu varsayılan nehrin kıta sahanlığı sınırına ulaşmadığı ileri sürülmüşse de (Demirbağ et al., 1999) gerek burada elde edilen ayrıntılı topoğrafya gerekse Akdeniz suyunun takip ettiği yol bunun aksini savunmaktadır.

Boğazlardaki alışveriş akımları ve karışım

Karadeniz ile Akdeniz'ın Ege Baseni arasında iletişim TBS aracılığıyla gerçekleşir. Bu sistemin su ve madde iletişimini en sınırlayıcı elemanı İstanbul Boğazı'dır, çünkü buradaki iki tabakalı iki yönlü akımlar özel bir hidrodinamik rejime uymaktadırlar. Ayrıca iklimsel değişimlerin ve kontrastların en önemli olduğu bir bölgede yer alması nedeniyle de (Özsoy, 1999) TBS komşu olduğu denizlerde büyük çevresel değişimleri kolaylıkla yaratabilecek bir yapıya sahiptir. Bunun en çarpıcı örneği, yakın zamanlarda ortaya konulduğu gibi (Ryan et al., 1998) son buzul çağını izleyen iklim değişimleri sonucunda Karadeniz'in su seviyesinin şimdikinden 100m daha alçak olduğu M.Ö. 5500 sıralarında, kapalı olduğu varsayılan İstanbul Boğazı'nın açılması ile o zamanlarda bir göl olan

Karadeniz'in Akdeniz sularınca birdenbire istila edilmesidir. Modern zamanlarda ise, İstanbul Boğazı'nın sahip olduğu özel akım rejimi ile Karadeniz - Akdeniz arası su seviyesi farklarının Boğazlar'dan geçen akılarda asimetrik değişimler yarattığı bilinmektedır (Özsoy et al., 1996, 1998).

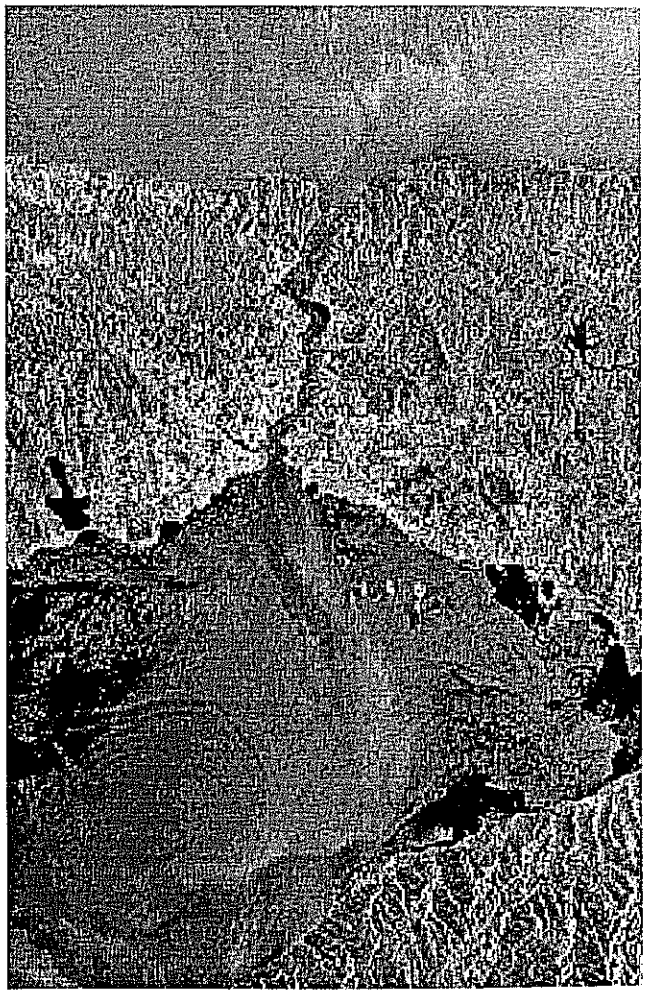

Şekil 4. Marmara Denizi'nin doğusu ve İstanbul Boğazı'nın ERS-1 uydusundan alınan Synthetic Aperture Radar (SAR) resmi, 25 Ekim 1995 8:49 GMT

İstanbul Boğazı akımları ve çevre denizlerdeki girişimleri Şekil 4 teki SAR uydu resminde açıkça gösterilmektedir. SAR (Synthetic Aperture Radar) verilerinde akıntılar genellikle yüzey pürüzleri (kısa yüzey dalgaları) üzerindeki etkilerinin algılanması ile görüntülenebilirler, ve ayrıca akıntıların sığ taban yapıları ile etkileşimleri de kullanılırsa bu verilerden taban topoğrafyasının elde edilmesi olanağı da vardır (Wensink and Campbell, 1997). Karadeniz'den kaynaklanan ve İstanbul Boğazı boyunca güneye akan yüzey akıntısı Marmara Denizi'ne bir yüzey ceti şeklinde girdiği bölgede belirgin bir şekilde gözlenebilmektedir. Bu cet akımı Marmara'nın Bozburun yarımadasına çarparak sığ güney kıta sahanlığı bölgesinde, yüzeye yansıyan yapısı SAR resminde izlenebilen iç dalgalar oluşturmaktadır. İstanbul Boğazı'nın kuzey çıkışında ise Belirgin bir şekilde taban topoğrafyasına karşılık gelen, özellikle Boğaz'dan Karadeniz'e uzanan

ve Akdeniz suyunu Karadeniz'e taşıyan kanal ve ilgili diğer yapılar gözlemlenmektedir (Özsoy, et al., 2000).

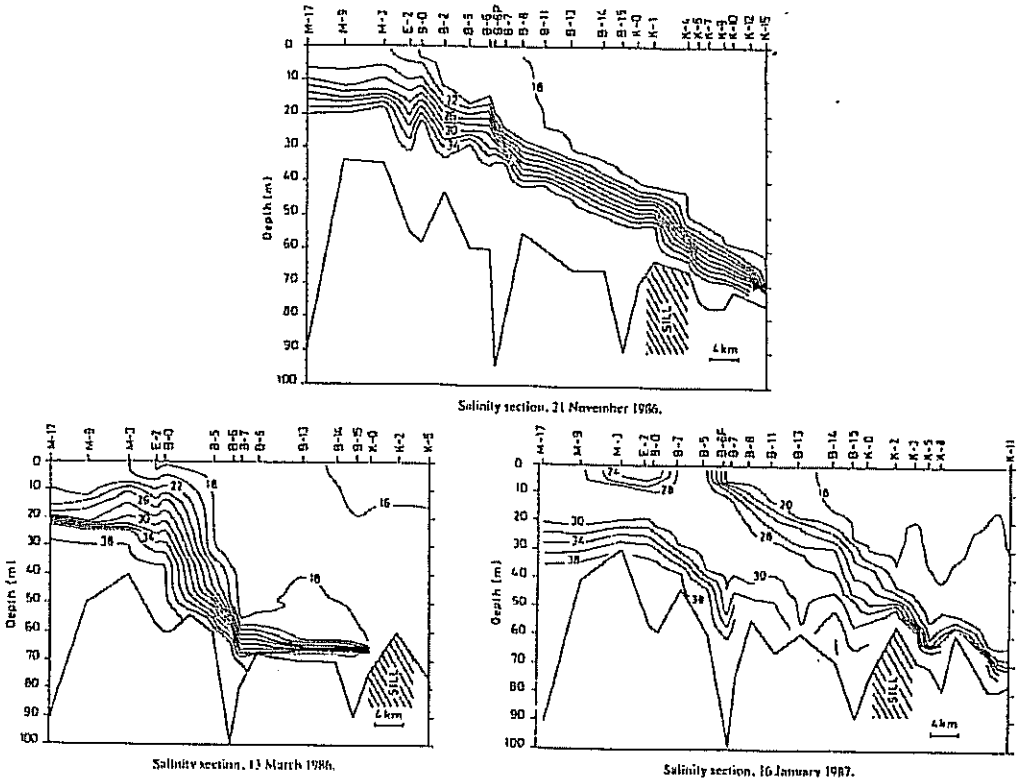

Figure 5. İstanbul Boğazı'nda tuzluluk dağılımı: (a) 'normal' durumdaki iki tabakalı alışveriş, (b) alt tabakanın kuzey eşiği'nde tıkandığı durum, (c) üst tabakanın bloke olduğu üç tabakalı akım durumu. Kuzey eşiğinde (K-2 istasyonu) ve güneydeki daralma bölgesinde (B-7 istasyonu) hidrolik kontrol bulunmaktadır.

İstanbul Boğazı Şekil 1b de gösterilen bazı önemli geometrik özellikleri sonucunda 'hidrolik kontrol'a sahip iki tabakalı boğaz akımları için özel bir durum olan 'maksimum alışveriş' (Farmer ve Armi, 1986) rejimine sahip görünmektedir (Ünlüata et al., 1990, Özsoy et al., 1998, Gregg ve Özsoy, 1999). Bu durum için gereken, iki tabakanin birden kontrol edildiği en dar kesit Boğaz'ın güney yarısında, ve sadece alt tabakanın kontrol edildiği eşik ise Boğaz'ın Karadeniz çıkışının 5 km kuzeyinde kanalın içinde, her ikisi de yoğunluk farkı açısından doğru yerlerde olmak üzere yer almaktadır (Şekil 1a). Hidrolik kontrol'un bulunduğu her iki kesitte de, iki tabakalı birleşik Froude sayısının $G^2 = 1$ olduğu ve akıntı hızının yerel iç dalga hızına oranla arttığı, akım rejiminde hızlı değişiklikler beklenir.

İstanbul Boğazı'ndan geçen akımlar, yerel çevreyi olduğu gibi Karadeniz'in anoksik dip sularının havalandırılması yoluyla, bu suların uzun dönemdeki karışımını ve fiziksel ve kimyasal yapısını doğrudan etkilerler (Latif et al., 1991; Ozsoy et al., 1993, 1995a, 1996, 1998, 2000; Özsoy ve Ünlüata 1997, 1998, Gregg et al., 1999, Gregg ve Özsoy, 1999). Uzun dönemli gözlemler, keskin bir yoğunluk tabakalaşması, boyuna doğrultuda hızlı değişimler, doğrusal olmayan hidrolik kontrol gibi etkenler ve her iki yöndeki akımların zaman zaman bloke olması gibi önemli fiziksel özellikleri bulunan İstanbul Boğazı'nın günlük, mevsimsel ve yıllararası zaman ölçeklerinde hidrodinamik olarak

Karadeniz-Akdeniz arası su seviyesi farkları, Karadeniz ve Marmara'daki rüzgar gerilimi dağılımı, barometrik basınç farkları ve bu denizlerdeki su bütçesi gibi faktörlerden etkilendiklerini göstermiştir (Özsoy 1996, 1998; Ducet et al., 1999). İstanbul Boğazı akımlarının iki tabakalı ve tek boyutlu modelleri (Oğuz et al., 1990) durağan koşullardaki akımlar ve hidrolik kontrol koşullarını anlamada yararlı olmuş ve ölçümlerden elde edilen kavramsal modeli doğrulamıştır.

Ortalama akılar durağan kütle dengesini sağlamalıdır; ancak her hangi bir andaki değişim akımları, komşu basenlerdeki zamana bağımlı meteorolojik ve hidrolojik zorlamalar sonucunda, bu ortalama değerlerden büyük sapmalar gösterir. İstanbul Boğazı taşınımının farklı zaman ölçeklerindeki değişkenliği tekrarlı ölçümlerle saptanmıştır (Özsoy *et al.*, 1986, 1988, 1994, 1995, 1996; Latif *et al.*, 1990, 1991, 1992; Oğuz *et al.*, 1990; Ünlüata *et al.*, 1990).

İstanbul Boğazı her iki yönde de etki eden ve zayıftan kuvvetliye kadar geniş bir aralıktaki barotropik zorlamalar aralığında çalışır. Olağan dışı koşullarda, her iki tabakadaki akımlar bloke olur ve bu durum her defasında bir kaç gün sürebilir (Şekil 5). Alt tabakanın bloke olduğu durumlar, genellikle Karadeniz'e tatlı su girdisinin arttığı ilkbahar ve yaz aylarında gerçekleşir. 'Orkoz' yerel adıyla anılan üst tabakanın bloke olması durumu ise daha çok yüzey akımını ters yöne dönebildiği veya yavaşladığı sonbahar ve kış aylarında oluşur (Özsoy *et al.*, 1986, 1988, 1994, 1996; Latif *et al.*, 1989, 1991). İstanbul Boğazı'nın seçilen enine kesitlerindeki kıntı-ölçer verileri ve Doppler akıntı profilleyicisi (ADCP) ölçümleri daha kesin bilgiler elde edilmesini sağlamış ve bazen aynı gün işerisinde bile önemli farklılık yaratan büyük geçici değişimler yaratabilmektedir (Özsoy *et al.*, 1994).

Bir daralma ve bir eşik kesitindeki iki kritik-ötesi geçiş bölümü dolayısı ile İstanbul Boğazı 'maksimum alışveriş' (Farmer ve Armi, 1986) rejimine sahip boğazlara en iyi örnektir (Özsoy *et al.*, 1986, 1996; Ünlüata *et al.*, 1990), ve bu durum sayısal modellerle de doğrulanmıştır (Oğuz *et al.*, 1990). İstanbul Boğazı özel durumunda basenler arası alışverişi önemli iki özellik belirler: (i) komşu basenlerdeki uygun rezervuar koşulları ve iki kesitteki hidrolik kontrol maksimum alışveriş sonucunu doğurur, ve (ii) eşiğin daha düşük yoğunluğa sahip olan basene diğerinden daha yakın olması durumunda, akım sistemi geometrik özelliklere duyarlı olan asimetrik bir davranış gösterir (Farmer and Armi, 1986; Armi and Farmer, 1987). İstanbul Boğazı'nın kontrollü akımları bir kaç günden bir kaç yıla kadar değişik zaman ölçeklerindeki zorlamalara farklı ve uzun dönemlerde oldukça değişken şekilde yanıt verir. Karadeniz ve Marmara Denizi su seviyesi ve Boğaz akımları su bütçesi ve barometrik basınç cinsinden zorlamalarla ilişkilidir (Özsoy *et al.*, 1990, 1996).

Çanakkale Boğazı'nda ise hidrolik kontrol'un bulunduğu tek yer Nara Burnu'dur, ve dolayısı ile buradaki su alışverişi 'sub-maksimal' olarak nitelenebilir (Farmer and Armi, 1986). Çanakkale Boğazı'nda tek hidrolik kontol bulunduğu ölçüm sonuçlarından bilindiği gibi sayısal modellerle de öngörülmüştür (Oğuz ve Sur, 1989).

17. yüzyılda İstanbul Boğazı'nda ilk ölçümleri ve konu ile ilgili bilimsel deneyleri yapan İtalyan Marsigli (Şekil 6a,b) yüzeyde Karadeniz'den Marmara'ya akan yüzey akıntısının altında yer alan, ve yerel balıkçıların çok iyi bildiği ters yöndeki akıntının hızını ölçmüş

OSSERVAZIONI
INTORNO
AL
BOSFORO TRACIO
OVERO
CANALE DI CONSTANTINOPOLI
Rappresentate in Lettera
ALLA SACRA REAL MAESTA
DI
CRISTINA
REGINA DI SVEZIA
DA
LVIGI FERDINANDO
MARSILII.

In Roma, Per Nicolò Angelo Tinassi 1681.
Con Licenza de' Superiori.

Şekil 6a. Luigi Ferdinando Marsigli'nin 1681 tarihli eserinin kapağı

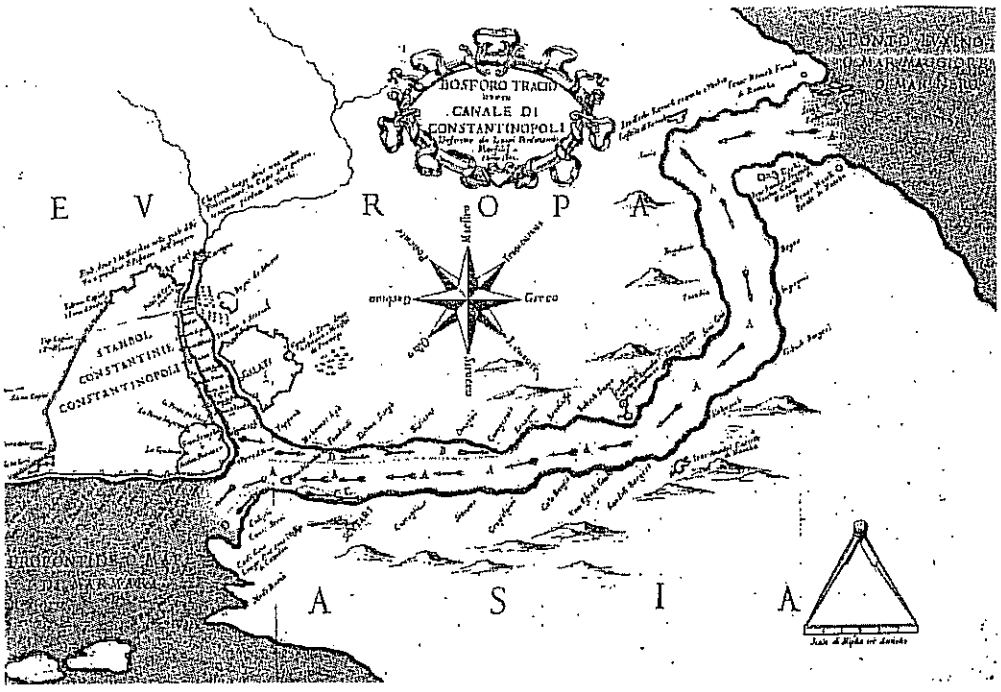

Şekil 6b. Marigli'nin ölçümlerine göre İstanbul Boğazı yüzey akıntıları

ve kuramsal olarak yoğunluk farklarından kaynaklandığını açıklamıştır (Marsigli, 1681). Bunu izleyen yıllarda yapılmış eksik gözlemlere dayanan bazı yanlış yorumlar sonucunda alt akıntının her zaman olup olmadığı tartışılmış ve hatta bu yüzyılın başında tekrarlanan eksik gözlemler sonucunda aynı konu zaman zaman yeniden ortaya çıkmışsa da,

yeterli zaman dilimini ve değişken koşulları kapsayan modern ölçümler sayesinde, her iki tabakada da akımın zaman zaman kısa süreli olarak bloke olduğu özel koşullar dışındaki uzun sürelerde iki tabakalı akım koşullarının genellikle geçerli olduğu (Ünlüata et al., 1990; Özsoy et al., 1998; Gregg et al., 1999), ve bunun sonucunda Karadeniz'e çıkan suların kıta sahanlığındaki akımı (Latif et al., 1991; Gregg ve Özsoy, 1999; Özsoy et al., 2000) ile kıta sahanlığı sonrasında ve Karadeniz iç sularındaki girişimleri (Özsoy et al., 1993; Özsoy ve Beşiktepe, 1996) ortaya konmuştur.

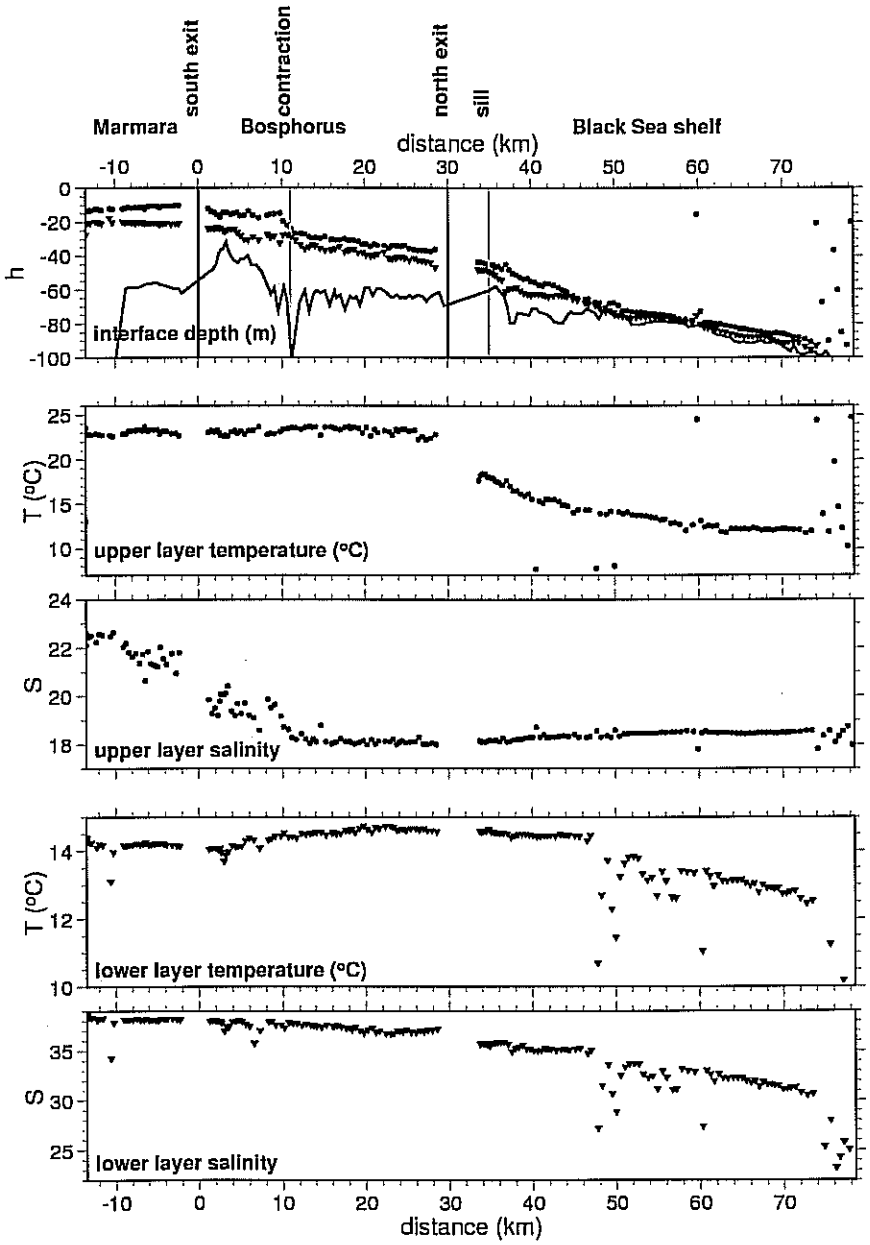

Şekil 7. 13-19 Eylül 1994 tarihlerinde İstanbul Boğazı'nda 179 istasyonda AMP cihazı ile ölçülen profillerden elde edilen (a) üst ve alt tabaka sınırları, (b), (c) üst tabaka ortalama sıcaklık ve tuzluluğu, (d), (e) alt tabaka ortalama sıcaklık ve tuzluluğu. Alt ve üst tabaka sınırları taban ve yüzeydeki tuzluluk değerleri arasındaki farklar temel alınarak belirlenmiştir.

Yüzey akıları ve her iki yönde de etkili olan türbülanslı girişim ('entrainment') nedeniyle TBS'den geçen su kütlelerinın katetikleri yol boyunca sürekli olarak değişime uğradıkları bilinmektedir. Değişimin en hızlı olduğu yerler ise özellikle Boğazlar'ın hidrolik kontrol sonrası bölgeleri (İstanbul Boğazı güneyi ve Karadeniz eşiği kuzeyi, Çanakkale Boğazı'nda Nara Burnu batısı) ile komşu denizlere bağlandıkları çıkış bölgeleridir (Ünlüata et al., 1991).

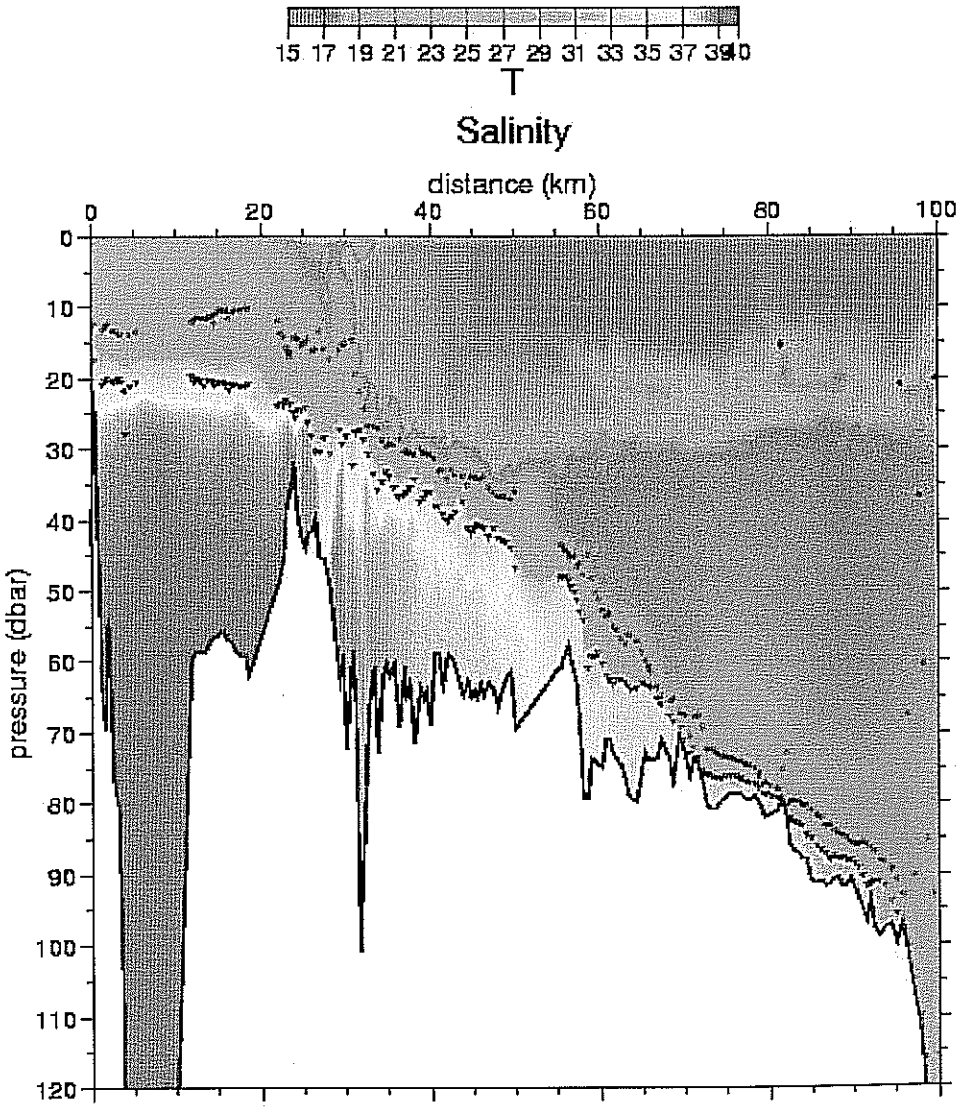

Şekil 9. 13-19 Eylül 1994 tarihlerinde İstanbul Boğazı'nda 179 istasyonda AMP cihazı ile ölçülen profillerden elde edilen tuzluluk kesiti. Üst ve alt tabaka sınırları noktalarla gösterilmiştir. (Özsoy et al., 2000).

Tuzluluk / sıcaklık ve akıntılar gibi parametrelere ek olarak türbülans parametreleri bakımından İstanbul Boğazı'nda bugüne kadar en detaylı ölçümler 1994'teki bir ortak çalışmada R/V BİLİM gemisi'nde elde edilmişlerdir (Gregg et al., 1999, Gregg ve Özsoy, 1999, 2000). Bu çalışmada türbülans ölçümleri için serbest düşme halinde kullanılan AMP (Advanced Microstructure Profiler) cihazı ile çok sık aralıklarla

fiziksel özelliklerin profilleri de elde edilmiştir. İstanbul Boğazı boyunca 179 profil kullanılarak elde edilen sıcaklık ve tuzluluk değişimleri Şekil 7 ve 8 de gösterilmiştir (Özsoy et al., 2000). Ayrıca, bir ara tabaka tarafından birbirinden ayrılan alt ve üst tabaka sınırları da her istasyonda işaretlenmiş olan bu Şekillerde türbülanslı girişim sonucunda her iki tabakanin ortam özelliklerinin Boğaz boyunca ve birbirine ters yönde hızlı bir şekilde değiştiği ve Karadeniz kıta sahanlığı'nda incelerek yayılan alt tabakanın özelliklerinin burada aynı yolla değişmeye devam ettiği izlenebilmektedir. Korunmalı bir fiziksel özellik olan tuzluluğun üst tabakada en hızlı değiştiği yer ise hidrolik kontrol'un bulunduğu Boğaz'ın en dar kesitinin güneyindeki karışım (hidrolik sıçrama ve Marmara çıkışındaki cet) bölgesinde bulunmaktadır.

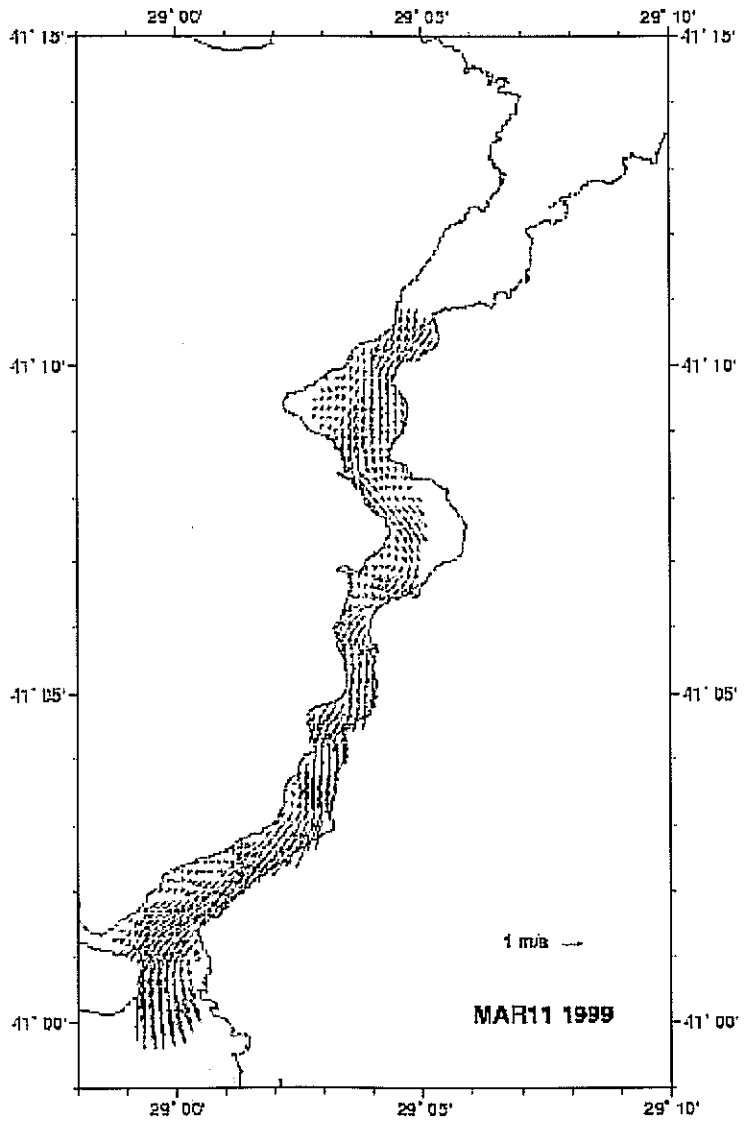

Sekil 9. 11 Mart 1999 te İstanbul Boğazında yapılan ayrıntılı ADCP akıntı ölçümlerine dayanılarak gride interpole edilmiş akıntılar.

1998 ve 1999 yıllarında yapılan bazı ölçümlerde ise İstanbul Boğazı içindeki geometrik ve batimetrik değişimlerin, örneğin küçük ölçekli körfezler ve burunlar gibi kıyısal yapıların akıntılara etkileri incelenmiştir (Şekil 9). Bu gibi etkilerin İstanbul Boğazı'ndan geçen gemilerin navigasyonunu olumsuz etkileyerek sıklıkla kazalara neden verdiği bilinmektedir. Kıyısal bölgelerde akıntının fazlasıyla hızlandığı veya ters yöne döndüğü yerlerde, önceden tahmin edilemeyen bu ani değişiklikler, gerek yüzen cismin eylemsizliği, gerekse kumandadaki gecikmeler sonucunda gemilerin manevrasını zorlaştırmakta ve gemi kazalarına yol açmaktadır. Şekil 9 da özellikle Beşiktaş, Çengelköy, Bebek, Yeniköy, Paşabahçe-Beykoz, Umuryeri ve Büyükdere gibi koylarında çevrimler ve ters akıntılar oluşmakta, ayrıca Boğaz'ın kesitindeki genişleme ve daralmalar nedeniyle akıntı hızları yerel olarak ve çevresel zorlamalarla zamana göre değişmektedir. Çeşitli zamanlarda elde edilen üç boyutlu akıntılar Merz (Möller, 1927) tarafından Birinci Dünya Savaşı öncesinde gözlenen akıntı çevrimleri ile benzerlik arzetmektelerse de çok daha ayrıntılı bilgiler içermektedir. Yine bu çevrimlerden olan Beşiktaş önlerindeki belirgin ters akıntı bundan yaklaşık 400 sene önce Kont Marsigli (1681) tarafından da gösterilmiştir.

Bir kaç yıl boyunca aylık zaman ölçeklerinde İstanbul Boğazı'nda yatay kesitler üzerinde tekrarlanan ADCP ölçümleri entegre edilerek alt ve üst tabaka akıları ayrı ayrı hesaplanmıştır. Bu ölçümler Karadeniz'den gelen üst tabaka akımının ve dolayısı ile toplam akımın ilkbahar-yaz aylarında artma ve sonbahar-kış aylarında azalması şeklinde genel bir mevsimselliğin dişinda belirgin bir zamana bağlı değişim tanımlamamaktadır, çünkü diğer ölçümlerin de ortaya koyduğu gibi, kısa süreli değişimler Boğaz akımlarının en belirgin özelliğidir (Özsoy et al., 1996, 1998).

İstanbul Boğazı'nın alt sularına verilen İstanbul Şehri'nin atıksularının üst sulara ne ölçüde karıştığı, yüzey sularına ulaşıp ulaşmadığı, üst tabaka akımlarıyla hangi oranda Marmara Denizi'ne döndüğü, gibi sorular zaman zaman tartışılan konular olmuştur. Bu konudaki en güvenilir tahminler, ortalama tuz ve su dengesine dayanan hesaplamalardır (Ünlüata et al., 1990) ve atıksu sisteminin tasarımında da en temel kriter olarak kullanılmışlardır. Buna rağmen, öncelikle Ahırkapı'da hizmete girmiş bulunan difüzör sistemleri ile ortama verilen ve deniz ortamına göre farklı yoğunluk ve kaynak özellikleri ile tanımlanan atıksuların bu tahminlerde elde edilenden farklı bir davranış gösterebileceği kaygısı kamuda ve ilgili kesimlerde duyulmuştur (Orhon et al., 1984). Bu nedenle yapılan genel izleme çalışmalarına ek olarak atıksuların izlek maddeler (boya) ve akustik yöntemlerle doğrudan ölçülmesini amaçlayan çalışmalar da yapılmıştır. Alt ve üst akımların bloke olduğu 'olağanüstü' koşulları da kapsayan doğrudan ölçümlerle, Ahırkapı deşarjı'ndan verilen atıksuların alt akımda öngörülen oranlarda seyrelerek Karadeniz'e ulaştığı ve oldukça zorlayıcı koşullarda bile atıksu girdisinin yüzeye ulaşan miktarlarının az miktarlarda olduğu gösterilmiştir (Özsoy et al., 1995; Beşiktepe et al., 1995).

Türk Boğazlar Sistemi ile Komşu Denizler arası Yoğun Su Alışverişi ve Yayılımı

Model ve Yöntem

Karadeniz'de Akdeniz kaynaklı suların yayılımını incelemek için kullanılan model Jungclaus ve Backhaus (1994) tarafından geliştirilmiş ve İstanbul Boğazı Karadeniz çıkışı'ndaki karmaşık taban topoğrafyasının etkilerini de içerecek şekilde kullanılmıştır.

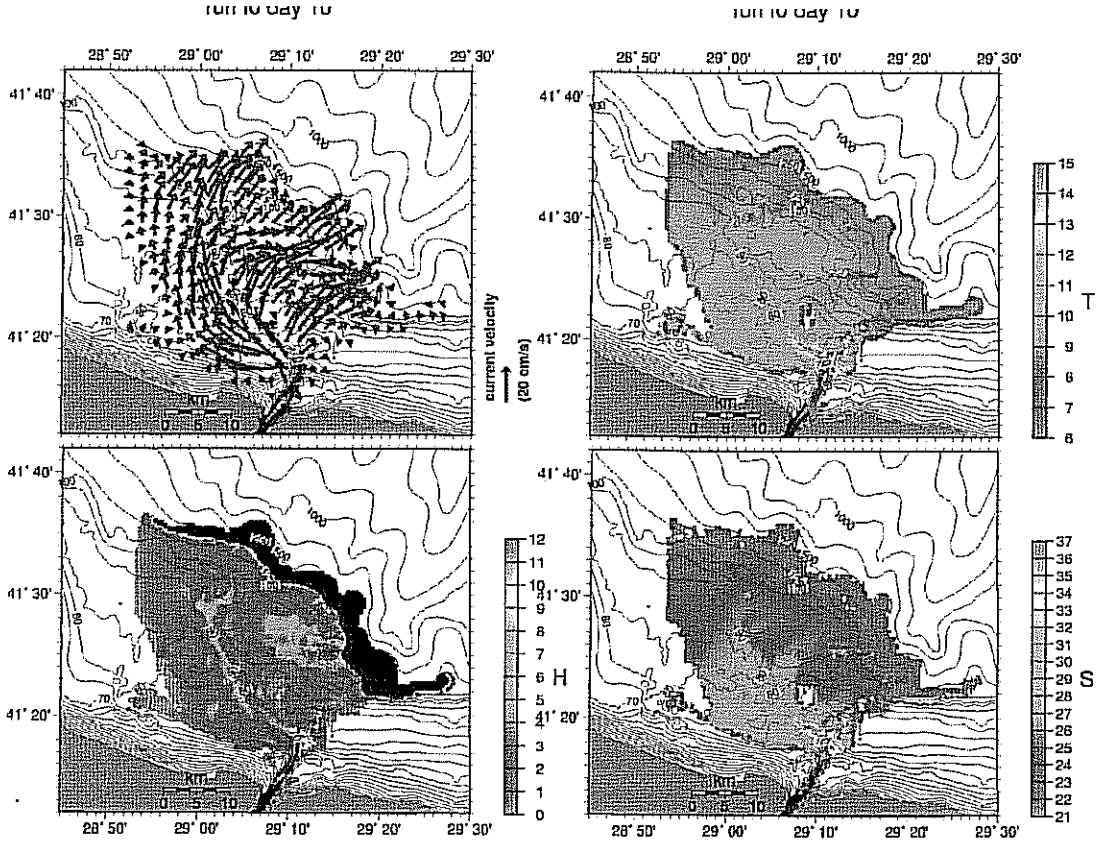

Şekil 10. İstanbul Boğazı Karadeniz kıta sahanlığında, model sonuçlarına göre, başlangıçtan 10 gün sonra tabanda yayılan Akdeniz sularının (a) akım hızı (cm/s), (b) tabaka kalınlığı (m), (c) sıcaklık (°C) ve (d) tuzluluğu. Bu merkezi denemede yatay ve taban sürtünme katsayıları A_h=150 m^2/s ve r=0.003, Boğaz çıkışındaki hız, tuzluluk, sıcaklık ve tabaka derinliği başlangıç koşulları sırasıyla u_o=0.7 m/s (yön kuzeyden 45°), S_o=37, T_o=14.5°C, H_o=40m alınmıştır. Modelin yatay ayırımı 200m dir. Hız vektörleri her 10 noktada bir çizilmiştir. Kıta eğimi bölgesindeki siyah bölge tanımlanan kontur sınırlarının dışında kalmaktadır.

Detayları anılan kaynaklarda bulunabilecek ve Hüsrevoğlu (1999) tarafından da tarif edilen 'reduced gravity' dinamiğine uyan modelde, 'primitive' denklemler temel olmakla birlikte, yoğunluk fazlası nedeniyle tabanda yayılan sular tek bir tabaka ile temsil edilir ve taban sürtünmesi ve yatay sürtünme kuvvetleri ile, çevresel sulardan tabaka içerisine türbülanslı girişim de dikkate alınır.

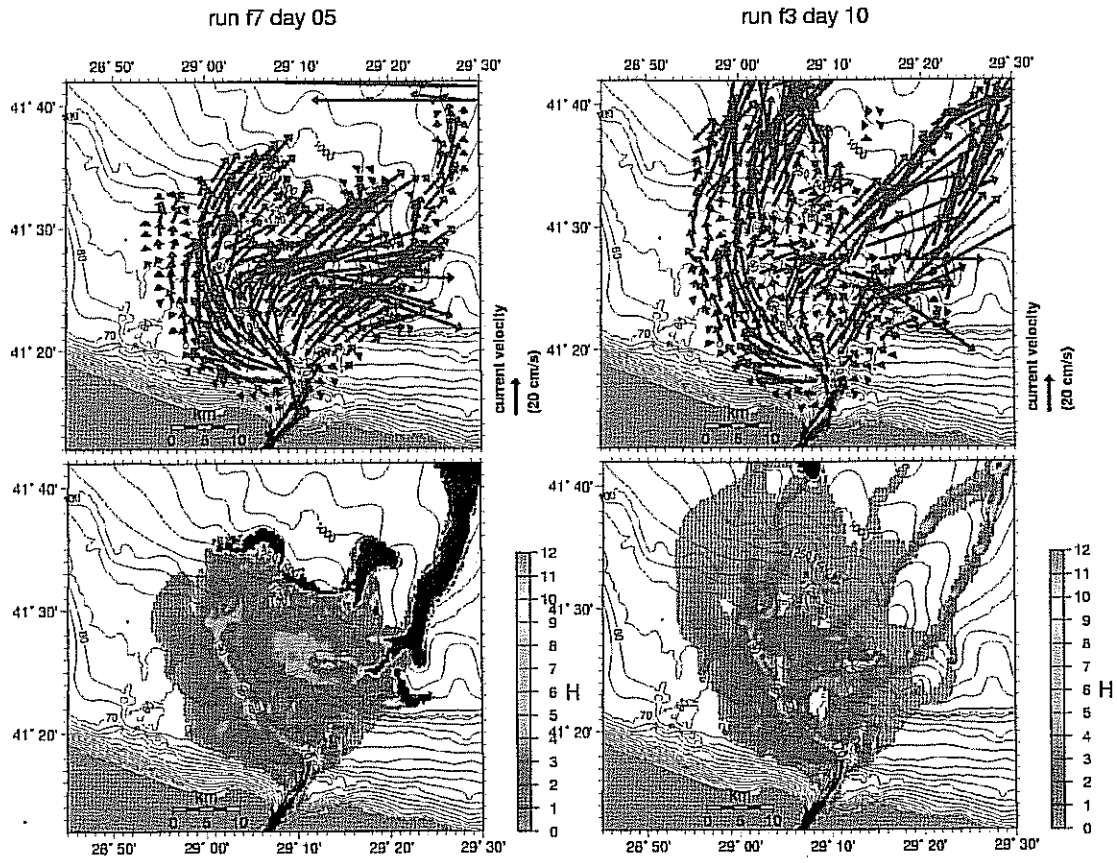

Şekil 11. (a) Sürtünme katsayısı r=0.001 için, (b) türbülanslı girişim ihmal edildiği durumda, başlangıçtan 10 gün sonra tabanda yayılan Akdeniz sularının tabaka kalınlığı (m). Diğer parametreler Şekil 12 ile aynıdır.

Akdeniz Suları'nın Karadeniz Kıta Sahanlığı'nda Yayılımı

Karadeniz'de Akdeniz kaynaklı suların yayılımını incelemek için, yukarıda ayrıntıları verilen İstanbul Boğazı Karadeniz çıkışı'ndaki karmaşık taban topoğrafyası dikkate alınmıştır ve 200m yatay ayırımla modelde kullanılmıştır. Ayrıca, Karadeniz çevresel tuzluluk ve sıcaklık tabakalaşması 1988 koşullarını temsilen R/V KNORR Leg 4 ölçümleri (Özsoy et al., 1993) temel alınarak belirlenmiştir.

Modelin tahmin edilen parametrelerle merkezi bir denemesinden elde edilen sonuçlar Şekil 11 de verilmektedir. Başlangıç koşullarında sadece İstanbul Boğazı çıkışında verilen ilk hız, derinlik ve tuzluluk değerleri modelin çalışması süresince sabit tutulmuş ve 10uncu günde akımın hemen hemen durağan hale ulaştığı durumdakı sonuçlar verilmiştir. 1995 ve 1996 tarihlerinde Karadeniz çıkış eşiğinde yapılan ölçümlerde boyutsuz taban sürtünme katsayısının değerleri r=0.003-0.015 aralığında bulunmuştur (DiIorio et al., 1996, 1997). Modelde de taban sürtünme katsayısı bu büyüklükte alınmıştır ve özellikle kıta sahanlığında yayılan Akdeniz suyu özelliklerinde bariz bir fark yaratmamıştır ve sonuçlar ölçümlerle (Latif et al., 1991; Gregg and Özsoy, 1999) uyumludur. Normal değerlere sahip parametreler için Akdeniz suyu püskülü kıta sahanlığı sınırına kadar seyrelerek geldiği için ve burada aniden değişen eğim ile hızlanıp çevreden daha çok su girişine neden olduğu için 500m derinlikten daha derine inememektedir.

Sürtünme katsayısın r=0.001 değerine düşürüldüğü, buna karşılık başlangıç hızının u_o=1.0 m/s değerine artırıldığı durumda akıntı hızı

artmakta ve sonuçta yoğun Akdeniz suyu kıta sahanlığından derine doğru sızarak Karadeniz'in tabanına kadar inebilmektedir (Şekil 11a). Benzer şekilde eğer türbülanslı girişim akısını tamamen ihmal etseydik sonuç Şekil 11b deki gibi olurdu ve seyrelme olmadığı için yoğun su Karadeniz'ın tabanına kadar ulaşabilirdi. Ancak bu durumun istisna olacağı ve gerçek duruma karşılık gelmediği hem burada verilen model sonuçlarından (Özsoy et al., 2000) hem de ölçümlerden (Özsoy et al., 1993, Özsoy and Ünlüata, 1997, 1998) bellidir.

Akdeniz Sularının Marmara Denizi'nde Yayılımı

Çanakkale Boğazı'ndan giren Akdeniz tuzlu suları, giren sularla Marmara alt suları arasındaki yoğunluk farkına ve Marmara alt sularının tabakalaşmasına bağımlı olarak topoğrafya boyunca dengeye ulaştıkları derinliğe kadar batarlar (Beşiktepe et al., 1994). Denge derinliğini, tabakalaşma kadar bir yoğunluk akıntısı şeklindeki taban püskülünün türbülanslı girişim hızı ile çevreden ithal ettiği sıcaklık ve tuzluluk da belirler (Beşiktepe et al., 1993). Yoğunluk farkının fazla olduğu durumlarda giren sular tabana kadar batabilir, aksi halde ise orta derinliklerde dengeye ulaşabilir. Bu durumun sonucu olarak Marmara Denizi alt sularında biri 200-300m derinliklerde, diğeri ise tabana yakın ve batıdan doğuya doğru dil şeklinde uzanan iki derinlikte tuzluluk anomalileri görülmektedir.

Ege Denizi'nden Çanakkale Boğazı'nın alt tabaka akımı ile Marmara Denizi'ne giren, ve buradaki deniz suyuna oranla göreceli olarak daha yoğun olan Akdeniz Suyu'nun Çanakkale Boğazı içerisindeki davranışı oldukça karmaşıktır. Öncelikle Çanakkale Boğazı'nın alışveriş akımları dinamiği ve taban topoğrafyası, İstanbul Boğazı'nda olduğu gibi burada da alt su özelliklerinin değişiminde etkindir. Çanakkale Boğazı'nın batı kesiminde iki tabakalı ve etkileşimli bir akım yer alırken, doğuda Boğaz'ın bir koni şeklinde genişlemesi ve taban topoğrafyasının bu geniş kanal içerisinde dar bir taban kanyonu oluşturması (Şekil 1a ve 1c) nedeniyle Ege Denizi kaynaklı yoğun sular üst tabakadan ayrılır ve burada üç tabakalı bir yapı oluşur (Ünlüata ve Özsoy, 1986, Özsoy et al., 1986, 1988).

Tabandaki yoğun su, derin bölgeye doğru hareketinde, önce Marmara ile Çanakkale Boğazı'nın birleştiği koni şeklindeki bölgenin güney kıyısı boyunca uzanan ve giderek derinleşen (en derin yeri ~60m) kanyon şeklindeki taban topoğrafyasını izler. Güney kıyıdaki bu kanyon ile, Marmara Denizi'nin derin üç çukuru'ndan en batıdaki derin çukur (derinlik >1000m) arasındaki bağlantı kuzeydoğu yönünde yavaş bir eğimle sağlanır. Ancak yaklaşık 80m derinlikten sonra, eğimin hızla arttığı derin bir kanyon yapısı ile kıta sahanlığı eğimi kuzeydoğu yönünde derin çukura bağlanır (Şekil 1c). Derin çukurların, en batıdaki de dahil olmak üzere kıta sahanlığına bağlanan derin yamaçları çok diktir. Üç derin çukurdan birbirine oldukça yakın olan en batıdaki ikisi arasındaki bağlantı 700m derinlikteki bir eşikle sağlanır. Oysa orta basenle doğu basen arasındaki bağlantıyı yaklaşık 50km uzunlukta ve en sığ yerinde 600m derinliği olan bir eşik sağlar (Şekil 1a).

Çanakkale Boğazı'ndan giren yoğun suların özellikleri, mevsimsel ve yıllararası değişkenlik göstermektedir (Özsoy et al., 1986, 1988, Beşiktepe *et al.*, 1994, Hüsrevoğlu, 1999). Bu suların Marmara Denizi

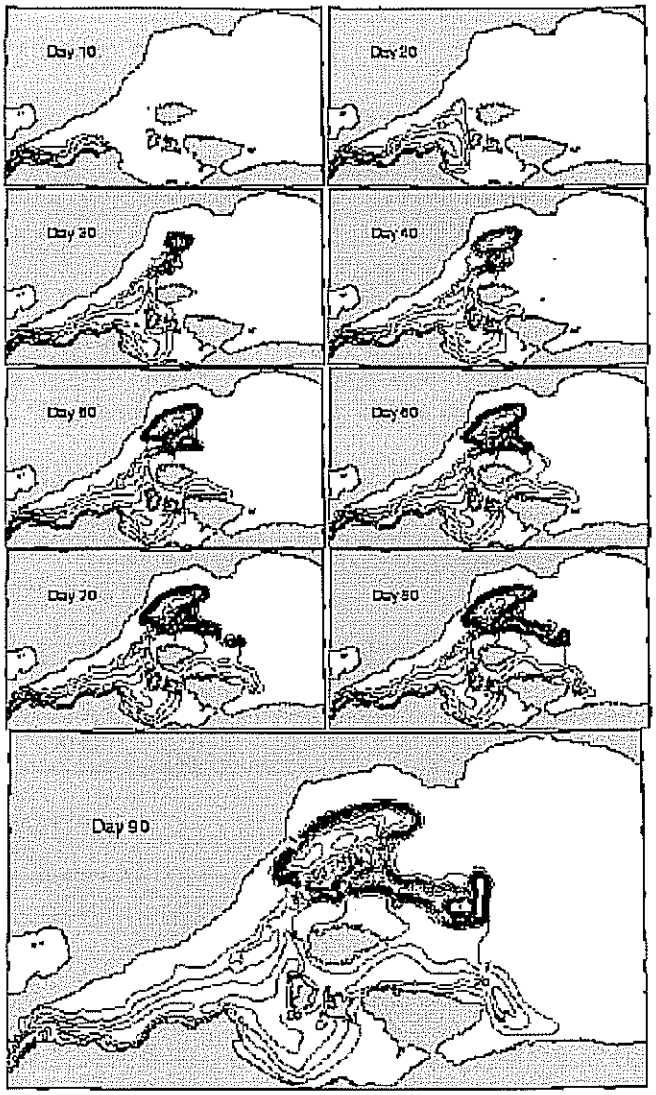

alt sularını yenilemesi, derine batan püskül (plume) ve iç suların sadece düşey yöndeki değişikliklerinin incelendiği bir 'filling box' modeli ile incelenmiş ve tuzluluk, sıcaklık ve oksijenin Marmara Denizi alt sularındaki değişimleri gerçeğe yakın bir şekilde hesaplanmıştır

Şekil 12. Marmara Denizi alt sularına Çanakkale Boğazı'ndan giren Akdeniz kaynaklı suların yoğunluk akıntısı oluşturarak basen tabanına çökmesinin 'reduced gravity' model simulasyonlarında, başlangıçtan sonraki 90 gün içindeki gelişimi. Çanakkale Boğazı alt tabakadan giren suların ilk hızı 0.3 m/s, ara yüzey derinliği 26.5m, sıcaklığı T=14.92, tuzluluğu S=38.86, Marmara iç sularının sıcaklığı T=14.5, tuzluluğu S=38.5 alınmıştır. Boyutsuz taban sürtünmesi katsayısı r=0.003, yatay karışım katsayısı A_H=50m^2/s alınmıştır. Doğrusal olmayan terimlerin, sürtünme ve Coriolis etkilerinin dahil edildiği modelin bu uygulamadaki yatay ayırımı 750m ve integrasyon zaman aralığı 60s dir (Hüsrevoğlu, 1999).

(Beşiktepe, 1993). Bu modelden farklı olarak, Çanakkale Boğazı'ndan giren yoğun suların taban topoğrafyası, başlangıç koşulları ve tabakalaşmaya bağımlı olarak tabanda yayılması ve baseni doldurması, daha ayrıntılı dinamiksel koşulları içeren bir 'reduced gravity' modeli ile incelenmiştir (Hüsrevoğlu, 1999).

Şekil 12 de merkezi parametrelerin seçimi durumunda taban püskülünün kalınlığının 90 günlük bir süredeki gelişmesi gösterilmiştir. Homojen bir su kütlesinin bulunduğu farzedilen Marmara Denizi iç sularına göre daha yoğun olan Çanakkale alt suları, yerçekimi ve dünyanın dönmesinin etkisiyle önce kıta sahanlığında geniş koni bölümünün güneyindeki derin

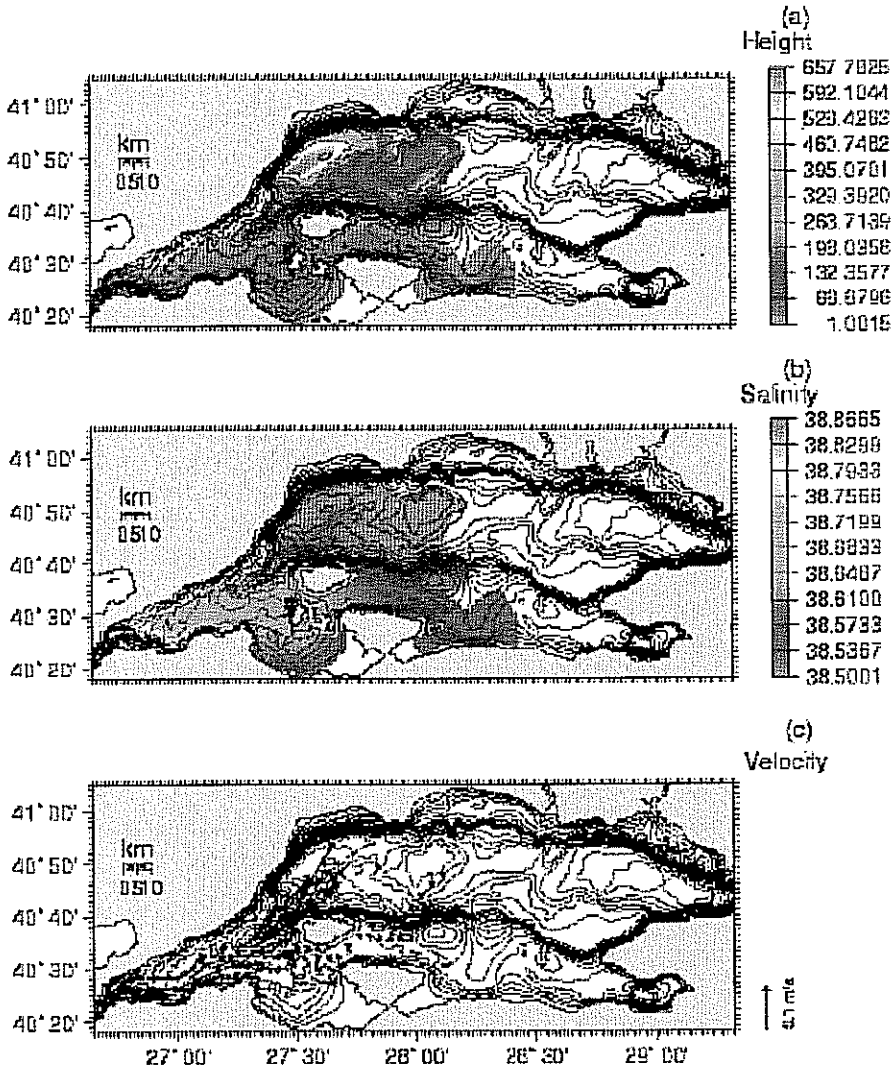

Şekil 13. Çanakkale Boğazı'ndan giren Akdeniz kaynaklı suların Marmara Denizi'ndeki yayılmasının Şekil 14 te verilen simulasyonunda başlangıçtan 180 gün sonra yoğun dip tabskasının (a) kalınlığı (m), (b) tuzluluğu ve (c) akıntıları (m/s) (Hüsrevoğlu, 1999).

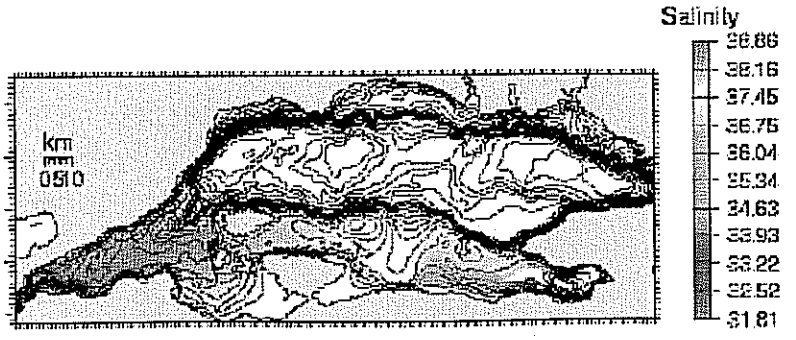

Şekil 14. Marmara Denizi alt sularına Çanakkale Boğazı'ndan giren Akdeniz kaynaklı suların yoğunluk farklarının az olduğu durumda güney kıta sahanlığı boyunca yayılımı sonucundaki tuzluluk dağılımı (Hüsrevoğlu, 1999).

kanyon boyunca ilerlemekte, başlangıçtan yaklaşık 20 gün sonra bu kanyonun sona erdiği bölgeye ulaşmakta ve yaklaşık 30 gün sonra da derin batı çukuruna doğru akmaya başlamaktadır. Bundan sonraki bir ay içerisinde batı çukurunu dolduran yoğun sular başlangıçtan iki ay sonra 700m derinliğindeki eşiği aşarak ikinci çukura doğru hareket etmektedir. Coriolis etkisi nedeniyle akım yönünün sağına doğru sapma gösteren yoğun su damarı öncelikle Marmara Adası kuzeyindeki batı çukuru ve eşik geometrisini güney kıta sahanlığına bağlayan dik kıta yamacı boyunca ilerlemektedir ve başlangıçtan 80 gün sonra orta çukuru doldurmaya başlamaktadır. Modelin toplam çalışma süresi olan 180 günde orta çukur güney yamaçtan beslenmeye devam etmekte fakat bu sürede tümüyle dolmamaktadır (Şekil 12). Şekil 12 ve 13 te derin çukura akan sular dışında, Marmara Adası ve Kapıdağ Yarımadası arasından güney kıta sahanlığı boyunca sızan yüksekliği en fazla 20m olan ince bir su damarının tabanda batıya doğru ilerlediği görülmektedir. Bu damar, yoğun suların Coriolis ve taban topoğrafyasının etkisiyle sığ kıta sahanlığı boyunca doğuya doğru sızmasıyla oluşmaktadır.

Şekil 14 te ise ilk yoğunluk farkının az olduğu ya da karışarak azaldığı, taban püskülünün Coriolis etkisi ile sığ güney Marmara kıta sahanlığı boyunca ilerleyerek derin basene batmadığı başka bir durumdaki tuzluluk dağılımı görülmektedir. Bu durumda tuzlu sular alt tabakada Gemlik Körfezine kadar ilerleyebilmektedir.

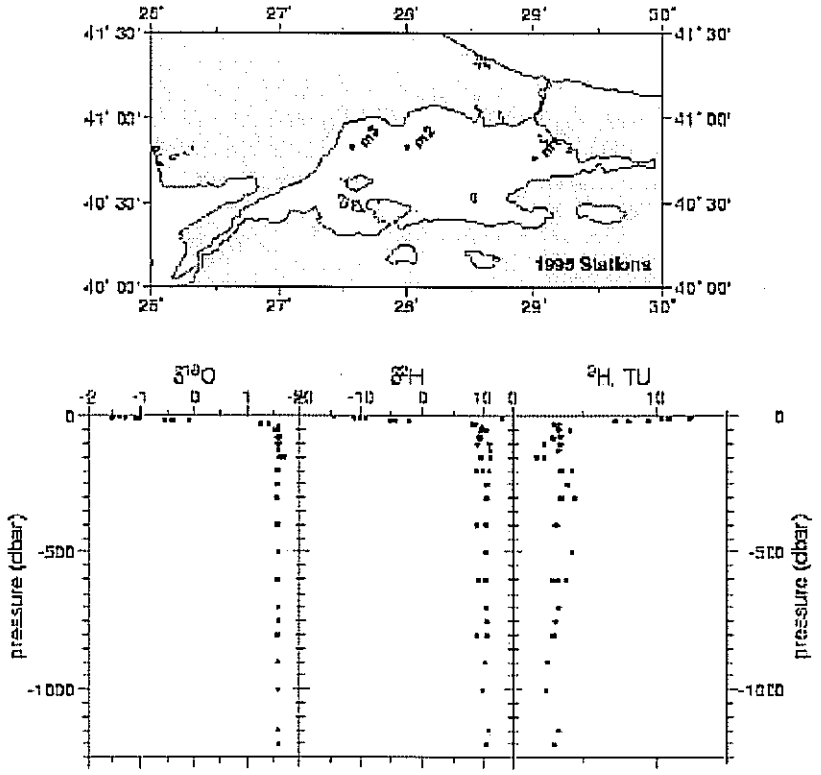

Şekil 15. Marmara Denizi'nde radyoizotop ölçüm istasyonları ve elde edilen oksijen-18, deuterium ve tritium profilleri (Rank et al., 1998).

İzlek Madde Yöntemi ile Su Kütleleri Analizi

Marmara Denizi alt sularının Çanakkale Boğazı'ndan giren sularca yenilenmesinin yoğun suların bazı durumlarda tabana kadar batması, diğer durumlarda da güneydeki kıta sahanlığını izleyerek orta derinliklerde olduğu hem yukarıdaki model sonuçları ile, hem de ölçümlerle (Beşiktepe et al., 1993, 1994) gösterilmiştir.

Marmara Denizi sularının yenilenme süreçlerinin araştırılması için, oksijen-18 ve deuteryum dengeli izotopları ve nükleer silah kaynaklı tritium izleyiciler kullanılmıştır (Rank et al., 1998). Bu araştırmalarda Marmara sularının dengeli (doğal) izotoplar yönünden Akdeniz ve Karadeniz sularının sürekli bir karışımı olduğu, tritium stokları açısından ise alt suların yeterli yenilenmeye sahip Akdeniz sularını yansıttığı izlenmiştir (Şekil 15). Diğer iz maddelerinden elde edilen sonuçlar doğrultusunda (Beşiktepe et al., 1993, 1994) orta derinlikte ve tabanda yüksek Trityum bulunması Marmara Denizi'ne bu derinliklerde girdi olduğunu doğrulamaktadır.

REFERANSLAR

Baştürk, Ö., Saydam, C., Salihoğlu, İ. and A. Yılmaz (1986). Oceanography of the Turkish Straits - First Annual Report, Volume III, Health of the Turkish Straits II: Chemical and Environmental Aspects of the Sea of Marmara, Institute of Marine Sciences, METU, Erdemli, İçel.

Baştürk, Ö., Saydam, C., Salihoğlu, İ. and A. Yılmaz (1988). Oceanography of the Turkish Straits - Second Annual Report, Volume II, Health of the Turkish Straits: Chemical and Environmental Aspects of the Sea of Marmara and the Golden Horn, Institute of Marine Sciences, METU, Erdemli, İçel, 130p.

Baştürk, Ö., Tuğrul, S., Yilmaz, A., Saydam, C. (1990). Health of the Turkish Straits: Chemical and Environmental Aspects of the Sea of Marmara. METU-Institute of Marine Sciences, Tech. Rep., No.90/4, Erdemli, İçel, 69 pp.

Beşiktepe, Ş., Özsoy, E. and Ü. Ünlüata (1993). Filling of the Marmara Sea by the Dardanelles Lower Layer Inflow, Deep-Sea Res., 40, 1815-1838,

Beşiktepe, Ş., Sur, H. İ., Özsoy, E., Latif, M. A., Oğuz, T., and Ü. Ünlüata (1994). The Circulation and Hydrography of the Marmara Sea, Prog. Oceanogr. 34, 285-334.

Beşiktepe, Ş., Özsoy, E., and M. A. Latif (1995). Sewage Outfall Plume in the Two-Layer Channel: An Example of İstanbul Outfall, Wat. Sci. Tech., 32(2), 69-75.

Demirbağ, E., E. Gökaşan, F. Oktay, M. Şimşek and H. Yüce (1999). The last Sea Level Changes in the Black Sea: Evidence from the Seismic Data. Mar. Geol., 157, 249-265.

Di Iorio, D. and H. Yüce (1998). Observations of Mediterranean Flow into the Black Sea, J. Geopys. Res., 104, 3091-3108.

Di Iorio, D., T. Akal, P. Guerrini, H. Yüce, E. Gezgin and E. Özsoy (1999). Oceanographic Measurements of the West Black Sea: June 15 to July 1996, Saclant Undersea Research Centre report SR-305, 59 pp.

Ducet, N., P.-Y. Le Traon, and P. Gauzelin (1999). Response of the Black sea mean level to atmospheric pressure and wind. J. Mar. Sys., 22, 311-327.

Farmer, D. M. and L. Armi (1986). Maximal Two-Layer Exchange over a Sill and Through the Combination of a Sill and Contraction with Barotropic Flow, J. Fluid Mech., 164, 53-76.

Gregg M. C., E. Özsoy and M. A. Latif (1999). Quasi-Steady Exchange Flow in the Bosphorus, Geophysical Research Letters, 26, 83-86.

Gregg M. C. and E. Özsoy (1999). Mixing on the Black Sea Shelf North of the Bosphorus, Geophysical Research Letters, 26, 1869-1872.

Gregg, M. C. and E. Özsoy (2000). Flow, Water Mass Changes and Hydraulics in the Bosphorus, (submitted).

Hüsrevoğlu, Y. S. (1999). M.Sc. Thesis, Institute of Marine Sciences, METU, Erdemli, İçel.

Jungclaus, J. H. and J. O. Backhaus (1994). Application of a transient reduced gravity plume model to the Denmark Strait Overflow, {\it J. Geophys. Res}, {\bf 99}, 12,375--12,396.

Latif, M. A., E. Özsoy, T. Oğuz and Ü. Ünlüata (1991). Observations of the Mediterranean inflow into the Black Sea, Deep Sea Research, 38, Suppl. 2, S711-S723.

Latif, M. A., Oğuz, T., Sur, H. İ., Ş. Beşiktepe, Özsoy, E. and Ünlüata Ü. (1990). Oceanography of the Turkish Straits - Third Annual Report, Volume I. Physical Oceanography of the Turkish Straits, Institute of Marine Sciences, METU, Erdemli, İçel.

Marsigli, L. F. (1681), Osservazioni Intorno al Bosforo Tracio overo Canale di Constantinopoli Rappresentate in lettera all Sacra Real Maesta di Cristina Regina di Svezia, Roma, 108+pp.

Möller, L. (1927). Alfred Merz' Hydrographisch Untersuchungen in Bosphorus and Dardanellen, Veroffentlichungen des Instituts für Meereskunde an der Universitat Berlin, Neue Folge A, 18, 3-284.

Oğuz, T. and H. İ. Sur (1989). A Two-Layer model of Water Exchange Through the Dardanelles Strait. Oceanol. Acta, 12 , 23-31.

Oğuz, T., Özsoy, E., Latif, M. A., and Ü. Ünlüata, (1990). Modelling of Hydraulically Controlled Exchange Flow in the Bosphorus Strait, J. Phys. Oceanogr. , 20 , 945-965.

Orhon, D., Uslu, O., Meriç, S., Salihoğlu, İ., Filibeli, A. (1994). Wastewater Management for İstanbul: Basis for Treatment and Disposal, Environmental Pollution, 84, 167-178.

Özsoy, E., Oğuz, T., Latif, M. A., and Ü. Ünlüata (1986). Oceanography of the Turkish Straits - First Annual Report, Volume I, Physical Oceanography of the Turkish Straits, Institute of Marine Sciences, METU, Erdemli, İçel, Turkey, 223pp.

Özsoy, E., Oğuz, T., Latif, M. A., Ünlüata Ü., Sur, H. İ. and Ş. Beşiktepe (1988). Oceanography of the Turkish Straits - Second Annual Report, Volume I. Physical Oceanography of the Turkish Straits, Institute of Marine Sciences, METU, Erdemli, İçel.

Özsoy, E. (1990). On the Seasonally Varying Control of the Black Sea Exchange Through the Bosphorus, presented at the AGU-ASLO Ocean Sciences Meeting, New Orleans, February 1990, EOS 71 (2), p.138.

Özsoy, E., Latif, M. A., Beşiktepe, Ş., Oğuz, T., Güngör, H., Ünlüata, Ü., Gaines, A. F., Tuğrul, S., Baştürk, Ö., Yilmaz, A., Yemenicioğlu, S., Saydam, C. and İ. Salihoğlu (1994). Monitoring via Direct Measurements of the Modes of Mixing and Transport of Wastewater Discharges into the Bosphorus Underflow (Hydrography, Sea-Level, Current and Flux Measurements in the Bosphorus Strait, and Acoustical Chemical and Rhodamine-B Dye Tracer Studies of the Ahirkapı Waste Discharge), Volumes 1, 2 and 3, METU Institute of Marine Sciences, Erdemli, İçel, Turkey.

Özsoy, E., M. A. Latif, S. Tuğrul, and Ü. Ünlüata (1995a). Exchanges with the Mediterranean, Fluxes and Boundary Mixing Processes in the Black Sea, In: F. Briand, (editor), Mediterranean Tributary Seas, Bulletin de l'Institut Oceeanographique, Monaco}, Special Number 15, CIESM Science Series No. 1, Monaco, 1-25.

Özsoy, E., Latif, M. A., Beşiktepe, Ş. and A. F. Gaines (1995b). Fluorescent Dye Measurements of the Mixing and Transport of Wastewater Discharge in the Bosphorus, Wat. Sci. Tech., 32(2), 61-68.

Özsoy, E. and Ş. Beşiktepe, (1995). Sources of Double Diffusive Convection and Impacts on Mixing in the Black Sea, pp. 261-274, in: Brandt, A. and H. J. S. Fernando (editors), {\it Double-Diffusive Convection}, Geophysical Monograph 94, American Geophysical Union, 334 pp.

Özsoy, E., M. A. Latif, H. I. Sur and Y. Goryachkin (1996). A Review of the Exchange Flow Regimes and Mixing in the Bosphorus Strait, in: F. Briand, (editor), Mediterranean Tributary Seas, Bulletin de l'Institut Oce\'eanographique, Monaco, Special Number 17, CIESM Science Series No. 2, Monaco.

Özsoy, E. and Ü. Ünlüata (1997). Oceanography of the Black Sea: A Review of Some Recent Results, Earth Sci. Rev., 42(4), 231-272.

Özsoy, E. and Ü. Ünlüata (1998). The Black Sea, in: A. R. Robinson and K. Brink (editors), The Sea: The Global Coastal Ocean: Regional Studies and Syntheses, 11, John Wiley and Sons, New York, pp. 889-914.

Özsoy, E., Latif, M. A., Beşiktepe, Ş., Çetin, N., Gregg, N. Belokopytov, V., Goryachkin, Y. and V. Diaconu (1998). The Bosphorus Strait: Exchange Fluxes, Currents and Sea-Level Changes, in: L. I. Ivanov and T. Oğuz (editors), Ecosystem Modeling as a Management Tool for the Black Sea, NATO Science Series 2: Environmental Security 47, Kluwer Academic Publishers, Dordrecht, vol. 1, 367pp + vol. 2, 385 pp.

Özsoy, E. (1999). Sensitivity to Global Change in Temperate Euro-Asian Seas (the Mediterranean, Black Sea and Caspian Sea): A Review, in P. Malanotte-Rizzoli and V. N. Eremeev, (editors), The Eastern Mediterranean as a Laboratory Basin for the Assessment of Contrasting Ecosystems, NATO Science Series 2, Environmental Security, 51, Kluwer Academic Publishers, Dordrecht, pp. 281-300.

Özsoy, E., D. Di Iorio, M. C. Gregg and J. O. Backhaus (2000). Mixing in the Bosphorus Strait and the Black Sea Continental Shelf: Observations and a Model of the Dense Water Outflow (submitted).

Rank, D., Özsoy, E. and İ. Salihoğlu (1998). Oxygen 18O, Deuterium and Tritium in the Black Sea and the Sea of Marmara, J. Env. Rad., 43, 231-245.

Ryan, W. B. F., W. C. Pitman, C. O. Major, K. Shimkus, V. Moskalenko, G. A. Jones, P. Dimitrov, N. Görür, M. Sakınç, H. Yüce (1998). An Abrupt Drowning of the Black Sea Shelf, Mar. Geol., 138, 119-126.

Ünlüata, Ü., and E. Özsoy (1986). Oceanography of the Turkish Straits - First Annual Report, Volume II, Health of the Turkish Straits, I. Oxygen Deficiencey of the Sea of Marmara, Institute of Marine Sciences, METU, Erdemli, İçel, Turkey, 81pp.

Ünlüata, Ü., T. Oğuz, M. A. Latif and E. Özsoy (1990). On the Physical Oceanography of the Turkish Straits, In: The Physical Oceanography of Sea Straits , L.J. Pratt, editor, NATO/ASI Series, Kluwer.

Yenigün, O. and E. Albek (1990). Two Dimensional Two Layer Hydrodynamical Model of the Marmara Sea, Doğa , 14 , 1-17.

Wensink, H. and G. Campbell (1997). Bathymetric Map Production Using the ERS SAR, Backscatter, 8(1), 16-22.

APPENDIX 2
PREVIOUSLY PUBLISHED PAPERS

Paper 3

Ünlüata, Ü., Oğuz, T., and E. Özsoy (1983).
Blocking of Steady Circulation by Coastal Geometry,
J. Phys. Oceanogr., **13**, *1055-1062.*

Paper 4

Sur, H. İ., Özsoy, E. and Ü. Ünlüata, (1994).
Boundary Current Instabilities, Upwelling,
Shelf Mixing and Eutrophication Processes In The Black Sea,
Prog. Oceanog., **33**, *249-302.*

Paper 3

Ünlüata, Ü., Oğuz, T., and E. Özsoy (1983).
Blocking of Steady Circulation by Coastal Geometry,
J. Phys. Oceanogr., **13**, *1055-1062.*

American Meteorological Society
Printed in U. S. A

Blocking of Steady Circulation by Coastal Geometry

ÜMIT ÜNLÜATA, TEMEL OĞUZ AND EMIN ÖZSOY

Middle East Technical University, Institute of Marine Sciences, P.K. 28, Erdemli, İçel, Turkey

(Manuscript received 23 November 1982, in final form 1 March 1983)

ABSTRACT

Along the southern Turkish continental shelf, the intensity of the observed mean flow has a considerable degree of variability. The relatively strong currents along the straight portion of the coast is reduced significantly in the nearshore region upon encountering irregularities in the form of bays and headlands. As a possible explanation of such blockage by coastal irregularities, a linear, homogeneous, wind-stress free model is presented incorporating the constraints of topographic steering and linear bottom friction. Solutions are given for an idealized case of an abrupt indentation on a straight coast adjoining a linearly deepening shelf. The directional preference of blocking and the applicability of boundary layer approximations are discussed. Numerical solutions are obtained for the realistic bathymetry and coastal configuration along the southern Turkish continental shelf. The concepts developed are applied to the observed blocking features.

1. Introduction

A cyclonic circulation in the eastern Mediterranean has been proposed as a dominant mean current system (Wüst, 1961; Lacombe and Tchernia, 1972). Accordingly, the steady surface current follows the coasts of Israel, Lebanon and Syria and turns west to flow along the southern Turkish coast. Using the observed density and wind fields, Ovchinnikov (1966), Engel (1967), Moskalenko (1974) and Gerges (1976) have confirmed computationally this picture of mean motion. Collins and Banner (1979) have utilized the computed geostrophic fields together with ERTS imagery and secchi depth measurements to provide the details of the flow in the northeastern corner of the Levantine basin. The patterns of the subsurface flow essentially follow that of the surface motion (Gerges, 1976).

Recent observations (Ünlüata *et al.*, 1978, Ünlüata *et al.*, 1980) confirm the existence of a mean westerly motion along the southern Turkish coast. These observations were made at station E2 off Erdemli (Fig. 1a). Additional long term current data obtained (unpublished) at the same station during 1980 provides further confirmation of the existence of the steady flow with velocities of the order of 10 cm s^{-1}.

While the westerly mean flow is detectable off the relatively smooth coastline extending from Mersin to Göksu river (Fig. 1a), its magnitude is found to be significantly reduced in the nearshore areas west of the Göksu river delta. In particular, during 1977–78 nearly a year-long, and in 1980 a four-month current measurement program was carried out at station A2 (Figs. 1a, b). The maximum observed mean flow was less than 4 cm s^{-1} in magnitude during all measurement periods, and there was no predominant direction. In 1980, the data collection at A2 was simultaneously carried out with that of E2. During this period the four-month average of the currents measured at E2 was near 15 cm s^{-1} while that at A2 was nearly zero.

A summary of current measurements in stations A2 and E2 with observed mean values are given in Table 1. The coordinates to which mean currents are referred are shown in Figs. 1a, b (the current components in station E2 have been aligned with the coastline). The overall mean values (statistical average weighted by data length) show that mean currents in station A2 are virtually non-existent, while in station E2 a south-westerly mean current of 7.5 cm s^{-1} is aligned with the isobaths. During the period 26 August 1978–31 January 1979, current-meters deployed continuously show reversals in the direction of mean current at E2 due to (Ünlüata, 1982) very low frequency oscillations (some periods larger than individual record lengths), but they too have a southwesterly mean of 4.3 cm s^{-1}. The better set of observations that can be used to compare station E2 with station A2 is the 1980 measurements, indicating mean southwesterly currents at 13.7 cm s^{-1} in station E2 and mean currents of less than 4 cm s^{-1} in station A2.

A distinguishing feature of the coastline between the Göksu River delta and Anamur is its ruggedness, reflecting the presence of a series of bays and headlands. The reduction in the intensity of mean motion along this segment of the coast evidently implies a significant amount of blockage of the flow by the well-

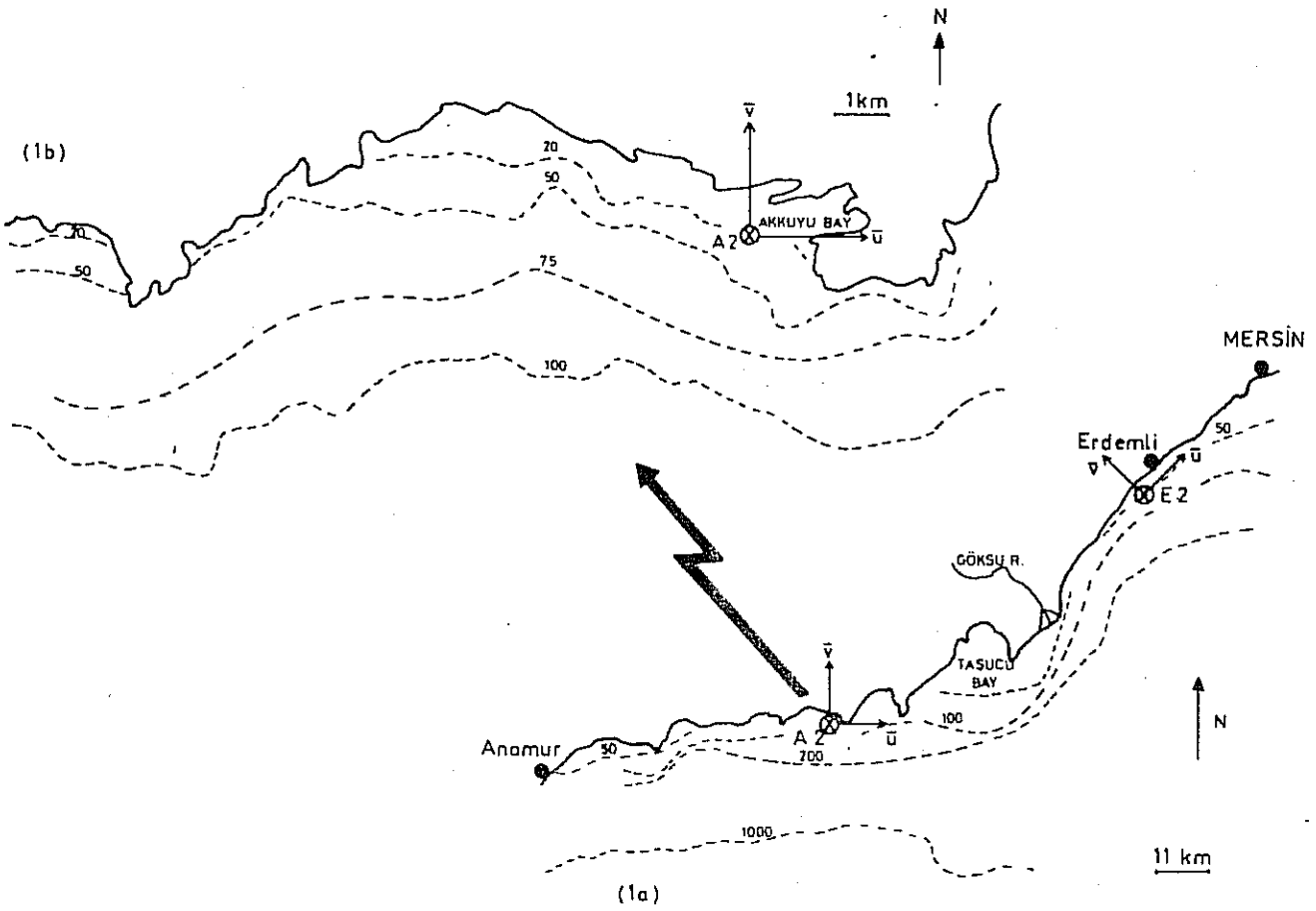

FIG. 1. Location maps.

pronounced coastal features. In particular, station A2 is located within a bay and to the west of a headland (Figs. 1a, b).

The blockage of the mean flow as far as the location of A2 is concerned may come about for various reasons. An earlier offshore deflection of the flow by the coastal perturbations on the east of A2 could lead to an effective blockage. On the other hand, the headland on the east may induce flow separation, leading to the formation of an eddy in the bay and a dead water area around A2.

Here we examine another possibility emerging from the fact that the steady flows free of wind stress tend to follow isobaths. Consider the simplest situation involving a single bay located on a coast with rapidly increasing water depth so that the coastline essentially acts as a vertical wall of height H_0 except in the bay area (Fig. 2). Within the bay, the water depth decreases from H_0. Now, in the absence of external and frictional forces, the water column moving along the coastline must preserve its height status. Consequently, upon arriving at the bay it would follow the isobath of value H_0, the flow penetrating only partially into the bay area. The vertical fluid column along the H_0 isobath thus acts as if it were a rigid barrier and the water mass in the dotted area in Fig. 2 stays stationary.

The form of blockage that is envisioned here constitutes just another result of the Taylor–Proudman theorem (Greenspan, 1968). We also note that if the other coastal perturbations are ignored, the situation depicted in Fig. 2 is sufficiently well approximated by the bay shown in Fig. 1b, where the water depth very rapidly attains a value of the order of 50 m off the headlands on the east and the west.

The lateral and the bottom frictional effects will undoubtedly influence the blockage arising as a result of the steering along isobaths. Especially, the competition between the lateral friction and the adverse pressure gradients is expected to lead to the separation of the approach flow. It is felt, however, that for sufficiently low intensity motions, the topographic effect will dominate the tendency of the flow to separate.

We study the blockage induced through topographic constraints by neglecting the horizontal diffusion of momentum but retaining the bottom friction (Section 2 and 3). An idealized case involving an abrupt semi-infinite intendation on an otherwise straight coastline (Fig. 3) is utilized to demonstrate the flow blockage in terms of analytical solutions

TABLE 1. Mean currents.

Measurement period (month/day/year)	Data length (h)	Depth (m)	Mean current (cm s^{-1}) $\bar{u}$	$\bar{v}$	
Station A2 (Akkuyu)					
8/23/77–9/11/77	490	5	0.4	−0.1	
8/23/77–10/14/77	1231	15	−0.2	0.2	
10/2/77–10/23/77	513	5	1.1	1.0	
10/24/77–12/12/77	1153	15	−0.5	−0.2	
2/13/78–3/14/78	746	5	3.3	2.1	
2/13/78–3/14/78	746	15	0.3	1.9	
4/9/78–5/13/78	856	5	0.3	−4.1	
4/9/78–5/13/78	826	5	−0.6	−1.0	
5/18/78–6/19/78	806	5	−2.7	−0.9	
5/18/78–6/19/78	860	15	−1.3	−0.8	
6/19/80–9/4/80	1878	20	−0.7	2.2	
6/19/80–9/20/80	2269	20	−2.0	3.5	
	Overall mean:		−0.5	0.9	
Station E2 (Erdemli)					
3/22/78–4/6/78	363	5	−8.3	0.3	
3/22/78–4/6/78	363	10	−4.6	0.2	
8/26/78–9/29/78	822	10	−9.4	−1.2	
10/4/78–10/30/78	628	15	0.9	1.2	
11/7/78–12/1/78	590	15	4.4 (−4.3)	1.7 (0.5)	
12/9/78–12/29/78	504	15	−12.7	0.6	
12/31/78–1/31/79	768	15	−4.4	0.6	
6/6/80–8/19/80	1777	20	−13.7	0.1	
	Overall mean:		−7.5	0.3	

(Section 3c). Numerical solutions relevant to the regional setting will then be provided in Section 4.

2. Formulation

We consider linear, barotropic motions taking place over variable topography on an f-plane. Forcing by wind and the effect of lateral friction will be neglected. The bottom friction is assumed to be linearly proportional to the velocity. The depth integrated equations of motion are then of the form

$$\left.\begin{aligned} f\mathbf{k}\times\mathbf{u} &= -g\nabla\eta - r\mathbf{u}/H \\ \nabla\cdot(H\mathbf{u}) &= 0 \end{aligned}\right\}, \qquad (2.1a, b)$$

where $\mathbf{u}$ is the averaged horizontal velocity, f the Coriolis parameter, $\mathbf{k}$ the unit vector along the vertical, g the gravitational constant, η the free surface displacement, r the frictional constant, H the depth and ∇ is the horizontal gradient operator.

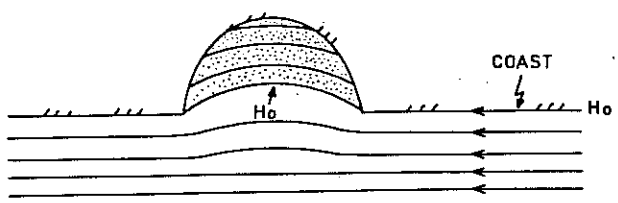

FIG. 2. Topographically induced blockage. Flow approaches from right. Solid lines imply the isobaths.

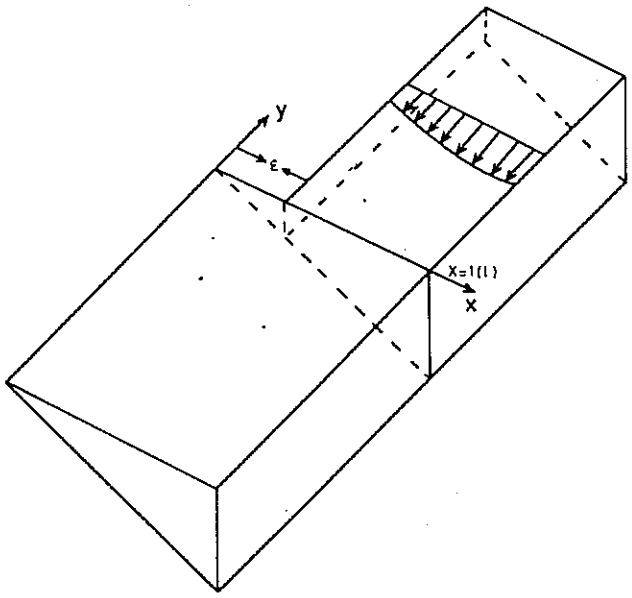

FIG. 3. A semi-infinite indentation on a coastline.

Eq. (2.1b) allows the introduction of a stream function such that

$$H\mathbf{u} = -\mathbf{k}\times\nabla\Psi \qquad (2.2)$$

and a single scalar equation for Ψ can then be obtained from (2.1.a), i.e.,

$$f\nabla H\cdot\mathbf{k}\times\nabla\Psi = r(\nabla^2\Psi - 2\nabla\Psi\cdot\nabla H/H). \qquad (2.3)$$

This is the vorticity equation of motion, expressing simply the static balance between the vorticity induced because of the changes in the height of a fluid column and the frictional torques exerted by the bottom.

If the bottom friction were negligible, the right-hand side of (2.3) would vanish, implying that $\nabla H\cdot\mathbf{u} = 0$, i.e., the motion is then directed along isobaths and the height of each water column is therefore preserved. If this were the case, the water mass in the dotted area in Fig. 2 would be completely stationary. The presence of bottom friction will augment a complete blockage in accordance with (2.3).

The extent in which the bottom friction will influence a complete blockage can be demonstrated by studying the relatively simple situation depicted in Fig. 3. This will be done after some general features of the solutions of (2.3) as applied to the flows in a channel are considered.

3. Analytical solutions

a. General features

In this section we first consider some general features of wind-stress free motions occurring in a chan-

nel of width l. The water depth is assumed to vary only in the transverse direction x (Fig. 4). The steady vorticity equation (2.3) can then be cast into the following dimensionless form

$$-\alpha\Psi_y + \gamma\Psi_x = \tfrac{1}{2}\nabla^2\Psi, \tag{3.1}$$

where

$$\alpha = H_x(fH_0/2r), \quad \gamma = H_x/H. \tag{3.2a, b}$$

In obtaining (3.1) the variables $[(x, y), H, \Psi]$ have been scaled by $\{l, H_0, V_0H_0l\}$ with V_0 being the scale of the velocity field $\mathbf{u}$, and H_0 being an appropriately chosen depth.

It is an easy task to show that, the solution of (3.1) that is independent of the longshore coordinate y, is of the form

$$\Psi_\infty = C\int_0^x H^2dx.$$

The constant of proportionality C can be found in terms of the discharge Q, and in dimensionless variables Ψ_∞ reads

$$\Psi_\infty = Q\left(\int_0^x H^2dx\right)\Big/\left(\int_0^1 H^2dx\right). \tag{3.3}$$

In particular, the values of Ψ_∞ on $x = 0$ and $x = 1$ are zero and Q, respectively. The solution expressed by (3.3) is valid for arbitrary $H(x)$ and implies a basic asymptotic state in which the motion occurs only in the y-direction, the transverse component u being zero. The corresponding longitudinal component is proportional to depth, implying intensification in the deeper sections of the channel.

Consider now the general problem in which interest lies with the motions occurring in the semi-infinite region $y < 0$ when an arbitrary along-shore velocity $v_0(x)$ is prescribed on $y = 0$ and $0 < x < 1$ in terms of Ψ as

$$\Psi_0(x) \equiv \Psi(x, 0) = \int_0^x v_0(x)H(x)dx. \tag{3.4}$$

It is worth noting that $\Psi_0(0) = 0$, while $\Psi_0(1) = Q$, and these values agree with those for Ψ_∞. Clearly, the flow prescribed on $y = 0$ will be perturbed, unless $\Psi = \Psi_\infty$ on $y = 0$ in which case the only solution of (3.1) satisfying (3.4) and the boundary conditions on $x = 0$, 1 is given everywhere by Ψ_∞. In the general case when Ψ_0 differs from Ψ_∞, the asymptotic state reached by Ψ as $y \to -\infty$ is Ψ_∞. We must set

$$\Psi = \Psi_\infty + \tilde{\Psi}, \tag{3.5}$$

with the function $\tilde{\Psi}$ describing the perturbations from the basic state and satisfying

$$\begin{aligned} &-\alpha\tilde{\Psi}_y + \gamma\tilde{\Psi}_x = \tfrac{1}{2}\nabla^2\tilde{\Psi},\\ &\tilde{\Psi} = 0 \quad \text{on} \quad x = 0, 1,\\ &\tilde{\Psi} = \Psi_0 - \Psi_\infty \equiv F(x) \quad \text{on} \quad y = 0,\\ &\tilde{\Psi} \to 0 \quad \text{as} \quad y \to -\infty. \end{aligned} \tag{3.6a–d}$$

If the problem were posed for the domain $y > 0$, then (3.5) and (3.6) still apply but now $\tilde{\Psi}$ must vanish as $y \to +\infty$.

Analytical solutions of the boundary value problem defined by Eq. (3.6) can be obtained by assuming the water depth to vary linearly with x. For such changes in depth, (3.6) is separable and the solutions can be found without invoking the boundary layer approximation that $\Psi_{xx} \gg \Psi_{yy}$. This will enable us to demonstrate explicitly a fundamental directional asymmetry, namely that unless the shallower depth is to the right of the flow, the boundary layer approximation cannot be utilized. Actually, this fact is implicitly imbedded in the character of the governing equation. When the right-hand side of (3.6a) is replaced by Ψ_{xx} the equation becomes parabolic. The problem is then ill posed in the domain $y < 0$ if $\alpha < 0$, and in the domain $y > 0$ if $\alpha > 0$. In an investigation of arrested topographic waves Csanady (1978) has encountered a similar situation, for his assumptions essentially amount to the boundary layer approximation. In a model of the flow of an estuary onto a continental shelf, Beardsley and Hart (1978) have in particular examined the motions generated by a source located on a straight coast discharging into a semi-infinite ocean. It is shown that the boundary layer approximation leads to a source solution that is (for the Northern Hemisphere) valid in the region lying to the right of the source (looking out onto the shelf) and the flow spreads by taking the shallower depth to its right. When the full equation is used, the solution valid for the entire half-space is obtained and it reveals that there exists a degree of asymmetry in the spread of the source depending on the parameter (fH_0/r). For small values of this parameter the source spreads symmetrically into the two quadrants of the half-space. Typically, however, $fH_0r^{-1} \gg 1$ and the flow favors spreading towards right. It is worth pointing out that we can infer this type of source behaviour directly from the governing Eq. (3.1). The equation is similar to the convective–diffusion equation with $-\alpha$ and γ standing for the "velocities" in the y and x directions, respectively. In this analogy then boundary layers will develop only

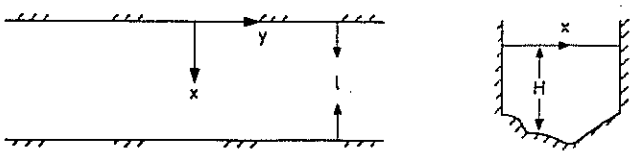

FIG. 4. Definition sketch for channel flows.

for sufficiently large values of $-\alpha$ viz., proportional to fH_0/r.

We now proceed to discuss the aforementioned type of asymmetry as it is related to the present problem. The salient aspects of this asymmetry will then be utilized in studying the blockage problem in an idealized situation.

b. The channel flow

Consider the boundary value problem (3.6) when the dimensionless water depth varies as $H = x$. Then $\alpha = fH_0/2r$ and $\gamma = x^{-1}$, with H_0 standing for the water depth along the coast on $x = 1$. The water depth on $x = 0$ could be taken non-zero but this does not influence the features to be demonstrated.

The solution to equation (3.6) is easily found to be of the form

$$\tilde{\Psi} = \sum_{n=1}^{\infty} A_n \psi_n(x) \phi_n^{<}(y), \tag{3.7a}$$

where the functions

$$\psi_n = \sin \lambda_n x - \lambda_n x \cos \lambda_n x \tag{3.7b}$$

form an orthogonal set in the sense that

$$\int_0^1 x^{-2} \psi_n \psi_m dx = \begin{cases} 0, & n \neq m \\ \tfrac{1}{2}\lambda_n^2 \sin^2 \lambda_n, & n = m \end{cases} \tag{3.7c}$$

with the eigenvalues λ_n being determined by the roots of

$$\tan \lambda = \lambda. \tag{3.7d}$$

In (3.7a) the functions ϕ_n are evanescent in y and are given by

$$\phi_n^{<} = \exp\{y[-\alpha + (\alpha^2 + \lambda_n^2)^{1/2}]\}, \quad y < 0, \tag{3.7e}$$

while the coefficients A_n are found by utilizing (3.7c).

$$A_n = \frac{2 \int_0^1 x^{-2} \psi_n(x) F(x) dx}{\lambda_n^2 \sin^2 \lambda_n}. \tag{3.7f}$$

If the problem is posed for the domain $y > 0$, then the solution is still given by (3.5) but the function $\phi^{<}$ appearing in (3.7a) must be replaced by

$$\phi_n^{>} = \exp\{-y[\alpha + (\alpha^2 + \lambda_n^2)^{1/2}]\}, \quad y > 0. \tag{3.8}$$

Consider first now the solution that is valid in $y < 0$. It is seen that the decay of the nth mode of the perturbation stream function $\tilde{\Psi}$ is measured by the normalized distance

$$y^{(n)} = [(\alpha^2 + \lambda_n^2)^{1/2} - \alpha]^{-1}. \tag{3.9a}$$

The parameter $\alpha = fH_0/2r$ is typically much greater than unity. Assuming the predominance of the first few modes of $\tilde{\Psi}$, $\lambda_n = O(1)$ and it therefore follows from (3.9a) that

$$y^{(n)} \approx 2\alpha/\lambda_n. \tag{3.9b}$$

Consequently, the development of the flow to Ψ_∞ occurs within distances much greater than the channel width. Moreover, it is a simple task to show that $v = -H^{-1}\tilde{\Psi}_x = O(1)$ while $u = H^{-1}\tilde{\Psi}_y = O(1/\alpha) \ll v$. Therefore, the boundary layer approximation for the problem in $y < 0$ would have been appropriate.

Considering next the problem posed for $y > 0$, we infer from (3.8) that the decay of $\tilde{\Psi}$ would occur, for $\alpha \gg 1$ and $\lambda_n = O(1)$, within a distance

$$y^{(n)} \approx \tfrac{1}{2}\alpha. \tag{3.10}$$

This implies a decay distance of the order of one percent of the channel width, i.e., the rapid variations occur in the direction of the flow. When the problem is posed for $y > 0$ the boundary layer approximation hence fails. Moreover, consistent with this failure we can show that $u = O(\alpha)$ and $v = O(1)$.

The fact that the motion very rapidly decays to the basic state for the region $y > 0$ has important ramifications with regard to the blockage problem to be studied next.

c. Blockage problem

Consider the following idealized problem involving the interaction of a wind-stress free flow with an abrupt semi-infinite indentation on an otherwise straight coast bounding the offshore extent of the water mass at a distance l ($x = 1$ in dimensionless units) which is qualitatively identified as a shelf width. The flow approaches the coastal transition from the $+y$ direction. In the region of $y > 0$ the shelf terminates at a coastal wall, while in the region $y < 0$ the depth vanishes at the coast. We assume that the approach flow is in the basic state, i.e., it is given, as $y \to +\infty$, by

$$\Psi_\infty^{>} = \frac{Q \int_\epsilon^x H^2(x) dx}{\int_\epsilon^1 H^2 dx}, \tag{3.11}$$

Q being the discharge.

The exact solution of the problem just posed is obtainable by first considering the regions $y > 0$ and $y < 0$ separately and matching the solutions later on the common boundary $y = 0$ (by requiring the continuity of pressure and the velocity components v). This procedure leads to an integral equation which is solvable by variational or numerical techniques. Instead of doing this we utilize the results of the earlier problem as follows.

In $y < 0$ the solution is given by (3.5) and (3.7) with $F(x)$ left yet unspecified and Ψ_∞ being determined through (3.3).

In the region $y > 0$, the solution is given by the superposition of (3.11) and (3.7a) with the understanding that $\phi_n^<$ are to be replaced by $\phi_n^>$. However, the functions of $\phi_n^>$ rapidly decay so that in effect the value of the stream function Ψ on $y = 0$, i.e., Ψ_0 is given by (3.11) in $\epsilon < x < 1$ while $\Psi_0 = 0$ in $0 < x < \epsilon$.

Consequently, from Eq. (3.6c),

$$F(x) = \begin{cases} -\Psi_\infty(x) & , \quad 0 < x < \epsilon \\ \Psi_\infty^>(x) - \Psi_\infty(x) , & \epsilon < x < 1 \end{cases} \tag{3.12}$$

with Ψ_∞ and $\Psi_\infty^>$ being given by (3.3) and (3.11), respectively. Eq. (3.12) specifies $F(x)$ and therefore the streamfunction $\tilde{\Psi}$ through (3.7a–f). For $H = x$, the complete solution (3.5) is found to be

$$\Psi = x^3 - \frac{6}{(1-\epsilon^3)} \sum_n \frac{\psi_n(x)\psi_n(\epsilon)\phi_n^<(y)}{\lambda_n^4 \sin^2\lambda_n}, \tag{3.13}$$

wherein we have set $Q = 1$.

It is important to note that (3.13) implies vanishing longshore velocity $v = -\Psi_x/H$ on $x = 0$. Consequently, it is expected that the horizontal diffusion of vorticity plays a minor role. We further note from (3.13) that in the absence of bottom friction complete blockage would occur in the region $x < \epsilon$. The role of bottom friction on the amount of blockage of the mean flow is deduced from (3.13) by varying the value of nondimensional parameter α. The results for different α values and for the case of $\epsilon = 0.25$ are depicted in Fig. 5. The streamline pattern corresponding to $\alpha = 100$ shows a significant amount of blockage along the coastline at $x = 0$ for the region $y < 0$. The increase in the bottom friction of almost one order of magnitude (i.e., $\alpha = 10$) still shows a considerable amount of blockage along the coastline without affecting the interior geostrophic flow pattern. Finally, the parameter ϵ reflects the amount of blockage in the sense that larger ϵ characterizes the region where more blockage might occur for the flow

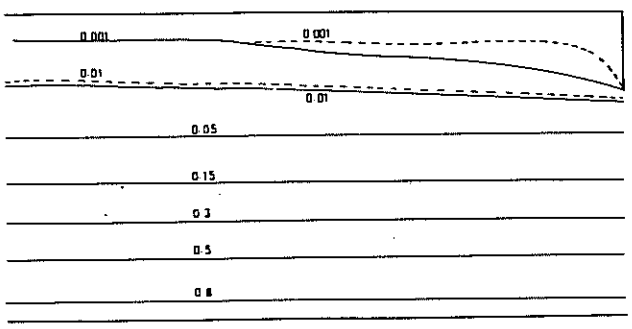

FIG. 5. The streamline pattern for a semi-infinite indentation on a coastline with $\epsilon = 0.25$. Continuous line corresponds to $\alpha = 100$, broken line to $\alpha = 10$.

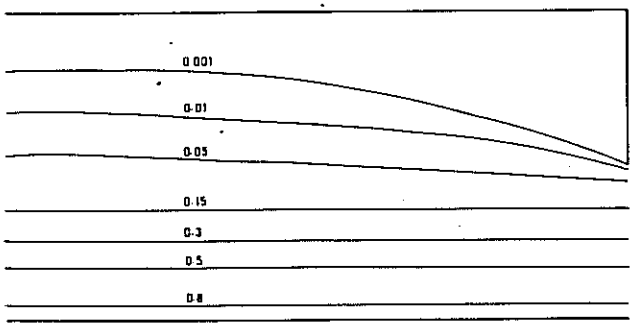

FIG. 6. As in Fig. 5, but for $\epsilon = 0.5$ and $\alpha = 100$.

approaching to the region. This is evident by comparing Figs. 5 and 6, the latter corresponding to the case of $\epsilon = 0.5$.

4. Numerical solutions

This section deals with the topographically controlled blockage of the mean flow along the southern Turkish coastal waters between the Göksu River delta and Anamur. The region has a complex coastal geometry associated with a series of bays and headlands and is further characterized by the presence of a steep and narrow shelf with rapid deepening to 1000 m in ~10–15 km offshore (Fig. 1a).

Considering that the cross-shelf depth variations are sufficiently rapid along the coast under study, topographic effects on the flow dominate and lateral diffusion effects become relatively unimportant. The wind-stress free mean circulation driven by the large-scale steady currents of the northeastern Levantine Sea is then described by numerical solution of Eq. (2.3).

The model incorporates realistic bathymetry of the shelf region. A false constant bottom is however, assumed for places deeper than 300 m, in a region 36 km wide in the offshore direction. The offshore extent of the region being modelled is terminated by a vertical wall across which the normal flow is set to zero as being consistent with the assumption of geostrophic balance.

Eq. (2.3) is discretized in a rectangular mesh of grid spacing $\Delta y = \Delta x = 3.0$ km in the longshore and transverse directions, respectively. The value $r = 0.003$ m s^{-1} is assumed for the linear bottom friction coefficient. Coriolis parameter takes the value $f = 1.0 \times 10^{-4}$ s^{-1} and gravitational acceleration $g = 9.81$ m s^{-2}. The vorticity equation (2.3) is solved for the boundary condition prescribed at the eastern open-boundary according to Eq. (3.4). The solution procedure is the Gauss–Seidel iterative method described by Ramming and Kowalik (1980).

The mean circulation in the shelf region driven by

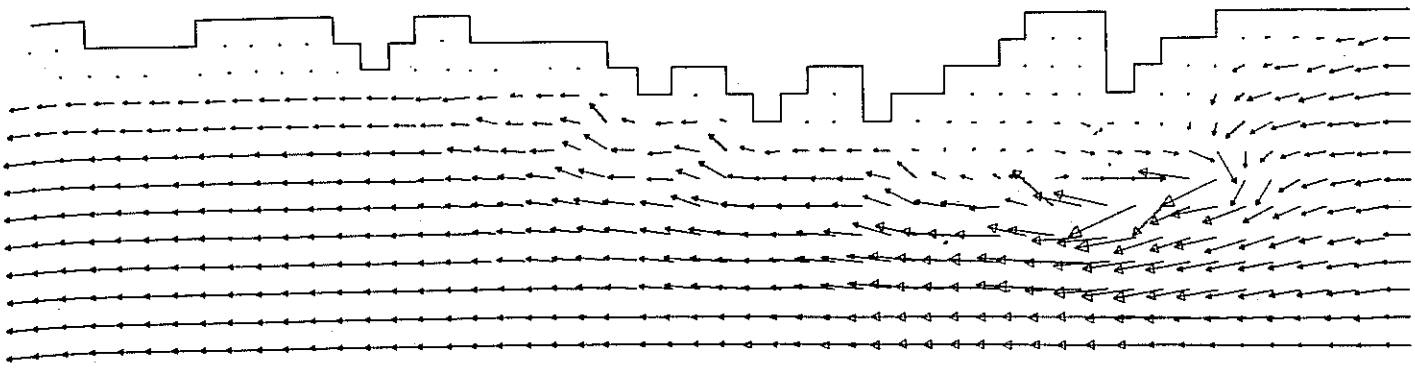

FIG. 7. The depth-averaged steady circulation in the southern Turkish continental shelf.

the large scale current system of Levantine Sea is shown on Fig. 7. The flow, which is almost in a geostrophic balance and tends to follow isobaths along the continental shelf, penetrates only partially into the bay areas due to topographic steering and leads to the aforementioned blockage. The situation is clearly shown within Taşucu Bay where the flow following the 100 m isobath is deflected partially into the bay to set up a weak clockwise circulation. Further experiments have confirmed that the bottom friction as well as rotation and lateral friction have a minimal influence on the circulation developed.

5. Summary and conclusions

A linear, barotropic model of wind-stress free steady motions on a shelf has been used in an attempt to explain the observed blocking of mean flow near coastal irregularities on the southern Turkish continental shelf. In geostrophic flow, regions with closed depth contours near the coast (such as bays of Fig. 2) should be completely blocked off from the mainstream flow on the shelf, but such solutions are indeterminate. To remove geostrophic indeterminacy, linear bottom friction has been introduced in the present linear model, although it may be noted that nonlinear advection terms have been kept in other applications (for example: Charney and De Vore, 1979). Nonlinear processes such as advection, flow separation at coastal boundaries and nonlinear bottom friction have not been taken into account on the basis of sufficiently weak mean currents.

In this model, vorticity changes induced by motions across depth contours are exactly balanced by torques applied by the bottom shear stress. Analytical solutions require that the currents on the shelf evolve into asymptotic states [Eq. (3.3)] and that this evolution has fundamental asymmetry. Consequently, boundary layer approximation may only be invoked if the shallower depth is to the right of the approaching flow.

The behavior of the flow can be directly explained utilizing Eq. (3.1) which is analogous to the convective diffusion equation with $-\alpha$ and γ standing for the convective velocities in the y and x directions, respectively. In this analogy, for $H_x < 0$, there exists the competitive effects of diffusion (which will tend to smear an initial profile in x, y) and convection in $-y$ and x directions. For sufficiently large values of α, boundary layers will develop in the region $y < 0$. Consider, for example, an approaching channel flow with zero initial vorticity specified at $y = 0$. Since the bottom stress (last term in 2.1a) is larger for shallower depths a negative bottom torque will be applied on the fluid, which will therefore deflect towards deeper water to balance this effect. Two boundary layers will develop along $x = 0$ and $x = 1$ in $y < 0$, and the flow will be pumped from one to the other boundary layer until the basic state (3.3) is reached within distances much greater than the channel width. In $y > 0$, the boundary layer approximation cannot be used due to directional asymmetry, and the flow reaches its eventual basic state only within a few percent of the width scale of the channel. Advantage is taken of this fact in Section 3 so that the basic state has been specified for $y > 0$ in solving the coastal indentation problem.

The solutions show how bottom friction augments the geostrophic blockage near coastal and topographic irregularities, though the effects of friction do not avoid blockage in a complete sense. While these conclusions are only valid in the absence of lateral diffusion of momentum and nonlinear effects, numerical experiments performed in investigating the flow structure of the southern Turkish continental shelf have verified that these effects are indeed negligible so far as blocking is influenced to any extent.

REFERENCES

Beardsley, R. C., and J. Hart, 1978: A simple theoretical model for the flow of an estuary onto a continental shelf. *J. Geophys. Res.*, **83**, 873–883.

Charney, J. G., and J. G. DeVore, 1979: Multiple flow equilibria in the atmosphere and blocking. *J. Atmos. Sci.*, **36**, 1205–1216.

Collins, M. B., and F. T. Banner, 1979: Secchi disc depths, suspensions and circulation, northeastern Mediterranean Sea. *Mar. Geol.*, **31**, M39–M46.

Csanady, G. T., 1978: The arrested topographic wave. *J. Phys. Oceanogr.*, **8**, 47–62.

Engel, I., 1967: Currents in the eastern Mediterranean. *Int. Hydrogr. Rev.*, **44**, 23–40.

Gerges, M. A., 1976: Preliminary results of a numerical model of circulation using the density field in the eastern Mediterranean. *Acta Adriat.* **18**, 165–176.

Greenspan, H. P., 1968: *The Theory of Rotating Fluids*, H. P. Greenspan, Ed. Cambridge University Press, 329 pages.

Lacombe, H., and R. Tchernia, 1972: Characterés hydrologiques et circulation des eaux on Méditerranée. *The Mediterranean Sea*, Dowden, Hutchison and Ross, 25–36.

Moskalenko, L. V., 1974: Steady-state wind-driven currents in the eastern half of the Mediterranean Sea. *Oceanology*, **14**, 491–494.

Ovchinnikov, I. M., 1966: Circulation in the surface and intermediate layers of the Mediterranean. *Oceanology*, **5**, 48–58.

Ramming, H. G., and Z. Kowalik, Ed., 1980, *Numerical Modelling of Marine Hydrodynamics*. Elsevier, 368 pp.

Ünlüata, Ü., 1982: On the low-frequency motions in the Cilician Basin. *J. Phys. Oceanogr.*, **12**, 134–143.

——, M. A. Latif, F. Bengü and H. Akay, 1978: Towards an understanding of shelf dynamics along the southern coast of Turkey, IV[es]. *J. Etud. Pollut.*, Antalya, Comm. Inter pour L'Exploration Scientifique de la Mer Méditerraneé, 535–542.

——, E. Özsoy and M. A. Latif, 1980: On the variability currents in the northeastern Levantine Sea, V[es]. *J. Etud. Pollut.*, Cagliari, Comm. Inter pour L'Exploration Scientifique de la Mer Méditerraneé, 929–936.

Wüst, G., 1961: On the vertical circulation of the Mediterranean Sea. *J. Geophys. Res.*, **66**, 3261–3271.

Paper 4

Sur, H. İ., Özsoy, E. and Ü. Ünlüata, (1994).
Boundary Current Instabilities, Upwelling,
Shelf Mixing and Eutrophication Processes In The Black Sea,
Prog. Oceanog., **33**, *249-302.*

Pergamon

Prog. Oceanog. Vol. 33, pp. 249-302, 1994

0079 - 6611/94 $26.00

0079-6611(94) 00005-0

Boundary current instabilities, upwelling, shelf mixing and eutrophication processes in the Black Sea

HALİL İ. SUR, EMİN ÖZSOY AND ÜMİT ÜNLÜATA

Institute of Marine Sciences, Middle East Technical University, PK28 Erdemli, İçel, Turkey

Abstract – Satellite and *in situ* data are utilized to investigate the mesoscale dynamics of the Black Sea boundary current system with special emphasis on aspects of transport and productivity. The satellite data are especially helpful in capturing rapid sub-mesoscale motions insufficiently resolved by the *in situ* measurements.

Various forms of isolated features, including dipole eddies and river plumes, are identified in the satellite images. Unstable flow structures at these sites appear to transport materials and momentum across the continental shelf. Species differentiation and competition are evident along the boundary current system and at the frontal regions during the development of early summer productivity.

A time series of Coastal Zone Colour Scanner (CZCS) images indicate dynamical modulation of the springtime surface productivity in the southern Black Sea. Unstable meandering motions generated at Sakarya Canyon propagate east with speeds of ~10-15km d^{-1}. Within weeks, a turbulent jet is created which separates from the coast, covering the entire southwestern sector. The nutrients driving the phytoplankton production (mainly *Emiliana huxleyi*) of the current system evidently originate from fluvial discharge entering from the northwestern region including the Danube river. The productivity pattern develops in early summer when the Danube inflow is at its peak, and through meandering motions spreads into an area several times wider than the continental shelf.

In 1980, the CZCS data, and in 1991 and 1992, the Advanced Very High Resolution Radiometer (AVHRR) data indicate patches of upwelling along the west Anatolian coastline between Sakarya Canyon and Cape İnce (*İnce Burun*) in summer. The upwelling phenomenon is outstanding because it occurs on a coast where normally the surface convergence near the coast implies downwelling, and under conditions of unfavourable winds.

In 1992, the hydrographic data indicated the upwelling to be the result of a surface divergence of the boundary current, and sequences of satellite data indicate the role of transient dynamics. The *in situ* data showed the upwelling centres to be devoid of phytoplankton as well as fish eggs and larvae.

The AVHRR and *in situ* hydrographic data in winter 1990 indicate cold water is formed over the entire western Black Sea continental shelf. The band of cold water decreases in width as it moves south and impinges on the headland at Baba Burnu, where it undergoes a sudden expansion. The maximum winter phytoplankton bloom sampled during the same period indicates explosive populations of diatoms following the band of cold water.

CONTENTS

1. INTRODUCTION

Exquisite observational detail of surface features is furnished by satellite remote sensing, an essential tool for studying dynamical processes often left unresolved by *in situ* measurements. This is especially true in the energetic environment of the Black Sea: whereas the *in situ* measurements yield 'hard' information, they necessarily lack sufficient resolution both in space and time to describe the rapidly changing mesoscale and sub-mesoscale fields. On the other hand, although satellite data may yield high resolution and time dependent information, this information is often qualitative and the results only describe surface features. It seems that the ultimate aim of reaching a sufficient understanding of the productivity and transport mechanisms operating in the Black Sea could only be accomplished by a synthesis of satellite and *in situ* data.

The high spatial frequency of sampling of the ocean surface with imaging sensors on board satellites has motivated detailed observations of complex oceanic processes. Although the ocean skin temperature measured by infra-red sensors (e.g. the Advanced Very High Resolution Radiometer - AVHRR) is frequently used to identify surface flow features in the ocean, diurnal solar heating can temporarily mask the ocean surface temperature, destroying any correlations with underlying dynamical features (e.g. DESCHAMPS and FROUIN, 1984). In addition, the heat stored by the surface mixed layer can be uniform in relatively large areas of the ocean, and therfore, many flow features may have a colour signature even when they do not appear on infra-red imagery (e.g. AHLNÄS, ROYER and GEORGE (1987).

In contrast, the CZCS collects data reflected from a depth range comparable with the attenuation distance of visible light in the ocean, and may thus give a better indication of the surface circulation (Appendix A). The CZCS was also a modern tool for assessing productivity in large areas of the ocean, though it must be recognized that phytoplankton pigments are not conservative tracers and often contain 'nutrient enrichment' effects in areas of the ocean where vertical mixing, density discontinuities, or upwelling of nutrients to within the photic zone lead to plankton growth (YENTSCH, 1984). In this way, they separate regions of increased fertility, which are typically the boundaries of major ocean currents or eddies. The transport patterns of plankton and suspended matter can serve to detect visually important features of the ocean current system, and are especially useful for studying interactions between the shelf and the deep ocean regions, because they allow

tracing of the pigment or suspended matter concentrations originating from coastal sources. Many collective programs recognize this potential of the analyses of the ocean colour as a tool of modern multi-purpose oceanographic assessments, e.g. the OCEAN Project aiming to develop a European colour data base and network (BARALE and FUSCO, 1992). The SeaWiFS ocean colour sensor expected to be operational in the coming decade is extremely promising for developing this technology further. In the Black Sea, comparative studies based on satellite and *in situ* data can reveal in full detail the ecological collapse stemming from eutrophication.

We use satellite and *in situ* data to identify a number of important dynamical processes in the Black Sea, and emphasize their impact on the biology and chemistry of the basin. As part of our discussion on the cross-shelf exchanges, we show filaments of river waters expanding from the shelf towards the deep basin region, among which are the ordered structures of dipole vortices. Similar oceanic dipole eddies have been illustrated by satellite observations elsewhere; for a review, the reader is referred to FEDOROV and GINSBURG (1989).

We also use satellite data in observing the features of the meandering boundary currents following the Black Sea basin periphery. Satellites have specifically been proved useful in similar environments where the rapid development and turbulent features can not be sufficiently resolved by *in situ* data. Unstable waves, meanders, dipoles, or paired eddies with opposite signed vorticity have frequently been reported along density-driven boundary currents in many parts of the world ocean: near Vancouver Island (THOMSON, 1984; IKEDA, MYSAK and EMERY, 1984), in the California Current (IKEDA and EMERY, 1985), off the southern coast of Alaska (AHLNÄS *et al*, 1987), in the Norwegian Coastal Current (CARSTENS, MCCLIMANS and NILSEN 1984; JOHANNESSEN, SVENDSEN, JOHANNESSEN and LYGRE, 1989; IKEDA, JOHANNESSEN, LYGRE and SANDVEN, 1989), in the Sea of Okhotsk and the Subarctic Polar Frontal Zone (FEDOROV and GINSBURG, 1989), in the Fram Strait Marginal Ice Zone (JOHANNESSEN, JOHANNESSEN, SVENDSEN, SCHUCHMAN, CAMPBELL and JOSBERGER, 1987; GINSBURG and FEDOROV, 1989), off the Labrador Coast (IKEDA, 1987), in the East China Sea (QIU, IMASATO and AWAJI, 1988), in the Leeuwin Current along western Australia (CRESSWELL and GOLDING, 1980; LEGECKIS and CRESSWELL, 1981; THOMPSON, 1984; GRIFFITHS and PEARCE, 1985), along the Ligurian Coastal Current (CREPON, WALD and MONGET, 1982), and along the Algerian Current (MILLOT, 1985, 1991).

An interesting consequence of the boundary current instability, of interest in the Black Sea, is the rather unexpected patterns of upwelling generated in summer. Similar transient features of unexpected upwelling has been found along boundary current systems by QIU *et al* (1988) and CHAO (1990), and near anticyclonic members of coastal eddy pairs along the Algerian Current (MILLOT, 1991; BECKERS and NIHOUL, 1992).

In addition to the basic baroclinically unstable flow situations reviewed above, the interaction of a boundary current with the coastline geometry, or with the continental shelf/slope topography appears to be another possible mechanism that could lead to the unstable meanders, eddies or filaments along the Black Sea periphery. A review of similar situations is given in the sequel, together with the interpretation of our observations.

Whatever may be the cause leading to the meandering and filamented structures of boundary currents, they are of primary importance in determining the exchange between the shelf regions and the deep ocean, with many biogeochemical implications. In a basin of relatively small size such as the Black Sea, cross-shelf exchanges are of central importance because (1) occasionally the horizontal scales in the bursts of exchanges are almost of the same scale as the basin itself, (2) a significant amount of the fresh water nutrients and other materials are inputed from major rivers (e.g. the Danube), and advected along the coast by the boundary current, finally being injected into the basin interior via turbulent exchanges.

The methods of observation and image analysis are discussed in Section 2. A description of the general features of the Black Sea circulation, river inputs, and productivity are given in Section 3. The results of our analyses are described in Section 4. In Section 4.1 we illustrate the effects of river plumes and describe cross-shelf transport caused by mushroom eddies. Then, in Section 4.2 we discuss the rapid development, separation and disintegration of a meandering jet flow along the Anatolian coast. Local upwelling along the same coast is discussed in Section 4.3. Winter mixing on the continental shelf, and the interactions with coastline geometry are described in Section 4.4. From the observations, we extract information concerning the impacts on productivity and eutrophication processes. Conclusions and discussion can be found in Section 5.

2. THE SATELLITE IMAGERY AND METHODS

Nimbus-7 CZCS and NOAA AVHRR images are used to infer the flow characteristics of the Black Sea boundary current. Imagery produced by visible and thermal sensors of these satellites are used to investigate regional flow dynamics by comparative studies of the optical and thermal properties. The processing details and the basis for the interpretations of these satellite data are given in Appendix A.

All of the image processing was done on the SEAPAK interactive processing system at the Institute of Marine Sciences, Middle East Technical University, excluding the images presented in Figs 19d,e which were processed by the KNMI (Royal Netherland Meteorological Institute). Approximately 100 relatively cloud free images of the Nimbus-7 CZCS and NOAA AVHRR were examined and geometrically transformed to Mercator projection.

The NOAA-10 thermal infra-red images could not be corrected for atmospheric effects because of the inapplicability of the method for this particular satellite; in these cases the images have been used with contrast enhancement of relative sea surface temperatures, resulting in east-west temperature gradients depending on solar and satellite altitude. Only a few NOAA-11 images were available (Figs 19d,e). The Nimbus-7 CZCS served as a secondary source of infra-red data, interpreted only in terms of relative temperatures since the radiometric performance of this sensor has been questionable (Robinson, 1991). A third source of data was the NOAA APT transmissions.

3. A BRIEF REVIEW OF THE CIRCULATION AND PRIMARY PRODUCTIVITY

3.1 Bottom topography

The bottom topography of the Black Sea basin is shown in Fig.1. The abyssal plain (depth >2000m) is separated from the margins by steep continental slopes, excluding the gentler slopes near the Danube and Kerch Fans. The wide northwestern continental shelf (mean depth ~50m) occupies the region between the Crimean peninsula and the west coast. This wide continental shelf extends along the western and southwestern coasts of the Black Sea with depth <100m at the shelf break. In fact the entire western Black Sea shelf extending from Crimea to the Sakarya River on the Anatolian coast is a continuous region of flat topography decreasing in width towards its southern terminus. The shelf becomes abruptly terminated at Sakarya Canyon, an abrupt feature where the depth suddenly increases from 100m to about 1500m along the Anatolian coast east of the Bosphorus. The canyon is delimited by Baba Burnu (Cape Baba) on its east, where the coast makes a sharp turn. Smaller continental shelf areas are found along the coast between the two Capes of Kerempe Burnu and Bafra Burnu, along the coast of Kerch, and at narrow stretches separated by canyons along the eastern coasts.

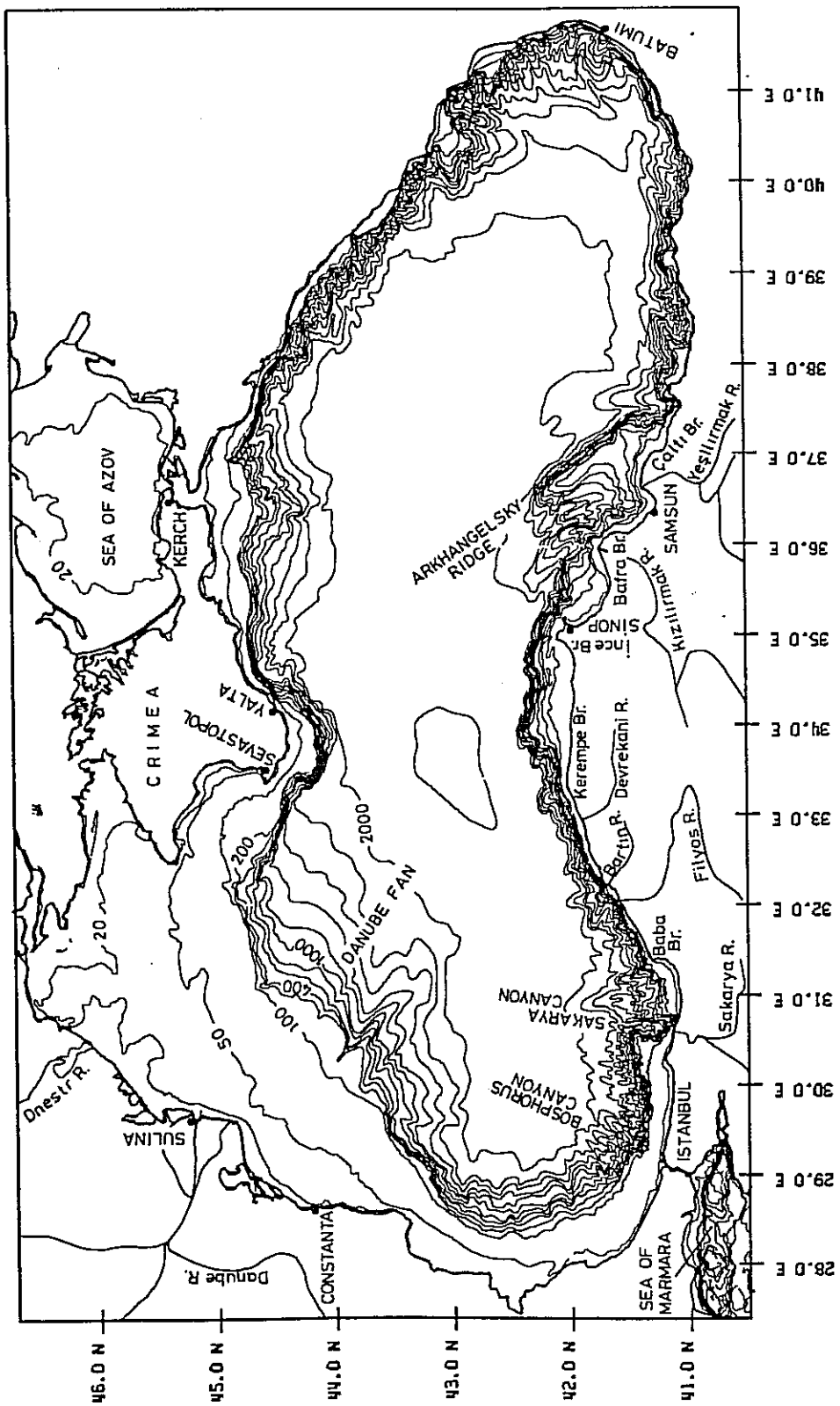

FIG. 1. Bathymetry and location map of the Black Sea.

Along the coast from Sakarya Canyon to Cape Kerempe, a steep continental slope topography is located adjacent to the coast. The cross-shore depth profile changes from a flat, step shaped continental shelf topography west of the Sakarya Canyon to a steep linearly deepening profile following the coastline between Sakarya Canyon and Cape Kerempe, and back to the step-like shelf profile west of Cape Kerempe. These transitions in bottom topography induce significant control on the dynamics of the boundary currents, as will be shown in Section 4.2.

The bottom topography becomes complicated near the Arhangelsky Ridge, a prominent deep feature (shallowest contour at 400m) east of the central Anatolian (Sinop) shelf; then along the remaining eastern Black Sea coast, the continental slope topography undulates between shallow and deep regions. The continental slope region is intersected by numerous canyons throughout the Black Sea.

3.2 The general circulation

A basin scale cyclonic boundary current is the main feature of the Black Sea general circulation. KNIPOVICH (1933) and NEUMANN (1942) were the first to note a division of the circulation pattern into two large cyclonic gyres in the eastern and western halves of the basin, with smaller scale circulations between the two gyres and in the easternmost corner of the basin. BLATOV, KOSEREV and TUZHILKIN (1980) confirmed this circulation and indicated that the centre of the eastern gyre was displaced to the west in summer. According to LATUN (1990), the winter circulation is stronger and better organised than in the summer, when increased mesoscale eddy activity breaks or masks the continuity of the basin circulation. STANEV's (1990) results also support this intensified winter circulation.

It is not clear what physical factors drive the Black Sea circulation. Classically, cyclonic winds (positive curl of wind stress) have been recognized as the main reason for the cyclonic surface circulation (e.g. NEUMANN, 1942; MOSKALENKO, 1976). On the other hand, the results of numerical studies by MARCHUK, KORDZADZE and SKIBA (1975) and STANEV (1990) indicate a seasonal thermohaline circulation driven by nonuniform surface fluxes, complementary to the wind driven circulation, and generating surface currents of comparable magnitude.

Relatively little is known on the role of freshwater runoff from major rivers in establishing a density driven component of the circulation. Although their effects are suspected to be of secondary importance, both the river inflows and the Bosphorus fluxes are expected to modify the circulation through local effects superimposed on the horizontal and vertical ambient stratification.

The northwestern shelf and the Bosphorus vicinity are the two major areas where lateral sources and convection modify the Black Sea circulation (STANEV, 1990). The competing effects of freshwater inflow and winter cooling respectively create and destroy vorticity in the first area, while intermediate depth intrusions driven by shelf mixing of the dense Mediterranean inflow (ÖZSOY, ÜNLÜATA and TOP, 1993) create disturbances including vertical motions in the second area. In both regions, the eddy kinetic energy increases at the expense of mean kinetic energy (STANEV, 1990).

While GAMSAKHURDIYA and SARKISYAN (1976) found the joint effect of baroclinicity and bottom relief (the 'jebar' effect) to be the most important factor in the dynamics of the Black Sea general circulation, the results of STANEV (1990) did not indicate a significant contribution, which according to the author was a result of the strong vertical stratification in the Black Sea. We suggest that these conflicting interpretations could result from insufficient resolution of either the topography or the density structure in the models, because observations often suggest that the core of the boundary current with the largest horizontal density gradients coincides with the narrow continental slope topography. Slope currents are quite common elsewhere, and a fair understanding of their dynamics exists; see HUTHNANCE (1992) for a review.

Mesoscale eddies are known to exist in the Black Sea, and are subject to large excursions and mutual interactions. Central basin features formed by merging of anticyclonic eddies shed from the coherent flows along the northern and southern coasts have been demonstrated by LATUN (1990) and GOLUBEV and TUZHILKIN (1990). Mesoscale eddies of stationary and travelling forms are also indicated by OGUZ, LAVIOLETTE and ÜNLÜATA (1992). In fact the eddies are an integral part of the boundary currents, and lead to the meandering of this current, as noticed earlier by BLATOV *et al* (1984).

The upper ocean circulation derived from recent hydrographic measurements (OGUZ, LATUN, LATİF, VLADIMIROV, SUR, MARKOV, ÖZSOY, KOTOVSHCHIKOV, EREMEEV and ÜNLÜATA 1993) is described by a well defined cyclonic boundary current approximately following the narrow continental slope region and a series of semi-permanent anticyclonic eddies on the periphery between the boundary current and the undulations of the coast (Fig.2). Of these the Batumi anticyclonic circulation is the most prominent closed circulation, existing in the eastern corner of the Black Sea for most of the time, and this is the only region where the cyclonic boundary current ceases to follow the basin slope boundary. This interpretation attempts to generalize the steady general circulation, assigning quasi-permanent anticyclonic cells to the periphery, which in our opinion is associated with the meandering structure of the boundary current, leading to standing structures as well as transient features.

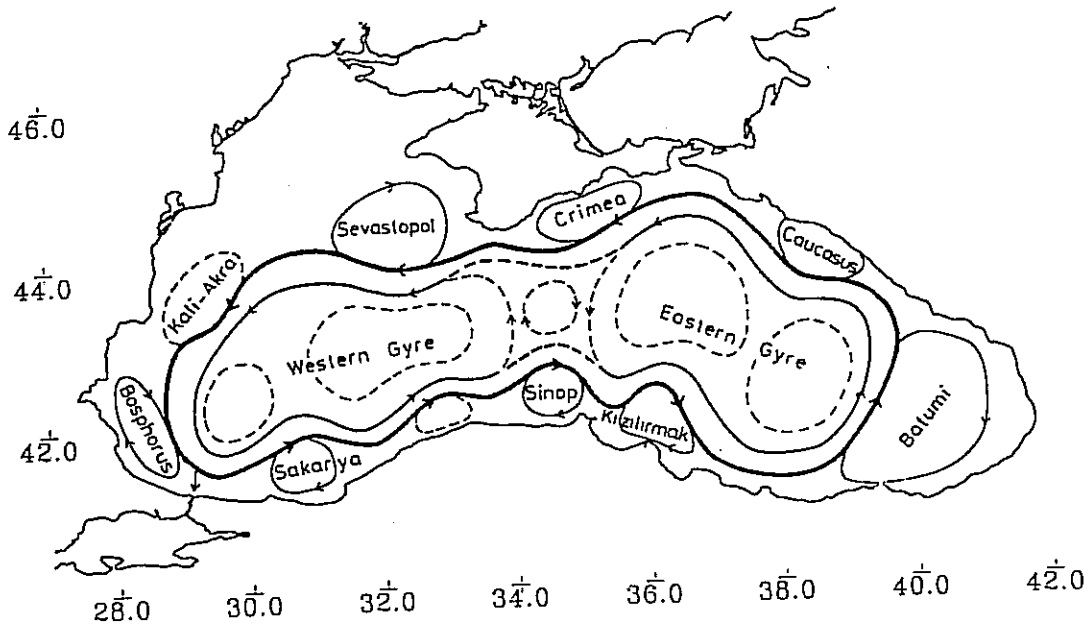

FIG.2. Schematized general circulation of the Black Sea (after OGUZ *et al*, 1993).

3.3 The effects of riverine discharges in the western Black Sea

Major rivers (the Danube, Dnepr and Dnestr) discharge into the northwest shelf of the Black Sea (the region between Crimea and Romania). The Danube River is the greatest contributor of river run off into the Black Sea, accounting for about one half of the total riverine influx. The total discharge of the Dnestr and Dnepr rivers is about a third that of the Danube, and the total discharge of the remaining rivers accounts for a small fraction (<1/5) of the total river runoff.

The annual mean discharge of the Danube, monitored for more than a century (Fig.3a) indicates large natural fluctuations within the range of 4000-9000m^3s^{-1}. In addition to this interannual variability, seasonal changes of about ±30% of the annual mean occur in the discharge (SERPOIANU, 1973; ÖZTURGUT, 1966; TOLMAZIN, 1985; BONDAR, 1989; SERPOIANU, NAE and MALCIU, 1992). Therefore one can expect variations of up to ~3-fold between the minimum and maximum seasonal discharges. The annual Danube influx is well correlated with the basin sea-level (Fig.3b) on seasonal and interannual time-scales (BONDAR, 1989). ÖZSOY (1990) and ÖZSOY, LATİF, TUGRUL and ÜNLÜATA (1992) suggest that the nonlinear mechanism of hydraulic controls imposed by the Bosphorus results in the long-term response of the mean sea level to net freshwater inflow. In addition, SERPOIANU *et al* (1992) show that the salinity decrease measured at Constanza (downstream of the Danube) is also closely correlated with the Danube discharge on seasonal and interannual time scales (Figs 3c,d). The Danube water usually flows cyclonically (to the south) around the basin, except during storms when strong southwesterlies push its waters back into the northwest shelf (TOLMAZIN, 1985).

Salinity data from near the Anatolian coast suggest that the freshwater from the northwest shelf reaches the southwest coast. Daily measurements in the Bosphorus (Figs 4a,c) indicate minimum salinity at different periods of each year, from spring to late summer (ACARA, 1958; ARTÜZ and OGUZ, 1976). Although salinity minima can be observed as early as March-April, the more prominent salinity minima are observed during summer, from June till September. The mean travel time between the Danube and the Bosphorus (~500km) is calculated to be on the order of 1-2 months assuming a mean current speed of 10-20cm s^{-1}. The irregularities and lags in the timing of minimum salinity waters observed along the Anatolian coast could result from mixing and dispersion effects of the circulation transporting the northwest shelf waters south.

To show the river effects, we computed the mean salinity of the surface waters within the upper 10m (Fig.5a) in the southwestern Black Sea (between 28° and 32°E, and 41° and 42°N) from the detailed coverage of the R/V *Bilim*, the research vessel of the Institute of Marine Sciences, Middle East Technical University, during 1985-1992, including offshore and inshore stations, as well as stations in the Bosphorus, where more frequent measurements were obtained. The weight of the data indicates a mean salinity of about 18 in the southwest sector of the Black Sea. The salinity decreases to 16-17 during the exceptional conditions when the Danubian influence is felt in the area. The minimum salinity periods in Fig.5a occur at different times varying from March to August each year, which are superposed in the seasonal plot of Fig.5b.

3.4 Primary production and eutrophication processes

A number of complex factors control the spatial/temporal distribution, variability and recycling of the primary production in the Black Sea, including the peculiar redox processes and their bacterial mediation at the oxic-anoxic interface, the vertical and horizontal transport of nutrients originating from the riverine, atmospheric and land sources, and their exchanges between the shelf and deep waters.

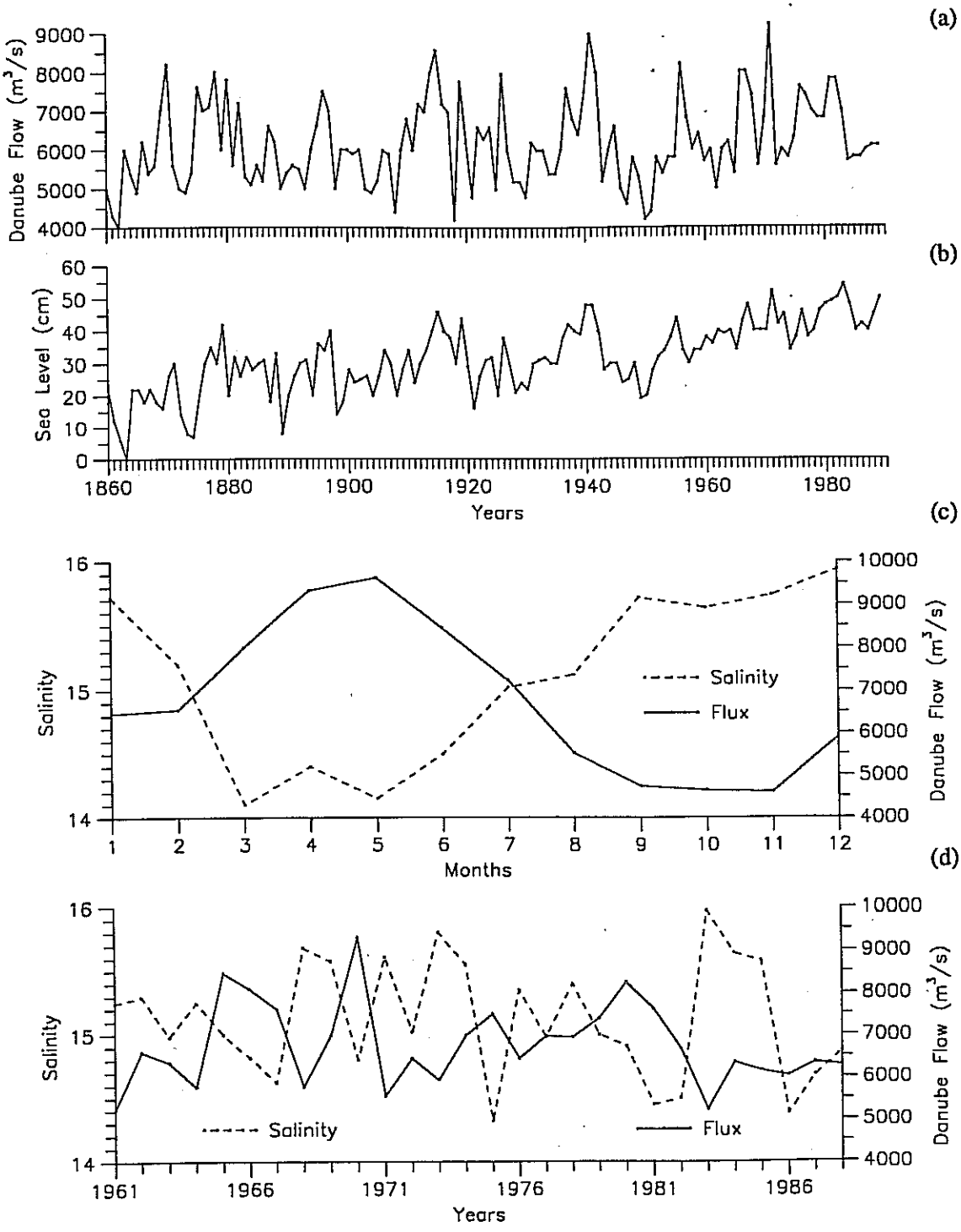

FIG.3. Long-term measurements of annual average (a) Danube discharge, (b) sea level at Sulina on the Romanian coast (after BONDAR, 1989), (c) monthly average and (d) annual average Danube discharge and salinity at Constantza, Romania (after SERPOIANU *et al*, 1992).

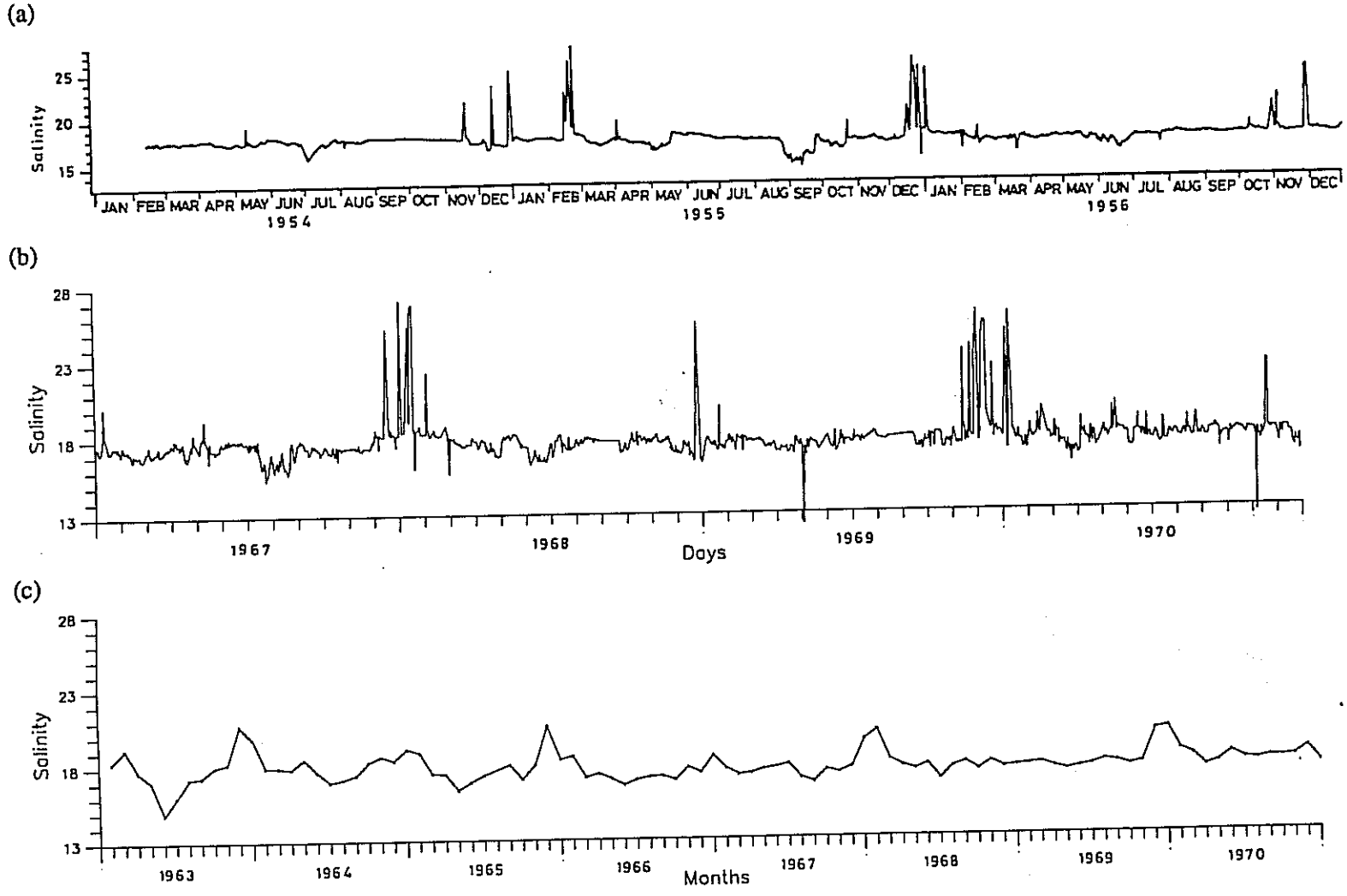

FIG.4. Time series of salinity within the Bosphorus: (a) daily measurements, 1954-1956 (redrawn after ACARA, 1958), (b) daily measurements, 1967-1970, (c) monthly averages of daily measurements, 1963-1970 (after ARTÜZ and UGUZ, 1976).

1967-1970, (c) monthly averages of daily measurements, 1963-1970 (after ARTUZ and [illegible]).

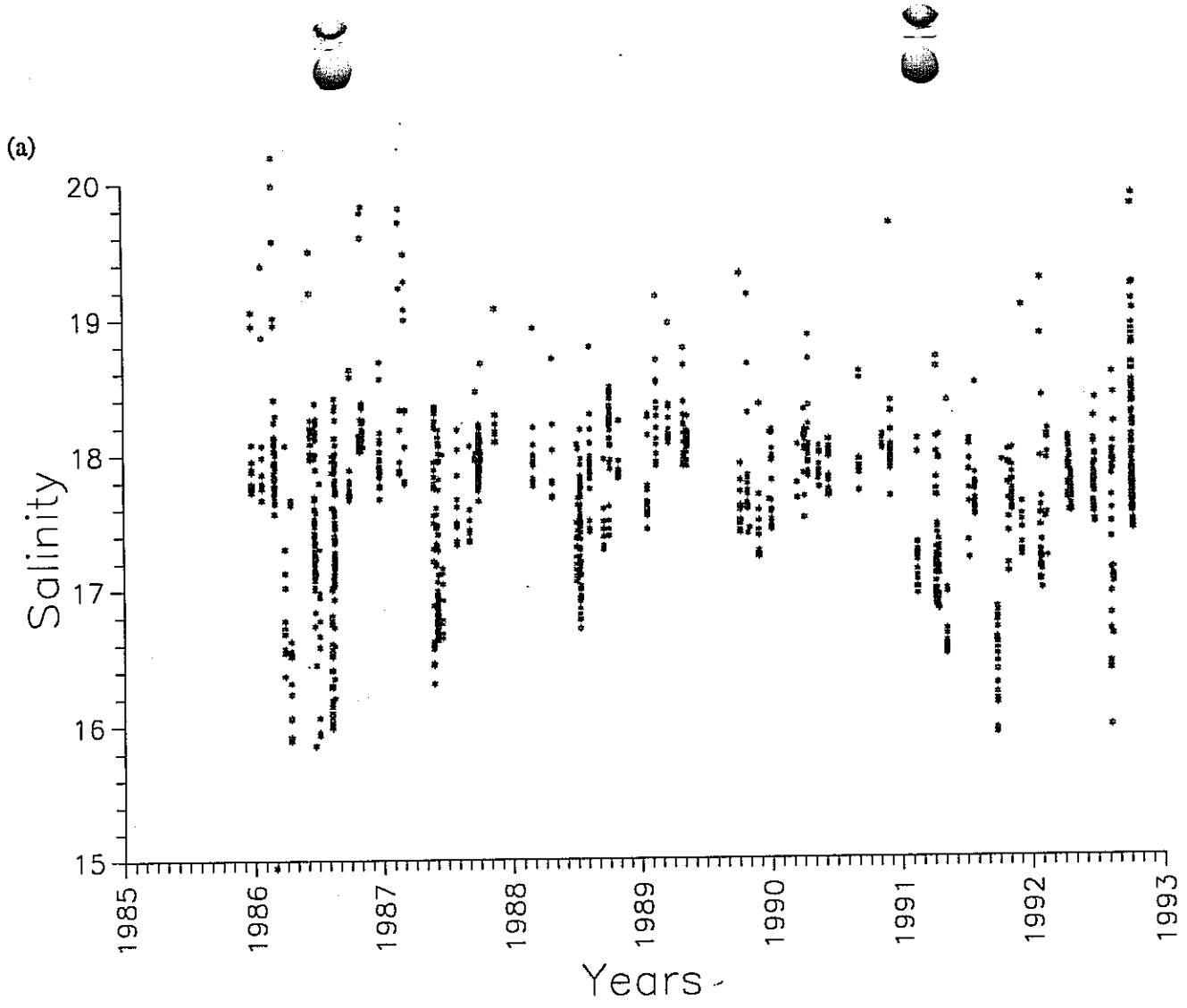

FIG.5. Surface salinity measurements (upper 10m average) in the southwestern Black Sea (between 28° and 32°E, and 41° and 42°N). Each data point corresponds to a hydrographic station occupied in the area, including the many measurements made in the Bosphorus. Time dependence with respect to (a) annual and (b, overleaf) seasonal time axes are shown separately to emphasize the different times of salinity minima in the spring-summer periods.

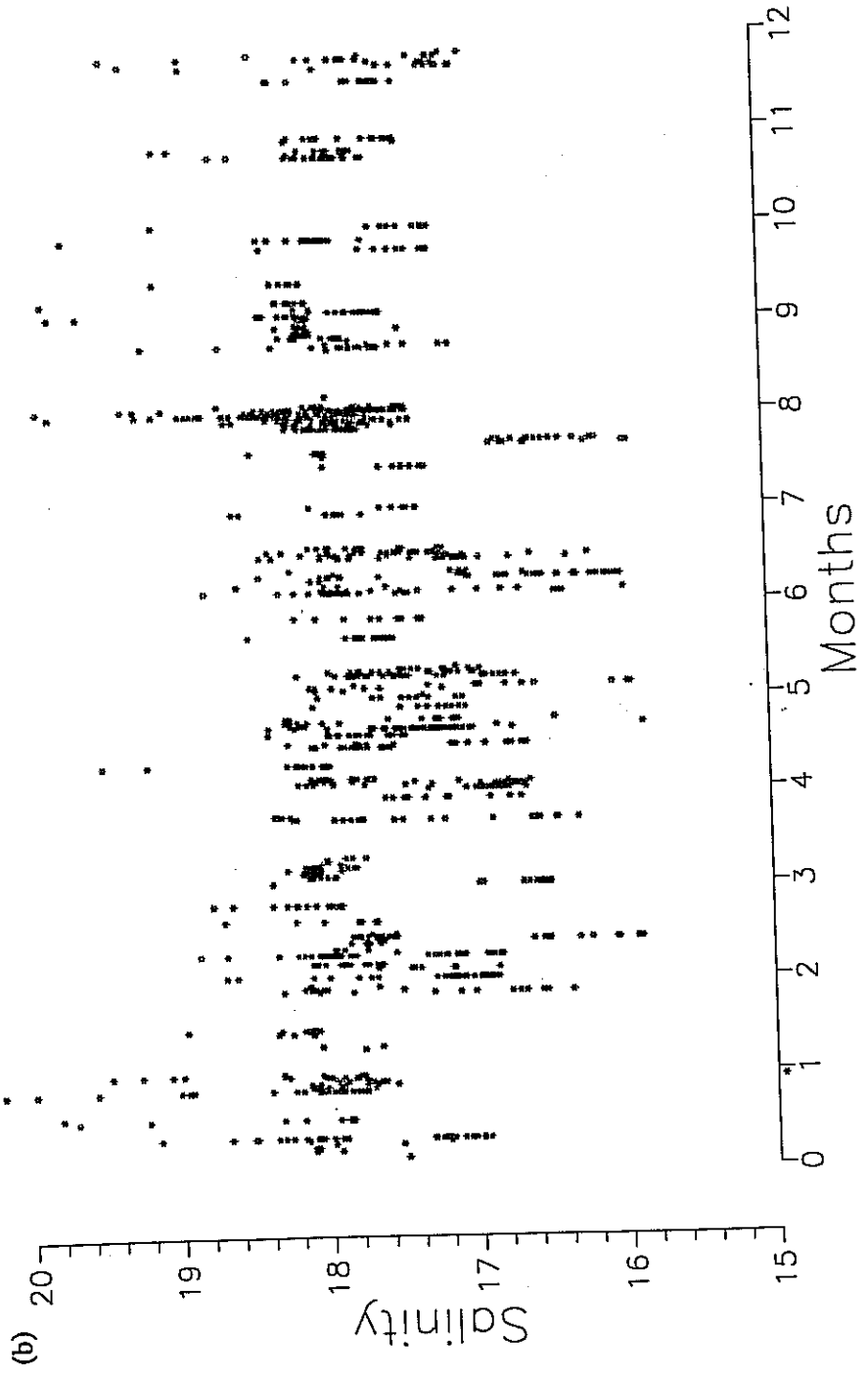
(b)
Salinity
20
19
18
17
16
15
Months
0
1
2
3
4
5
6
7
8
9
10
11
12

Fed by a rich supply of nutrients, the Black Sea is known to be a region of moderate to high productivity (KOBLENTZ-MISHKE, VOLKOVINSKY and KABANOVA 1970), compared with other parts of the world ocean. In the past (before the last decade), the peaks in primary productivity of the Black Sea were known to occur twice a year, with a major bloom mainly of diatoms (several species of *Chaetoceros*) in early spring, followed by a secondary bloom mainly of coccolithophorids in autumn (SOROKIN, 1983). Occasional blooms of coccoliths and dinoflagellates occurred mainly in coastal areas. Recently, additional summer blooms with predominance of dinoflagellates and coccoliths (*Emiliana huxleyi*) have increased in occurrence to become common in the region (BOLOGA, 1986; BENLI, 1987; HAY and HONJO, 1989; HAY, HONJO, KEMPE, ITEKKOT, DEGENS, KONUK and IZDAR, 1990; HAY, ARTHUR, DEAN and NEFF (1991). In addition, SOROKIN (1983) first reported the spring and summer development of red tides in the eutrophic waters of the western shelf. Massive red tides have been created along the Romanian and Bulgarian coasts by dinoflagellates (mainly *Exuviaella cordata*, as well as *Prorocentrum micans*, SUKHANOVA, FLING, HIBAUM, KARAMFILOV, KOPYLOV, MATVEEVA, RAT'KOVA and SAZHIN, 1988, and references cited therein) and by ciliate infusoria (*Mesodinium rubrum*, TUMANTSEVA, 1985).

Not much is known about the winter productivity, which should be expected to follow convection events bringing nutrients up from the halocline into the upper layers. SOROKIN (1983) indicates a late winter - early spring (February-March) bloom comprised of sub-arctic species with a biomass even larger than the spring-autumn blooms, but he notes that the existing sampling, mainly carried out during the good weather season may have missed the peak winter primary production. On the other hand, most winter measurements were obtained in the offshore waters; the available observations within the northwest shelf zone either do not indicate winter blooms or seem to have missed the winter peak of production (M.E. VINOGRADOV, personal communication). Our limited winter observations during February 1990 (UYSAL, 1993) indicate a massive explosion of plankton, mainly *Chaetoceros sp.* along the west Anatolian coast (see Section 4.4).

The maximum spring-autumn primary productivity (60% of the Black Sea production) is found in the northwest shelf where 87% of the total fresh water input reaches the Black Sea from major rivers contributing large amounts of nutrients and detritus onto the shallow shelf region, reducing the surface salinity and transparency (<60% of the total incident radiation reaching below 1m depth). The maximum daily assimilated carbon in this area is estimated to be on the order of 1-2gC $m^{-2}d^{-1}$. Open sea primary productivity at the centres of the western and eastern gyres of the Black Sea are typically low (0.05-0.2gC $m^{-2}d^{-1}$). Next to the high productivity areas in the northwest shelf and the northeast regions, the highest primary productivity (0.2-0.5gC $m^{-2}d^{-1}$) is reported to occur along the Anatolian (southwestern) and Romanian (western) coasts, and extends into the central region separating the eastern and western gyres (BOLOGA, 1986).

The primary productivity measurements during the Atlantis II Cruise in March-April 1969 indicated maximum values of 2.3gC $m^{-2}d^{-1}$ near the Sakarya Canyon. High values of 0.4-2.0gC $m^{-2}d^{-1}$ were also observed when following the western shelf, along the Anatolian coast, in the central region between the eastern and western basins, and in northeastern region. More recent data in the western Black Sea in May 1982 indicates a high surface primary productivity values of 1-3.9gC $m^{-3}d^{-1}$ near the Bosphorus, and 14-153gC $m^{-3}d^{-1}$ in the Danube region, verifying the eutrophication levels (BOLOGA, 1986).

Although there are limited observations, some of the above measurements suggest the western part of the Anatolian coast is a region of relatively high productivity. The algal production rate was estimated to be in the range of 0.3-0.44gC $m^{-2}d^{-1}$ from chlorophyll *a* measurements (<1.0μg l^{-1}) of the R/V *Bilim* in September 1988 and January and April 1989 along the Anatolian coast (OGUZ, BINGEL and TUGRUL, 1990). On the other hand, May 1986 measurements near the Sakarya Canyon seemed to indicate a spring bloom with high values of chlorophyll *a* (~1.6μg l^{-1}; GÖÇMEN, 1988).

The increased influxes of highly mineralized nutrients from major rivers (such as the Danube) draining large areas of the continent have initiated eutrophication processes in recent decades; the environmental deterioration, now on the scale of a catastrophy, is being acknowledged with an increasing sense of urgency (BOLOGA, 1986; CHIREA and GOMOIU, 1986; MEE, 1992). At present the Danube introduces 60,000t y^{-1} of total phosphorus and about 340,000t y^{-1} of total inorganic nitrogen to the Black Sea, representing large increases in the last two decades (MEE, 1992). In comparison, major Turkish rivers are estimated to contribute 1700t y^{-1} of o-PO_4 and 25,000t y^{-1} of total inorganic nitrogen, and the nutrient export versus import through the Bosphorus roughly balance each other (ÖZSOY *et al*, 1992).

The eutrophication started in the northwestern shelf area influenced by the Danube and Dniestr river mouths (TOLMAZIN, 1985), and progressed south, along the western shelf (MUSAYEVA, 1985; BOLOGA, 1986). It is now evident that the eutrophication is reaching the southwestern sector, and is in fact, creating some of the adverse changes observed in the neighboring Marmara Sea. It seems that the eutrophication increased sharply in the last decade: for example a time series of more than 1100 historical Secchi disc readings in the central parts of the Black Sea illustrate that the white disc visibility has decreased from 20m in the 1920s to about 15m until the mid-1980s; recent measurements indicate that it has decreased to 5-6m in the early 1990s (EREMEEV, VLADIMIROV and KRASHENINNIKOV, 1992). In the shelf regions, eutrophication has led to hypoxia of the bottom sediments within the oxic zone (TOLMAZIN, 1985; ZAITSEV, 1991). Significant decreases have occurred in the total stocks and species of fish, many organisms have disappeared from the region, and part of the food web has been invaded by opportunistic species imported from outside the region (ZAITSEV, 1991). In the meantime, the high productivity of the region, prized by bordering countries which were not properly alert to the impending adverse changes, resulted in a massive exploitation of the fisheries.

It has been shown that the adverse changes have not been restricted to the shelf regions alone: the nutrient distribution has changed drastically throughout the entire basin (TUGRUL, BASTÜRK, SAYDAM and YILMAZ, 1992; SAYDAM, TUGRUL, BASTÜRK and OGUZ, 1992), in spite of the stability with time of the anoxic interface relative to density surfaces. The results indicate that ammonia and silicate have been depleted in the near surface waters by increased utilization in the last few decades.

The recycling mechanisms of nutrients within the basin are not clearly identified. The major source of nutrients entering the euphotic zone is often assumed to be the reserve of nutrients in the oxic and anoxic waters below the photic zone (DEUSER, 1971; FONSELIUS, 1974; SOROKIN, 1983). On the other hand, no new nitrogen seems to reach the euphotic zone from the deep water (J.W. MURRAY, personal communication); this may be one of the peculiarities of the Black Sea, leaving the atmospheric and riverine supply as the only sources of new production.

4. RESULTS

4.1 River plumes, dipole eddies and plankton blooms

Riverine influence is easily recognised in the CZCS images such as those showing the Anatolian coast on September 19, 1980 (Figs 6a,b). The feature near 32°E is the plume of the Filyos River. We also see a separated filament of river water (possibly originating from the small Bartin and Devrekani Streams near 33°E) near Cape Kerempe. The eastward bending plumes from these perennial runoff sources extend up to 50km offshore, with a colour signature indicating terrigenous sediment and organic inputs. HAY and HONJO (1989) attributed part of the deposition in offshore

sediment traps to sediments supplied by these rivers. The properties of the wide patch with wavy edges between 29°E and 31°E contrasts with those of the river dominated features described above. Firstly, the feature is essentially confined to the shelf region west of the Sakarya Canyon (Fig.1), and does not appear to be river driven. If the material yielding the visible signal were to originate from the Sakarya River (located downstream at 30°40'E) the plume would be expected east of the mouth in response to the eastward flowing boundary currents, as for the other rivers observed in the same picture. Secondly, this patch of water displays a more uniform distribution of reflectance than the river plumes. Thirdly, its reflectance is large both with respect to particulates (Fig.6a) and pigment concentration (Fig.6b), indicating that this feature is likely to be a coccolithophore bloom. We also note other patches of the same nature along the Thracian and Bulgarian coasts, which may indicate that such blooms are characteristic of the western shelf.

In Figs 7a,b (October 7, 1980) plumes originating from the Kizilirmak and Yesilirmak rivers, and from other small streams along the central Anatolian coast are observed to bend eastwards as a result of the boundary current system, and to form small eddies in the adjoining bays (east of Cape İnce, Cape Bafra and Cape Çalti). As with Figs 6a,b we note a clear predominance of inorganic particulates. The pigment calculations in Fig.7b depend on information from different bands of visible light, including some contribution of channel 3 reflectance. Yet the pigment signal of the plumes, partly associated with river-borne organics (e.g. plant debris and yellow substance) is typically smaller than the particulate signal.

In Fig.8a (October 13, 1980) the plume at the mouth of Filyos River has become weaker as a result of decreased runoff during autumn. Note that the plume from the Sakarya River, a relatively large river compared to Filyos, has very narrow coastal influence during the autumn period reviewed. This is because it drains the dry interior region, whereas the Filyos receives its water from the north Anatolian mountains, which continue to receive rainfall throughout the summer and autumn.

A mushroom eddy is visible in Fig.8a, offshore of the mouth of the Kizihrmak river at Cape Bafra. In the enlarged image of the Anatolian coast (Fig.8b) specific features can be observed. The antisymmetric spiral pattern of the tracer field trapped in the doublet, and the pattern of streamers surrounding the eddies are remarkably similar to the patterns generated in laboratory simulations.

Similar coherent structures of dipole eddies have been reproduced in laboratory experiments with rotating/stratified (FEDOROV, GINSBURG and KOSTIANOY, 1989) or stratified flows (VAN HEIJST and FLOR, 1989; VOROPAYEV, 1989). Nonlinear advective dynamics and two-dimensional dipole eddies from the collapse of impulsively generated three-dimensional flows. For example, FEDOROV and GINSBURG (1989) and FEDOROV, GINSBURG and KOSTIANOY, (1989) view dipole structures to be the universal reaction of a rotating fluid to an impulse applied to it. The momentum impulse could result from local dynamical instabilities, local winds, or river discharges. During initial development, the dipoles are often assymmetric or immature, but when a surface tracer is present (for example, sea surface temperature, biota, sediments, sea-ice), the basic surface signature of a dipole eddy is a mushroom-like pattern. Numerical studies by MIED, MCWILLIAMS and LINDEMANN (1991) confirm generation by a localized pulse; advection by the dipole velocity field then leads to a mushroom pattern in tracer fields. Dipole eddies are also the most common structures resulting from the instability of boundary currents (cf Section 4.2). For example, some laboratory experiments (GRIFFITHS and LINDEN, 1981) indicate that when long waves generated by the instability of a boundary current break, they form cyclonic/anticyclonic vortex pairs or dipoles.

The tracer pattern in Fig.8b appears mainly related to river sediments, as well as some pigments (weaker, not shown) carried by river water. The mushroom feature consists of equal sized cyclonic

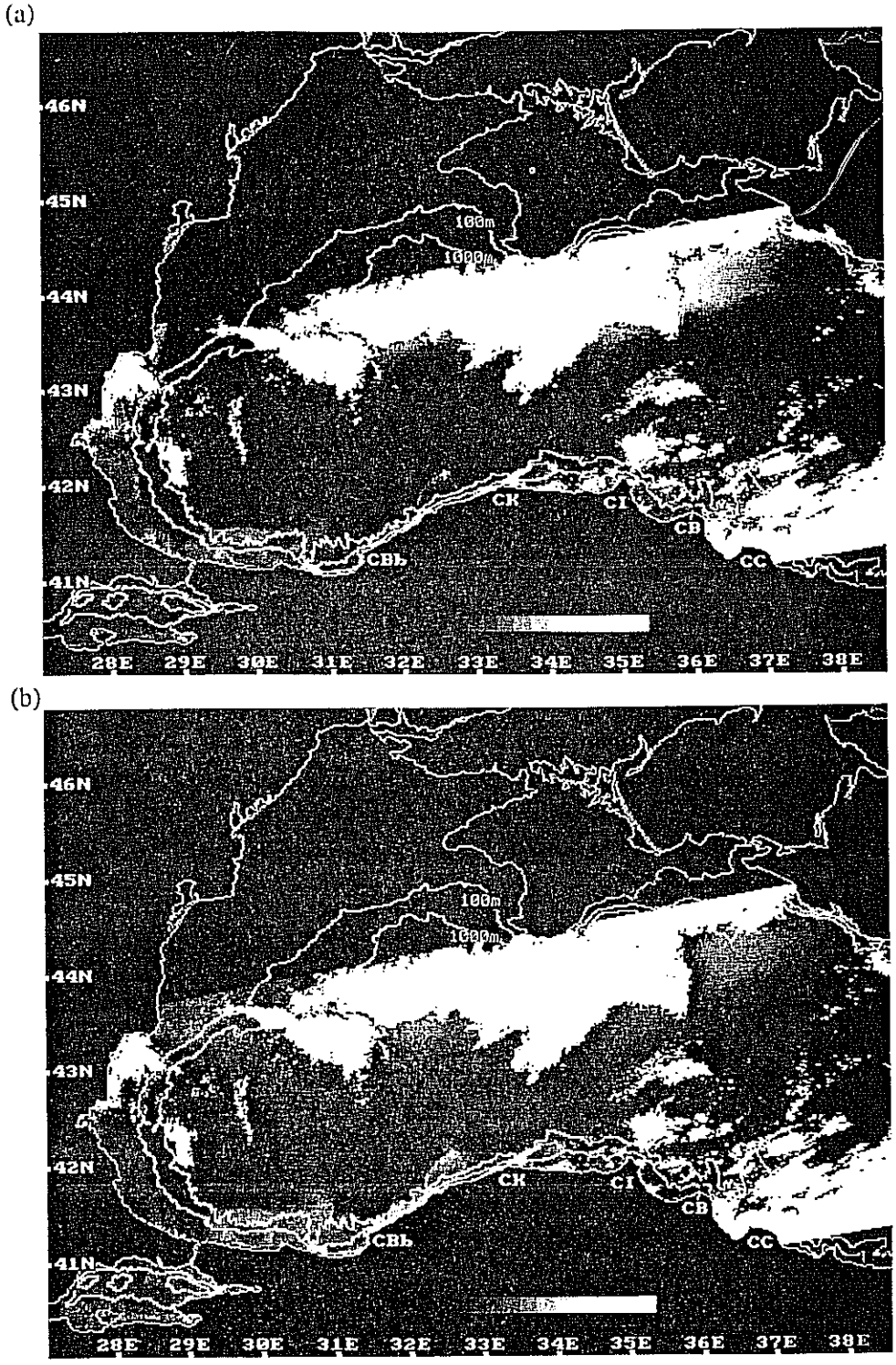

FIG.6. Coastal Zone Colour Scanner (CZCS) satellite images on September 19, 1980 showing the plumes of the Filyos and the other small rivers, and a bloom of coccolithophores on the southwestern shelf. The images represent the atmospherically corrected (a) channel 3 (550nm), (b) the calculated pigment concentration. Abbreviations used: CBb:Cape Baba, CK:Cape Kerempe, CI:Cape İnce, CB:Cape Bafra, CC:Cape Çalti.

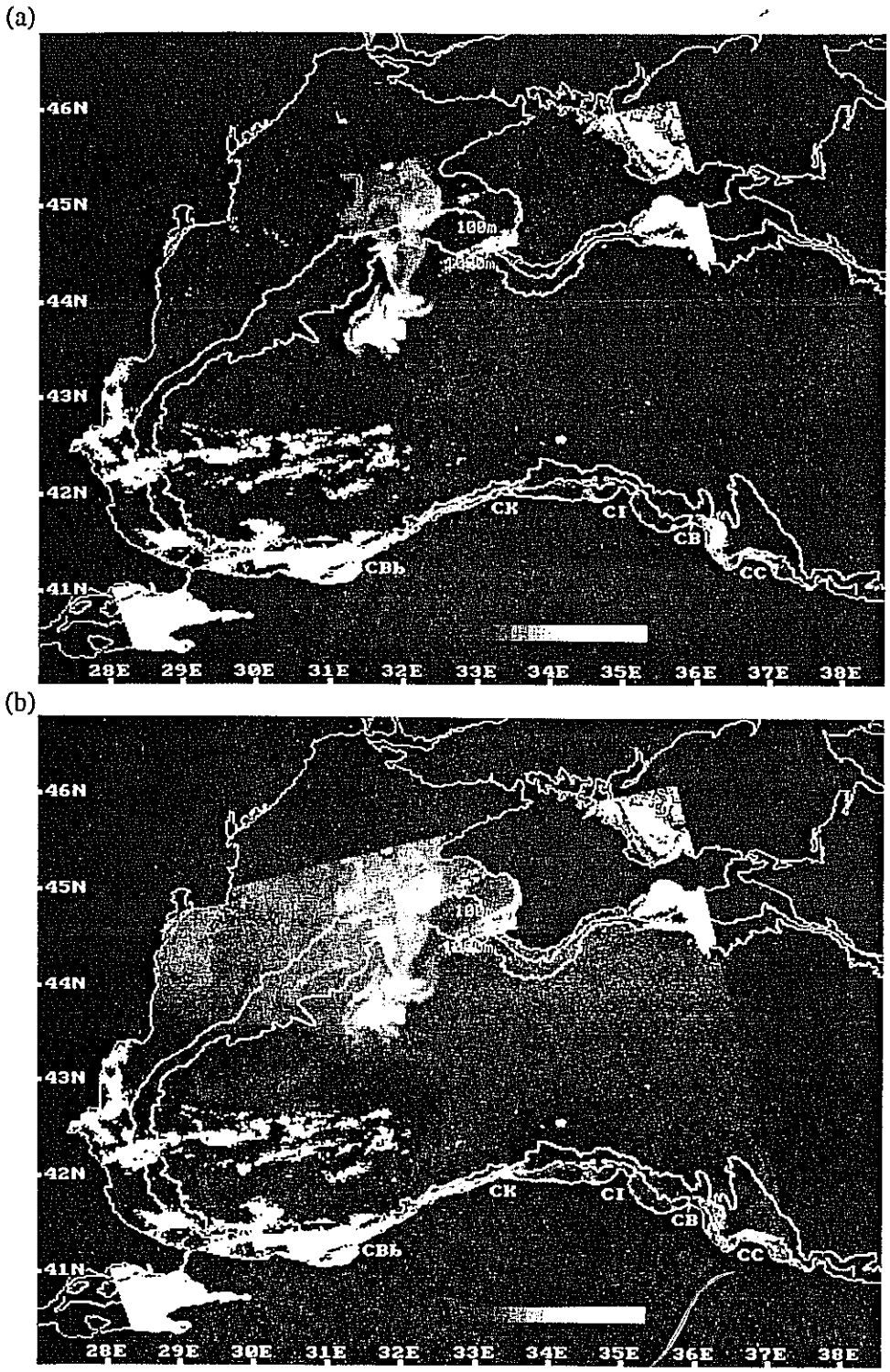

FIG.7. Coastal Zone Colour Scanner (CZCS) satellite images on October 7, 1980. The images represent the atmospherically corrected (a) channel 3 (550nm) and (b) the pigment concentration showing development of flow and associated sediment along the southwestern coast of the Black Sea, and a distinct offshore plume of Dnepr, Bug, and Dnestr Rivers.

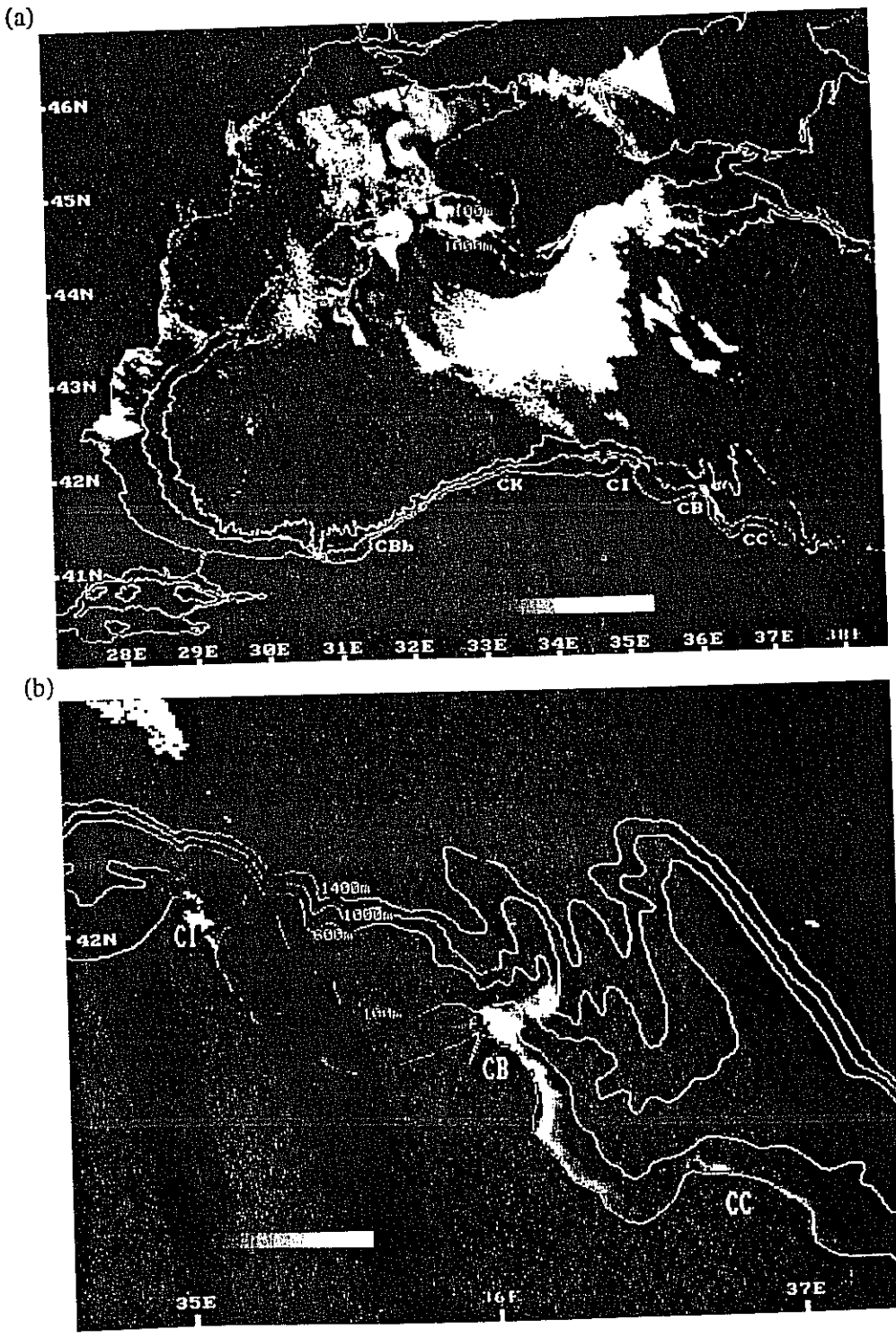

FIG.8. (a) Coastal Zone Colour Scanner (CZCS) satellite image on October 13, 1980, showing the massive plankton bloom in the northeast sector and unstable filaments near Cape Kerempe, and (b) its enlarged form showing a dipole eddy near the mouth of the Kizilirmak river. Both images are the atmospherically corrected channel 3 (550nm) of the CZCS.

and anticyclonic eddies, extending 60km offshore, and connected to the coast by a filament (the river plume) that seems to follow the depth contours of the local canyon topography adjacent to the Arhangelsky Ridge (Figs 1 and 8b). This topographic control is surprising since we suspect the flow to be confined in the surface layers. The dipole vortex could be an unstable feature generated by a pulse of momentum imparted by local winds, the river plume itself, or instabilities of the boundary current. Support for the instability hypothesis is given by similar features observed not far from the dipole: a number of filaments extending offshore from the coast near Cape Kerempe suggest an instability of the boundary current flowing along this coast.

In addition to the effects of Anatolian rivers displayed in Figs 7 and 8, a massive plankton bloom originating from the northwestern shelf can be identified. The bloom appears in both the particulate (Fig.7a) and calculated pigment (Fig.7b) fields. The high pigment concentration could well correspond to an *Emiliania huxleyi* bloom, since high spectral reflectance is obtained in all visible CZCS channels, which is characteristic of these organisms (HOLLIGAN, VIOLLIER, HARBOUR, CAMUS and CHAMPAGNE-PHILIPPE, 1983). Note that the bloom extends south from the shelf, reaching the middle of the basin, in spite of the minimum river discharges (Fig.3) expected during this season. This may suggest either the influence of northerly winds or the bloom to be independent of the size of the river plume. Investigating more closely, we see that the pigment distribution covers the entire northwest sector of the basin (Fig.7b), but the particulate signal (Fig.7a) is more confined to the region northwest of Crimea. This spectral pattern may indicate species differentiation between the shelf and open ocean plankton blooms. Only 6 days later, on October 13, 1980 (Fig.8a), the plankton bloom in the northeastern sector has become larger in size, and more complicated in texture.

Earlier during the same year, a summer plankton bloom was in progress, identified in Figs 9-13. The summer bloom originated over the northern shelf and then extended into part of the interior and across the entire western shelf region. We only discuss the northwestern sector in this section; the Danubian influence and transport in the southwest region are discussed in Section 4.2.

In Fig.10a-d different bands of the CZCS are shown for June 12, 1980, about 4 months before the data of Fig.6 were collected. The visible channel 1 data show a dark band covering the entire western shelf (Fig.1), indicating absorbance of sunlight by chlorophyll *a*, i.e. a massive bloom limited to the shelf. We note that the darkest region occurs in the northwest shelf near the Danube, where the production, under direct influence of the riverine nutrient supply, is largest. Channel 3 of the CZCS in Fig.10b indicates particulate material in the same area, and the pigment distribution in Fig.10c combined with the information given by Figs 10a and b, indicate that the particulates are mainly phytoplankton. Finally, the thermal infra-red image in Fig.10d shows a band of shelf water that is warmer than the interior, outlining the convergence region where warm surface water accumulates at the coast in agreement with the cyclonic basin circulation.

The visible data of Fig.10 can be used for the identification of multiple species of plankton. Light absorption (darker tones) in Channel 1 is maximum in the northwestern shelf region near the mouth of the Danube, with decreasing values observed along the entire western shelf (Fig.10a). In principle this maximum of absorption could result from chlorophyll *a* supported by the uniform pigment distribution in Fig.10c. In contrast to this region of absorbance, a region of Channel 1 reflectance (lighter tone) is identified at the front separating the shelf water from the interior. The frontal region is most likely populated with *E. huxleyi* as confirmed by high reflectance in the other visible bands (Figs 10a-c). As a result of the above discussion, we distinguish two populations of plankton, one occupying the western shelf region and the other populating the outer edge of the first group in the offshore frontal region. The nitrogen to phosphorus ratio of the Danube discharge determines the strength of summer phytoplankton blooms (D. AUBREY, personal communication). Particularly in June 1980, favourable N:P ratios were found in the immediate neighbourhood of the discharge,

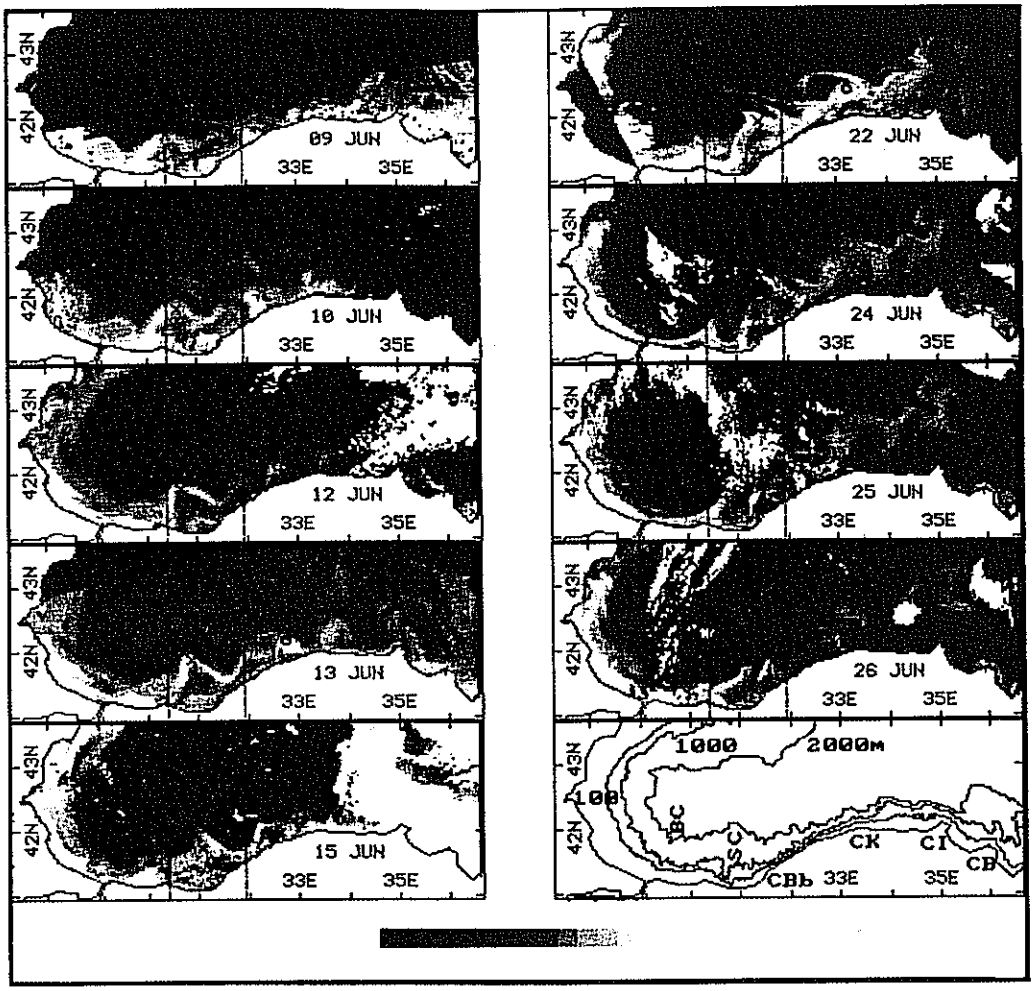

FIG.9. A sequence of CZCS channel 3 (550nm) images showing the development of the motions along the Turkish coast for the period 9 June through 26 June 1980. Abbreviations used: BC:Bosphorus Canyon, SC:Sakarya Canyon, CBb: Cape Baba, CK: Cape Kerempe, CI:Cape İnce, CB:Cape Bafra.

decreasing rapidly along the coast as a result of phytoplankton consumption.

Three days later (Figs 11a,b) we observe that the frontal region occupied by *E. huxleyi* has become unstable, and is ejecting a large filament (size ~150km) from the northwest shelf region into the interior. Note that the core of this filament contains chlorophyll *a* (Channel 1 absorption), encapsulated by high spectral reflectance species on the periphery of the filament. In Figs 11a,b and 12a,b, observed 10 and 13 days respectively after the initial image of Figs 9a-d, the filament has retained its identity, but a dipole eddy (with a better defined cyclonic member) has developed near its cap. We also note that the filament on these last two images does not seem to contain a core of visible light absorption at Channel 1; rather the entire filament becomes a region of high spectral reflectance. Also note that the area of Channel 1 absorption which initially covered the entire northwest shelf and extended south partially to cover the western shelf, has become smaller and more confined to the Danube mouth in the later images.

The above observations seem to suggest there is competition between the shelf species and the

coccolithophore bloom on its periphery. Initially the high reflectance species at the shelf edge forms a contrast with the other species distributed in the shelf region. In the sequence of following images, the shelf species are observed to become more confined, and the high reflectance species dominates the entire region excluding the vicinity of river mouths. The observed features suggest segregation behaviour (e.g. OKUBO, 1980) typically encountered between similar but competing species.

4.2 A time series study of meandering flow and primary production along the Anatolian coast

In addition to the other aspects discussed above, outstanding dynamical processes of shelf-open ocean interaction, with important impact on productivity are investigated in Figs 9-13. The open ocean production activity of a filament originating from the northwestern region has been revealed above. Similarly, a unique pattern of meandering currents along the Anatolian coast with efficient dispersion result in a massive plankton bloom in that region.

The fields derived from the CZCS serve as tracer fields visualizing the motions transporting them. The motion along the Anatolian coast basically consists of a pattern of eastward propagating waves with an embedded train of mesoscale eddies. The series of images in Fig.9 are used to calculate (by following points with fixed phase) an eastward propagation speed of 10-15cm s^{-1} ($\cong$10-15km d^{-1}) for the meandering motion. Based on a review of several images used in their study, OGUZ *et al*, (1992) claimed that they had not been able to detect any translation of features along the boundaries, and suggested that the translation speeds could be too small to be detectable. In the present case, we find noticeably fast propagation of wave motions superimposed on mean boundary currents.

There is close correlation of the flow features with the continental slope topography. The eastward propagating oscillatory motions are generated at the abrupt termination of the western continental shelf at Sakarya Canyon. As the whole pattern moves east in Fig.9 and in Figs 10-13, the eastern terminus of the shelf region appears as the generation region for the wave motion. The uniform distribution of tracers observed along the western shelf, e.g. in Figs 10b,c, verifies uniform flow of the cyclonic boundary current. This uniform flow in the west is replaced by undulating features east of Sakarya Canyon.

During early development (Fig.10) the wave pattern is regular, though filaments with offshore extensions are visible near Cape Kerempe. Ten days later (Figs 9 and 12), the meander has developed into a train of cyclonic and anticyclonic regions with a complex pattern of filaments extending offshore. In fact, the overall appearance of the motion in Fig.12 is reminiscent of a turbulent jet flow, with a core containing numerous meanders and filaments. This jet follows the 30° (from east) oriented western Anatolian coast from Sakarya Canyon to Cape Kerempe, where it begins to separate from the coast, and becomes more complex to the east. Note that this is also the region where the steep bottom topography adjacent to the coast is replaced by a wide continental shelf extending from Cape Kerempe to Cape Bafra.

In Fig.13, only 3 days after the image in Fig.12, we observe that the jet flow that developed earlier has widened and become totally separated from the coast east of Cape Kerempe. The wide jet terminates with a dipole-like cap extending to the mid-basin region east of Cape Ince. In this fully developed state, we observe numerous cyclonic and anticyclonic eddies within the turbulent jet. (Note that this particular image has also been used by MURRAY and IZDAR, 1989, and on the cover of MURRAY, 1991).

Also note the rapidity of the development observed in Figs 9-13: in merely two weeks, an entire

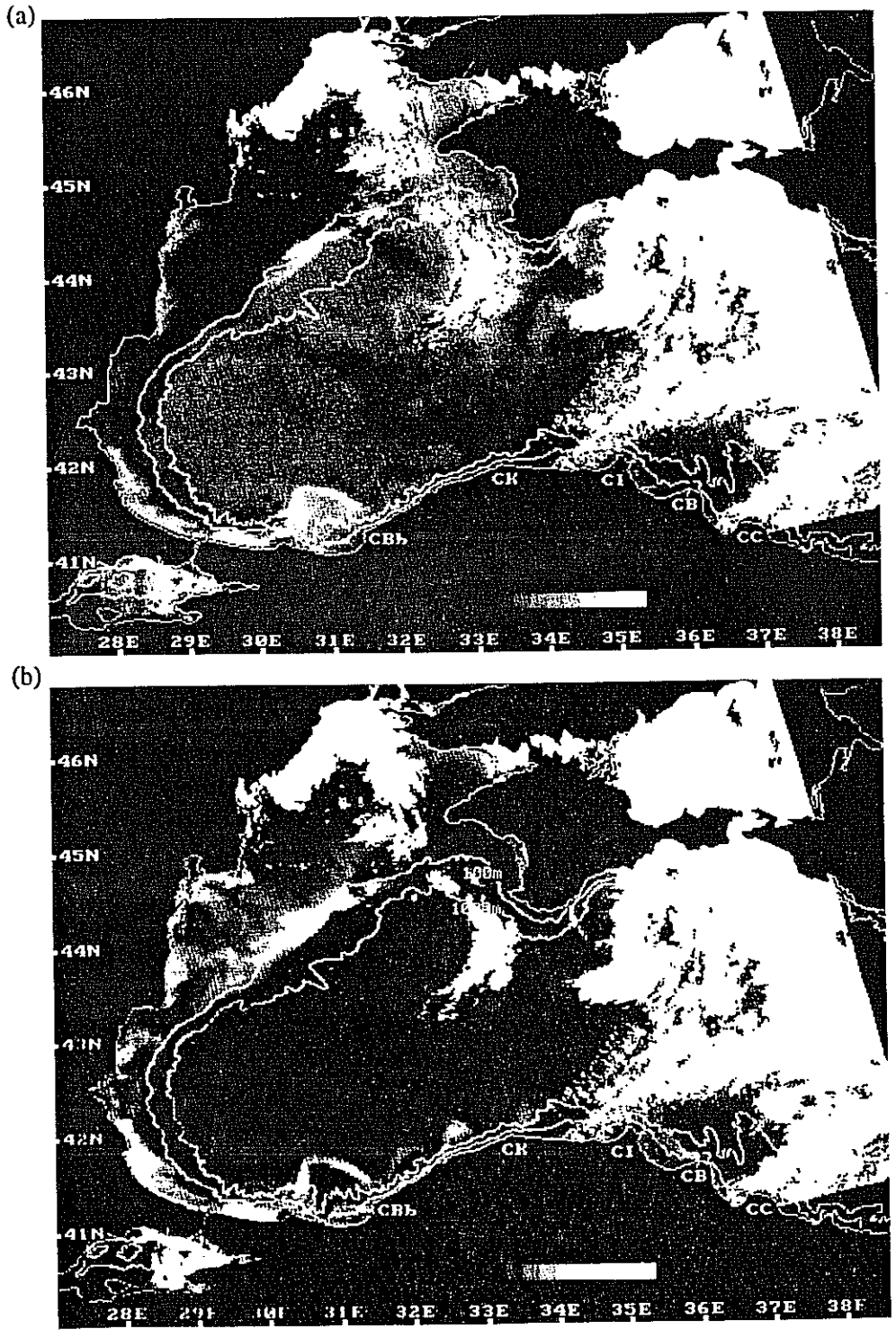

FIG.10. Coastal Zone Colour Scanner (CZCS) satellite images on June 12, 1980. The images represent the atmospherically corrected (a) channel 1 (443nm), (b) channel 3 (550nm), (c) the calculated pigment concentration and (d) thermal infra-red channel, showing development of flow and associated primary productivity along the west and southwestern coast of the Black Sea. (In this and the following thermal images, the darker tones represent warmer and the lighter tones represent colder water.)

(c)

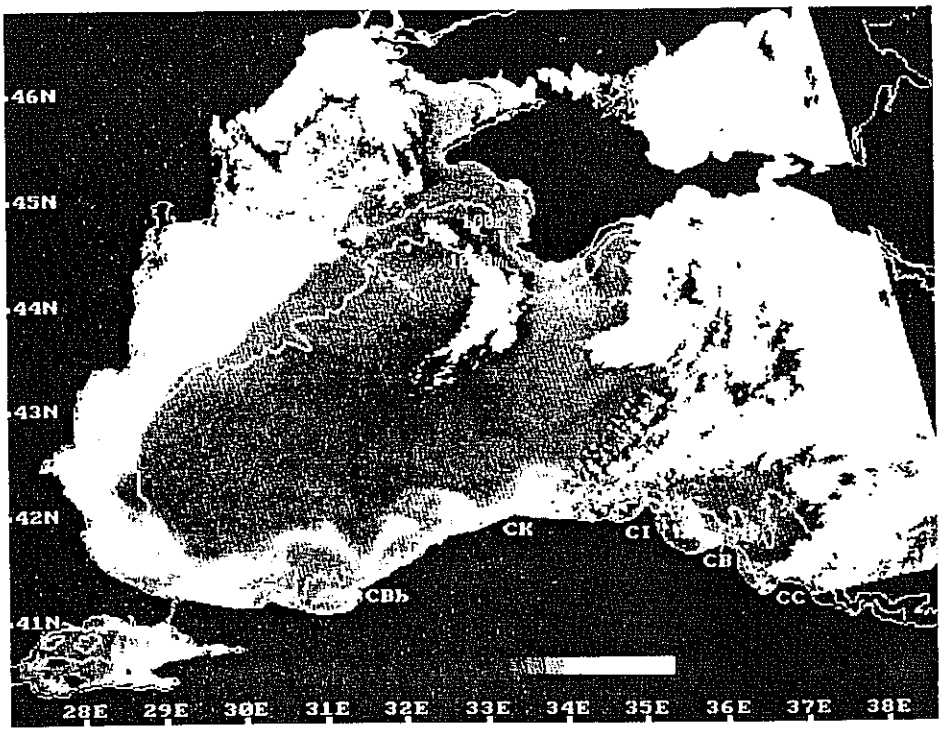
46N
45N
44N
43N
42N
41N
CK
CI
CB
CC
CBb
28E 29E 30E 31E 32E 33E 34E 35E 36E 37E 38E

(d)

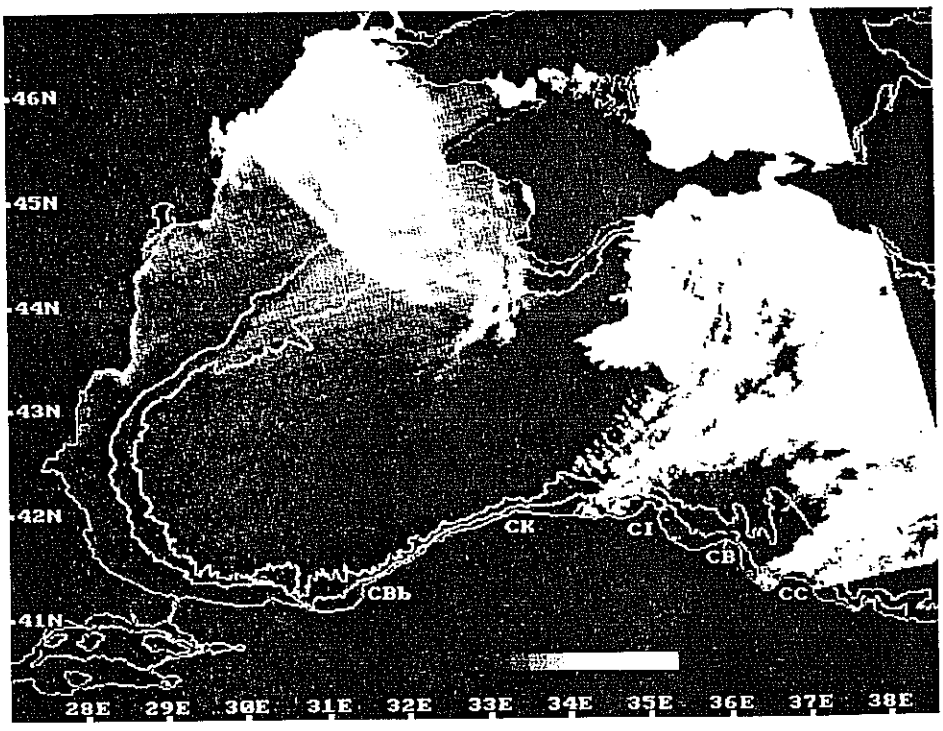
46N
45N
44N
43N
42N
41N
CK
CI
CB
CC
CBb
28E 29E 30E 31E 32E 33E 34E 35E 36E 37E 38E

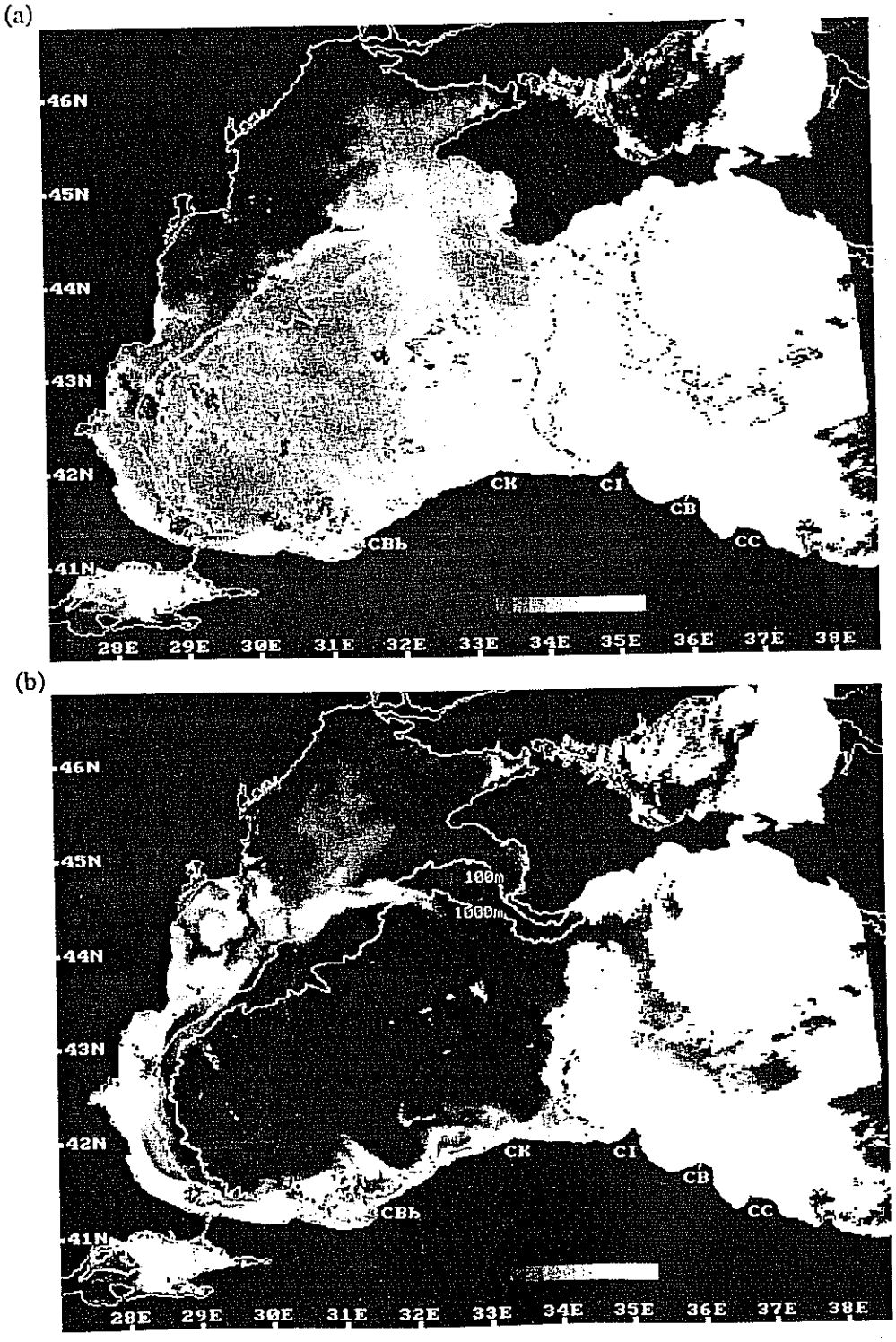

FIG.11. Coastal Zone Colour Scanner (CZCS) satellite images on June 15, 1980. The images represent the atmospherically corrected (a) channel 1 (443nm), (b) channel 3 (550nm) showing development of flow and associated primary productivity along the west and southwestern coast of the Black Sea.

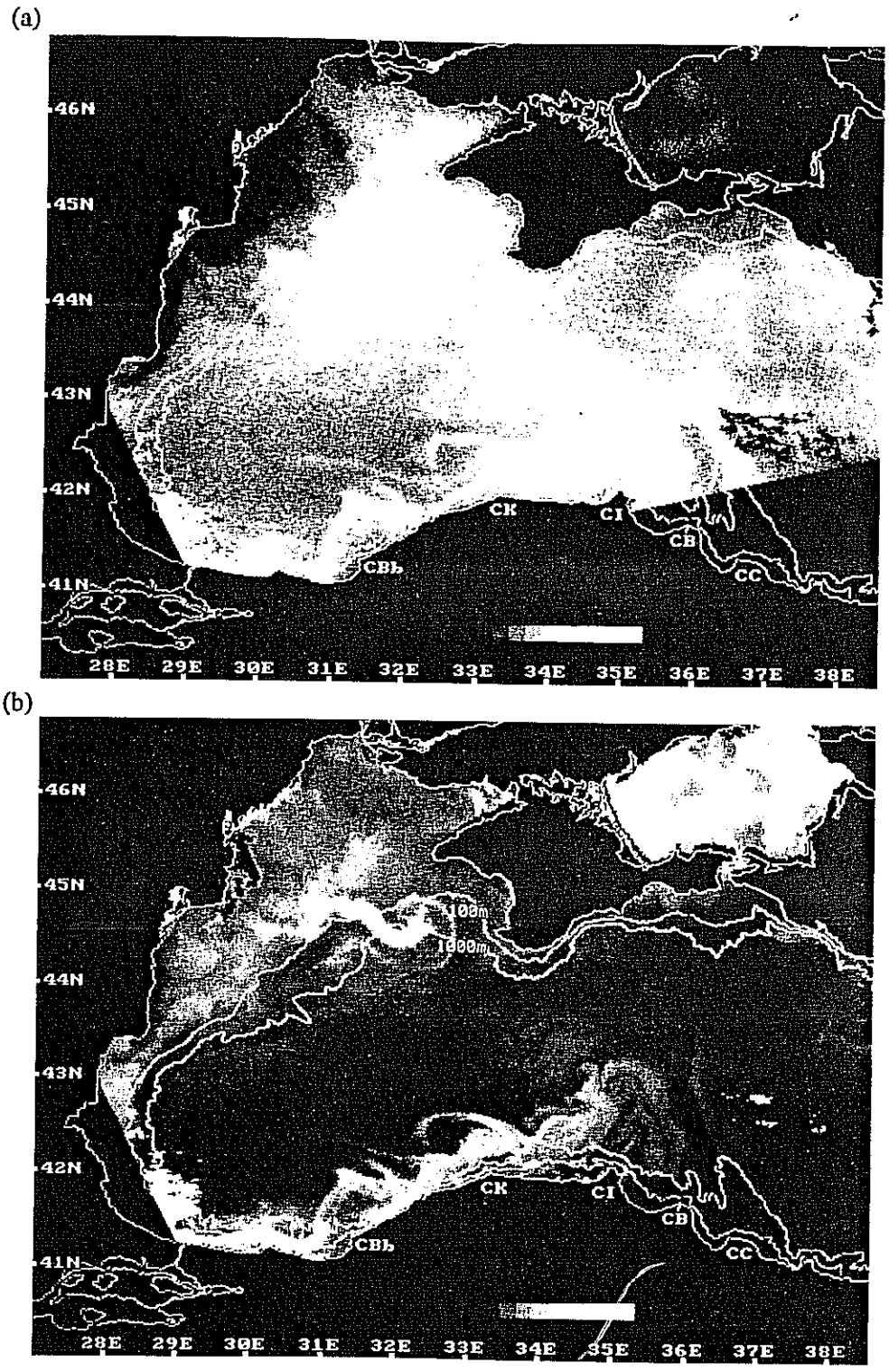

FIG.12. Coastal Zone Colour Scanner (CZCS) satellite images on June 22, 1980. The images represent the atmospherically corrected (a) channel 1 (443nm), (b) channel 3 (550nm) showing development of flow and associated primary productivity along the west and southwestern coast of the Black Sea.

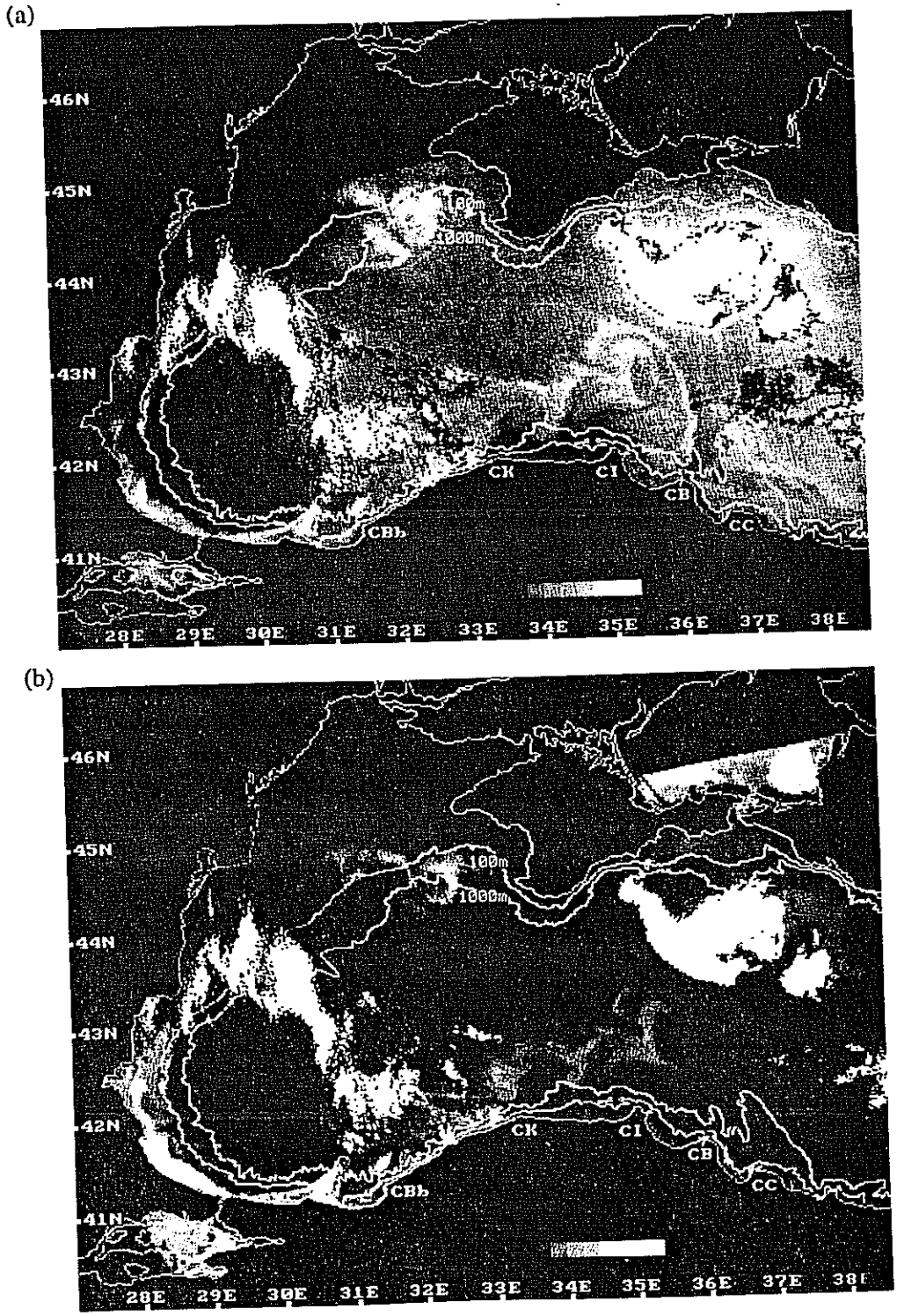

FIG.13. Coastal Zone Colour Scanner (CZCS) satellite images on June 25, 1980. The images represent the atmospherically corrected (a) channel 1 (443nm), (b) channel 3 (550nm) showing development of flow and associated primary productivity along the west and southwestern coast of the Black Sea.

current system has become modified in character, and unstable eddies and filaments have developed within time scales of a few days. This is in marked contrast with the circulation dynamics in the neighbouring regions, for example in the Levantine Basin of the Eastern Mediterranean Sea (e.g. ÖZSOY, HECHT, ÜNLÜATA, BRENNER, OGUZ, BISHOP, LATIF and ROZENTRAUB, 1991), where long-term persistence is a basic property of coherent structures. This comparison reveals the roles of strong ambient stratification and of lateral sources of buoyancy in supporting unstable motions in the Black Sea environment.

Baroclinic instability is the mechanism most frequently used (numerous examples given in Section 1) to explain unstable motions in buoyant coastal flows. Although we oberve that the meandering motion of the west Anatolian boundary current is triggered by a discontinuity in shelf topography, baroclinic instability appears to contribute to its subsequent growth. Instability of fronts leading to large meanders, bores or breaking waves was examined by STERN (1980). It is these motions that lead to exchanges across the front, as indicated by the large excursions in Figs 9-13. It is noticeable from the increasing sizes of the eddies that significant entrainment is taking place.

Baroclinic instability could be one of the most relevant mechanisms generating time-dependent motions along frontal regions. Realistic boundary flows with horizontal density gradients are often found to be unstable to small perturbations (e.g. MYSAK and SCHOTT, 1977; GRIFFITHS and LINDEN, 1981; IKEDA *et al*, 1984, 1989; QIU, 1988; CHAO, 1990; BECKERS and NIHOUL, 1992), and as a result the unstable waves in many cases grow into large amplitude meanders or paired coherent vortices. Laboratory experiments of CONDIE (1989) show that the energy of the unstable motions, including coalescent eddies and dipoles, is extracted from the mean flow at the Rossby deformation radius scales, and later transferred to larger scales by nonlinear processes. During the nonlinear growth stage of the instability, QIU *et al* (1988) showed that disturbances starting at the grid-scale were transformed into finite amplitude meanders with 'backward breaking' tendency, enhancing the cross-shelf exchanges. Laboratory experiments of CARSTENS *et al* (1984) indicated anomalous current loops separated from the coast. CHAO (1990) differentiated between prograde (fronts rising to the surface in the same direction as the bottom topography, e.g. Gulf Stream or upwelling fronts) and retrograde (isobaths and isopycnals slanted in opposite senses, e.g. density driven boundary currents with buoyant water near the coast, such as in the Black Sea) fronts, arguing that prograde fronts are more amenable to slanted convection (baroclinic instability) than retrograde fronts. However, it was demonstrated that enhanced meander and eddy growth could occur as a result of relaxation processes, e.g. temporally varying buoyancy forcing, which seemed to be more important in the case of retrograde fronts and more effective than the other possible forms of external forcing (such as winds or small topographic variations).

The observations also illustrate how the dynamics of the meandering jet flow along the Anatolian coast of the Black Sea is influenced by strong interactions with topography and by changes in the coastline orientation. The flow along the western shelf is most probably in a state of geostrophy, following the bathymetric contours of the shelf/slope region. Once triggered by the sudden depth change at Sakarya Canyon, the ensuing motions are unstable and, therefore, not able to readjust to a steady uniform flow along the remaining part of the coast. The jet flow becomes wider and more turbulent with distance from the step, and with time.

The mechanism of generation of the oscillatory motions by the step topography is not clearly understood. We expect oscillatory motions to be generated by the interaction of a topographic barrier with barotropic shelf/slope flows taking the coast (shallower depths) to the left in the northern hemisphere. Considering that the analogous effects of planetary vorticity gradient (β) and topography (i.e. contributions to variations in f/H, where f is the Coriolis parameter and H the depth

of the flow), we can compare flows bounded on the left hand side with eastward flows in the case with planetary vorticity gradient. Oscillatory motions are created when an eastward flowing β-plane barotropic jet crosses a step topography, while a smooth readjustment occurs for westward flowing jets (SHETYE and RATTRAY, 1982), confirming well known results of BATCHELOR (1970). The above results suggest that the western Anatolian jet flowing across the Sakarya Canyon would not be subjected to meandering or oscillatory motions if this jet were to be purely barotropic. On the other hand, SPITZ and NOF (1991) indicate that a barotropic boundary current would be forced to separate from the coast when it encounters a large step with the depth increasing downstream, regardless of the direction of flow relative to the coast.

Sudden changes in topography are expected to lead to oscillatory motions even in the case of a right hand side coast, when baroclinic modes are included. In fact, barotropic flows impinging on a step topography can be expected to generate large amplitude baroclinic motions (e.g. CUSHMAN-ROISIN and O'BRIEN, 1987). Oscillatory motions created by interacting baroclinic and barotropic components of a boundary current near canyon or ridge topographies are illustrated by HÄKKINEN (1987).

Interactions with coastline perturbations were found to create standing waves, as well as baroclinic eddies and filaments in the case of upwelling fronts (NARIMOUSA and MAXWORTHY, 1987), and to lead to meanders by pure geometrical adjustment to depth contours (without imposing baroclinic instability) in the case of ice-edge fronts (IKEDA, 1987). The role of bottom topographic features was found to augment the baroclinic instability in the case studied by IKEDA (1989). In the case of upwelling fronts, NARIMOUSA and MAXWORTHY (1985) found large stationary meanders and filaments generated by a bottom ridge. HAIDVOGEL, BECKMANN and HEDSTRÖM (1991) and HOFFMANN, HEDSTRÖM, MOISAN, HAIDVOGEL and MACKAS (1991) found offshore filaments generated by the interaction of a boundary current (upwelling front) with topographic variations. During later stages of development, the evolving filaments were shown to lead to self-advecting dipole eddies detached from the coastal region.

An important effect of topography we observe in the case of the west Anatolian boundary current is the separation of the jet from the coast at Cape Kerempe, where the flow encounters a widening shelf topography. LEAMAN and MOLINARI (1987) studied the effects of a linearly widening shelf and found that this situation can lead to vertically sheared flows perpendicular to the coast, resulting in flow separation. The change in the angle of the coastline near Cape Kerempe can be a secondary factor leading to flow separation. Laboratory studies illustrate eddy shedding and separated flows downstream of headlands (e.g. BOYER and CHEN, 1987).

Although the flow is made visible by productivity and particulate material on the western continental shelf, these tracers are neither conservative nor have uniform sources. For example, we observe changes of reflectance both along the western shelf and at the Sakarya Canyon in Figs 10a-d. In particular, sharper changes of concentration occur across the Canyon. Vertical mixing and resuspension of bottom sediments created by three dimensional motions at the edge of the Canyon (ÖZSOY *et al*, 1993), and local increases in productivity (GÖÇMEN, 1988) can contribute to these changes.

The cyclonic circulation of the Black Sea is outlined by the bio-optical properties modified along the western shelf. Much of the interior and the eastern basin have considerably smaller pigment and particulate concentrations. Note also that the satellite data in Figs 9-13 correspond to the period when the Danube discharge is maximum. Furthermore, the data of SERPOIANU *et al* (1992) (Section 3.3) suggest that 1980 was characterized by relatively high runoff and lower salinities near the Romanian coast.

HAY and HONJO (1989) examined the vertical particle flux at two sites in the southwestern Black

Sea using sediment traps during the 1982-1987 period. They observed that the dominant fraction of the annual flux was deposited during short plankton bloom periods lasting less than a month at a site 80km offshore from the Sakarya Canyon. At the other site 40km offshore from Amasra (west of Cape Kerempe), the short term fluxes were less dominant. The nearshore traps indicated *E. huxleyi* blooms in the summer, autumn and early winter, in contrast to the offshore traps where more than half of the annual particle flux was deposited during short (~one month) periods of spring/ summer blooms. Some spring blooms of *E. huxleyi* were accompanied by the diatom *Rhizosolenia*.

It appears that the images in Figs 9-13 were obtained in the short period (<1 month) of an early summer bloom, during which rapid changes in the spatial distribution of species were observed, with *E. huxleyi* dominating the western basin towards the end of the observation period, excluding the near field of the Danube delta.

About 20 days later than the fully developed bloom in Fig.13, we observe absorption at channel 1 in the Azov Sea, the northwestern shelf and along the Anatolian coast (Fig.14a). The regions of strong absorption in channel 1 in the northwest shelf and the Azov Sea appear to delineate regional blooms of phytoplankton chlorophyll other than *E. huxleyi* (possibly dinoflagellates), characterized with high reflectance in channel 3 accompanying channel 1 absorption. The same period marks the termination of the *E. huxleyi* bloom along the Thracian and Anatolian coasts, because no colour signature of either particulates (Fig.14b) or pigments (not shown) are present in these regions. The channel 1 absorption without any channel 3 reflectance in the patches along the Anatolian coast could be a result of flavins released into the water during bacterial production, since these dissolved chemicals can lead to absorption at 450nm (COBLE, GAGOSIAN, CODISPOTI, FRIEDERICH and CHRISTENSEN, 1991). Although the depth distribution of flavins has a maximum below the euphotic zone in the Black Sea (COBLE *et al*, 1991), eddy-induced upwelling along the central part of the Anatolian coast, as indicated by the infra-red data (Fig.14c) may have increased their surface concentrations. The upwelling structures observed in Fig.14c are typical of the summer months, a fact we investigate further in Section 4.3.

Note that the spreading pattern of production displayed in Figs 9-13, and confirmed by *in situ* measurements, implies that the eutrophication must have started near the Danube, proceeded south along the shelf, and finally reached the interior via cross-frontal turbulent exchanges during the early part of the last decade, when the CZCS data were obtained. It is suspected that this pattern has been significantly altered in recent years, leading to a recent decrease in the optical transparency o the surface waters even at the central regions of the Black Sea (EREMEEV *et al*, 1992), implying basin-wide intense phytoplankton blooms, confirmed by some of our recent data (not presented).

Figures 9-13 emphasize the production on the western shelf and the importance of horizontal spreading by the interactions between the shelf and deep sea regions. D. AUBREY (personal communication) has reviewed monthly averaged CZCS pigment data from 1979, 1980 and 1981 and has found the same region of influence for phytoplankton blooms with similar cross-shelf influences. In fact, he indicates a higher production in 1981 as compared to 1980 represented by our data. This higher production in 1981 seems to be a result of a Danube discharge with a high ratio of inorganic nitrogen to phosphorus (N:P), preceding the summer productivity maximum observed during that year.

Finally in this section, we note that the summer productivity in the western Black Sea shelf appears to influence the productivity in the eastern half of the Sea of Marmara. Earlier results (ÜNLÜATA and ÖZSOY , 1986; BASTÜRK, SAYDAM, SALİHOGLU and YILMAZ, 1986) suggest that the upper layer transport from the Black Sea and the entrainment/recycling of nutrients from the underlying Mediterranean water into the jet flow issuing from the Bosphorus are the main processes leading to production in the Sea of Marmara. In fact, the highest productivity in the Sea of Marmara

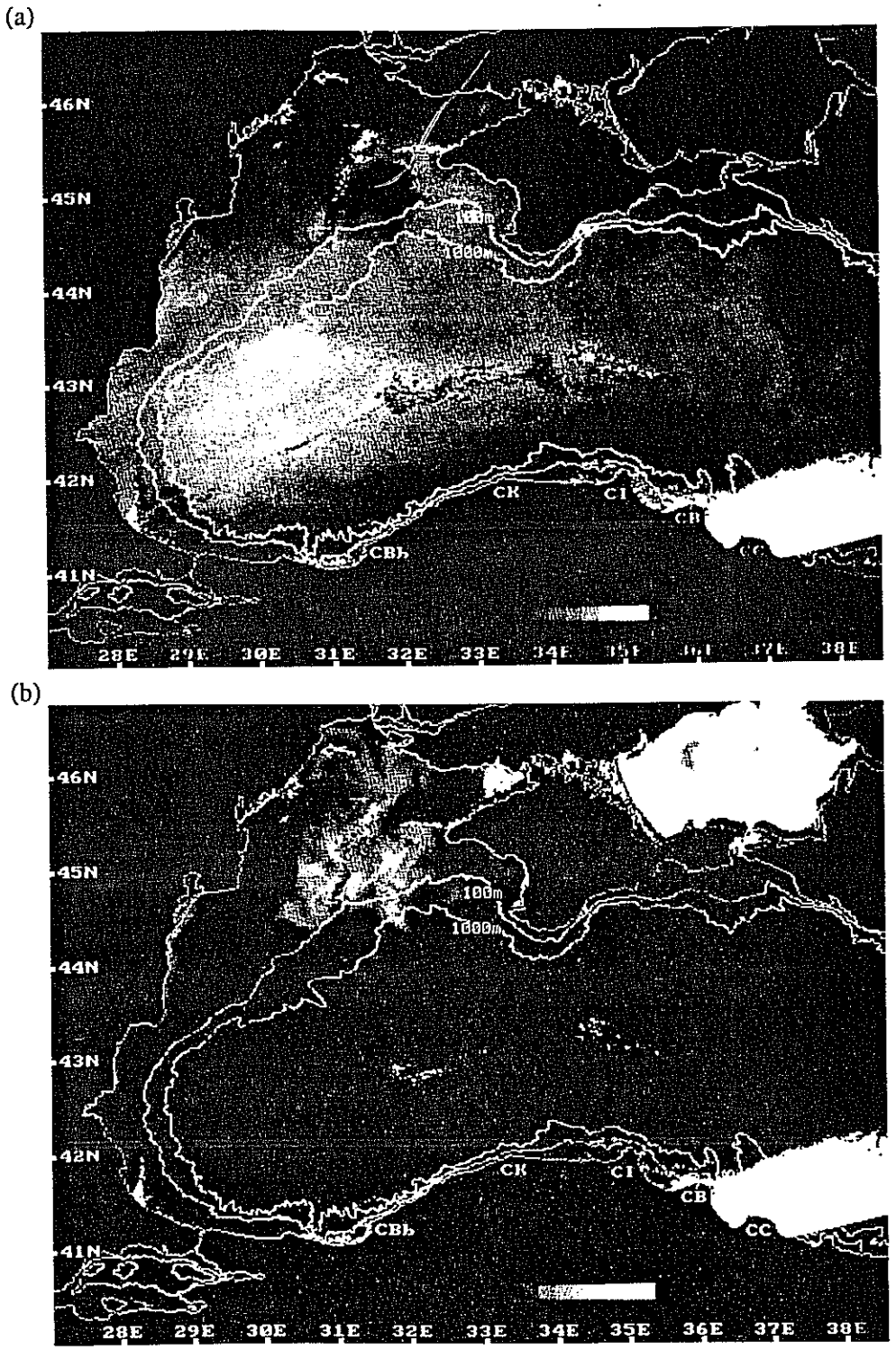

FIG. 14. Coastal Zone Colour Scanner (CZCS) satellite images on July 15, 1980. The images represent the atmospherically corrected (a) channel 1 (443nm), (b) channel 3 (550nm) and (c) thermal infrared channel, showing the phytoplankton blooms in the northwestern shelf and the Sea of Azov, simultaneously with the development of an upwelling event and post-bloom dissolved materials along the Anatolian coast.

(c)

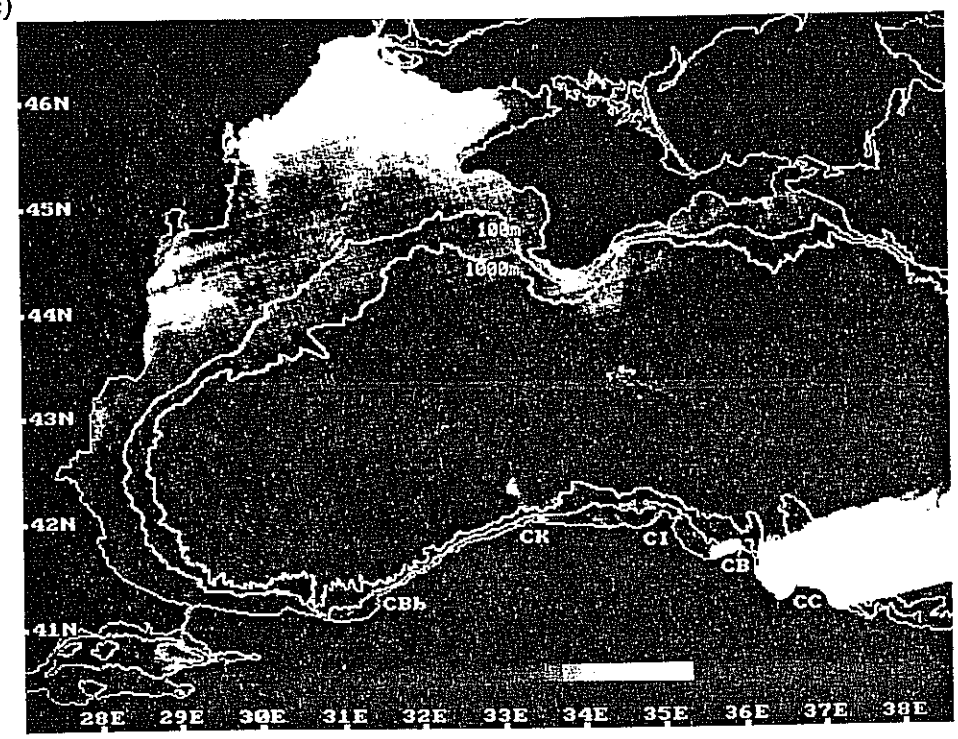

occurs in winter, when wind mixing enhances nutrient inputs into the upper layer, but secondary particle and chlorophyll maxima are found in summer, following peak discharges of the Bosphorus. A plankton bloom in the Sea of Marmara is shown in Figs 10-13 at the same time as the bloom along the shelf region in the western Black Sea. Figures 14 and 15 confirm that the intensity of the Marmara productivity subsides together with the productivity in the Black Sea. These results indicate a direct influence in summer of Black Sea surface waters transported through the Bosphorus.

4.3 Summer upwelling along the Anatolian coast

Based on a set of individual images from different years, the Anatolian coast from Cape Baba to Cape Ince can be identified as a region of upwelling starting in early summer and lasting until early fall.

Upwelling along the Anatolian coast is indicated in the CZCS thermal infra-red image of July 15, 1980 (Fig.14c). The successive images in Figs 14c and 15a-3 indicate a persistent upwelling event during the two month period of July-September 1980. It is remarkable that the upwelling event starts about one month after the period of Figs 9-13, when a cyclonic (downwelling) basin circulation with warm coastal waters (e.g. Fig.9d) was observed in the same region.

The cold water patches initially occur in the form of regular eddies in Fig.14c. Only two days later, in Fig.15a, we observe that the initial forms have been stretched in the offshore direction,

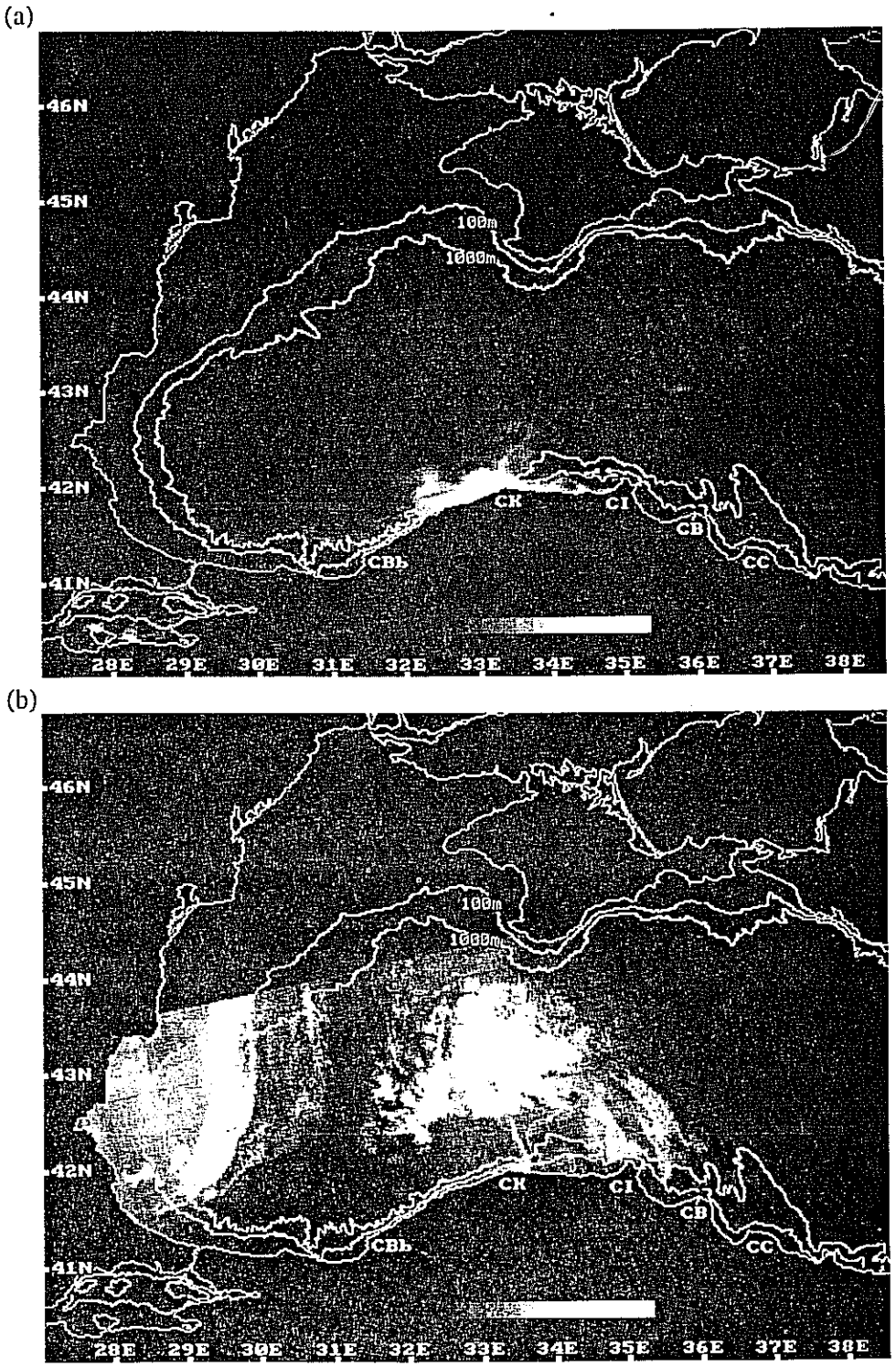

FIG.15. Coastal Zone Colour Scanner (CZCS) satellite images on (a) July 17, (b) July 22, (c) August 29, (d) August 31, and (e) September 9 1980, representing the atmospherically corrected thermal infra-red channel.

(c)

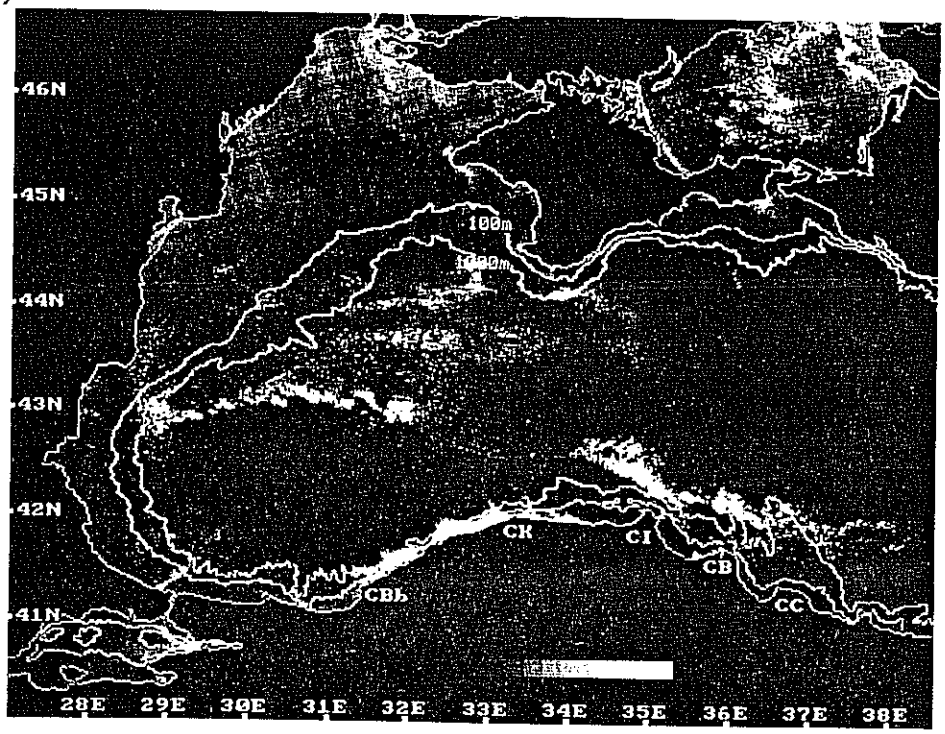

(d)

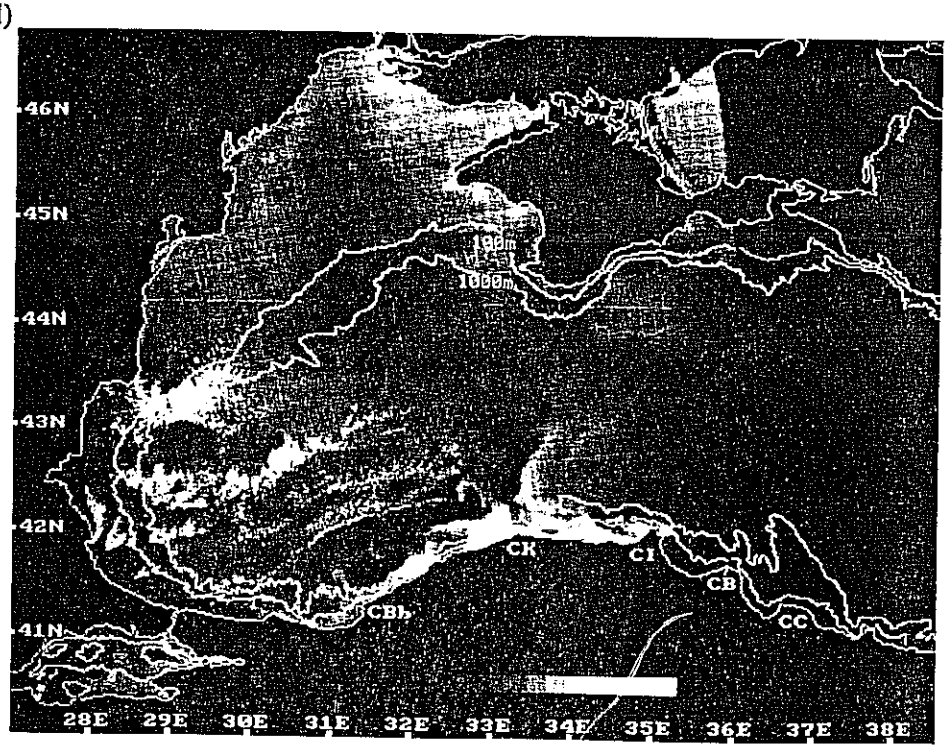

ugust
ermal

(c)

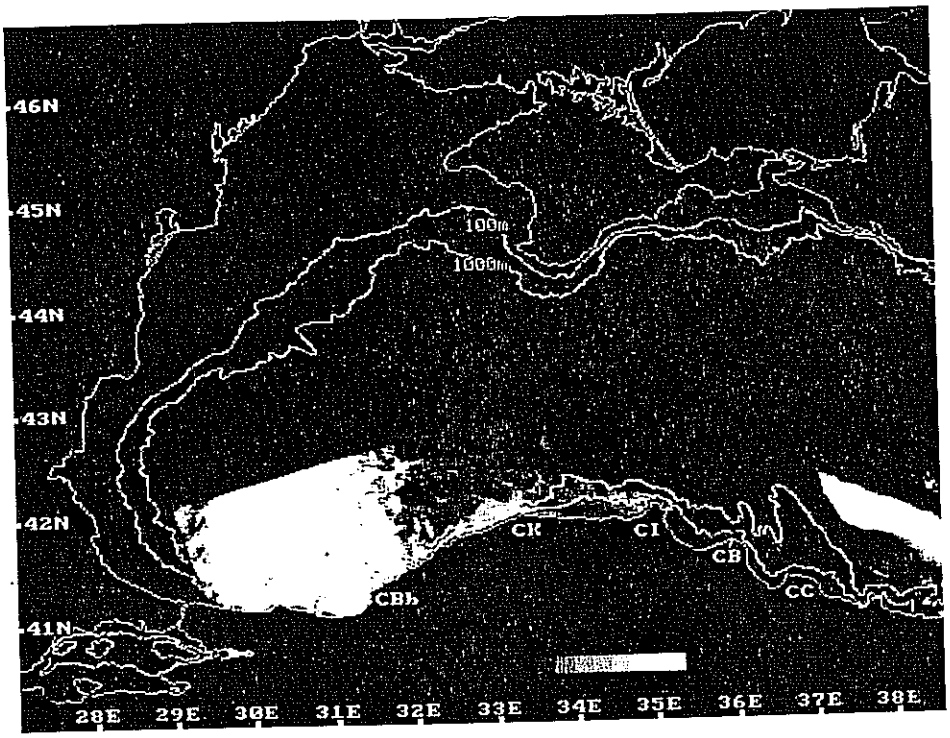

taking the form of filaments. In the remaining images of Figs 15b-e we observe rapidly growing and dissipating filaments, extending ~150km offshore. In Fig.15c we observe periodic wave motion along the coast from Cape Baba to Cape Kerempe, growing rapidly into filaments during the next two days until Fig.15d.

The fact that upwelling takes place along a coast ordinarily associated with a downwelling circulation of the cyclonic boundary current is most remarkable. The upwelling can not be attributed to local winds, because they are not particularly strong or favourable in summer (e.g. the summer winds at Sinop, largely sea-breezes, are mainly from the northwest).

Although the wind distribution and circulation do not appear to support continuous upwelling along the Anatolian coast, transient dynamics could ressult in the short-term upwelling. For density driven boundary flows, QIU *et al* (1988) found upwelling related reversals of surface salinity near the coast. Similarly, CHAO (1990) indicated upwelling near the coast, even in the case of retrograde fronts. In numerical experiments simulating the Algerian Current (BECKERS and NIHOUL, 1992), a possibility of upwelling was found within anticyclonic eddies as well as within cyclonic ones. Despite the fact that the Algerian Current normally pools low density Atlantic water against the coast, upwelled water occasionally occurs along the coast and within filaments wrapped around coastally attached anticyclonic eddies (MILLOT, 1991).

We note that the upwelling motions start past Capa Baba, and the coldest waters and filaments with greatest offshore extension occur near Cape Kerempe. Despite the lack of *in situ* data showing the flow structure at the time of these observations, we may speculate that the local dynamics, e.g. headland geometry and widening topography, rather than wind forcing, are largely responsible for creating the Anatolian coastal upwelling. We recognise the effects of the widening topography near Cape Kerempe leading to the flow separation observed two months earlier in Figs 9 and 13.

Sharp corners in coastline geometry can lead to localized upwelling, even in the case of buoyant boundary currents with the coast on the right hand side, as shown by CHERNIAWSKY and LEBLOND (1986). Most observations of topographically or geometrically induced upwelling elsewhere have been obtained either near permanent upwelling fronts (e.g. the California coast, IKEDA and EMERY, 1985; NARIMOUSA and MAXWORTHY, 1985, 1987; the southeastern coast of the USA, JANOWITZ and PIETRAFESA, 1982), or under conditions of favorable winds (e.g. the Gulf of Lions, HUA and THOMASSET, 1983).

Similar upwelling is observed in the available AVHRR images of the summers of 1990, 1991 and 1992 (Figs 16-20). *In situ* data during some of these periods are used to verify the upwelling features.

On June 20, 1990 and the following August 22 1990 images (Figs 16a,b) cold water patches can be seen along the Anatolian coast. The August 29, 1990 image (Fig.16c) shows the development of a wave-like feature (wavelength ~100km) with regularly spaced offshore filaments (10-20km wide and ~70km long) of cold water in the region between Sakarya Canyon and Cape Ince. We also note the similarity of the wave-like features occurring in the same area, in the two images of August 29, 1980 (Fig.15c) and August 29, 1990 (Fig.16c) taken at the same time of the year. We have *in situ* data observed later, in September 1990, which indicate anticyclonic recirculation in the region of Cape Kerempe to Cape Bafra (OGUZ *et al*, 1993), but there was no indication of cold surface water in the area, perhaps because the upwelling had ceased to exist in the autumn.

Imagery from summer 1991 (Figs 17a,b) similarly indicate upwelling to the east of Cape Kerempe (Figs 20a,b). In just one day, between September 14 and 15, 1991, a large change occurs in the area covered by the upwelled water. Wave-like features with scales of about 100km are evident in Fig.17b. Within the next ten days until the next image on September 24, 1991 (Fig.17c), the upwelling disappeared along the Anatolian coast. This is in agreement with the hydrographic data taken during the later part of September 1991 (Figs 18a,b). Figure 18a shows warm water along the coast in the recirculating area west of Cape Ince, except between Cape Baba and Cape Kerempe where the boundary current is discontinuous as shown by the streamlines in Fig.18b. This region of discontinuous currents could either indicate a coastal attachment of the current not sufficiently resolved by the geostrophic analyses, or they could indicate residual downwelling/ upwelling along the coastline, although the transient events were observed somewhat earlier.

A remarkable feature in Figs 17a-c is the pair of warm water filaments extending from the northeastern (Caucasian) shores towards the interior of the eastern basin, each with a length of ~250km, a width of several tens of km, and horizontal spacing of ~150km. These features are associated with the dynamics of the boundary current in the eastern basin, downstream of the large anticyclone trapped in the southeast corner (a permanent feature found almost every time, including the 1991 and 1992 surveys, Figs 18b and 20b). These features indicate that the interaction between the boundary current and the basin interior is not confined to the western basin, but similar interactions, though with different types of instability, also occur in the eastern basin.

Returning back to the Anatolian upwelling, a persistent summer event of long duration is evident in infra-red images of August-September 1992 (Figs 19a-c). Data obtained by the R/V *Bilim* (Figs 20a-c) indicate that the upwelling occurred earlier during July 1992. Both the survey data and the APT image obtained in early August indicated the upwelling region to be small. The *in situ* data located its centre west of Cape Ince, and infrared image located it near Cape Kerempe. In the AVHRR images later in August, the upwelling region had grown in size, covering the entire region from Cape Baba to Cape Ince. Periodicity in the upwelling features is evident in the last image.

The surface temperature distribution (Fig.20a) indicates a cold water patch between Cape Kerempe and Cape Ince with a temperature of 10°C at its center (compared to surface temperatures

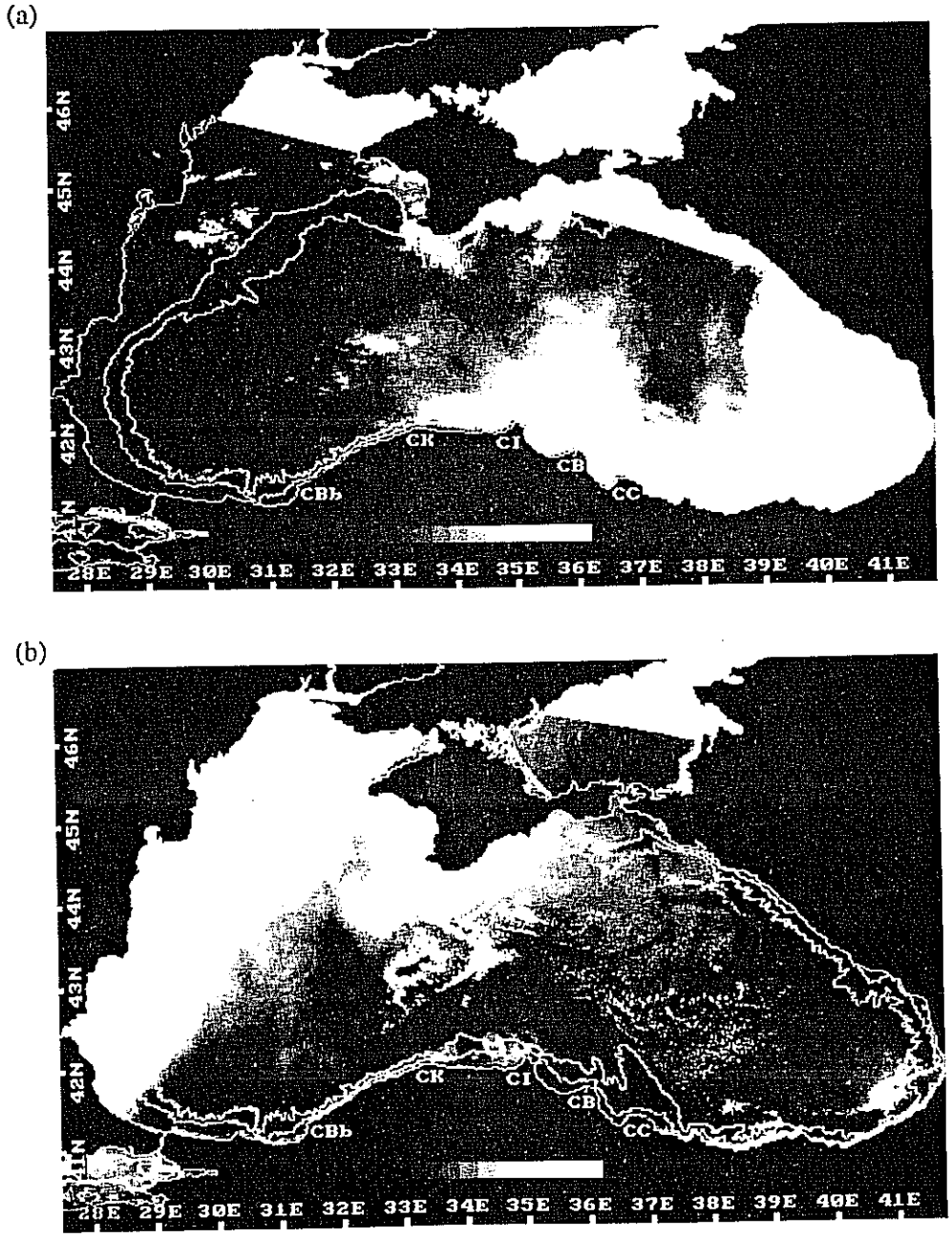

FIG.16. Advanced Very High Resolution Radiometer (AVHRR) satellite images on (a) June 20, (b) August 22, and (c) August 30, 1990 representing the atmospherically uncorrected (NOAA-10) channel 4.


41E
40E
39E
38E
37E
36E
35E
34E
33E
32E
31E
30E
29E
28E
41N
42N
43N
44N
45N
46N
1000m
CC
CB
CI
CH
CBh

(c)

(a)

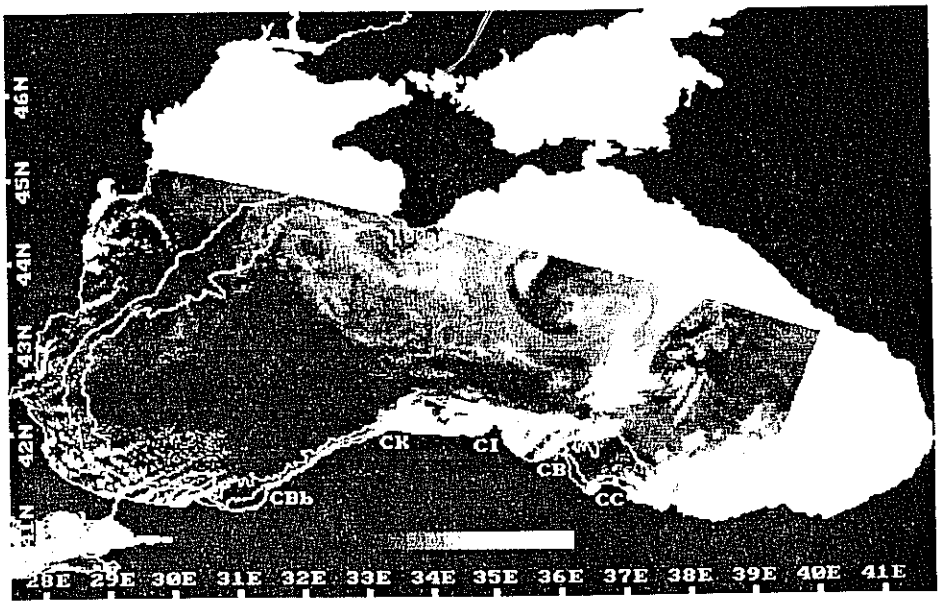

(b)

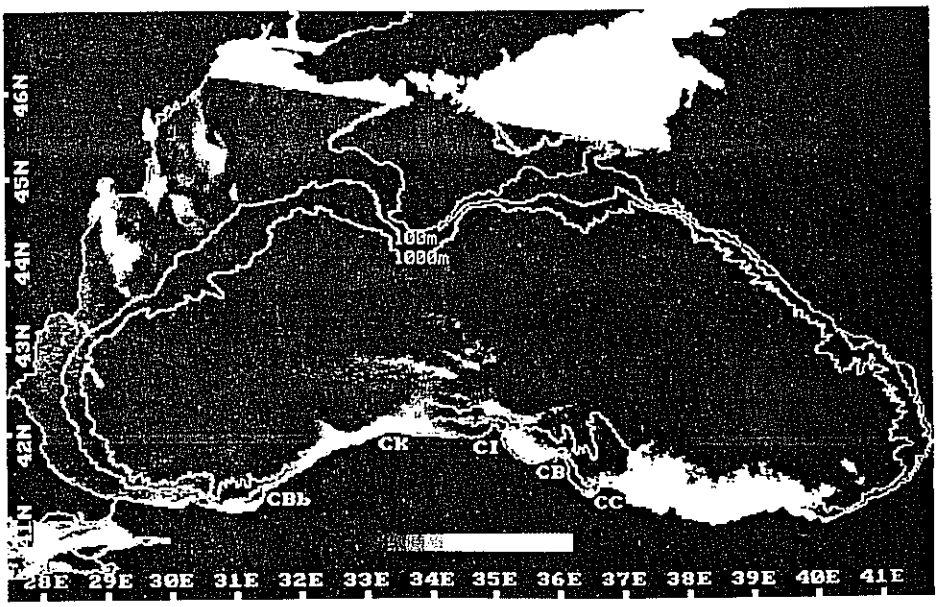

FIG. 17. Advanced Very High Resolution Radiometer (AVHRR) satellite images on (a) September 14, (b) September 15 and (c) September 24, 1991, representing the atmospherically uncorrected (NOAA-10) channel 4.

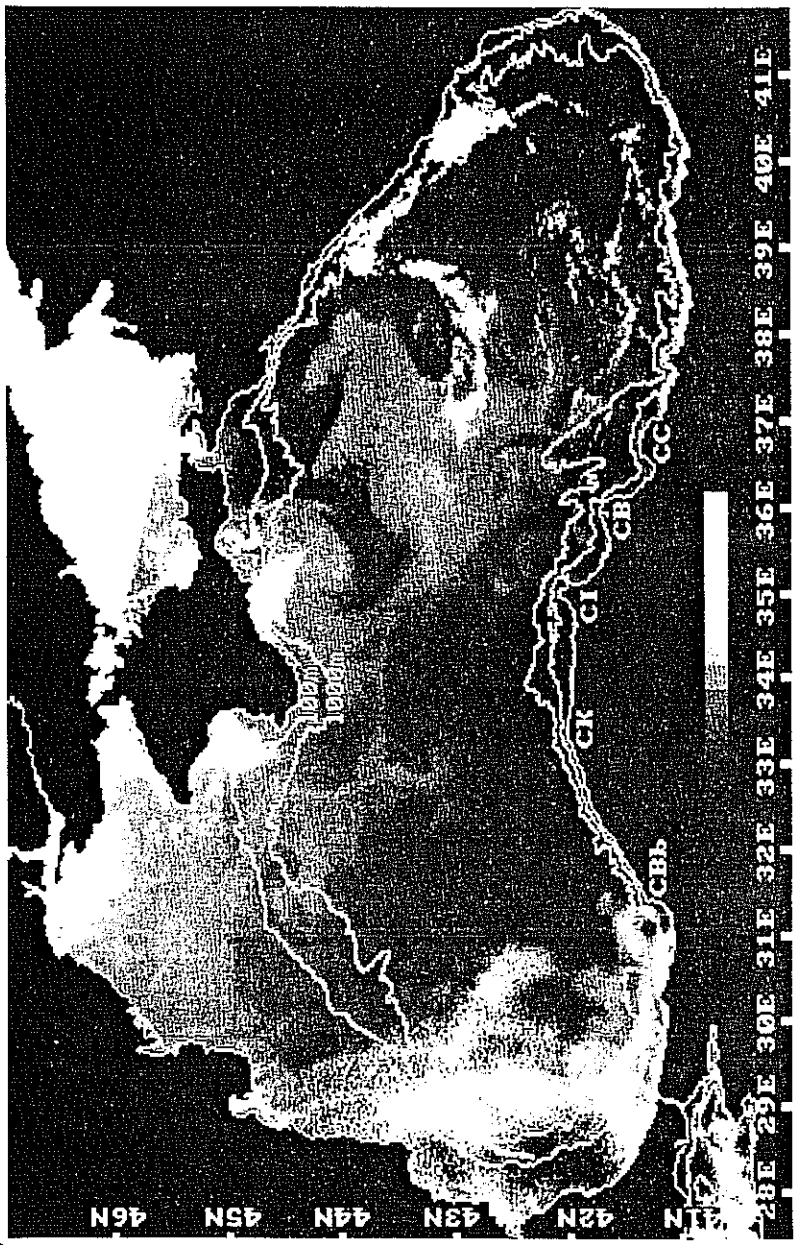
28E
29E
30E
31E
32E
33E
34E
35E
36E
37E
38E
39E
40E
41E
41N
42N
43N
44N
45N
46N
CR
CI
CB
CC
CBs
1000
2000

(c)

(a)

SEPTEMBER 1991

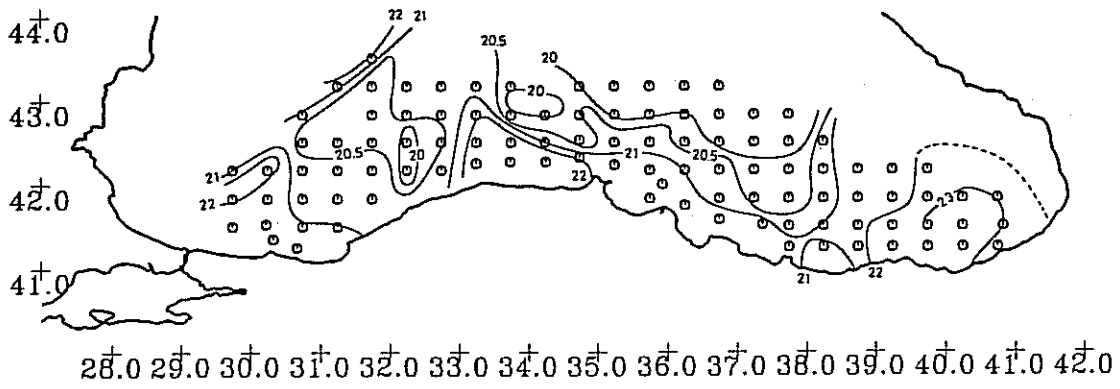

(b)

SEPTEMBER 1991

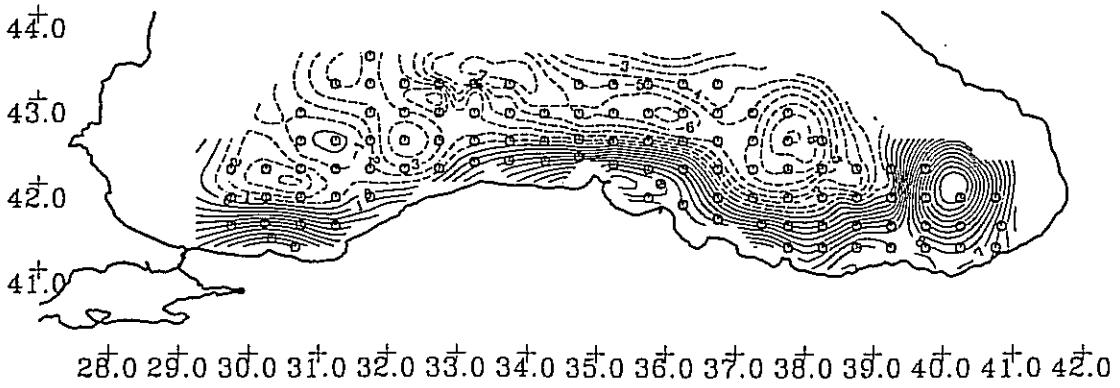

FIG. 18. (a) Surface temperature and (b) surface dynamic topography (cm), referenced to 300m during the September 1991 cruise of the R/V *Bilim*.

of 21-24°C elsewhere). The dynamic topography in Fig.20b displays boundary currents with alongshore variations similar to those indicated in Fig.18b. The current either becomes discontinuous or attached to the coast between Cape Baba and Cape Kerempe, but becomes separated downstream of Cape Kerempe. The cold water patch in Fig.20a occurs at the same location where the streamlines indicate a surface divergence in Fig.20b.

In Fig.20c, the cross-shore transects across the cold water patch show a localized structure with upwelling at its centre. Note that there are three layers of density: at the base of the shallow mixed layer density gradients are dominated by the contribution of the vertical gradient of temperature; below this, the permanent core of the Cold Intermediate Water (ÖZSOY *et al*, 1993; OGUZ *et al*, 1992) has minimum temperatures of <7°C at a depth of about 50m. The permanent pycnocline below this layer of cold water is dominated by the contribution of salinity gradients and, in general, slopes down towards the periphery of the basin in accord with the cyclonic basin circulation. Note, however, that the main pycnocline dips down towards the coast at the offshore part of the section in Fig.20c; then a reversal in its slope occurs near the coast, as a result of the upwelling activity. Near the surface, the vertical motions appear at some distance from the coast, leading to the penetration of the thin mixed layer zone by the underlying Cold Intermediate Water. This is perhaps the most favourable condition for upwelling: the shallow (10-20m) mixed layer can expose the underlying cold water when a surface divergence is created by the dynamics of the unstable boundary currents.

Notice that the width of the boundary current increases as it separates from the coast near Cape Kerempe (Fig.20b). This is reminiscent of a shock, or a critical transition, which may be associated with the effects of the Cape. CHERNIAWSKY and LEBLOND (1986) suggested that travelling shocks or bores could be formed near a cape although they predicted that stationary shocks were not possible. NOF (1984) showed that propagating shock waves can be generated along buoyant boundary currents by a sudden increase in the upstream transport.

During the observations of 1990-1991, the upwelling region is variable in character, with rapid changes in total area of the cold water patterns under the influence of local dynamics. Based on a sequence of images for an upwelling filament between Cape Kerempe and Cape Ince, OGUZ *et al* (1992) concluded that the upwelling features do not translate along the coast. Although our observations show rapid changes, the rapidity of creation and dissipation of filaments could mask organized motions. In any case, it is difficult to recognize any phase propagation during upwelling (e.g. Figs 14c and 15a-3). This apparently static nature of the patterns would be consistent with recirculation shoreward of the separated boundary current east of Cape Kerempe (Fig.13), and with the relatively smaller current velocities to the west of it (Figs 18b and 20b). We also speculate that the upwelling is usually observed in summer, when the relaxation in the strength of the circulation (e.g. STANEV, 1990) could create conditions favourable for upwelling.

Measurements during the detailed survey of July 1992 (NIERMANN, BINGEL, GORBAN, GORDINA, GÜCÜ, KIDEYS, KONSULOV, RADU, SUBBOTIN and ZAIKA (1993) indicate that only very few eggs and larvae of Anchovy were found in the cold water patch of Fig.20a, although they were abundant elsewhere. At the same location both phyto- and zoo-plankton were present in the near surface layers; in fact some yet unidentified species of phytoplankton and some copepods (especially the cold water species *Pseudocalanus elongatus*) were more abundant in the cold water patch, as compared to the surroundings. The decreased abundance of ichtyoplankton, despite a presence of phyto- and zoo-plankton, in the cold water patch seems to suggest that either the spawning of anchovy was suppressed, or the eggs and larvae could not survive the temperature shock created by the cold, upwelled waters.

It is worth noting that the same situation also occurred during a survey in July 1957 (EINARSSON

(a)

(b)

(c)

FIG. 19. (a) Automatic Picture Transmission (APT) infra-red image on August 4, 1992 (NOAA-10) without atmospheric and geometric corrections, (b) and (c) AVHRR (NOAA-11) infra-red images on August 30 and September 3, 1992, respectively. Lighter shades correspond to colder temperatures in satellite imageries. The AVHRR imageries were supplied by Paul Gerdeers from the Royal Netherlands Meteorological Institute (KNMI).

(b)

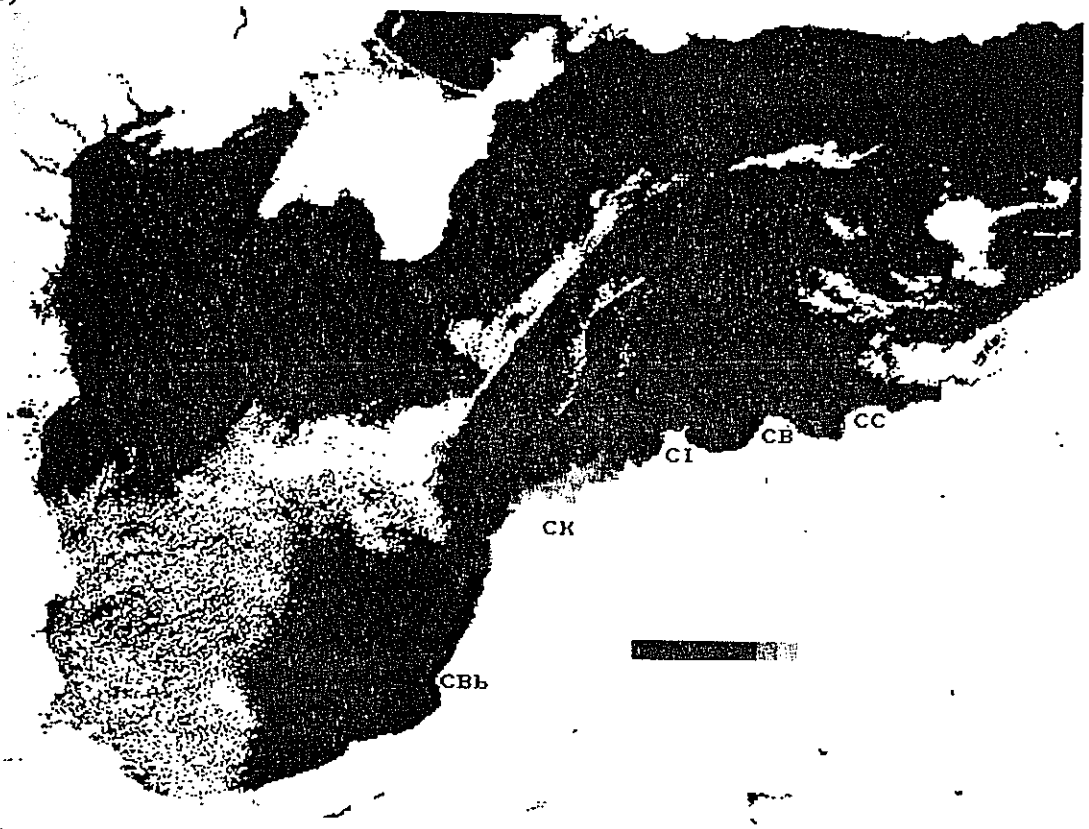

(c)

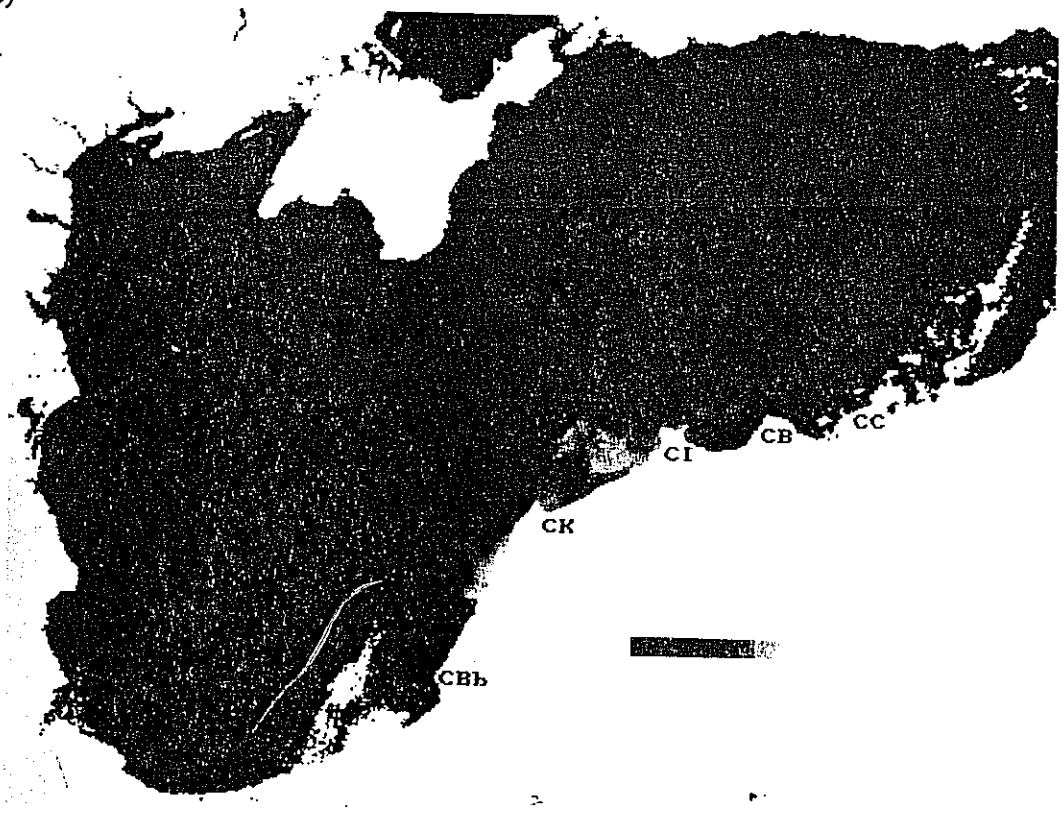

(a)

JULY 1992

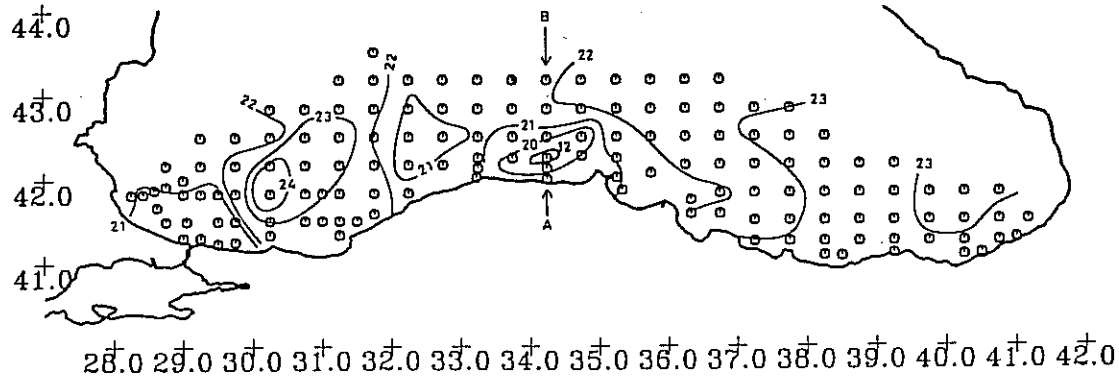

(b)

JULY 1992

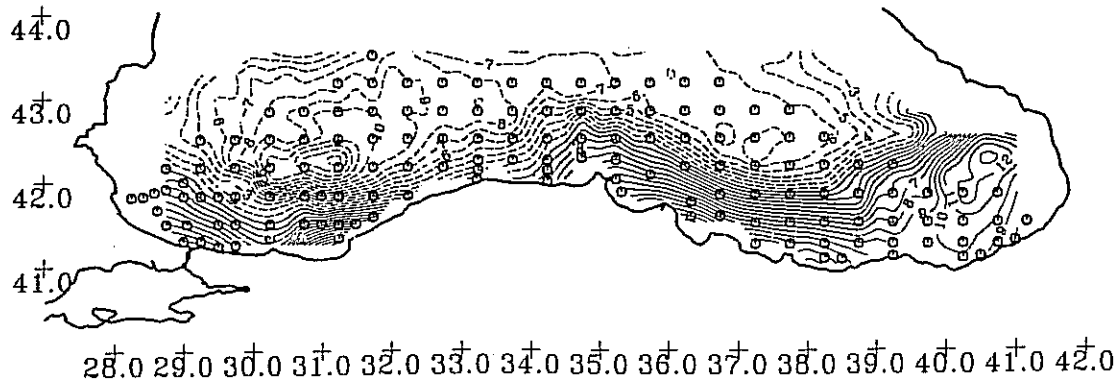

DENSITY JULY 1992

SALINITY JULY 1992

TEMPERATURE JULY 1992

(c)

FIG.20 (a) Surface temperature (°C), (b) dynamic topography (cm) referenced to 300m, and (c) the distribution of properties on a cross-shore transect passing through the upwelling region marked in (a), during the July 1992 cruise of the R/V *Bilim*.

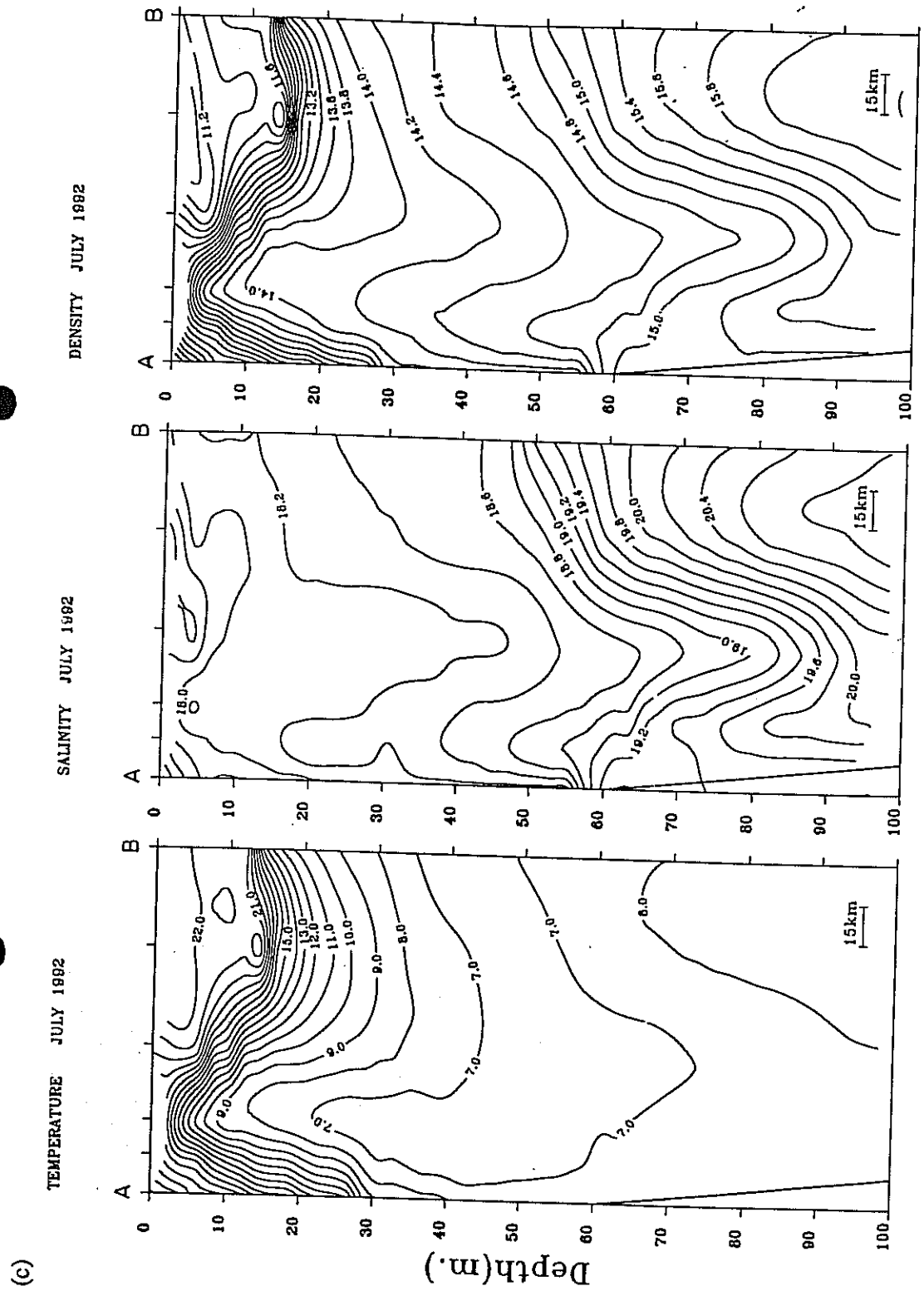
TEMPERATURE JULY 1992
SALINITY JULY 1992
DENSITY JULY 1992
A
B
15km
Depth(m.)
0
10
20
30
40
50
60
70
80
90
100

(c)

and GÜRTÜRK; 1960, NIERMANN *et al*, 1993). In this case, the upwelling region extended from Cape Baba to Cape Ince region, with temperatures as low as 11.6°C (at 10m depth) occurring in the same location as the 1992 upwelling. The distribution of anchovy eggs showed a total lack of eggs in the upwelling region (NIERMANN, *et al*, 1993).

4.4 Winter convection and productivity on the western shelf

Our limited winter data yield unique observations of shelf and slope processes. An infra-red (AVHRR) image on February 27, 1990 (Fig.21) indicates cold water with uniform temperatures along the entire western continental shelf. This well-mixed water has a uniform temperature of ~6.5°C and salinity <18 in the upper 30-40m along the southern coast (Figs 22a,b), and water with similar properties is expected to occupy the shallower part of the northwestern and western shelf regions as witnessed in Fig.21. The width of this band of cold water decreases towards the south, parallel to the decreasing width of the shelf. In fact, it can be verified that the boundary of the cold water follows a constant depth contour between 50 and 100m along the entire western shelf.

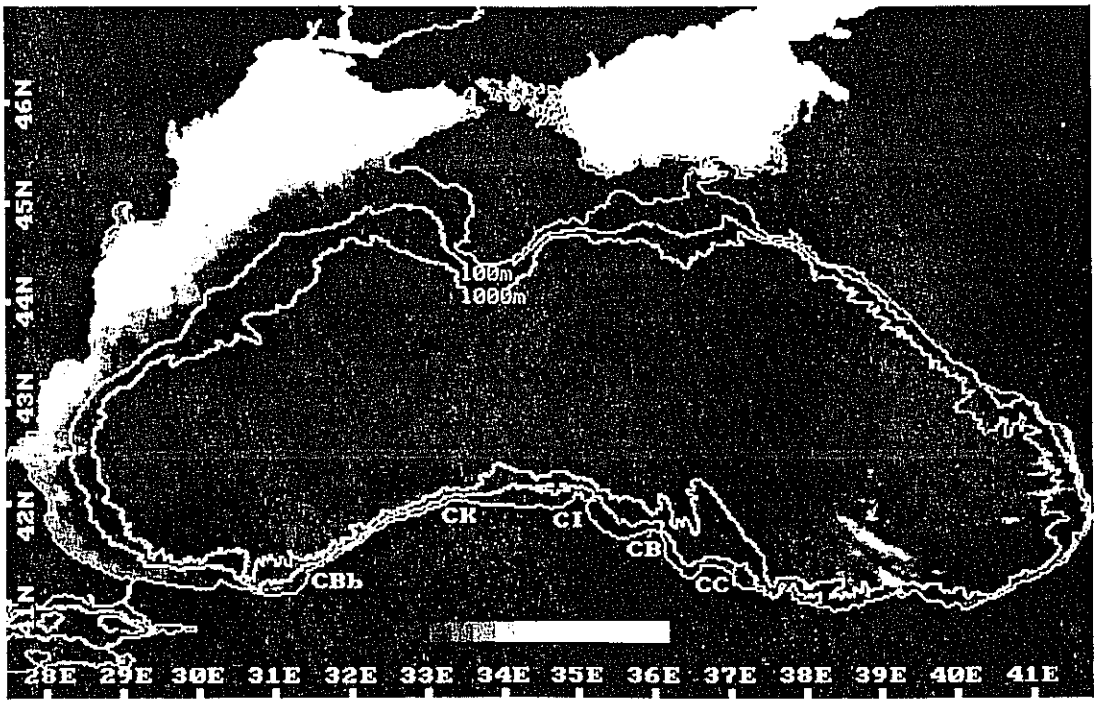

FIG.21. Advanced Very High Resolution Radiometer (AVHRR) satellite image on February 27 1990. The satellite images represent atmospherically uncorrected (NOAA-10) channel 4.

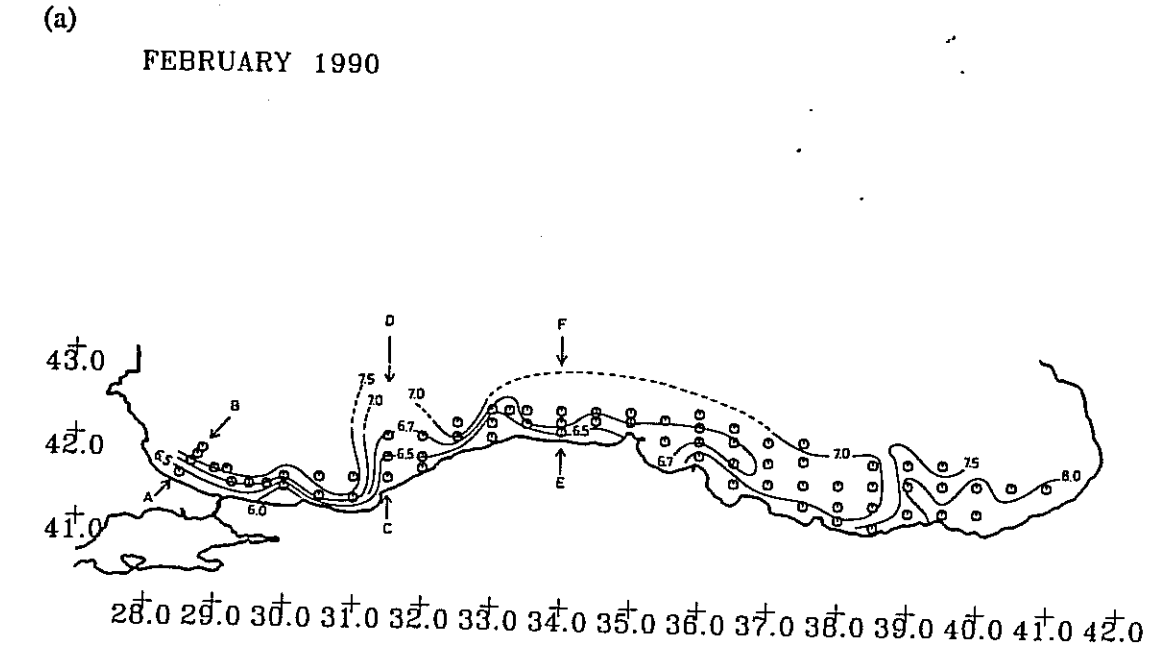

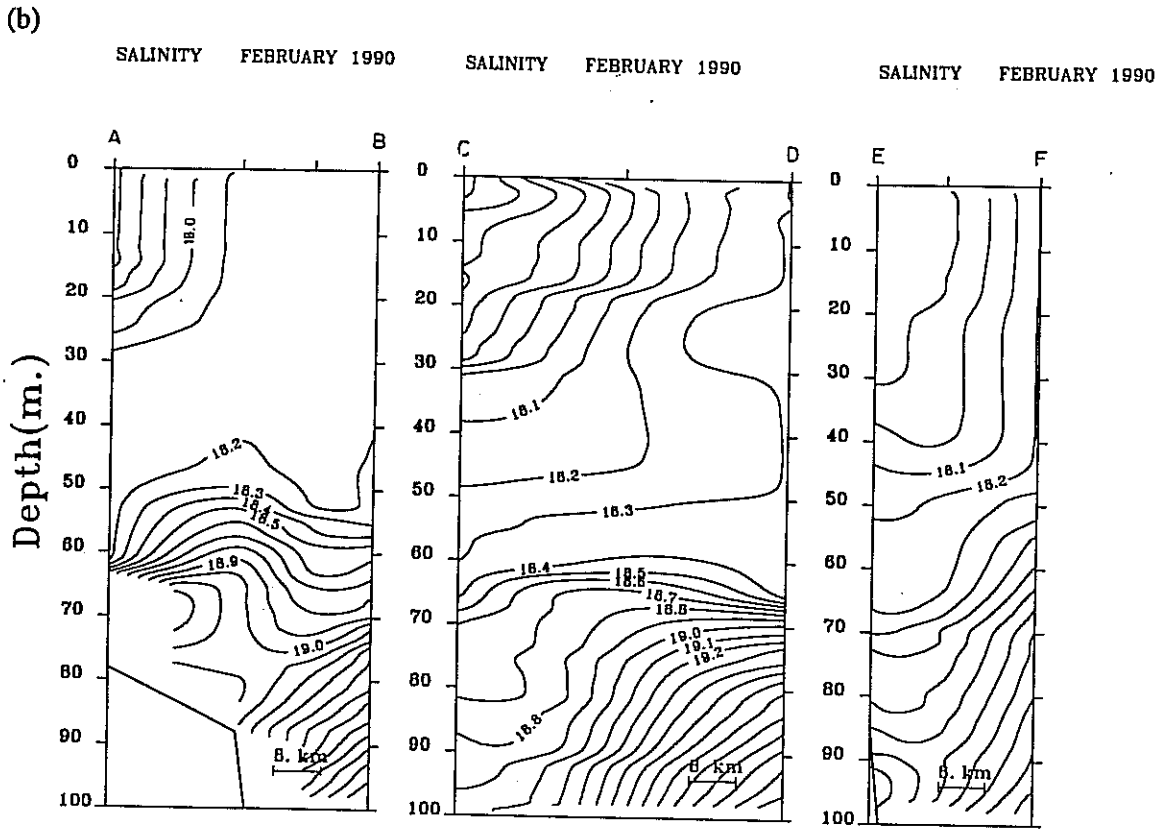

FIG.22. (a) Surface temperature distribution and (b) cross-shore hydrographic sections marked in (a), during the February 1990 cruise of the R/V *Bilim*.

The band of cold water flowing along the western shelf in Fig.21 becomes so thin that it is hardly detectable along the southeastern shelf. Because it is so thin, the cold water hugs the coast and is transported along the shallow inner part (<100m) of the Sakarya Canyon without setting up any disturbance there (compare with Fig.10). When the boundary current transporting the cold water reaches the concave coastline to the east of the Canyon it flows north, and becomes separated from the coast near Cape Baba, where the shallow region suddenly ends. The temperature structure displayed in Figs 21 and 22a near the Cape is most striking: the shape of the front delineating the flow is very similar to a shock; the narrow band of cold water suddenly expands and continues to flow along the coast with a sudden increase in width.

Our review in Section 4.3 of the effects of Sakarya Canyon indicates that the abrupt changes in depth can excite oscillatory motions supplied by baroclinic energy conversions. On the other hand, the possibility of flow separation has been predicted by SPITZ and NOF (1991), for a barotropic flow meeting a sudden depth increase (such as the well-mixed shelf-bound flow of cold water proceeding offshore near Cape Baba in Fig.21). This result is obtained for a coastal jet, keeping all nonlinear terms in the equations of motion. The hydraulics of nonlinear rotating flows seem to have directional preference. ARMI (1989) found an analogy of zonal flows with the hydraulic control theory, with two possible states for the width of an eastward flowing barotropic β-plane jet for a given flux; no controls were found for westward flowing jets (results confirmed by other analyses, e.g. HUGHES, 1985). If the planetary β-effect is exchanged with the effects of topographic slope, we would not expect such hydraulic transitions for a steady jet flowing in the Kelvin wave propagation direction, i.e. with the coast on the right. A transition from subcritical to supercritical flow was found in the case of the two-layer coastal jet studied by GILL and SCHUMANN (1979), with combined effects of shelf topography and coastal curvature. However, when their results are translated to the northern hemisphere, they can only be applied for coastal jets bounded by a left hand side coast, in line with the above results for barotropic flows. CHERNIAWSKY and LEBLOND (1986) suggested that for a buoyant boundary current along a coastline, flow separation could occur near sharp re-entrant corners.

For the above reasons, we suspect the sudden expansion at Cape Baba is the result of the flow separation as it crosses into the deep water region and turns around the corner made by the coastline, rather than a steady state hydraulic transition.

It is also important to recognise the relation of the cold shelf water relative to the boundary current system in Fig.21. Note that a band of warm water is present along the northern and eastern boundaries in this winter image of the Black Sea. Along the western and southern coasts, the warm water occurs along the continental slope offshore of the shelf waters and gradually disappears through frontal mixing with the cold shelf water. This gradual blending of cold and warm waters proceeds along the coast from west of Crimea to near Cape Baba on the Anatolian coast where the expanded ribon of cold water mixes efficiently with the warm slope waters. As a result, the tongue of cold water diminishing towards the east and its separation from the coast after Cape Ince is evident in Fig.22a.

Phytoplankton counting along the Turkish coast during February 1990 indicated an intense bloom along the coast, first following the ribbon of cold water to Cape Baba, and then in the separated flow region up to Cape Kerempe, in the same area as the cold water is seen in the satellite image. Throughout the survey area, the diatom *Chaetoceros sp.* was dominant, having abundances amounting to >91% of the total phytoplankton population of size >55μm. This percentage increased further in the coastal area adjacent to Cape Baba. The total number of individuals increased logarithmically to ($>10^6$ cells l^{-1}) near the coast at Cape Baba, but then decreased gradually towards the east. In the same region, there was a parallel increase of the observed number

of species near the coast (54 coastal species versus ~10 offshore species; species richness index increasing from a value of 1.2 in the offshore region to about 3.8 near the coast), but the corresponding measures of diversity decreased abruptly within the coastal band of cold water (Shannon-Weaver index <0.1, evenness index ~0.02) as compared to the offshore regions (Shannon-Weaver index >1.0, evenness index >0.5) (UYSAL, 1993). It is not clear whether this high abundance of dominant phytoplankton species was linked with the transport of plankton from the northwest shelf, local production resulting from nutrients either supplied via the ribbon of cold water, or entrained from the deep water. It is also not clear whether such a winter bloom supports higher trophic levels or collapses rapidly by sedimentation.

5. SUMMARY AND CONCLUSIONS

Relative to remotely-sensed thermal images which yield data restricted to a thin layer of surface water influenced by short-term surface heat fluxes, the CZCS data for the Black Sea have greatly enhanced value in producing depth-integrated signature of the available colour tracers, faithfully reproducing the transport patterns of the underlying flow dynamics. We have used phytoplankton pigment and particulate fields of CZCS together with or separately from infra-red images to study the current structures, the distribution of competing species of phytoplankton productivity and the progression of eutrophication in the Black Sea.

It is evident that materials originating from lateral sources are transported by the boundary current flowing along the continental slope topography, and are later dispersed along the coast and across frontal region by turbulent, meandering motions. These unstable motions, translating eastward along the Anatolian coast, are initiated by interactions with the sharp topographic variations in the along-shore direction. Flow separation caused by widening shelf topography or headlands is also evident, and influences the transport and vertical motions along the coast.

Upwelling is revealed, with rapidly varying distribution along a particular stretch of the Turkish coast, and persisting for extended periods in summer. However, the basic mechanism leading to upwelling remains largely unexplained. We suggest that interactions of the current system with the coastline geometry and bathymetry induces upwelling without any need for wind forcing to be present.

The advection of materials along the periphery of the basin and the cross-shelf transports created along the boundary current are important for the spreading of productivity and the subsequent basin-scale eutrophication processes, and sets the time and space scales of a succession of plankton blooms and their transformation into higher trophic levels. It is also recognised that these circulation features are important for the migration/spawning behaviour of the mainly pelagic fish stocks of the Black Sea, although they are now under an increasing threat of extinction. Only a better understanding of the system and a massive effort by collaborating European and Asian states to control their harmful effluxes can save *Pontos Euxeinos* (i.e. the hospitable sea, named after the early Greek civilisations and trading colonies who inhabited its coasts).

6. ACKNOWLEDGEMENTS

This study was made possible through the TU-Fisheries Project of the NATO Science for Stability Program, and partially funded by the Turkish Scientific and Technical Research Council (TÜBITAK). We would like to thank Paul Geerders who obtained the AVHRR images for August 1992 from the Royal Netherlands Meteorological Institute (KNMI) and to Paul E. LaViolette, who supplied most of the other level-1 CZCS and AVHRR data as part of a collaborative agreement within the TU-Fisheries project.

7. REFERENCES

ACARA, A. (1958) Fluctuation of the surface water temperature and salinity of the Bosphorus. *Rapports et Procès-verbaux des Reunions de la CIESMM*, **15**(3), 255-258.

AHLNÄS, K., T.C. ROYER and T.H. GEORGE (1987). Multiple dipole eddies in the Alaska Coastal Current detected with Landsat Thematic Mapper Data. *Journal of Geophysical Research*, **92**, 13041-13047.

ARMI, L. (1989) Hydraulic control of zonal currents on a β-plane. *Journal of Fluid Mechanics*, **201**, 357-377.

ARNONE, R.A. and P.E. LAVIOLETTE (1986) Satellite definition of the bio-optical and thermal variation of coastal eddies associated with the African Current. *Journal of Geophysical Research*, **91**, 2351-2364.

ARTÜZ, M.I. and H.C. UGUZ (1976) Daily observations on the hydrographic conditions of the Bosphorus during the period of 1967-1970. *Publications of the Hydrobiology Research Institute, Faculty of Science, University of Istanbul*, **16**, 35pp. (in Turkish).

BARALE, V. and L. FUSCO (1992) Ocean colour, planktonic pigments and productivity. *Rapports et Procès-verbaux des Reunions de la CIESMM*, **33** 10.

BASTÜRK, Ö, A.C. SAYDAM, I. SALIHOGLU and A. YILMAZ (1986) Health of the Turkish Straits II: Chemical and environmental aspects of the Sea of Marmara. In: *Oceanography of the Turkish Straits, First Annual Report, Vol.II,* Institute of Marine Sciences, Middle East Technical University, Erdemli, Içel, Turkey. 86pp.

BATCHELOR, G.K. (1970) *An introduction to Fluid Dynamics*, Cambridge University Press, 615pp.

BECKERS, J.M. and J.C.J. NIHOUL (1992) Model of the Algerian Current's instability. *Journal of Marine Systems*, **3**, 441-451.

BENLI, H. (1987) Investigations of plankton distribution in the Southern Black Sea and its effects on particle flux. In: *Particle flux in the Ocean*, E.T. DEGENS, E. IZDAR and S. HONJO, editors, Mitteilungen des Geologisch-Paleontologischen Institut, Universität Hamburg, **62**, 77-87.

BLATOV, A.S., A.N. KOSEREV and V.S. TUZHILKIN (1980) Variability of the hydrographic structure of the Black Sea Water and its links with the external factors. *Vodnyye Resursy* (Water Resources), **6**, 71-82, (in Russian).

BLATOV, A.S., N.P. BULGAKOV, V.A. IVANOV, A.N. KOSEREV and V.S. TUZHILKIN (1984). *Variability of hydrophysical fields in the Black Sea.* Hydrometeoizdat, Leningrad, 240pp. (in Russian).

BOLOGA, A.S. (1986) Planktonic primary productivity of the Black Sea: A Review. *Thalassia Jugoslavica*, **22**, 1-22.

BONDAR, C. (1989) Trends in the evolution of the mean Black Sea level. *Meteorology and Hydrology* (Romania), **19**, 23-28.

BOYER, D.L. and R. CHEN (1987) On the formation and shedding of vortices from side-wall mounted obstacles in rotating systems. *Dynamics of Atmospheres and Oceans*, **11**, 59-86.

CARSTENS, T., T.A. MCCLIMANS and J.H. NILSEN (1984) Satellite imagery of boundary currents. In: *Remote sensing of shelf sea hydrodynamics*, J.C.J. NIHOUL, editor, Elsevier, 235-256.

COBLE, G.P., R.B. GAGOSIAN, L.A. CODISPOTI, G.E. FRIEDERICH and J.P. CHRISTENSEN (1991) Vertical distribution of dissolved and particulate fluorescence in the Black Sea. *Deep-Sea Research*, **38**, S985-S1001.

CONDIE, S.A. (1989) Mesoscale structures on density driven boundary currents. In: *Mesoscale/synoptic coherent structures in geophysical turbulence*, J.C.J. NIHOUL and B.M. JAMART, editors, Elsevier, Amsterdam, 197-210.

CHAO, S-Y. (1988) Instabilities of fronts over a continental margin. *Journal of Geophysical Research*, **95**, 3199-3211.

CHERNIAWSKY, J. and P.H. LEBLOND (1986) Rotating flows along indented coastlines. *Journal of Fluid Mechanics*, **169**, 379-407.

CHIREA, R. and T. GOMOIU (1986) Some preliminary data on the nutrient influx into western Black Sea. *Cercetari Marine*, IRCM Constanta, **19**, 171-189.

CREPON, M., L. WALD and J.M. MONGET (1982) Low-frequency waves in the Ligurian Sea during December 1977. *Journal of Geophysical Research*, **87**, 595-600.

CRESSWELL, G.R. and T.G. GOLDING (1980) Observations of south-flowing current in the southeastern Indian Ocean. *Deep-Sea Research*, **27**, 449-466.

CUSHMAN-ROISIN, B. and J.J. O'BRIEN (1987) The influence of bottom topography on baroclinic transports. *Journal of Physical Oceanography*, **13**, 1600-1611.

DESCHAMPS, P.Y. and R. FROUIN (1984) Large diurnal heating of the sea surface observed by the HCMR Experiment. *Journal of Phyusical Oceanography*, **14**, 177-184.

DEUSER, W.G. (1971) Organic carbon budget of the Black Sea. *Deep-Sea Research*, **18**, 995-1004.

EINARSSON, H. and N. GÜRTÜRK (1960) Abundance and distribution of eggs and larvae of the Anchovy (*Engraulis encrasicholus ponticus*) in the Black Sea (Results of the Pektas Expedition). *Hydrobiological Research Institute, Faculty of Science, University of Istanbul, Series B*, **5**(1-2), 79-94 + 2 plates.

EREMEEV, V.N., V.L. VLADIMIROV and B.N. KRASHENINNIKOV (1992) Long-term variability of the Black Sea Water transparency. In: *Hydrophysical and hydrochemical studies of the Black Sea*, Marine Hydrophysical Institute, Ukraine Academy of Sciences, Sevastopol, 28-30.

FEDOROV, K.N. and A.I. GINSBURG (1989) Mushroom-like currents (vortex dipoles); one of the most widespread forms of non-stationary coherent motions in the ocean. In: *Mesoscale/synoptic coherent structures in geophysical turbulence*. J.C.J. NIHOUL and B.M. JAMART, editors, Elsevier, Amsterdam, 1-14.

FEDOROV, K.N., A.I. GINSBURG and A.G. KOSTIANOV (1989) Modelling of 'mushroom-like' currents (vortex dipoles) in a laboratory tank with rotating homogeneous and stratified fluids. In: *Mesoscale/synoptic coherent structures in geophysical turbulence*, J.C.J. NIHOUL and B.M. JAMART, editors, Elsevier, Amsterdam, 15-24.

FONSELIUS, S.H. (1974) Phosphorus in the Black Sea. In: *The Black Sea - Geology, Chemistry, Biology*. American Association of Petroleum Geologist, Memoir No.20, 144-150.

GAMSAKHURDIYA, G.R. and A.S. SARKISYAN (1976) Diagnostic calculations of current velocities in the Black Sea. *Oceanology*, **15**, 164-167.

GILL, A.E. and E.H. SCHUMANN (1979) Topographically induced changes in the structure of an inertial coastal jet: Application to the Agulhas Current. *Journal of Physical Oceanography*, **9**, 975-991.

GINSBURG, A.I. and K.N. FEDOROV (1989) On the multitude of forms of coherent motions in Marginal Ice Zones (MIZ). In: *Mesoscale/synoptic coherent structures in geophysical turbulence*. J.C.J. NIHOUL and B.M. JAMART, editors, Elsevier, Amsterdam, 25-40.

GÖÇMEN, D. (1988) *Fluctuations of chlorophyll a and primary productivity as related to physical chemical and biological parameters in Turkish coastal waters*. MS Thesis, METU, Institute of Marine Sciences, Erdemli, Içel, Turkey, 137pp.

GORDON, H.R., O.B. BROWN, R.H. EVANS, J.W. BROWN, R.C. SMITH, K.I.S. BAKER and D.K. CLARK (1988) A semianalytic model of ocean colour. *Journal of Geophysical Research*, **93**, 10909-10924.

GRIFFITHS, R.W. and P.F. LINDEN (1981) The stability of buoyancy-driven coastal currents. *Dynamics of Atmospheres and Oceans*, **5**, 281-306.

GRIFFITHS, R.W. and A.F. PEARCE (1985) Instability and eddy pairs on the Leeuwin Current south of Australia. *Deep-Sea Research*, **32**, 1511-1534.

HAIDVOGEL, D., A. BECKMANN and K. HEDSTRÖM (1991) Dynamical simulations of filament formation and evolution in the coastal transition zone. *Journal of Geophysical Research*, **96**, 15017-15040.

HÄKKINEN, S. (1987) Feedback between ice flow, barotropic flow and baroclinic flow in the presence of bottom topography. *Journal of Geophysical Research*, **92**, 3807-3820.

HAY, B.J. and S. HONJO (1989) Particle deposition in the present and holocene Black Sea. *Oceanography*, **2**, 26-31.

HAY, B.J., S. HONJO, S. KEMPE, V.A. ITEKKOT, E.T. DEGENS, T. KONUK and E. IZDAR (1990) Interannual variability in particle flux in the southwestern Black Sea. *Deep-Sea Research*, **37**, 911-928.

HAY, B.J., M.A. ARTHUR, W.E. DEAN and E.D. NEFF (1991) Sediment deposition in the late holocene abyssal Black Sea: Terrigenous and biogenic matter. *Deep-Sea Research*, **38**, (Suppl), S1211-S1235.

HOFFMANN, E.E., K. HEDSTRÖM, J. MOISAN, D. HAIDVOGEL and D.L. MACKAS (1991) Use of simulated drifter tracks to investigate general transport patterns and residence times in the coastal transition zone. *Journal of Geophysical Research*, **96**, 15041-15152.

HOLLIGAN, P.M., M. VIOLLIER, D.S. HARBOUR, P. CAMUS and M. CHAMPAGNE-PHILIPPE (1983) Satellite and ship studies of coccolithophore production along a continental shelf edge. *Nature*, **304**, 339-342.

HOLLIGAN, P.M., T. AARUP and S.B. GROOM (1989) The North Sea: Satellite colour atlas. *Continental Shelf Research*, **9**, 667-765.

HUA, B-L. and F. THOMASSET (1983) A numerical study of coastline geometry on wind-induced upwelling in the Gulf of Lions. *Journal of Physical Oceanography*, **13**, 678-694.

HUGHES, R.L. (1985) On inertial currents over a sloping continental shelf. *Dynamics of Atmospheres and Oceans*, **9**, 49-73.

HUTHNANCE, J.M. (1992) Extensive slope currents and the ocean-shelf boundary. *Progress in Oceanography*, **29**, 161-196.

IKEDA, M. (1984) Coastal flows driven by a local density flux. *Journal of Geophysical Research*, **89**, 8008-8016.

IKEDA, M. (1987) Modelling interpretation of the ice edge off the Labrador coast observed in NOAA satellite imagery, Northern California. *Journal of Physical Oceanography*, **17**, 1468-1483.

IKEDA, M. and M.J. EMERY (1985) Observation and modelling of meanders in the California Current System off Oregon and Northern California. *Journal of Physical Oceanography*, **14**, 1434-1450.

IKEDA, M., L.A. MYSAK and W.J. EMERY (1984) Observation and modelling of satellite-sensed meanders and eddies off Vancouver Island. *Journal of Physical Oceanography*, **14**, 3-21.

IKEDA, M., J.A. JOHANNESSEN, K. LYGRE and S. SANDVEN (1989) A process study of mesoscale meanders and eddies in the Norwegian coastal current. *Journal of Physical Oceanography*, **19**, 20-35.

JANOWITZ, G.S. and L.J. PIETRAFESA (1982) The effects of alongshore variation in bottom topography on a boundary current. *Continental Shelf Research*, **1**, 123-141.

JOHANNESSEN, J.A., E. SVENDSEN, O.M. JOHANNESSEN and K. LYGRE (1989) Three-dimensional structure of mesoscale eddies in the Norwegian coastal current. *Journal of Physical Oceanography*, **19**, 3-19.

JOHANNESSEN, O.M., J.A. JOHANNESSEN, E. SVENDSEN, R.A. SCHUCHMAN, W.J. CAMPBELL and E. JOSBERGER (1987) Ice-edge eddies in the Fram Strait marginal ice zone. *Science*, **236**, 427-429.

KNIPOVICH, N.M. (1993) Hydrologic research in the Black Sea. *Trudy Azovo-Chernomorskoi Nauchnopromsylovoy Expeditsii*, **10**, 274pp (in Russian).

KOBLENTZ-MISHKE, O.J., V.V. VOLKOVINSKY and J.G. KABANOVA (1970) Plankton primary production of the world ocean. In: *Scientific exploration of the South Pacific*, W.S. WOOSTER, editor, National Academy of Sciences, Washington, 183-193.

LATUN, V.S. (1990) Anticyclonic eddies in the Black Sea in summer 1984. *Soviet Journal of Physical Oceanography*, **1**, 279-286 (in Russian).

LEAMAN, K.D. and R.L. MOLINARI (1987) Topographic modification of the Florida Current by Little Bahama and Great Bahama Banks. *Journal of Physical Oceanography*, **17**, 1724-1736.

LEGECKIS, R. and G. CRESSWELL (1981) Satellite observations of sea surface temperature fronts off the coast of Western and Southern Australia. *Deep-Sea Research*, **28**, 279-306.

MARCHUK, G.I., A.A. KORDZADZE and Y.N. SKIBA (1975) Calculation of the basic hydrological fields in the Black Sea. *Fizika Atomosfery: Okeana, Izvestiya Academiya nauk USSR*, **11**(4), 379-393 (in Russian).

MCCLAIN, E.P., W.G. PICHEL, C.C. WALTON, Z. AHMAD and J. SUTTON (1982) Multichannel improvements to satellite-derived global sea surface temperatures. *Advances in Space Research*, **2**, 43-47.

MEE, L.D. (1992) The Black Sea in crisis: The need for concerted international action. *Ambio*. **21**, 278-286

MIED, R.P., J.C. MCWILLIAMS and G.J. LINDEMANN (1991) The generation and evolution of mushroom-like vortices. *Journal of Physical Oceanography*, **21**, 489-510.

MILLOT, C. (1985) Some features of the Algerian Current. *Journal of Geophysical Research*, **90**, 7169-7176.

MILLOT, C. (1991) Mesoscale and seasonal variabilities of the circulation in the western Mediterranean. *Dynamics of Atmospheres and Oceans*, **15**, 179-214.

MOSKALENKO, L.V. (1976) Calculation of stationary wind driven currents in the Black Sea. *Oceanology*, **15**, 168-171.

MURRAY, J.W. (1991) (editor) Black Sea oceanography, results from the 1988 Black Sea Expedition. *Deep-Sea Research*, **38**, Supplementary Issue 2A, S665-S1266.

MURRAY, J.W. and E. IZDAR (1989) The 1988 Black Sea Oceanographic Expedition: Overview and new discoveries. *Oceanography*, **2**, 15-21.

MUSAYEVA, E.I. (1985) Mesoplankton near the Bulgarian coast. *Oceanology*, **25**, 647-652.

MYSAK, L.A. and F. SCHOTT (1977) Evidence for baroclinic instability of Norwegian Current. *Journal of Geophysical Research*, **82**, 2087-2095.

NARIMOUSA, S. and T. MAXWORTHY (1985) Two-layer model of shear-driven coastal upwelling in the presence of bottom topography. *Journal of Fluid Mechanics*, **159**, 503-531.

NARIMOUSA, S. and T. MAXWORTHY (1987) A note on the effects of coastal perturbations on coastal currents and fronts. *Journal of Physical Oceanography*, **17**, 1296-1303.

NEUMANN, G. (1942) Das Schwarze Meer. *Zeitschr. Ges. f. Erdkunde*, Berlin, **3**, 92-114.

NIERMANN, U., F. BINGEL, A. GORBAN, A.D. GORDINA, A. GÜCÜ, A.E. KIDEYS, A. KONSULOV, G. RADU, A.A. SUBBOTIN and V.E. ZAIKA (1993) Distribution of anchovy eggs and larvae (*Engraulis encrasicolus* Cuv.) in the Black Sea in 1991 and 1992 in comparison to former surveys, ICES, CM1993/H:48, 19pp.

NOF, D. (1984) Shock waves in currents and outflows. *Journal of Physical Oceanography*, **14**, 1683-1702.
OKUBO, A. (1980) *Diffusion and ecological problems: Mathematical Models*, Springer-Verlag, 254pp.
OGUZ, T., F. BINGEL and S. TUGRUL (1990) Stock assessment studies for Turkish Black Sea coast. *Technical Report*, METU, Institute of Marine Sciences, Erdemli, Içel, Turkey, 122pp.
OGUZ, T., P.E. LA VIOLETTE and Ü. ÜNLÜATA (1992) The upper layer circulation of the Black Sea: Its variability as inferred from hydrographic and satellite observations. *Journal of Geophysical Research*, **97**, 12569-12584.
OGUZ, T., V.S. LATUN, M.A. LATIF, V.V. VLADIMIROV, H.I. SUR, A.A. MARKOV, E. ÖZSOY, B.B. KOTOVSHCHIKOV, V.V. EREMEEV, Ü. ÜNLÜATA (1993) Circulation in the surface and intermediate layers of the Black Sea. *Deep-Sea Research*, **40**, 1597-1612.
ÖZSOY, E. (1990) On the seasonally varying control of the Black Sea exchange through the Bosphorus. AGU-ASLO Ocean Sciences Meeting, New Orleans, February 1990. *Eos*, **71**.
ÖZSOY, E., Ü. ÜNLÜATA and Z. TOP (1993) The Mediterranean water evolution, material transport by double diffusive intrusions and interior mixing in the Black Sea. *Progress in Oceanography*, **31**, 279-320.
ÖZSOY, E., M.A. LATIF, S. TUGRUL and Ü. ÜNLÜATA (1992) Water and nutrient fluxes through the Bosphorus, an exchange between the Mediterranean and Black Sea. In: *Problems of the Black Sea, International Conference*, MHI Sevastopol, Ukraine, Plenary reports, 54-67.
ÖZSOY, E., A. HECHT, Ü. ÜNLÜATA, S. BRENNER, T. OGUZ, J. BISHOP, M.A. LATIF and Z. ROZENTRAUB (1991) A review of the Levantine Basin circulation and its variability during 1985-1988. *Dynamics of Atmospheres and Oceans*, **15**, 421-456.
ÖZTURGUT, E. (1966) Water balance of the Black Sea and flow through the Bosphorus. *CENTO Symposium on Hydrology and Water Resources development, Ankara, Turkey, February 1966*. 107-112.
QIU, B., N. IMASATO and T. AWAJI (1988) Baroclinic instability of buoyancy-driven coastal density currents. *Journal of Geophysical Research*, **93**, 5037-5050.
ROBINSON, I.S. (1991) *Satellite Oceanography. An introduction for oceanographers and remote-sensing scientists.* Ellis Horwood, 455pp.
SAYDAM, C., S. TUGRUL, Ö. BASTÜRK and T. OGUZ (1992) Identification of the oxic/anoxic interface by isopycnal surfaces in the Black Sea. *Deep-Sea Research*, **40**, 1405-1412.
SERPOIANU, G. (1973) Le Bilan Hydrologique de la Mer Noire, *Cercetari Marine, IRCM* No: **5-6**, 145-153.
SERPOIANU, G., I. NAE and V. MALCIU (1992) Danube water influence on sea water salinity at the Romanian Littoral. *Rapports et Procès verbaux des Reunions de la CIESMM*. **33**, 233.
SHETYE, S.R. and M. RATTRAY (1982) The effect of varying bathymetry on steady zonal equivalent barotropic jets. *Deep-Sea Research*, **29**, 17-44.
SIMPSON, J.H. and J. BROWN (1987) The interpretation of visible band imagery of turbid shallow seas in terms of the distribution of suspended particulates. *Continental Shelf Research*, 7, 1307-1313.
SOROKIN, YU. I. (1983) The Black Sea. In: *Estuaries and enclosed seas, ecosystems of the world.* B.H. KETCHUM, editor, Elsevier, 253-292.
SPITZ, Y.H. and D. NOF (1991) Separation of boundary currents due to bottom topography. *Deep-Sea Research*, **38**, 1-20.
STANEV, E.V. (1990) On the mechanisms of the Black Sea circulation. *Earth-Science Reviews*, **28**, 285-319.
STERN, M.E. (1980) Geostrophic fronts, bores breaking and blocking waves. *Journal of Fluid Mechanics*, **99**, 687-703.
SUKHANOVA, I.N., M.V. FLINT, G. HIBAUM, V. KARAMFILOV, A.I. KOPYLOV, E. MATVEEVA, T.N. RAT'KOVA and A.P. SAZHIN (1988) *Exuviaella cordata* red tide in Bulgarian coastal waters (May to June 1986). *Marine Biology*, **99**, 1-8.
THOMPSON, R.O.R.Y. (1984) Observations of the Leeuwin Current off Western Australia. *Journal of Physical Oceanography*, **14**, 623-628.
THOMSON, R.E. (1984) A cyclonic eddy over the continental margin of Vancouver Island: Evidence for baroclinic instability. *Journal of Physical Oceanography*, **14**, 1326-1348.
TOLMAZIN, D. (1985) Changing coastal oceanography of the Black Sea. I: Northwestern shelf. *Progress in Oceanography*, **15**, 217-276.
TUGRUL, S., Ö. BASTÜRK, C. SAYDAM and A. YILMAZ (1992) Changes in the hydrochemistry of the Black Sea inferred from water density profiles. *Nature*, **359**, 137-139.
TUMANTSEVA, N.I. (1985) Red Tide in Black Sea. *Oceanology*, **25**, 99-101.

ÜNLÜATA, Ü. and E. ÖZSOY (1986) Health of the Turkish Straits I: Oxygen deficiency of the Sea of Marmara. *Oceanography of the Turkish Straits, First Annual Report Vol.II*, Institute of Marine Sciences, Middle East Technical University, Erdemli, Içel, Turkey, 82pp.

UYSAL, Z. (1993) *A preliminary study on some plankters along the Turkish Black Sea coast: Species composition and spatial distribution.* PhD Thesis, Institute of Marine Sciences, Middle East Technical Universioty, Erdemli, Içel, Turkey. 138pp.

VOROPAYEV, S.I. (1989) Flat vortex structures in a stratified fluid. In: *Mesoscale/Synoptic coherent structures in geophysical turbulence.* J.C.J. NIHOUL and B.M. JAMART, editors, Elsevier, Amsterdam, 671-690.

VAN HEIJST, G.J.F. and J.B. FLOR (1989) Laboratory experiments on dipole structures in a stratified fluid. In: *Mesoscale/Synoptic coherent structures in geophysical turbulence.* J.C.J. NIHOUL and B.M. JAMART, editors, Elsevier, Amsterdam, 591-608.

YENTSCH, C.S. (1984) Satellite representation of features of ocean circulation indicated by CZCS colorimetry. In: *Mesoscale/Synoptic coherent structures in geophysical turbulence.* J.C.J. NIHOUL and B.M. JAMART, editors, Elsevier, Amsterdam, 336-354.

ZAITSEV, YU.P. (1991) Cultural eutrophication of the Black Sea and other South European Seas. *Lamer (Societé franco-Japanaise d'océanographie, Tokyo)*, **29**, 1-7.

8. APPENDIX A

PROCESSING AND INTERPRETATION OF CZCS AND AVHRR SATELLITE IMAGES

The Nimbus-7 CZCS is a six channel, multispectral scanning sensor with visible channels (1-5) at 443±10, 520±10, 550±10, 670±10, 700-800nm and one infra-red channel of 10.5-12.5μm (ROBINSON, 1991). The satellite acquired data at about 11:00 (local solar time) each day near the Black Sea.

The bio-optical properties derived from CZCS are assumed to be integrated over one attenuation depth of visible light (ARNONE and LA VIOLETTE, 1986), typically on the order of 25m for open ocean waters and 5m for coastal waters (probably smaller in the case of the Black Sea).

The CZCS visible bands yield information on chlorophyll *a*, a most abundant constituent of live phytoplankton, with strong absorbance in the blue (443nm) and secondarily in the red (670nm) bands of the light spectrum. Accessory pigments have absorption maxima in the green (520nm) and yellow (550nm) bands. The measured reflectance in these bands also depends on the visible light scattering properties of the particulates, especially in the case of diatoms and coccolithophores (HOLLIGAN *et al* 1983). In coastal waters, suspended particulates backscatter in a wide band (channels 1-3 of CZCS) of the visible spectrum (SIMPSON and BROWN, 1987). In low salinity (<30) waters, reflectance can result from dissolved organic matter (DOM) or yellow substance of terrestrial or marine origin (HOLLIGAN, AARUP and GROOM, 1989).

The atmospheric correction algorithm for CZCS images involves the subtraction of a weighted measure of atmospheric aerosol concentration (channel 4, 670nm), and a signal proportion to the Rayleigh (molecular) scattering. The corrected upwelling radiance from the ocean surface is then computed for the first three channels (GORDON, BROWN, EVANS, BROWN, SMITH, BAKER and CLARK, 1988).

The AVHRR data obtained from the thermal infra-red sensors of NOAA-9 and NOAA-11 satellites are calibrated and atmospherically corrected utilizing the AVHRR channels 4 (10.3-11.3nm) and 5 (11.5-12.5nm), and the split-window multichannel technique developed by MCCLAIN, PICHEL, WALTON, AHMAD and SUTTON (1982).